Individual Blade Pitch and Disturbance Accommodating Control of Floating Offshore Wind Turbines

Hazim Namik

A thesis submitted in fulfilment of the requirements for the degree of Doctor of Philosophy in Mechanical Engineering, The University of Auckland.

February 2012

Abstract

Floating wind turbines offer a feasible solution for going further offshore into deep waters. However, using a floating platform introduces additional motions that must be taken into account actively or passively. Therefore, the control system becomes an important component in controlling these motions.

In this work, the development, implementation, and simulation of multi-objective state feedback and disturbance accommodating controllers applied on the three main floating concepts are described. The three concepts are the barge, tension leg, and spar-buoy floating platforms. These controllers utilise individual blade pitching to create asymmetric aerodynamic loads in addition to the symmetric loads created by collective blade pitching to increase the platform restoring moments.

Simulation results, according to design load case 1.2 of the IEC 61400-3 standard for offshore wind turbines, show that state feedback controllers improve the performance relative to a collective blade pitch gain scheduled proportional-integral controller in terms of power and rotor speed regulation as well as reducing tower fore-aft and side-side bending loads. However, the magnitude of the improvements depends on the dynamics of each platform, its responsiveness to individual blade pitching and sensitivities to external wind and wave disturbances. Furthermore, interesting physical phenomena, such as the platform roll to pitch coupling caused by the controller, are identified.

Disturbance accommodating controllers for rejecting wind speed perturbations further improve rotor speed regulation and reduce tower fore-aft bending loads except on the barge platform; the barge platform motion is dominated by incident waves and therefore rejecting wind speed perturbations has no noticeable impact. Wave moment disturbance rejection is also investigated but in a limited case study. While the approach taken can theoretically cancel the effects of incident wave moments, practically, the required actuation force cannot be generated by the wind turbine blades. Furthermore, using the blades for rejecting wave moments increases the tower bending due to the load path of the restoring moment through the tower.

Out of the three investigated platforms, the tension leg platform with a disturbance accommodating controller has the best overall performance with fatigue loads close or less than that of an onshore wind turbine. The other two platforms, in their current design form, experience large tower fore-aft bending loads that would prevent them from being deployed in rough sea conditions.

To my loving parents

Acknowledgements

First and foremost, I would like to thank my main supervisor *Dr. Karl Stol* for his guidance, support, patience, and encouragement. Karl's excellent supervision style has definitely made the journey enjoyable for the most parts.

A special thanks for *Dr. Jason Jonkman* at the National Renewable Energy Laboratory for providing the simulation models and continued support over the years. Without his support, I wouldn't have been able to do all the work that is in this thesis.

Thanks to *Edith Willson*, *Lesley Darby*, and *Anu Sunkari* for helping me out with the many bureaucratic processes of the university and for making things happen in the department.

I would like to thank the Tertiary Education Commission of New Zealand for funding the first three years through the Top Achiever Doctoral Scholarship and The University of Auckland for extending the scholarship for another six months. The scholarship has allowed me to focus on my research and attend important conferences and meetings.

Thanks to my good friends *Andrew, Avi, Claudio, Ehad, Nasser, Ramin,* and *Rav* for their companionship, support, and the unusually long lunch *hours* and afternoon "tea breaks"!

Finally, I would like to thank my parents *Ban* and *Said*, brother *Salim*, and sister *Hana* for their support, understanding, patience, and constant encouragement to finish *as soon as possible*.

Contents

1 Introduction **1**

1.1 Introduction to Offshore Wind Turbines 1

1.1.1 Overview of Wind Energy 1

1.1.2 Offshore Wind Energy 2

1.1.3 Historical Development of Floating Offshore Wind Turbine Concepts . . . 5

1.2 Introduction to Wind Turbine Control 10

1.2.1 Operating Regions 11

1.2.2 Overall Controller Objectives 12

1.2.3 Control of Floating Wind Turbines 13

1.3 Research Objectives and Scope 14

1.4 Thesis Outline 16

2 Review of Floating Wind Turbine Controllers **17**

2.1 Gain Scheduled PI Control 19

2.1.1 Barge Platform 21

2.1.2 Tension Leg and Spar-Buoy Platforms 22

2.2 Variable Power Pitch Control 23

2.3 Estimator Based Control 24

2.4 Active Structural Control 25

2.5 Other Controllers 26

2.6 Onshore Wind Turbine Control 26

2.7 Controller Objectives 26

2.8 Chapter Summary 28

3 State Feedback Control **29**

3.1 State-Space Approach 30

3.2 Collective vs. Individual Blade Pitching 32

3.2.1 Collective Blade Pitching 32

3.2.2 Individual Blade Pitching 34

3.3 Multi-Blade Coordinate Transformation . . . 36
3.4 Implementation . . . 37
3.4.1 Generator Torque . . . 39
3.4.2 Azimuth Angle Correction due to Platform Rolling . . . 39
3.4.3 Actuator Saturation . . . 40
3.4.4 Azimuth State Anti-windup . . . 41
3.5 Stability Assessment . . . 41
3.6 Chapter Summary . . . 42

4 Disturbance Accommodating Control **43**
4.1 Introduction to DAC . . . 43
4.2 DAC Theory Overview . . . 44
4.2.1 Disturbance Estimator . . . 45
4.3 DAC After MBC Transformation . . . 47
4.4 Implementation . . . 48
4.4.1 DAC Limitations and Challenges . . . 49
4.5 Wind Speed Disturbance Rejection . . . 50
4.5.1 Collective Blade Pitch Drift . . . 51
4.6 Chapter Summary . . . 53

5 Modelling, Simulation, and Analysis Tools **55**
5.1 Wind Turbine Modelling and Simulation Tools . . . 55
5.1.1 FAST Simulation Code . . . 56
5.2 5MW Wind Turbine Model . . . 60
5.3 The IEC 61400-3 Standard . . . 61
5.4 Performance Metrics . . . 62
5.5 Simulation and Comparison Set Up . . . 64
5.6 Weibull Scaling . . . 65
5.7 Chapter Summary . . . 68

6 The Barge Platform **69**
6.1 The Barge Platform . . . 70
6.2 Controller Design . . . 71
6.2.1 Collective Blade Pitch State Feedback Control . . . 71
6.2.2 Platform Roll-Pitch Coupling . . . 71
6.2.3 Final Controller Design . . . 74
6.3 Offshore DLC Results . . . 75

6.3.1 Averaged Normalised Results . . . 75
6.3.2 Time Series Results . . . 77
6.4 Chapter Summary . . . 78

7 The Tension Leg Platform **81**
7.1 The Tension Leg Platform . . . 81
7.2 Controller Design . . . 83
7.3 Offshore DLC Results . . . 83
7.3.1 Averaged Normalised Results . . . 83
7.3.2 Time Series Results . . . 86
7.4 Chapter Summary . . . 86

8 The Spar-Buoy Platform **89**
8.1 The Spar-Buoy Platform . . . 89
8.2 Effects of Lowering the Platform's Pitch Natural Frequency in Control Design . . . 91
8.2.1 Platform Surge DOF . . . 91
8.2.2 Effectiveness of Individual Blade Pitching . . . 92
8.2.3 Final Controller Design . . . 92
8.3 Offshore DLC Results . . . 95
8.3.1 Averaged Normalised Results . . . 95
8.3.2 Times Series Results . . . 99
8.4 Chapter Summary . . . 99

9 Platform Comparisons **103**
9.1 Comparison Approach . . . 103
9.2 Platform Pitch Input and Disturbance Sensitivities . . . 104
9.3 DLC Results Relative to an Onshore Wind Turbine . . . 108
9.3.1 The Barge Platform . . . 108
9.3.2 The Tension Leg Platform . . . 110
9.3.3 The Spar-buoy Platform . . . 110
9.4 Chapter Summary . . . 111

10 Wave Disturbance Rejection: A Case Study **113**
10.1 Wave Disturbance Rejection . . . 113
10.1.1 Simplified Modelling Approach . . . 114
10.2 Case Study: Wave Disturbance Rejection on Floating Wind Turbines . . . 116
10.2.1 Linear Time-varying Model . . . 116
10.2.2 Nonlinear Periodic Model . . . 119

10.2.3 Case Study Summary 120
10.3 Chapter Summary 123

11 Conclusions and Recommendations **125**

Appendices **131**

A MBC Transformation of Linear State-Space Models **133**
A.1 Overview of Approach and Notation 133
A.2 The State Equation 135
A.3 The Output Equation 137
A.4 Summary 138

B Implementation Options for DAC After MBC Transformation **139**

C Design Load Cases **143**

D Relative Performance Trends for Controllers on Floating Platforms **147**

E Adaptive Disturbance Estimator **155**
E.1 Dealing with Periodic Waves 155
E.1.1 Case Study: Simple Linear System with Periodic Disturbances 156
E.2 ADE for Disturbances with Variable Frequency 157
E.2.1 Frequency Estimation 158
E.2.2 On-line Estimator Design 159
E.2.3 Case Study: ADE Performance with Mismatched Frequency 159
E.2.4 Case Study: ADE Performance on a Linear Floating Wind Turbine Model 160
E.3 Summary 163

References **165**

List of Figures

1.1 Offshore wind energy growth history 3
1.2 The floating platform's 6 DOFs 5
1.3 The three main floating concepts 6
1.4 The Tri-floater concept 8
1.5 Hywind and SWAY concepts 10
1.6 Main components of a wind turbine 11
1.7 Wind turbine operating regions 12

2.1 Baseline controller implementation in above rated wind speed region 20

3.1 Platform pitch restoring forces with different blade pitch operation 33
3.2 Collective and individual blade 1 gains as a function of rotor azimuth 35
3.3 Block diagram implementations of an IBP state-space controller 38
3.4 Azimuth angle correction due to platform roll motion 40

4.1 DAC with FSFB implementation for floating wind turbines 49
4.2 Wind disturbance rejection by a DAC on a simple nonlinear model 52
4.3 Collective blade pitch drift 52

5.1 Baseline controller model showing Simulink/FAST interface 58
5.2 Offshore FAST structure 59
5.3 The Weibull distribution 66
5.4 Weibull scaling factors 67

6.1 The barge platform 70
6.2 Normalised results for 2 DOFs CBP SFC relative to the Baseline controller . . . 72
6.3 Blade 1 B matrix elements for platform roll and pitch of a 3 DOFs model 73
6.4 Typical platform yaw motion envelope for the barge platform 74
6.5 Averaged DLC results for the barge platform 76
6.6 Sample time series response of the barge platform 79
6.7 Frequency content of the tower side-side base moment 80

7.1 The tension leg platform . . . 82
7.2 Averaged DLC results for the tension leg platform . . . 84
7.3 Sample time series response of the tension leg platform . . . 87
7.4 Frequency content of tower base moments . . . 88

8.1 The spar-buoy platform . . . 90
8.2 Effects of adding the surge DOFs on frequency response . . . 93
8.3 Platform pitch frequency response with different sets of DOFs . . . 94
8.4 The three platforms' pitch frequency response to blade 1 pitch . . . 94
8.5 Averaged DLC results for the spar-buoy platform . . . 96
8.6 Rotor speed and power errors trends with increasing wind mean speed . . . 98
8.7 Effect of platform roll on tower SS bending trend . . . 98
8.8 Sample time series response of the spar-buoy platform . . . 100
8.9 Frequency content of tower base moments . . . 101

9.1 Platform pitch frequency response to blade 1 pitch input . . . 105
9.2 Blade pitch frequency content . . . 106
9.3 Platform pitch frequency response to disturbance inputs . . . 107
9.4 Averaged DLC results relative to an onshore wind turbine . . . 109

10.1 Wave disturbance rejection on a linear 2 DOFs model . . . 118
10.2 Wave disturbance rejection on a nonlinear 2 DOFs model . . . 119
10.3 Blade 1 pitch rates with different α . . . 120
10.4 Wave DACs with different α simulated with a nonlinear 2 DOFs model . . . 121
10.5 Wave minimisation moment load path . . . 122

B.1 General DAC implementation options . . . 141

D.1 Performance trends for the SFC on the barge platform . . . 148
D.2 Performance trends for the DAC on the barge platform . . . 149
D.3 Performance trends for the SFC on the TLP . . . 150
D.4 Performance trends for the DAC on the TLP . . . 151
D.5 Performance trends for the SFC on the spar-buoy platform . . . 152
D.6 Performance trends for the DAC on the spar-buoy platform . . . 153

E.1 Periodic disturbance cancellation with matched estimator frequency . . . 156
E.2 Mismatched frequency disturbance estimate and state regulation . . . 157
E.3 Quantised response of the estimated frequency . . . 159
E.4 Adaptive disturbance estimator implementation block diagram . . . 160

E.5 Variable frequency disturbance estimates and state regulation 161
E.6 Constant mismatched frequency case 162
E.7 Continuously changing wave disturbance frequency case 163

List of Tables

1.1 Total installed wind energy capacity for the top 10 countries in 2010 2
1.2 Water depth distribution for different regions up to 100km offshore 4
1.3 Differences between single or multiple turbine floaters 7
1.4 Comparison between different floating platform designs 7
1.5 Relative comparison between the major floating platform concepts 9

2.1 Overview of most important controllers applied on floating wind turbines 18
2.2 Types of controllers implemented on onshore wind turbines 27

5.1 Floating wind turbine simulation codes 57
5.2 NREL 5MW wind turbine properties 60
5.3 DLC 1.2 conditions summary 61
5.4 Relative importance of performance metrics 63
5.5 Types of observed performance trends 64
5.6 Simulated controllers' comparison summary 65
5.7 Wind speed region limits 68

6.1 Barge platform properties 71
6.2 Performance trends of the barge platform controllers relative to Baseline controller 77

7.1 Tension leg platform properties 82
7.2 Performance trends of the TLP controllers with increasing mean wind speed . . 85

8.1 Spar-buoy platform properties 90
8.2 DOFs list for Figure 8.3 92
8.3 Performance trends of the spar-buoy platform controllers 97

9.1 Platform controllers to be compared to the onshore wind turbine 104

10.1 Effect of DAC gain scaling factor α on $\|B\alpha G_d + B_d\Theta\|$ 117

11.1 Summary of most important controllers applied on floating wind turbines 127

C.1 Stochastic wind and wave parameters used for DLC analysis 143

Nomenclature

Abbreviations

ADE	Adaptive Disturbance Estimator
CBP	collective blade pitch or pitching
DAC	Disturbance Accommodating Control or Controller
DLC	Design Load Case
DOF	degree(s) of freedom
FA	fore-aft
FAST	Fatigue, Aerodynamics, Structures, and Turbulence
FSFB	Full State Feedback
GSPI	Gain Scheduled Proportional-Integral
IBP	individual blade pitch or pitching
IEC	International Electrotechnical Commission
LQR	Linear Quadratic Regulator
LSS	low speed shaft
LTI	linear time-invariant
MBC	multi-blade coordinate
MIMO	multi-input multi-output
OC3	Offshore Code Comparison Collaboration
PID	Proportional-Integral-Derivative
RMS	root mean square
RNA	Roto-Nacelle Assembly

SFC	State Feedback Control or Controller
SISO	single-input single-output
SS	side-side
TLP	Tension Leg Platform
TMD	Tuned Mass Damper

Alphabetical Symbols

A	state matrix
$\overline{A}$	augmented A matrix
B	actuators gain matrix
B_d	disturbances gain matrix
$\overline{B}$	augmented B matrix
C	matrix that relates the states, $\underline{x}$, to the measurements, $\underline{y}$
c	Weibull distribution scaling parameter
C_d	damping matrix
$\overline{C}$	augmented C matrix
$C_{P,max}$	maximum power coefficient of the wind turbine
D	matrix that relates the controlled inputs, $\underline{u}$, to the measurements, $\underline{y}$
D_d	matrix that relates the disturbance inputs, $\underline{u}_d$, to the measurements, $\underline{y}$
F	actuators gain matrix for second order system
F_d	disturbance inputs matrix for second order system
g	acceleration due to gravity
G_d	disturbance minimising gain matrix
H	significant wave height
I_{I}	drivetrain inertia from the low speed shaft end
K	state feedback control gain matrix
k	Weibull distribution shape parameter
K_e	state estimator gain matrix
K_{P}, K_{I}	proportional and integral gains

K_s	stiffness matrix
K_{T}	optimum generator torque gain in below rated wind speed region
M	mass/inertia matrix
N	gearbox ratio
P_{Rated}	rated generator power
$\underline{q}$	degreees of freedom vector
R_{Rotor}	rotor radius
T	boolean transition matrix
T_{Gen}	applied generator torque
$T_c\,(\psi)$	control input $\underline{u}$ transformation matrix
$T_d\,(\psi)$	transformation matrix for augmented states vector $\underline{w}$
$T_o\,(\psi)$	output measurements $\underline{y}$ transformation matrix
$T_s\,(\psi)$	state $\underline{x}$ transformation matrix
T_w	wave period
$\underline{u}$	actuators inputs vector
U	ten–minute mean wind speed
$\underline{u}_d$	disturbance inputs vector
$\underline{v}$	augmented estimator inputs ($\underline{u}$ and $\underline{y}$) in the mixed frame of reference
$\underline{w}$	augmented state vector $\underline{x}$ with disturbance states $\underline{z}$
$\underline{x}$	states vector
$\underline{y}$	measurements vector
$\underline{z}$	disturbance states vector

Greek Symbols

α	DAC gain scaling factor
η_{Gen}	generator efficiency
Γ	disturbance state matrix
λ_o	optimum tip speed ration that yields maximum power
Ω	rotor speed

ω_n	natural frequency
Ω_r	rated rotor speed in revolutions per second
ψ	azimuth angle
ψ_a	actual azimuth angle of the rotor
ρ	air density
Θ	matrix that relates disturbance states, $\underline{z}$, to disturbance inputs, $\underline{u}_d$
θ	blade pitch angle
ξ	platform roll angle
ζ	damping ratio

Notation

Δx	perturbation about an operating or linearisation point
$\dot{x}$	rate of change with respect to time
$\hat{x}$	estimate
x_{NR}	an entity transformed to the non-rotating frame of reference
x^{op}	operating point
x^*	commanded or desired signal
$\underline{x}$	vector

1 Introduction

Contents

1.1 Introduction to Offshore Wind Turbines 1
1.2 Introduction to Wind Turbine Control 10
1.3 Research Objectives and Scope 14
1.4 Thesis Outline 16

Growing demand for more renewable energy sources to reduce the emission of greenhouse gases is one of the main drivers for the substantial growth of the global wind energy sector. Part of that growth is to deploy wind turbines further offshore into deep water. This chapter gives a brief introduction to offshore wind energy, especially floating wind turbines, and wind turbine control. Research objectives and scope are also outlined.

1.1 Introduction to Offshore Wind Turbines

1.1.1 Overview of Wind Energy

Wind energy is a clean, renewable, and sustainable source of energy. According to the International Energy Agency, as of May 2011, wind energy along with solar, geothermal and other renewable sources (excluding hydro) produce around 4% of the global energy supply [1]. Wind energy is the fastest growing harvested energy source in the world and continues to grow exponentially [2, 3].

In 2010, China surpassed the United States to become world leader in installed wind energy capacity with 44.7 GW of total installed capacity [4]; Table 1.1 lists the top 10 countries that account for 86% of the global installed capacity as of December 2010. Also in 2010, China

Table 1.1: Total installed wind energy capacity for the top 10 countries in 2010 (adapted from [4])

#	Country	Installed Capacity (MW)	% of Global Total
1	China	44,733	22.7
2	USA	40,180	20.4
3	Germany	27,214	13.8
4	Spain	20,676	10.5
5	India	13,065	6.6
6	Italy	5,797	2.9
7	France	5,660	2.9
8	UK	5,204	2.6
9	Canada	4,009	2.0
10	Denmark	3,752	1.9

installed 18,928 MW of wind energy accounting for 49.5% of the new installed capacity globally followed by USA and India with installed capacities of 5,115 MW and 2,139 MW respectively. In terms of wind energy penetration, Denmark is the world leader with 26% of its energy generated from wind [5].

With global warming caused by green house gases and drive for sustainability, some governments have set goals by which a certain percentage of their power supply is generated from renewable energy sources (mainly wind) [3]. Two examples are given: Australia has set a goal of 20% energy generation from renewable sources by 2020, and France has set the goal of 25 GW of wind power with 6 GW of offshore installations by 2020 to meet the EU directive of 23% renewable energy generation [4].

According to the Global Wind Energy Council [4], New Zealand's onshore wind energy resource is sufficient to meet its annual demand several times. In 2010, the total installed wind energy capacity reached 506 MW accounting for 4% of the energy supply. There is no explicit target for wind energy set by the New Zealand government but it is planned that by 2025, 90% of power supply sourced from renewable sources; to date, 70% of the energy supply is generated using hydroelectric and geothermal sources and only 26% is generated using non-renewable sources such as natural gas and coal [4, 6]. Unlike other countries, such as Germany for example, New Zealand does not have an incentive programme to promote investing in wind energy. However, New Zealand's wind energy sector is competing successfully with other energy sources; this globally unique achievement demonstrates the cost-effectiveness and competitiveness of wind energy without any form of government subsidy [4].

1.1.2 Offshore Wind Energy

The first commercial offshore wind farm is Vindeby wind farm located 2.5 km off the Danish coast which became operational in 1991 [2, 7]. It is still operational, has eleven 450 kW wind

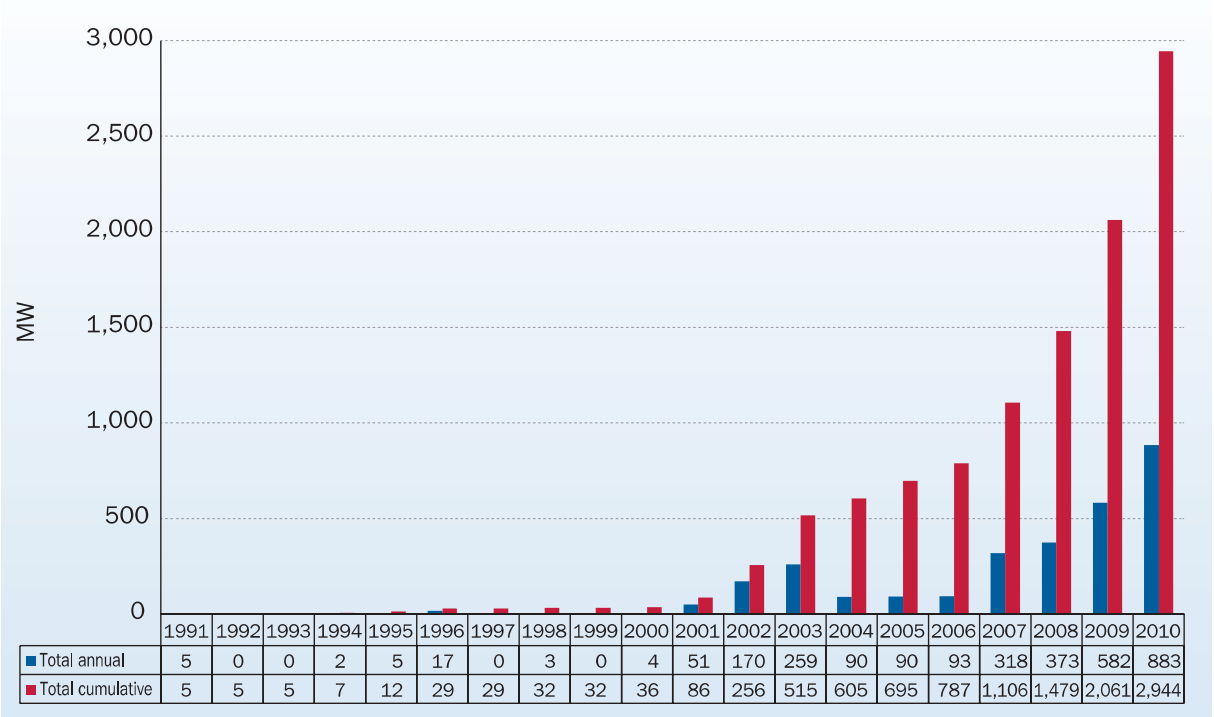

	1991	1992	1993	1994	1995	1996	1997	1998	1999	2000	2001	2002	2003	2004	2005	2006	2007	2008	2009	2010
Total annual	5	0	0	2	5	17	0	3	0	4	51	170	259	90	90	93	318	373	582	883
Total cumulative	5	5	5	7	12	29	29	32	32	36	86	256	515	605	695	787	1,106	1,479	2,061	2,944

Figure 1.1: Offshore wind energy growth history in the European Union [5]

turbines with total capacity of 4.95 MW, and is installed in water depths ranging from 2.5 m to 5 m. Since then, the growth in the offshore wind industry has been exponential (Figure 1.1). In 2010, the offshore wind energy market grew by 51% while the onshore market decreased by 13% [4].

The majority of offshore wind farms are located around Europe (North, Baltic, and Irish seas) with some offshore wind farms in USA, Japan, and China [2]. Historically, Denmark has been the world leader in offshore wind energy, but in 2010, the UK became the world leader with total installed capacity of 1,341 MW compared to Denmark's 854 MW [4, 5]. To date, all commercial offshore wind farms are located in shallow water (less than 30 m deep) and use fixed foundations such as mono-piles or lattice structures.

The main reason for going offshore is due to better wind resource attributes when compared to onshore wind; these include [8–10]: stronger and steadier wind; less turbulence resulting in longer turbine life; less vertical shear (i.e. higher wind speeds at lower altitudes) and higher annual mean wind speed. On average, offshore winds are 20% faster. However, offshore winds also have greater extremes, interact with surface waves, and are harder to measure.

In addition to having better offshore wind resource attributes, placing wind turbines offshore has several design and location advantages; these include [8, 11]:

- Turbines operate closer to maximum efficiency since no restrictions are imposed due to noise and other operational regulations.
- Proximity to load centres (large cities) thus requiring less transmission distance and access the less heavily used transmission lines.

- Reduced visual impact.
- Energy balance: An offshore wind turbine can recover the energy cost used during manufacture, transport, installation, operation, maintenance, and decommissioning in three months. Over its lifetime, the turbine can generate over 100 times that energy.

Placing the turbines offshore has the following challenges [12]: increased capital cost due to foundations, integration with the electrical network, and installation, operation and maintenance being subject to weather conditions.

The offshore wind energy potential is very large. For example, the UK's offshore energy potential is estimated to be 986 TWh/year while demand is estimated to be 321 TWh/year (based on 2003 estimates); i.e. more than three times the demand [8]. The US wind energy potential between 10 km and 100 km offshore is estimated to be more than 900 GW which is more than the currently installed electricity generation capacity in the US; however, much of this potential is located in deep water that is deeper than 30 m [13]. Table 1.2 shows the percentage of water depths for different regions up to 100 km offshore. It shows that in Northern Europe 47% of water depth is below 50 m while in Southern Europe 72% is deeper than 50 m [14]. Similarly in Japan, 69% is deeper than 50 m. However, in the USA 76% is below 50 m deep.

Floating Wind Turbines

Currently, the deepest installed fixed-bottom offshore wind turbine is the Beatrice wind farm off the coast of Scotland [15]; it is constructed in 44 m deep water. However, for water deeper than 60 m the most feasible option is to deploy floating wind turbines [10, 16].

Due to the lack of rigid foundations, floating wind turbines have 6 additional degrees of freedom (DOFs); 3 linear (surge, sway, and heave) and 3 rotational (roll, pitch, and yaw) DOFs as shown by Figure 1.2. A main challenge of floating wind turbines is that the motions induced by wind and wave conditions are almost impossible to eliminate. Therefore, the design of these turbines must take into account the added degrees of freedom due to platform motions.

Figure 1.3 illustrates the three main floating platform concepts. Each concept uses a different principle to achieve hydrostatic stability. The three floating concepts shown in Figure 1.3 are: a

Table 1.2: Water depth distribution for different regions up to 100km offshore [14]

	Water Depth (m)			
Region	<25	25-50	50-100	100-300
North Europe	21%	26%	32%	20%
South Europe	16%	11%	23%	49%
Japan	22%	9%	18%	51%
USA	50%	26%	13%	11%
North West USA	27%	29%	25%	19%

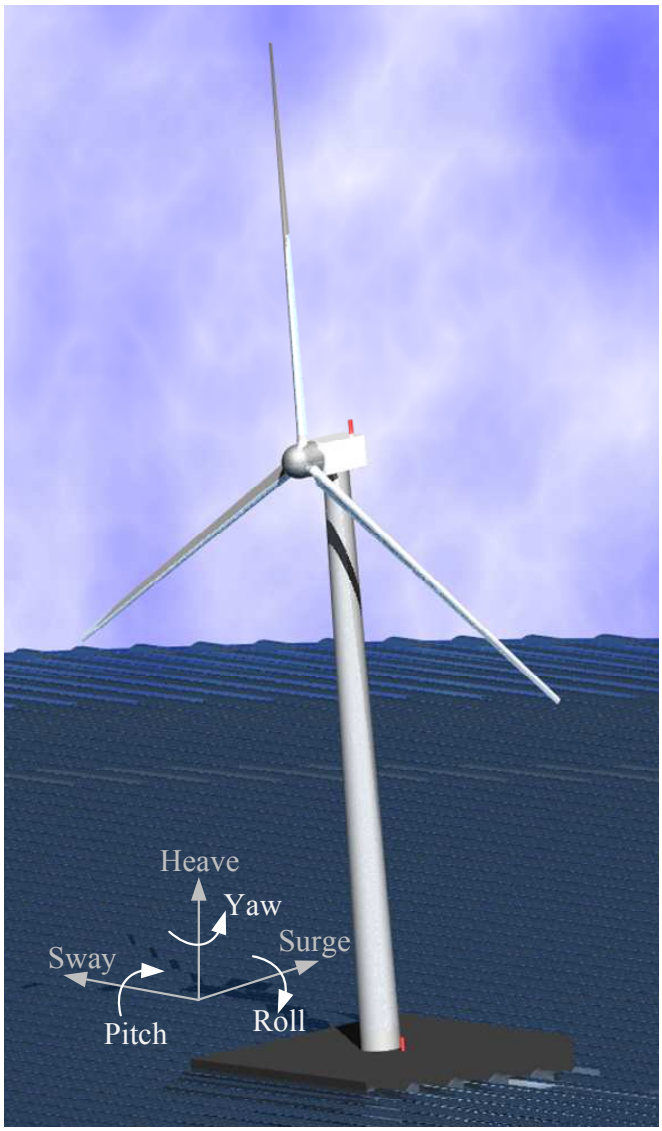

Figure 1.2: The floating platform's 6 DOFs

buoyancy stabilised barge platform, a mooring line stabilised Tension Leg Platform (TLP), and a ballast stabilised spar-buoy platform. Of course, each concept has its advantages and limitations. Early comparisons of all three platforms used simple static or dynamic models that usually excluded the effect of the control system [10, 17–20]. Note that the three floating principles (buoyancy, mooring lines, and ballast) are not mutually exclusive. That is, a combination of these principles into a single platform is possible; for example, semi-submersible platforms, not shown in Figure 1.3, use a combination of ballast and buoyancy for stability.

1.1.3 Historical Development of Floating Offshore Wind Turbine Concepts

The concept of floating offshore wind turbines was originally introduced in 1972 [18]. Only until the 1990's, when wind turbines were successful commercially, that floating offshore wind turbines became a topic for research. Initial studies conducted in the early 1990's showed that a floating wind turbine is technically possible but not feasible [17]. It was estimated that the

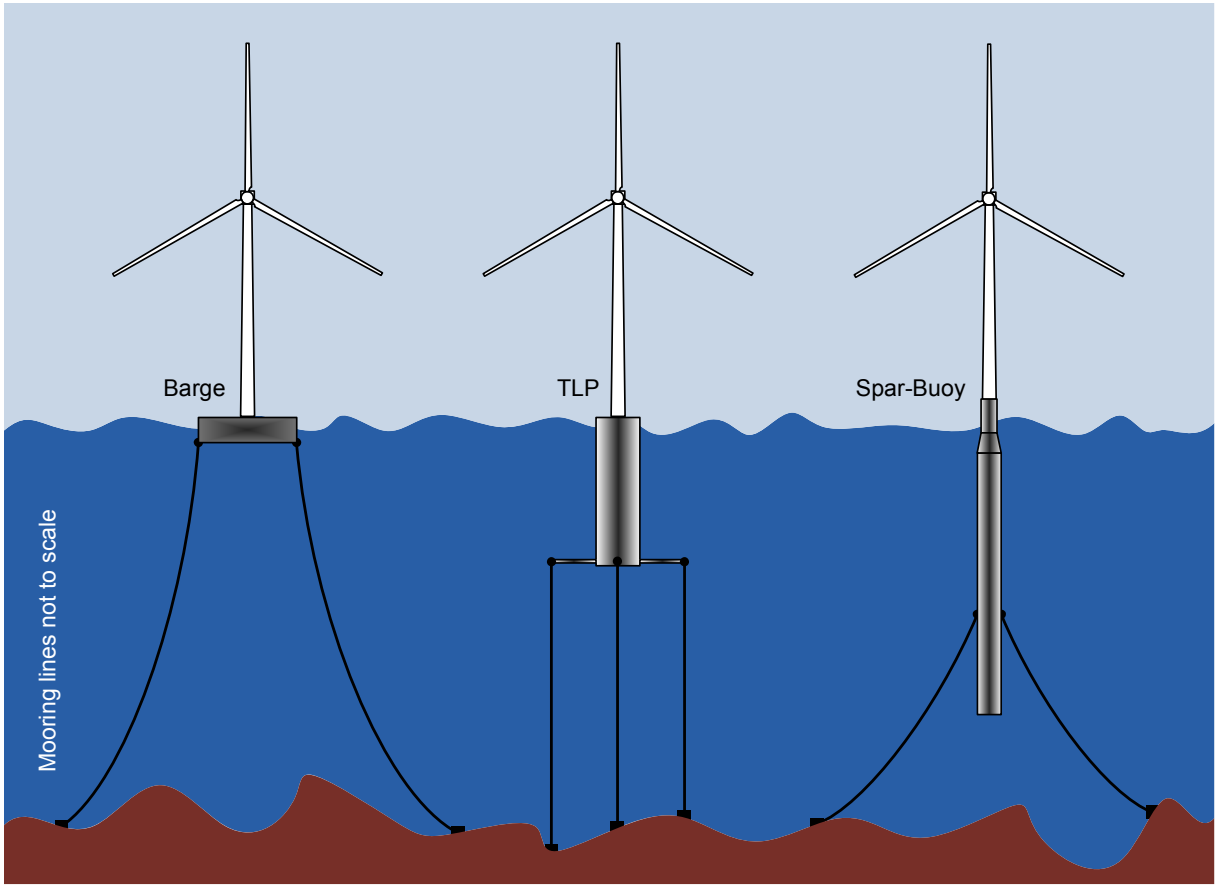

Figure 1.3: The three main floating concepts

cost of energy would be three times the cost of an onshore wind turbine. However, at the time of these studies, shallow water offshore wind turbines were also considered uneconomical and cost twice as much as an onshore turbine. Clearly, today's shallow water offshore turbines are used on a utility scale for power production.

In 1998, Tong [21] designed a 1.4 MW floating turbine utilising the spar-buoy concept with catenary mooring lines. The turbine was downwind[1] to have a free yawing system because it was believed that the platform could not support the moment reaction for an active yaw system. This was proven to be incorrect in later analyses. Tong found that wave loadings were prominent mainly on the tower but were not severe such that it became a main design driver for the tower. Furthermore, gyroscopic yaw motion caused by platform pitch was found to be small and of no serious concern.

Bulder *et al.* [17] considered several design options in 2003; these include: single or multiple turbines per floating platform; and single or multi-rotor turbines. First, they concluded based on qualitative analysis that a single turbine per floating platform (or floater) with spread mooring was the best technical and economic solution. This was confirmed by Musial et al [18] in 2004; Table 1.3 lists the advantages and disadvantages of both concepts. Second, Bulder *et al.* [17] also compared several single platform concepts listed in Table 1.4 and concluded that the Tri-floater,

[1]When the rotor is downwind of the tower (i.e. the wind hits the tower before the blades) it is attributed as a downwind wind turbine. Similarly, an upwind wind turbine has the rotor is upwind of the tower.

Table 1.3: Differences between single or multiple turbine floaters [18]

	Advantages	Disadvantages
Multiple Turbine Floaters	– Wave stability – Shared anchors – Mass optimisation possibilities	– High cost support structure – Wave loading – Complex yaw control
Single Turbine Floaters	– Simplicity – Modularity for manufacture – Lower structural requirements – Standard yaw control	– Individual anchors cost

Table 1.4: Comparison between different floating platform designs

Concept	Description	Advantages	Disadvantages
Single Cylindrical Floater	Simple cylinder platform held by spread moorings	Good static stability	Motion behaviour was not acceptable in terms of motion periods coinciding with wave periods (high energy region of wave spectrum)
Cylindrical with Tension Legs	Reduced cylinder size but held by tensioned mooring lines	Good vertical stiffness (heave)	Not suitable for water depths considered because gains in stability from adding the tensioned line were marginal
Tri-floater	Single column carrying the turbine connected to three floating cylinders via trusses	Requires less steel than the rest. Good stability with modification of floater cylinders	Initially the heave motion was still in the high energy region but this was solved through increasing the hydrodynamic mass by adding circular plates to the 3 floaters
Jack-up	Floating legs but the platform is above water	Simple installation and convenient for transportation Minimises wave induced motion	Cost. It is estimated to cost 12 million Euros to carry an estimated 4-5 MW turbine

shown in Figure 1.4, was the best design. However, their analysis was not comprehensive and several issues need to be addressed; among these:

- The need to consider and evaluate barge platforms.
- Use of simple equations of motion to describe heave and roll.
- Effects of mooring lines and waves were not included in analysis.

Musial *et al.* [18] have conducted a similar study to Bulder *et al.* [17], however, they found that a Tension Leg Platform (TLP), having vertical moorings, has excellent stability due to multiple tension legs that are spread out. With a tension leg platform, the majority of the platform

Figure 1.4: The Tri-floater concept [17]

is submerged thus experiencing lower wave loading. However, the vertical anchors have to withstand larger forces than anchors used with catenary mooring lines. A cost analysis was carried out to compare their TLP concept with the Tri-floater concept; results showed that the TLP would cost less mainly due to its smaller structure size. However, both concepts are estimated to be able to bring energy cost down to US$0.05/kWh which is required for large scale development as identified by the US Department of Energy.

In 2004, Ushiyama *et al.* [19] considered several floating turbine concepts to be deployed in Japanese waters. Vertical axis wind turbines were also considered to be placed on top of the floating structure because they have a low centre of gravity and can receive the wind from any direction without the need for a yawing system. However, their preliminary study did not find a clear winning concept which is the case for most floating structures. Each type had certain advantages and disadvantages, thus the choice of the platform concept would be site and application dependent. This was further illustrated by the study carried out by Butterfield *et al.* [20] where they compared the relative advantages and disadvantages of the three main floating concepts. The comparison in shown in Table 1.5; for further details please refer to [20].

In 2006, Nielsen *et al.* [10] carried out scale model testing for a spar-buoy type platform known as the Hywind concept being developed by a Norwegian company Norsk Hydro in cooperation with Siemens Power Generation [22]. The 1:47 scale model was tested in an 80 m×50 m basin at the Ocean Basin Laboratory at Marintek in Trondheim [10,23]. Their scale model testing results agree with their simulation results which tested a new control algorithm to add active damping of tower motions; the controller was effective in reducing induced tower motions [10].

Also in 2006, Vijfhuizen [24] developed a wind and wave power barge platform. This barge

Table 1.5: Relative comparison between the major floating platform concepts (reproduced from [20])

Platform Design Challenge	Platform Stability Classifications		
	Buoyancy (Barge)	Mooring Line (TLP)	Ballast (Spar-Buoy)
Design tools and methods	-	+	-
Buoyancy tank cost/complexity	-	+	-
Mooring line system cost/complexity	-	+	-
Anchors cost/complexity	+	-	+
Load out cost/complexity (potential)	+	-	
On-site installation simplicity (potential)	+	-	+
Decommissioning and maintainability	+	-	+
Corrosion resistance	-	+	+
Depth independence	+	-	-
Sensitivity to bottom condition	+	-	+
Minimum footprint	-	+	-
Wave sensitivity	-	+	+
Impact of Stability Class on Turbine Design			
Turbine weight	+	-	-
Tower top motion	-	+	-
Controls complexity	-	+	-
Maximum healing angle	-	+	-

Key
+ relative advantage
- relative disadvantage
blank neutral advantage

platform has a wind turbine to extract energy from the wind and an oscillating water column to extract energy from the waves. The barge platform was chosen because it was assumed to cost the least among other concepts; this was confirmed by Wayman in 2006 [25] where she showed that a shallow drafted barge would have the least capital cost and estimated cost of energy (excluding operation and maintenance costs) of US$ 0.0129/kWh and US$ 0.0089/kWh for mean wind speeds of 5.8 m/s and 8 m/s respectively. Vijfhuizen's main conclusions were [24]:

- The barge's motions and stability were acceptable even under severe conditions.
- With the wind turbine operating the motions were reduced while the oscillating water column operation had no effect.
- The barge's design can withstand at least 25 years of fatigue life.

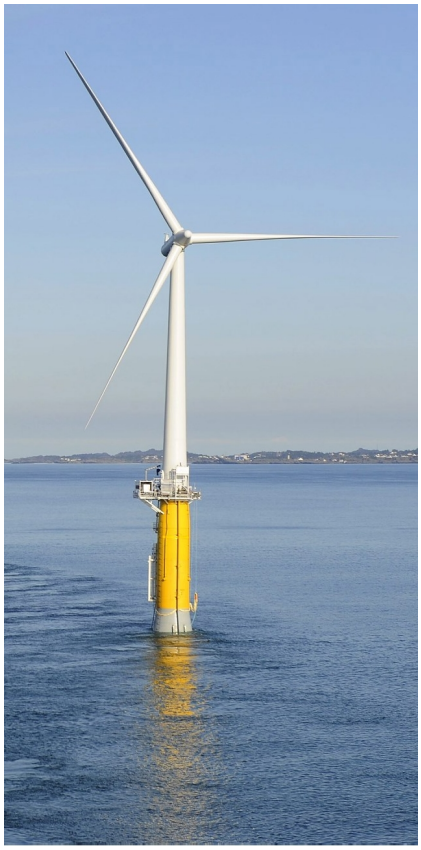

(a) Hywind (Photo: Øyvind Hagen/Statoil)

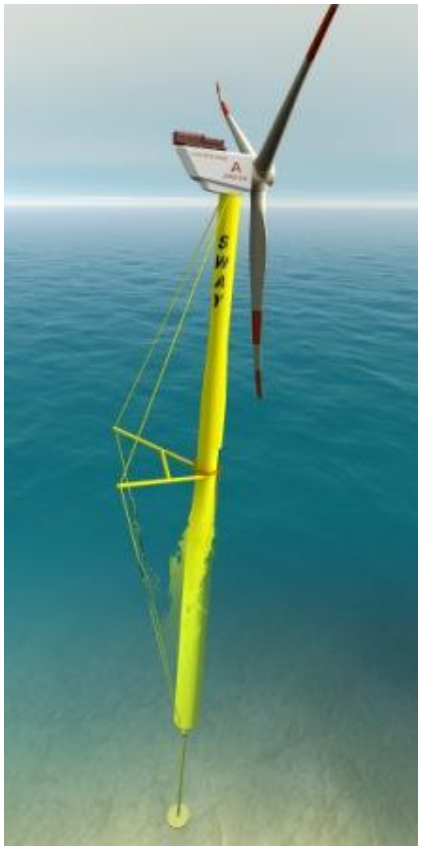

(b) SWAY [27]

Figure 1.5: Hywind and SWAY concepts

In June of 2009, the world's first full scale floating wind turbine prototype, the spar-buoy Hywind concept with a 2.3 MW wind turbine, was installed off the coast of Norway in 220 m deep water [26] (Figure 1.5a). In March 2011 another Norwegian company, SWAY, deployed a small scale floating wind turbine prototype for testing [27]; the full scale prototype with a 2.6 MW downwind turbine (Figure 1.5b) is scheduled for deployment in 2013. The tower is moored by a single tension leg cable that allows the tower to yaw freely with the wind; the concept is a hybrid between and a tension leg and a spar-buoy concept.

1.2 Introduction to Wind Turbine Control

Large wind turbines (utility scale) generally have an active control system that is used to regulate the operation of the turbine [28]. As wind turbines get larger in size and power capacity, the role of the control system in reducing loads becomes more important as the turbine structure becomes more flexible.

There are two types of wind turbine control: supervisory and closed-loop control [29]. Supervisory control determines the high level operation of the wind turbines such as when to start-up and when to shut-down. Closed-loop control operates between these two states and

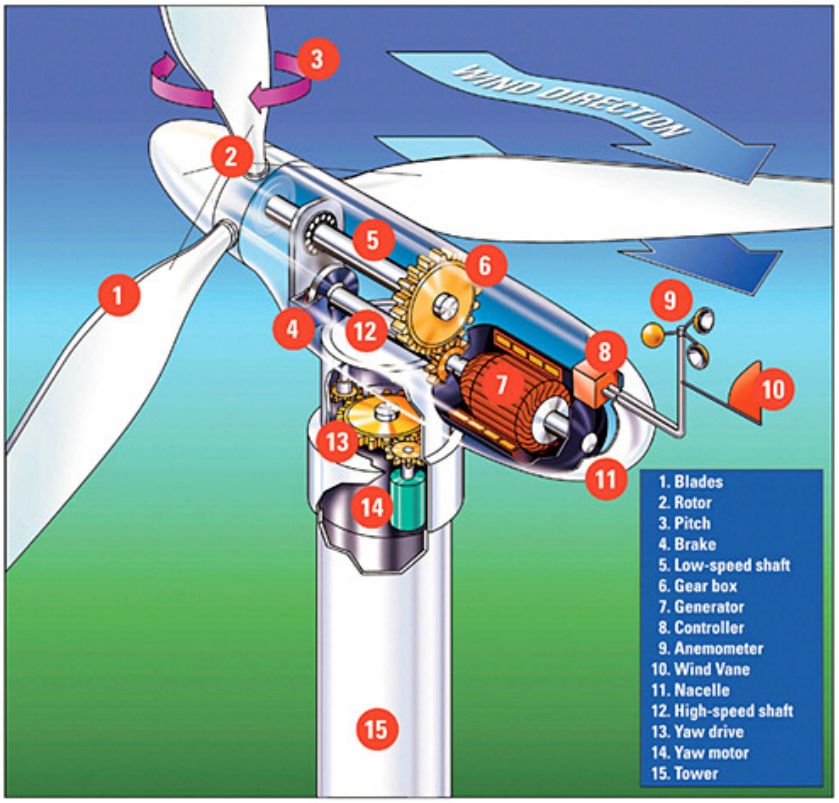

Figure 1.6: Main components of a horizontal axis wind turbine [31]

is responsible for the power production objectives such as minimising turbine yaw error and regulating rotor speed to maximise or limit power capture.

Horizontal axis wind turbines are generally under-actuated systems where the number of actuators or control inputs is significantly less than the controlled degrees of freedom. On a typical large wind turbine, there are three types of control inputs [30]: commanded generator torque, blade pitch angle, and the yaw drive giving a total of five available actuators (for a three-bladed wind turbine) as shown in Figure 1.6. Depending on the control algorithm, the blades can either be operated collectively or individually; differences between the two are discussed in Chapter 3. The yaw drive is only used to correct the turbine's yaw error[2] due to a change in mean wind direction. It is normally a slow actuator and ineffective for power production and regulation.

1.2.1 Operating Regions

Wind turbines have three regions of operation. In each region the turbine has a different operational objective according to the mean wind speed [30, 32, 33]. These are summarised below and the ideal power captured in each region is shown in Figure 1.7.

Region 1 The wind speed is too low for operation.

[2]Yaw error is the angle between the mean wind direction and the turbine yaw angle.

Region 2 This is where the turbine will spend most of its operational life in the designed wind speed region. Therefore, the main objective is to maximise power capture in this region. This region is also known as the *below rated* wind speed region.

Region 3 This is the *above rated* wind speed region where the extracted power of the wind must be limited to the rated power to avoid damaging the turbine components. Hence, the turbine is reducing its aerodynamic efficiency to limit power capture to the rated power of the generator.

An upper limit for region 3 exists where the wind speed is too fast for safe operation of the wind turbine. Therefore, the wind turbine goes into shut-down mode for wind speeds higher than the cut-off wind speed. The blades are feathered into the wind to minimise the lift generated and the shaft brakes are applied. The control logic that determines the operational state of the wind turbine and controls start-up and shut-down is the supervisory control. This higher control layer is not considered in this work.

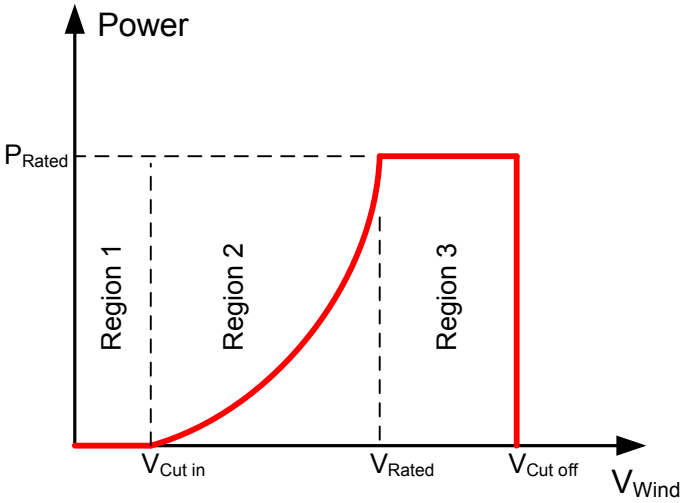

Figure 1.7: Wind turbine operating regions

1.2.2 Overall Controller Objectives

The main purpose of a wind turbine is to generate power with a competitive cost of energy. There are many factors that affect the cost of energy such as the location and wind speed distribution, turbine efficiency, etc. From a control system point of view, there are two factors that the controller can influence to reduce the cost of energy: power capture and component fatigue life. To reduce the cost of energy, the control system must

1. maximise power capture subject to
   (a) limits on the captured power according to the operating regions (i.e. limit power capture in regions 1 and 3);
   (b) actuation constraints for each region.
      i. To maximise power in region 2, the blade pitch is set to the fixed optimum angle that maximises the aerodynamic torque and the generator torque is used to control the rotor speed to achieve a desired tip speed ratio[3] [33, 34].

[3]Tip speed ratio is dimensionless number defined as the ratio of the blade's tip velocity to the upstream wind velocity [28, 29].

ii. In region 3, generator torque is not allowed to vary greatly (e.g. within 5% of rated torque) to limit power fluctuations.

2. prolong the operational life of the wind turbine. Apart from regular maintenance, the life of the wind turbine can be increased by reducing fatigue loads on its components[4] (blades, drivetrain, and tower).

To reduce the cost of energy utilising both approaches of maximising power and reducing fatigue loads, ideally one would require a single multi-objective controller implementation. Due to the abovementioned actuation needs for each region and the nonlinearity of wind turbines, a single multi-objective controller for all operating regions is very difficult to design and implement. The standard approach is to use a separate controller for each region and switch between them using certain rules [29,30,35].

1.2.3 Control of Floating Wind Turbines

Floating wind turbines experience additional motion due to the lack of rigid foundations. These additional motions, especially the platform pitch motion, can significantly affect power regulation and turbine loads. Therefore, reducing these motions becomes an important part of the design of the floating system. Several methods can be used separately or collectively to reduce these motions; these include:

- the design of the platform itself and the way it interacts with the waves,
- additional passive modifications to the system such as modifying the wind turbine to include a Tuned Mass Damper, and/or
- using the control system to actively reduce the platform motions using available or additional actuators.

The latter is the main focus of this research. Studies on the control of floating wind turbines have been conducted prior to this work; these are discussed in Chapter 2. These studies primarily use a single objective controller for rotor speed regulation utilising collective blade pitching. Structural control using active and passive Tuned Mass Dampers have also been investigated on floating wind turbines to reduce platform pitching. However, the controller set-up consisted of two separate single objective control loops: one for rotor speed regulation using collective blade pitch and the other for platform pitch regulation using the Tuned Mass Damper. Of all the reviewed works *on floating wind turbine control*, none used a single multi-objective controller to regulate rotor speed and reduce platform pitch motion. Furthermore, the effectiveness of individual blade pitching has not been investigated on floating wind turbines.

[4] A control system may also be capable of reducing the peak/maximum load on turbine components. However, peak loads are not usually design drivers from a control system point of view.

1.3 Research Objectives and Scope

The main research objective is to quantify the performance of multi-objective and Disturbance Accommodating Controllers applied to the three main floating platform concepts: the barge, tension leg, and spar-buoy platforms. The results and conclusions in this work are intended to be used by designers and developers of floating turbines to aid and guide the development of their floating concepts, such as in a multi-disciplinary optimisation.

The research undertaken uses model-based control theory to design and implement multi-objective controllers to reduce the induced motions by the floating platforms while maintaining rotor speed and power regulation *under normal operating conditions*. Time domain control design using linear state-space models for State Feedback Control is utilised.

The results presented in this thesis are based entirely on hi-fidelity simulations and, therefore, the results are bound by the limitations of the simulation tools used and their associated assumptions. However, the results are presented in a relative sense such that the absolute values of the simulation results are not used. Furthermore, the relative results are used to draw conclusions based on physical interpretations of the the floating systems. Design Load Case (DLC) 1.2 in the IEC 61400-3 standard for offshore wind turbines is used to analyse the *fatigue load* performance of the floating wind turbines under normal operating conditions. Simulations are carried out using FAST (Fatigue, Aerodynamics, Structures, and Turbulence) [36], a well established wind turbine design and simulation tool, in conjunction with MATLAB® Simulink® for control design and implementation; more details are given in Chapter 5.

Finally, the research undertaken in this thesis answers the following research questions (in no particular order of importance):

1. Does using individual blade pitching help improve the performance over collective blade pitching on a floating wind turbine?
2. Similarly, does using a multi-objective controller help improve the performance relative to a single-objective Gain Scheduled Proportional-Integral controller on floating wind turbines, consistent with findings for onshore wind turbines?
3. Can a Disturbance Accommodating Controller designed to reject wind and wave disturbances help improve the performance?
4. How will the three floating platforms perform when compared to each other under normal operating conditions especially when controlled by multi-objective controllers?
5. Is it possible to maintain fatigue loads to a level comparable to an onshore wind turbine of similar size?
6. With the addition of the platform's 6 DOFs, are the current actuators capable of addressing the control needs of the system?

In addition to the above objective and research questions, it is important to define what is out of scope of this research. Below are several items that are not part of the research undertaken in this thesis.

- No below rated wind speed region analysis: All controllers are simulated in the above rated wind speed region since it is in this region where the platform motions are affected the most due to high wind speeds as well as large incident waves. Furthermore, region transition methods/algorithms between the regions are not implemented.

- No stress analysis: Stress analysis is not part of this research; only structural loads are calculated and analysed. Performing stress analysis is usually performed at the final stages of the design whereas the aim of this research is to compare between different concepts rather than produce a solution ready for testing/implementation.

- No turbine/platform design changes or optimisations: Design changes such as adding extra actuators is not considered here as the objective is to assess the limitations of available actuators on the floating wind turbine. Optimisation of floating concepts is usually carried out to finalise a concept for prototyping or manufacture. Again, this is deviating from the objectives of this research.

- No meteorological modelling: Interaction between the wind and water surface where the wind influences the incident wave height and direction is beyond the scope of this research. However, realistic wind and wave conditions are used in the simulations but they are not coupled.

- No nacelle yaw control: The yaw control loop for correcting wind direction errors is separate from the main power and speed regulation control loop. Furthermore, DLC 1.2 does not specify a change in wind direction or a misalignment error.

- No state estimator design for state regulation: This work is of an exploratory nature and will not focus on implementation issues such as cost of sensors, effects of noise, sensor failure, etcetera. Therefore, the State Feedback Controllers are implemented using Full State Feedback where all the necessary measurements are assumed to be available.

- No actuator dynamics: A static actuator model with saturation limits is used due to the lack of a blade pitch time constant of a 5 MW or similar sized wind turbine in the literature. In the static model, the actuators are assumed to be fast enough such that their dynamics can be neglected. However, absolute and rate saturations are implemented in the simulation model to represent the operating limits of real actuators. These limits, defined in [37] and listed in Chapter 5, are based on data collected from several similar sized wind turbines.

- No ultimate load or extreme operating cases: This work only focuses on fatigue loads under normal operating conditions as this is where the major contribution of the multi-objective controllers is expected. Generally, ultimate loads occur under extreme operating conditions where the controller is in shut-down mode (e.g. during a fault). These cases are well documented for floating wind turbines [32, 38].

- No experimental testing: Scale model testing of such concepts requires substantial funding and a large facility that are not available.

1.4 Thesis Outline

Chapter 2 reviews the state of the art in the control of floating wind turbines thereby answering the first research question. Of particular interest is the Gain Scheduled Proportional-Integral controller. This controller is used as a reference controller for comparing the performance of the developed multi-objective controllers and is referred to as the Baseline controller.

Chapter 3 briefly describes the theory for State Feedback Control using linear time-invariant state-space models, implementation and stability assessment for floating wind turbines. Wind turbines are periodic systems, therefore, multi-blade coordinate (MBC) transformation (also known as the Coleman or Fourier transformation) is used to transform the system to a non-rotating frame of reference. The resultant transformed model becomes time-invariant allowing for linear time-invariant control design. Differences between the mechanisms of individual and collective blade pitching at regulating platform pitch are discussed since State Feedback Control theory can accommodate multi-input multi-output systems.

Chapter 4 presents the background theory for Disturbance Accommodating Control, its implementation and limitations on floating wind turbines after MBC transformation is applied. The design of a Disturbance Accommodating Controller for rejecting wind speed perturbations on floating wind turbines is outlined as well.

In Chapter 5, the selected simulation tool (FAST) is briefly described along with the assumptions used to model wind turbines with floating platforms. The chapter also describes the simulation set-up according to DLC 1.2 of the IEC 61400-3 standard and the performance metrics used to analyse the simulation results.

Simulation results for the barge, tension leg, and spar-buoy platforms are analysed and discussed in Chapters 6, 7, and 8 respectively. The analysis is based on overall averaged performance metrics to compare the performance of the State Feedback and Disturbance Accommodating Controllers relative to the Baseline controller on each floating platform. Performance trends across the above rated wind speed region and time series results are also used in the analysis.

The platforms' simulation results are then compared relative to an onshore wind turbine in Chapter 9. Normalising the results relative to an onshore wind turbine allows for comparison between the floating platforms. It also allows for the evaluation of the required strength of turbine components (tower, blades, and drive-shafts) in relative terms to well established onshore wind turbine designs.

Chapter 10 presents results for simple case studies used to implement wave disturbance rejection on floating wind turbines.

Finally, conclusions and recommendations for future work are presented in Chapter 11.

2

Review of Floating Wind Turbine Controllers

Contents

2.1 Gain Scheduled PI Control **19**
2.2 Variable Power Pitch Control **23**
2.3 Estimator Based Control **24**
2.4 Active Structural Control **25**
2.5 Other Controllers **26**
2.6 Onshore Wind Turbine Control **26**
2.7 Controller Objectives **26**
2.8 Chapter Summary **28**

A review of the most important contributions made towards designing and testing controllers for floating wind turbines is presented in this chapter. These controllers range in complexity, description detail, simulation results and testing styles, and floating platform structure. Furthermore, they have not yet been compared against each other quantitatively using the same simulation conditions. However, the attributes of each control approach documented in the literature are listed in this chapter. The main attributes of these controllers are given in Table 2.1. In the table, the platform types barge, TLP, and spar-buoy refer to the ITI Energy barge, MIT/NREL TLP, and OC3-Hywind spar-buoy respectively whose properties are listed in Chapters 6, 7, and 8 respectively; The Hywind spar-buoy is a slightly different model than the OC3 spar-buoy where it has a different wind turbine mounted from the NREL 5MW baseline wind turbine. Description of each controller follows.

Table 2.1: Overview of most important controllers applied on floating wind turbines

Controller Name	Blade Pitch Control	Torque Control	Additional Control Features	Simulation Code	Number of Simulations	Model Fidelity	Simulation Regions	Platform
GSPI	CBP GSPI	Constant power	TTF loop, pitch to stall, or detuned gains	FAST	Extensive	High	2, 3	Barge, TLP, Spar-buoy
GSPI Hywind	CBP GSPI	Constant torque	Constant speed region just below rated with PI torque control loop	HAWC2 / SIMO-RIFLEX	Limited	High	2, 3	Hywind spar-buoy
VPPC	CBP GSPI	Constant torque	Variable rotor speed set-point. IBP for blade load reduction	FAST	Limited	High	3	Barge
EBC	Unknown	Unknown	Wind turbine estimator to hide tower dynamics	HywindSim / SIMO-RIFLEX	Limited	Low	3	Hywind spar-buoy
ASC	Unknown	Unknown	Tuned mass damper with active control	FAST-SC	Moderate	High	3	Barge

Legend:

ASC	Active Structural Control
CBP	Collective Blade Pitch
EBC	Estimator Based Control
GSPI	Gain Scheduled Proportional-Integral control
IBP	Individual Blade Pitch
TTF	Tower-Top Feedback
VPPC	Variable Power Pitch Control

Number of Simulations Guide:

Limited	<10
Moderate	<100
Extensive	>100

2.1 Gain Scheduled PI Control

A Collective Blade Pitch (CBP) Gain Scheduled Proportional-Integral (GSPI) controller was implemented on a floating wind turbine by Jonkman to assess the dynamic performance of the barge floating platform [32]. The GSPI control loop only operates in the above rated wind speed region (region 3) to regulate the rotor speed to the rated speed by pitching the blades collectively to reduce their aerodynamic efficiency.

The GSPI control law is given by equation (2.1) where $\theta(t)$ is the commanded collective blade pitch angle, $K_P(\theta_-)$ and $K_I(\theta_-)$ are the proportional and integral gains respectively. The error signal is denoted $e(t)$ with ω_{Rated} and ω_{Gen} as the rated and actual generator speed respectively. The GSPI controller is a single-input single-output (SISO) controller with a single objective of rotor speed regulation.

The gains are scheduled as a function of blade pitch angle at the previous time step θ_- such that the controlled rotor DOF has the same prescribed closed-loop natural frequency, ω_n, and damping ratio, ζ, for all above rated wind speeds. θ_- is given by equation (2.2) where Δt is the simulation time-step. The scheduled gains are given by equations (2.3) and (2.4) where I_{D} is the drivetrain inertia from the low speed shaft end, Ω_r is the rated rotor speed in revolutions per minute (rpm), N is the gearbox ratio, and $\frac{\delta P}{\delta \theta}$ is the sensitivity of the rotor aerodynamic power to collective blade pitch angle. For more details on the power sensitivity and controller gains derivation, please refer to [32].

$$\theta(t) = K_{\mathrm{P}}(\theta_-)e(t) + K_{\mathrm{I}}(\theta_-)\int_0^t e(\tau)d\tau \tag{2.1}$$

where

$$e(t) = \omega_{Gen} - \omega_{Rated}$$

$$\theta_- = \theta\left(t - \Delta t\right) \tag{2.2}$$

$$K_{\mathrm{P}}\left(\theta_-\right) = \frac{2I_{\mathrm{D}}\Omega_r\zeta\omega_n}{N\left(-\frac{\delta P}{\delta \theta}\right)} \tag{2.3}$$

$$K_{\mathrm{I}}\left(\theta_-\right) = \frac{I_{\mathrm{D}}\Omega_r\omega_n^2}{N\left(-\frac{\delta P}{\delta \theta}\right)} \tag{2.4}$$

In addition to the blade pitch control loop, a separate generator torque control loop was used to maximise power capture in below rated wind speeds and regulate power in above rated wind speeds. The torque controller varies the applied generator torque as a function of filtered generator speed. In below rated wind speed (region 2), the relationship that maximises power capture is given by equation (2.5) where ρ, R_{Rotor}, $C_{P,max}$, and λ_o are air density, rotor radius, maximum power coefficient and tip speed ratio that yields $C_{P,max}$ respectively [33]. In above

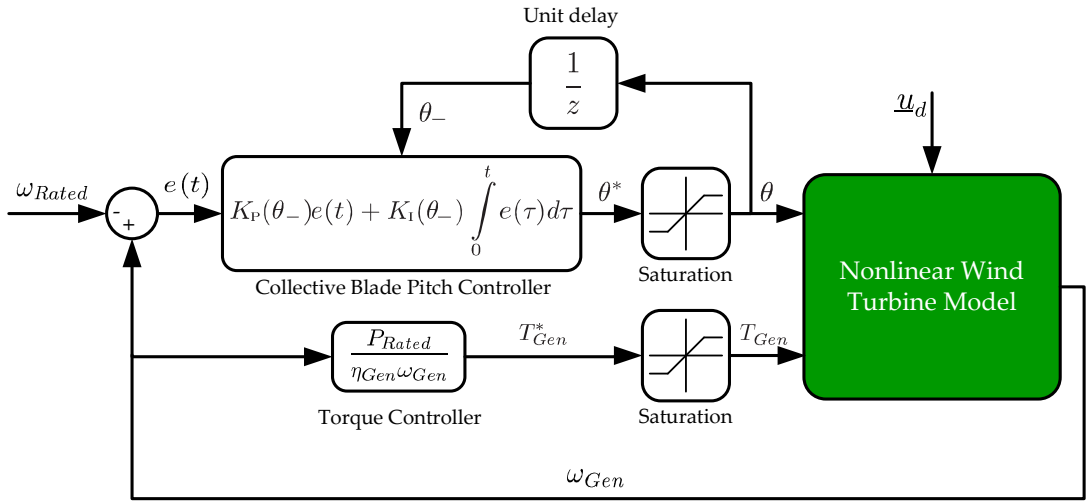

Figure 2.1: Baseline controller implementation in above rated wind speed region

rated wind speed region where the objective is to regulate power to the rated, the relationship is given by equation (2.6) where P_{Rated} is the rated generator power and η_{Gen} is the generator efficiency.

$$T_{Gen} = \frac{\pi\rho R^5_{Rotor} C_{P,max}}{2\lambda_o^2 N^3}\omega^2_{Gen} = K_T\omega^2_{Gen} \tag{2.5}$$

$$T_{Gen} = \frac{P_{Rated}}{\eta_{Gen}\omega_{Gen}} \tag{2.6}$$

The generator speed, used by both CBP GSPI and generator torque controllers, was filtered using a low pass filter with a cut-off frequency of 0.25 Hz. This frequency was chosen to be a quarter of the blades edgewise natural frequency to prevent the controller from exciting these modes [32]; this behaviour was also observed by Wright [35] where he found that a PI controller with a fast actuator can destabilise certain modes due to the actuation frequency.

Since the GSPI controller was one of the first well documented controllers implemented on floating wind turbines, it became the reference or baseline controller for other researchers to compare more advanced control strategies. In this work, the GSPI controller with Jonkman's [32] detuned gains (see next section) will be referred to as the Baseline controller. Block diagram implementation of the Baseline controller in the above rated wind speed region is shown in Figure 2.1 where θ^* and T^*_{Gen} are the commanded actuator inputs and $\underline{u}_d$ includes all disturbance inputs to the floating system, namely wind and waves. Not shown in the figure is the integrator anti-windup modules. Integrator anti-windup is used to prevent blade saturation from significantly affecting the performance by holding the integrator value during blade saturation. Blade saturation can occur from having aggressive gains or from operation close to region transition conditions.

2.1.1 Barge Platform

Jonkman, using his newly developed FAST simulator with the HydroDyn module [32] (described in Chapter 5), conducted an extensive set of simulations using the CBP GSPI controller on the ITI Energy barge floating platform in accordance with the IEC 61400-3 standard for ultimate loads [39]. The IEC 61400-3 is a standard for offshore wind turbines with fixed foundations developed by the International Electrotechnical Commission (IEC). To date, no standards for floating wind turbines have been released.

The barge platform exhibited large platform oscillations especially in the pitch direction (fore-aft rocking motion) resulting in large tower loads and power fluctuations. To mitigate these effects, Jonkman implemented three modifications to the controller ; these were:

Tower-Top Feedback Loop

An additional proportional control loop that designed to reduce tower fore-aft motion based on the measurement of the tower top acceleration was implemented. However, the addition of a tower top feedback control loop did not improve platform damping due to conflicting blade pitch commands issued by the separate control loops; the mechanics of issuing conflicting blade pitch commands are discussed in §3.2.

Active Pitch to Stall Control

The purpose of using pitch to stall was to get extra restoring thrust force once the blades are stalled when the turbine pitches forward. The active pitch to stall controller had excellent power regulation, however, platform motions were not reduced but were increased instead. This contradictory result was explained by examining the open and ideal closed loop damping ratios. Jonkman concluded that the pitch to stall damping was actually positive. And, since the pitch to feather controller had better damped response, he concluded that the actual closed loop damping of the pitch to feather controller is greater than that of the pitch to stall; i.e. the system has positive damping.

Reduced Controller Gains

Lowering the controller gains reduced the use of the blades and possibly reduced the negative damping effect. These gains, referred to by Jonkman as detuned gains, produced the best results out of the four controllers. Reducing the controller gains made the response of the system closer to that of the open loop response hence increasing the damping. This produced reasonable power regulation and slightly reduced the platform oscillations.

Barge Platform Summary

The increase in the main turbine loads is staggering. For example, the tower base loads are 6 times that of an onshore wind turbine. Jonkman concludes in his PhD dissertation that further

reductions in platform motions is necessary and suggests many possibilities to improve platform pitch damping such as the use of a constant torque algorithm, use of MIMO state-space controllers to avoid conflicting blade pitch commands, and implementing individual blade pitching control strategies.

2.1.2 Tension Leg and Spar-Buoy Platforms

Larsen and Hanson [40], working on the Hywind spar-buoy (slightly different from the OC3-Hywind model that has a different mounted wind turbine), also implemented a GSPI pitch control strategy in above rated wind speed region. However, to avoid the platform pitch damping issue, they used a constant torque algorithm in the above rate wind speed region and introduced a constant speed region just below rated wind speed. A variable speed control below rated region was used to maximise power capture. In the constant speed region, a PI torque control was used to regulate the rotor speed. Switching between regions was handled by a set of variable min/max operations in addition to low pass filters to ensure smooth transition. Simulation results using HAWC2 coupled with SIMO-RIFLEX from MARINTEK showed a 30% increase in rotor speed and power fluctuations. The motion response of the floating system was acceptable and tower loads were "reasonable" but were not compared to an onshore system. Larsen and Hanson accidentally simulated the floating system with an active pitch to stall controller and achieved surprisingly good results and recommended further investigations. However, this contradicts with what Jonkman [32] found when he investigated pitch to stall on the ITI Energy barge. The difference in behaviour is most likely due to different platform dynamics, simulation tool, and/or model complexity used.

Matha [38], continuing on Jonkman's work, extended the simulations on the Barge platform to include fatigue loads analysis. He also carried out a series of extensive simulations in accordance with the IEC 61400-3 standard on the TLP and Spar-Buoy platforms. Comparisons were made relative to an onshore wind turbine with the same controller. The Baseline controller was used on all three platforms, however, some modifications were made to the controller on the Spar-Buoy platform. A constant torque instead of constant power algorithm was used in the above rated wind speed region to improve platform pitch damping. Furthermore, the controller bandwidth was limited to avoid resonance issues due to lower natural frequencies of the system than the other platforms. Below is a brief summary of results obtained by Matha on each platform.

ITI Energy Barge

The barge concept has some advantages such as cost effective construction, ability to be assembled in any port due to its shallow draft, and relatively inexpensive slack anchoring system. However, fatigue loads analysis results were no different to the ultimate results found by Jonkman [32] in terms of their relative increase to an onshore system; e.g. tower fatigue loads were approximately 8 times that of an onshore wind turbine. Matha concluded that the barge

may not be suitable for sites with severe sea states but could provide a cost effective solution to more sheltered sites such as the Great Lakes in the USA.

OC3-Hywind Spar-Buoy

Results from the extensive simulations showed that the spar-buoy experienced significantly less loading on the turbine structure when compared to the barge. However, fatigue loads relative to an onshore wind turbine were still approximately 1.5 to 2.5 times more than an onshore system. Furthermore, the deep draft of the spar-buoy limits the number of ports where the hull can be fabricated and assembled. It is important to note that the first full-scale floating wind turbine prototype is the Hywind project which is a spar-buoy floating system. To date, the outcome of this project, which the offshore wind turbine community is very interested in, are yet to be published.

MIT/NREL TLP

The performance of the TLP relative to the onshore wind turbine is excellent. Almost all of the turbine loads are close to parity with the exception of tower Fore-Aft (FA) loads which are on average 1.5 times that of an onshore system. Therefore, the TLP probably has the best potential, with more advanced controllers, to achieve similar loading to that of an onshore wind turbine. However, the TLP may not be always the most economical choice due to the relatively high cost of the taut anchoring system.

Platform Instabilities

Jonkman [32] and Matha [38] have identified certain instabilities for each platform. These arise from a unique Design Load Case specified by the IEC 61400-3 standard such as operating with a faulty blade or in extreme conditions. For example, all three platforms experience yaw instability in a certain DLC where the turbine is idling with two of its blades fully feathered and one stuck at the maximum lift position (blade pitch angle of 0 degrees). Most of these instabilities are due to the design of the system rather than being caused by the controller.

2.2 Variable Power Pitch Control

A simple, empirical, yet effective solution to avoid the reduced or negative damping in the pitch motion was developed by Lackner [41]. A standard rotor speed controller exacerbates platform pitching motion as it attempts to regulate rotor speed to the rated speed in above rated wind speed region (see §3.2 for more details). Lackner's solution was to change the speed set-point for the collective blade pitch GSPI controller from a constant to a linear function of platform pitching velocity and implemented a constant torque algorithm in above rated wind speed region. The idea is to increase the rotor speed as the turbine is pitching forward

(negative pitching velocity according to the coordinate system) forcing the rotor to increase the aerodynamic torque to accelerate the rotor and hence create a pitch restoring moment due to increased rotor thrust force. Also, when the wind turbine is pitching backwards, the desired rotor speed is less than the nominal rated speed forcing the speed controller to feather the blades to reduce the rotor speed and thereby reducing the rotor thrust allowing the turbine to pitch forward. By holding the generator torque constant, turbine power becomes a linear function of platform pitch velocity. Furthermore, rotor speed fluctuations are reduced resulting in reduced blade pitching which limit the changes in rotor thrust that causes the reduction in platform pitch damping. This simple control strategy essentially trades power fluctuations for reduced pitching motion.

The rated rotor speed is given by equation (2.7) where ω_R and ω_o are the reference and the nominal rated rotor speeds respectively, $\dot{\varphi}$ is the platform pitch velocity and k is the gradient of the linear relationship – a design parameter. It can be seen from equation (2.7) that if the platform pitch velocity is zero, the desired rotor speed is the nominal rated speed. When the turbine is pitching forward (negative $\dot{\varphi}$), the desired rotor speed is increased and vice versa.

$$\omega_R = \omega_o \left(1 - k\dot{\varphi}\right) \tag{2.7}$$

Lackner applied this control strategy on the ITI Energy barge using FAST. Results were obtained after running two 600 second simulations with turbulent wind and irregular waves for three different slopes, k, of equation (2.7). Results show that platform pitch and pitch rates were, on average, reduced by 8-20% under different k values but power and rotor speed fluctuations, on average, only increased by 3-11% and 1.5-5% respectively. Of course, the higher the slope, the bigger the reductions in platform motions and increased power fluctuations.

In addition to the variable power pitch control method, Lackner also implemented individual blade pitch control to reduce blade loads in a similar way to Bossanyi's method [42] of using MBC (or Coleman) transformation (described in Chapter 3) with PID control for the cosine-cyclic and sine-cyclic components. However, Lackner found that the individual blade pitch controller was not as effective at reducing blade loads when compared to an equivalent onshore wind turbine. Blade load reductions were small (0.6-1.6% reduction) despite a significant increase in blade pitch usage. Furthermore, the IBP controller increased platform rolling and hence tower side-side fatigue loads. This effect was also observed during the controller design stage in this work on the barge platform and later resolved; see Chapter 6 for more details

2.3 Estimator Based Control

Because the Hywind concept was designed with much lower tower resonance frequencies to avoid the wave energy spectrum [40, 43], Skaare *et al.* [43] implemented an estimator based control strategy in the above rated wind speed region to "hide the tower motions for the wind turbine control system and thereby avoid the negative damping effect of the tower motion". The wind turbine estimator contains a simplified SISO model of the wind turbine with the

wind speed as an input and the rotor speed as an output. The wind speed is assumed to be either directly measured or estimated via a wind speed estimator.

In below rated wind speed region, the control system takes the *measured* rotor speed and commands the generator torque to maximise power capture. In above rated wind speed region, the controller commands the blade pitch based on the *estimated* rotor speed from the wind turbine estimator whose output is based on the estimated wind speed. Seven simulations were carried out using HAWC2 coupled with SIMO-RIFLEX using the same wind and wave conditions but with different turbulence intensities. Results show noticeable reductions in nacelle motions and hence large reductions in tower and rotor loads were observed along with increased rotor speed fluctuations and a maximum of 3.81% reduction in the average power output.

Under these limited cases, the controller seems to be regulating the floating turbine well with promising results. However, since the controller in above rated wind speed region depends on the estimated rotor speed and not the actual which is calculated/estimated based on wind speed estimates, the robustness of such controller will heavily depend on the quality of estimates.

2.4 Active Structural Control

An active structural control of floating wind turbines using a Tuned Mass Damper (TMD) was developed by Rotea *et al.* [44]. The idea is to add a Tuned Mass Damper with an active component in the nacelle to influence the platform pitching motion of the floating wind turbine. Rotea *et al.* derived the general equations of motion of the newly added TMDs (one along each of the pitching and rolling directions) and incorporated these changes into FAST resulting in a special version called FAST-SC (for structural control).

In their work in [44], only the TMD along the platform pitching direction is activated and analysed. The TMD parameters (mass, spring stiffness, and damping) were chosen such that they reduce the platform pitching motion on the ITI Energy barge passively (i.e. without a controller input). This is followed by designing a family of H_∞ controllers to actively introduce additional damping by driving the TMD.

Simulation results show that the passive TMD system achieves 10% reduction in the tower fore-aft fatigue damage equivalent load (DEL)[5] relative to a "baseline system" without structural control. However, no details were provided about the baseline system/controller. With active structural control, the tower loads are reduced by an average of 15-20% relative to the passive TMD system at the cost of 3-4% energy consumption of the rated power of the 5MW wind turbine. However, the stroke of the TMD (passive or active) is large when the dimensions of the nacelle are considered. Rotea *et al.* recommend the use to nonlinear control to implement an active TMD with stroke stop limits.

A major benefit from using a TMD (active or passive) is achieved when the turbine is operating in extreme conditions. In these conditions the blade pitch controller is normally switched off

[5]Fatigue DELs are used as a metric to replace the stochastic loads on a component by a periodic load with a calculated magnitude at a known frequency.

and the blades are feathered. Having a passive TMD will help improve the pitching (and rolling when implemented) motion(s) in these situations. The performance in these conditions are yet to be analysed.

2.5 Other Controllers

In this section, the remaining works, to the author's best knowledge, that have been carried out on control of floating wind turbines are briefly discussed. These works either have limited information available and/or limited conclusions can be drawn.

In 2006, Nielsen *et al.* [10] implemented a blade pitch control algorithm for active damping of the platform pitching motion in above rated wind speed region on the Hywind floating concept. Simulation results using HywindSim (a tool used to model a simple floating wind turbine) coupled with SIMO-RIFLEX agree to some degree with scale model testing. The pitch control algorithm seems to improve the platform pitching response. Scale model testing was carried out at the Ocean Basin Laboratory at Marintek in Trondheim, Norway with a scale of 1:47 [23].

Henriksen [45] implemented a model predictive controller primarily on an onshore wind turbine but a simple model for a floating wind turbine was also used. However, little insight into the performance of the floating system can be offered due to limited floating model fidelity.

2.6 Onshore Wind Turbine Control

More advanced controllers than previously discussed have been applied on onshore wind turbines for many reasons including but not limited to reducing fatigue loads, dealing with turbine nonlinearities and model uncertainties. These techniques can be applied to floating wind turbines to address the additional induced motions. Table 2.2 gives a non-exhaustive list of the types of controller that have been applied on onshore wind turbines; the entries are listed in perceived increasing complexity.

Obviously, as controller complexity increases the computational requirement also increases. In some cases, this limits the fidelity of the controller used to ensure real-time control. It's important to note that a more advanced controller does not necessarily guarantee better performance. For example, some form of nonlinear control requires the system model to be represented in a certain format. This format may not be possible to obtain or can only be obtained for low fidelity models.

2.7 Controller Objectives

The current range of controllers applied on floating wind turbines have the following limitations:

Table 2.2: Types of controllers implemented on onshore wind turbines

Type	Feature(s)	
LQR/LQG	Multi-objective, optimal for linear systems	[35, 46]
DAC	Minimises/cancels effects of persistent disturbances	[35, 47]
Periodic	Accounts for turbine periodicity	[48–50]
MPC	Predictive control, allows for setting saturation limits	[45, 51]
Adaptive	Adapts to model changes uncertainties to guarantee performance	[52, 53]
Nonlinear	Accounts for turbine nonlinearities including saturation	[54, 55]

Legend:
LQR/LQG Linear quadratic regulator/Gaussian
DAC Disturbance accommodating control
MPC Model predictive control

- Most had a single control objective of rotor speed control. Where an additional objective was included, it was implemented as a separate control loop; coupling between controlled DOFs is ignored.
- Fatigue load reduction was not an explicit control objective despite high tower loads.
- Used collective blade pitching. Collective blade pitching has limited actuation when multiple control objectives are considered (discussed in the next chapter).
- Not all of these controllers were simulated on all three main floating platforms.

To recap and expand on the research objectives discussed in Chapter 1, this work aims to implement *multi-objective* controllers that utilise *individual blade pitching* on the *three main floating wind turbines* using a state space approach.

For reducing tower fatigue loads on the wind turbine, the approach taken is to reduce tower base load variations via reducing tower-top motion relative to the platform coordinate system. Tower-top displacement relative to the platform coordinate system corresponds to the actual tower bending due to the applied forces and moments.

The controllers implemented in this work have the following objectives in the above rated wind speed region (region 3):

- Regulate the captured power to the rated (5 MW) via regulating rotor speed and varying generator torque.
- Reduce tower-top motion in order to reduce tower fatigue loads.
- Reduce platform motions (especially platform pitch) to:
  - improve rotor speed regulation via reducing the induced relative velocity caused by platform pitching; and
  - reduce loading on the tower base by reducing the deviations of the centre of mass due to platform rolling and pitching.

2.8 Chapter Summary

A recurring issue with floating wind turbines in terms of control is reduced or negative platform pitch damping in the above rated wind speed region. Several ways of dealing with this issue were proposed and below is a summary of the most important findings (in no particular order):

- Using constant torque instead of constant power algorithm for the generator torque control in above rated wind speed region helps to improve the platform pitching response by reducing the use of the blade pitch actuator responsible for the reduction in damping. This is not a complete solution but it can help when used with other controllers.
- The addition of Tuned Mass Dampers (TMDs) can noticeably improve the pitching motion on certain floating platform designs. Active TMDs further improve performance, however, based on current studies to date, the stroke length required to achieve these reductions cannot be used inside the nacelle of the wind turbine. A major benefit of using TMDs (active or passive) is that it has the potential to reduce pitching motion in extreme conditions where the blade pitch controller is not active.

3

State Feedback Control

Contents

3.1 State-Space Approach **30**
3.2 Collective vs. Individual Blade Pitching **32**
3.3 Multi-Blade Coordinate Transformation **36**
3.4 Implementation **37**
3.5 Stability Assessment **41**
3.6 Chapter Summary **42**

Multi-objective control of floating wind turbines is the next logical step to address the limitations of current controllers implemented on floating wind turbines as previously discussed. State feedback control is a model based approach that uses a linear state-space model to regulate multiple states. For brevity, the term state-space *control or controller* refers to a State Feedback Control (SFC) or Controller designed based on a linear state-space model. This approach allows the control of MIMO systems such as a floating wind turbine. As discussed in Chapter 2, this approach has not yet been applied to floating wind turbines.

This chapter describes the approach used to design, implement and assess the stability of such controllers on floating wind turbines. Furthermore, because state feedback control allows for the use of multiple actuators, the merits of individual over collective blade pitching and how each one operates are also described. A description of the selected approach to achieve individual blade pitching using a multi-blade coordinate transformation is given.

3.1 State-Space Approach

Linear state feedback control is one of the preferred types of controllers when dealing with MIMO systems with multiple objectives. This approach requires a linearised state-space model of the *nonlinear* floating system. As a result, the system states $\underline{x}$ become perturbations, $\Delta\underline{x}$, about a selected operating point $\underline{x}^{op}$ such that $\underline{x} = \Delta\underline{x} + \underline{x}^{op}$. This notation also applies for the measurements vector $\underline{y}$, actuators vector $\underline{u}$ and disturbance inputs vector $\underline{u}_d$. A generic linearised state-space model is given by equations (3.1) and (3.2) where A is the state matrix, B is the actuator gain matrix, B_d is the disturbance gain matrix, C relates the measurements to the states, D relates the measurements to the control inputs, and D_d relates the measurements to the disturbance inputs.

$$\Delta\dot{\underline{x}} = A\Delta\underline{x} + B\Delta\underline{u} + B_d\Delta\underline{u}_d \tag{3.1}$$

$$\Delta\underline{y} = C\Delta\underline{x} + D\Delta\underline{u} + D_d\Delta\underline{u}_d \tag{3.2}$$

The state feedback control law is given by equation (3.3) where K is the state feedback control gain matrix. In this work, the state matrix is defined as $\underline{x} = \begin{bmatrix} \underline{q} & \dot{\underline{q}} \end{bmatrix}^{\mathrm{T}}$ where $\underline{q}$ is a vector that contains the motions of the linearised degrees of freedom. The order or number of states of the linearised state space model chosen for control design is platform dependant and is discussed in relevant chapters.

$$\Delta\underline{u} = -K\Delta\underline{x} \tag{3.3}$$

The control law requires *all* the states information to be available through measurement or estimation. In this work, the state-space controllers are implemented with Full State Feedback (FSFB); that is, all the states are directly being measured. The selected design states for all the state-space controllers designed in this work can be easily measured by readily available sensors. In practice, it is desirable to reduce the number of sensors required by implementing a state estimator; however, this work is of an exploratory nature and will not focus on implementation issues such as cost of sensors, effects of noise, sensor failure, etcetera. Furthermore, from a stability point of view of linear systems, the separation principle allows the design of the controller to be independent of the state estimator. Since a state estimator can be designed separately, it is considered outside the scope of this work. Adding a state estimator only degrades the performance. Therefore, the state estimator is excluded from the system design because one of the objectives of this research is to assess the effectiveness/potential of advanced control strategies on floating platforms under ideal estimation conditions. The performance is assessed based on metrics defined in Chapter (5) that measure power regulation, fatigue loads, and platform motions.

It may be possible to express the cost of energy using a mathematical cost function for controller optimisation. However, that function will be nonlinear and maybe difficult to solve. Instead, Linear Quadratic Regulator (LQR) theory is used to obtain an optimal controller gain matrix given a set of weighting matrices that correspond to a quadratic cost function given by

equation (3.4) where Q and R are the state and actuator weighting matrices. These weighting matrices are *manually* chosen to emphasise the regulation of certain states over others to improve performance. This method is used for all the controllers that had a state regulation component including the disturbance accommodating controllers discussed in Chapter 4.

$$J = \int_0^\infty \left(\underline{x}^{\mathrm{T}} Q \underline{x} + \underline{u}^{\mathrm{T}} R \underline{u}\right) dt \tag{3.4}$$

So far, all of the above approach and equations only apply if the system is time-invariant. However, wind turbines are time-varying system that are governed by the period of the rotor; they are periodic systems. Therefore, when linearising such systems, the results is a linear *periodic* state-space model given by equations (3.5) and (3.6) where ψ is the azimuth angle of the rotor.

$$\Delta\dot{\underline{x}} = A(\psi)\,\Delta\underline{x} + B(\psi)\,\Delta\underline{u} + B_d(\psi)\,\Delta\underline{u}_d \tag{3.5}$$

$$\Delta\underline{y} = C(\psi)\,\Delta\underline{x} + D(\psi)\,\Delta\underline{u} + D_d(\psi)\,\Delta\underline{u}_d \tag{3.6}$$

Due to the periodic nature of the wind turbine, standard time-invariant control techniques cannot be applied directly. However, there are three ways to address the periodicity of the system; they are: averaging, Multi-Blade Coordinate (MBC) transformation, and direct periodic technique.

Averaging

Averaging the periodicity of each matrix across the azimuth angle resulting in a time-invariant state-space model. Direct averaging allows Linear Time-Invariant (LTI) control techniques to be applied. However, some information is lost by averaging and Individual Blade Pitching (IBP) cannot be used to control the rotor speed. Individual blade pitching may still be achieved for other control objectives if they are driven by a periodically changing error signal such as regulating blade flapwise load.

Multi-blade Coordinate Transformation

Multi-blade coordinate transformation can be used to facilitate individual blade pitching [48, 50, 56]. MBC transformation captures periodic properties of a system in a linear time-invariant model – useful for control design; see §3.3 for more details. Although MBC transformation does not capture all the periodic effects, it has been shown that the residual periodic effects are negligible for analysis and control design for three bladed wind turbines [50]. Bossanyi [57] implemented IBP control using PI controllers to mitigate blade loads. He used a direct and quadrature (d-q) axis representation (a form of MBC) to be able to allow for MIMO control using PI controllers.

Direct Periodic Technique

Direct periodic control allows the controller gains to change depending on the rotor azimuth position and control objectives [46, 58]. Periodic control captures all the periodicity of the system. However, it is more complicated and computationally more demanding than the previous two methods. Stol *et al.* [50] showed that there were no noticeable differences between the performance of controllers designed after MBC transformation and controllers with direct periodic control.

Both MBC transformation and direct periodic technique facilitate the use of IBP. However, the MBC transformation method allows for the utilisation of IBP control via LTI control design without the computational complexity of direct periodic control method.

3.2 Collective vs. Individual Blade Pitching

There are several actuators available for use by a control system on wind turbines in general. These include: blade pitch, generator torque, turbine yaw drive, smart blades with distributed actuators such as trailing edge flaps [59], and passive devices such as tuned mass dampers. For floating systems, passive devices such as oscillating water column can also be used to absorb energy from the waves. For active control, the most commonly used actuators for an onshore turbine are the blade pitch angle (operated either collectively or individually) and the commanded generator torque.

In this section, the physical mechanism behind Collective Blade Pitching (CBP) and individual blade pitching are described. The objective is to illustrate the differences between the two pitching schemes in terms of implementation, effectiveness at regulating multiple control objectives, and limitations with an emphasis on their impact on floating wind turbines.

3.2.1 Collective Blade Pitching

Collective blade pitch control is widely used in wind turbine control simply because it provides the necessary actuation required for rotor speed control. CBP changes the symmetric thrust and torque loads on the rotor. It is also easy to implement since all three blades are commanding the same pitch angle hence combining the actuation of the three blades into one single rotor actuator, which is useful for SISO control. However, when multiple objectives are to be regulated, collective blade pitching may not always provide the necessary actuation without sacrificing the regulation of other objectives or affecting other uncontrolled and/or un-modelled turbine DOFs.

With regards to floating offshore wind turbines, a major limitation of CBP is conflicting blade pitch commands issued by the control system with multiple objectives (whether implemented as separate SISO loops or a single MIMO controller) [60]. The objectives that conflict with each other in terms of actuator demand are rotor speed regulation and platform pitch motion regulation This type of conflict also exists but to a lesser degree in onshore turbines between

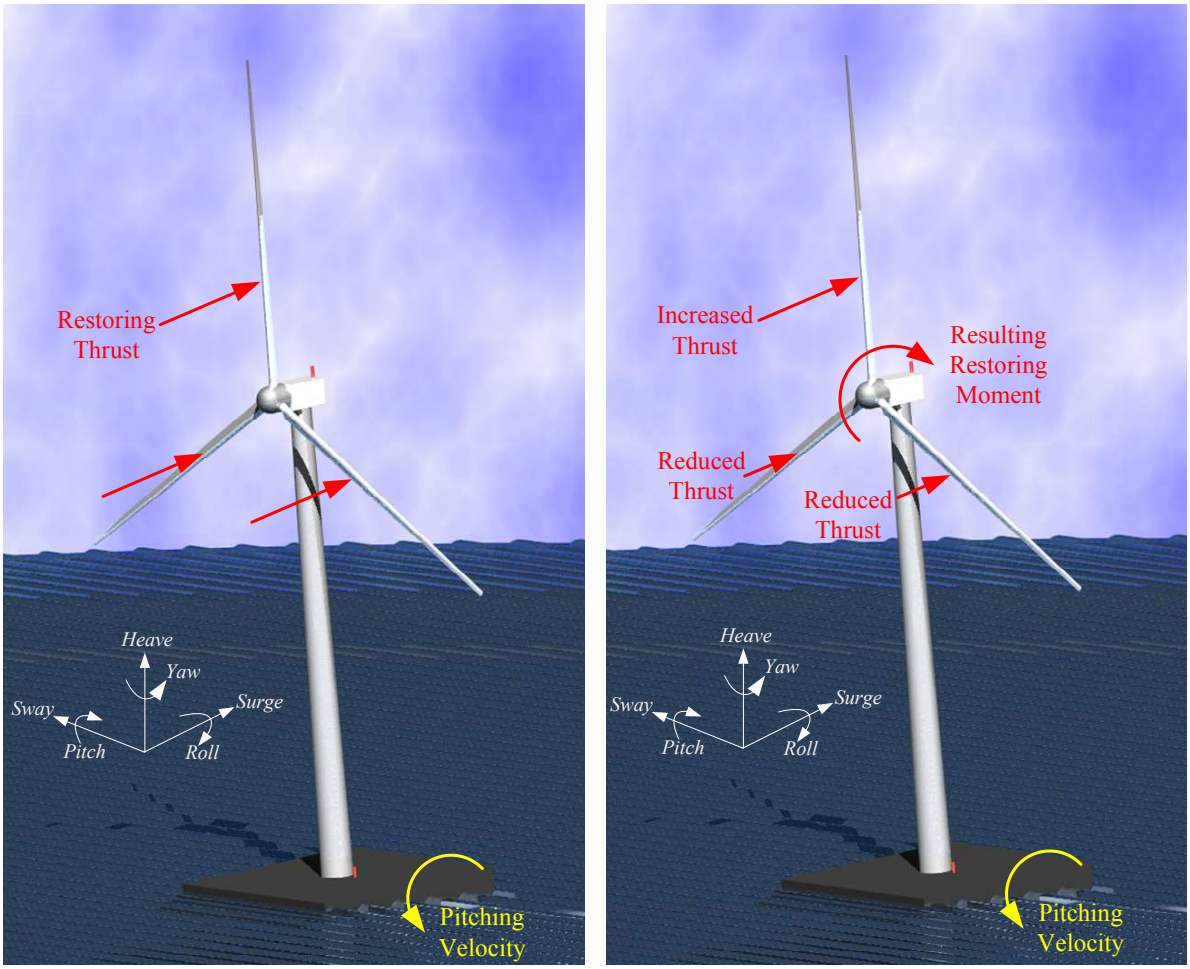

(a) Collective blade pitching

(b) Individual blade pitching

Figure 3.1: Platform pitch restoring forces with different blade pitch operation

rotor speed regulation and tower fore-aft motion. Below is a description using a hypothetical example of how these conflicting blade pitch commands are issued based on physical insight into the floating system.

For simplicity, assume there are two separate control loops: rotor speed controller and platform pitch controller. For regulating platform pitch, the most useful force generated by the blades is rotor thrust. Since the blades cannot influence the platform pitch angle directly but only through the thrust force, let the platform pitch controller regulate the pitching velocity which, ideally, must be reduced to zero. Now consider a forward pitching velocity shown in Figure 3.1a (negative pitch velocity according to the coordinate system). To keep the turbine in its equilibrium position (not necessarily upright due to the effect of constant wind), the platform pitch controller must generate a positive restoring pitch moment. This restoring moment can be achieved by increasing the aerodynamic thrust of each blade collectively where it will create a positive pitching moment about the pitch axis as shown in Figure 3.1a. Therefore, the blade pitch angles will have to be *decreased* to increase the torque and thrust loads generated by the blades.

Now, consider the effect of the same pitching velocity on the rotor speed. As the platform pitch

controller decreases the blade pitch to restore platform pitch, it is also accelerating the rotor by generating additional aerodynamic torque. This is coupled by the fact that as the turbine pitches forward, the wind speed relative to the blade increases thus further accelerating the rotor. Observing an increase in rotor speed, the rotor speed controller commands the blades to reduce the generated torque by *increasing* the collective blade pitch angle to reduce the aerodynamic efficiency of the blades. Therefore, the two objectives of speed and platform pitch regulation are competing for commanded blade pitch.

Multi-objective control using SFC with collective blade pitching can improve the performance with the abovementioned objectives but the conflict in objectives is present as it is still using CBP [61]; more details are given in Chapter 6. Therefore, SFC with CBP is not considered as one of the main controllers presented in this work.

3.2.2 Individual Blade Pitching

Individual blade pitch control where each blade is commanded independently uses a different mechanism from CBP control. It creates asymmetric aerodynamic loads in addition to the symmetric loads created by collective pitching thus enhancing the platform pitch restoring moment [60]. Due to the periodic nature of wind turbines, implementing IBP control results in time-varying gains that vary periodically with the rotor azimuth. That is, the controller "knows" how the effectiveness of the blade changes as it rotates and acts accordingly to create the necessary restoring forces/moments to achieve its control objectives.

There are many ways to achieve individual blade pitch control depending on the control objectives. MBC transformation and direct periodic techniques (discussed in §3.1) are the main methods to implement IBP for general purpose control objectives (rotor speed control, load mitigation, etc.). Wright [35] achieved IBP control using a disturbance accommodating controller. He used an internal model for the wind disturbance and the effect of vertical wind shear[6] to drive the individual blade pitching. This method uses IBP to only reject wind disturbance; the turbine states are regulated using a collective blade pitch controller.

As an example to illustrate the difference between individual and collective blade pitching, consider two controllers designed to regulate platform pitch DOF. The first is a CBP SFC and the second is an IBP SFC. Both controller gains are obtained using the same LQR cost function and weightings. The difference is that the IBP SFC is designed in the non-rotating frame after MBC transformation; this results in a *periodic* gain when it is transformed back. Figure 3.2 illustrates the variations with the rotor azimuth angle of both controller gains (or commanded blade pitch angle in radians) for blade 1 acting on platform pitch velocity error. The zero azimuth position is at the 12 o'clock position on the rotor with angle increasing clockwise when looking downwind; initially blade 1 is at the 0 azimuth position. The periodic gain changes sign twice as the blade goes through a full rotor revolution. The figure does not show the gains for the other two blades as the gains are the same but shifted 120° and 240° out of phase for blades 2 and 3 respectively. The significance of the sign change will be explained next.

[6] Vertical wind shear describes the increasing horizontal wind speed with height/elevation known as the boundary layer.

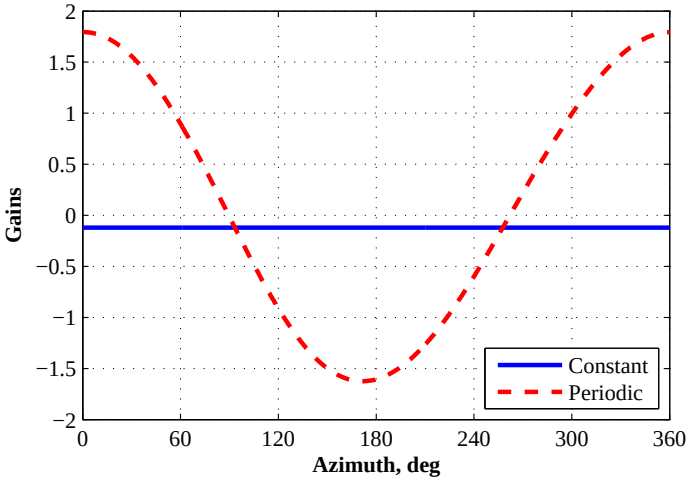

Figure 3.2: Collective and individual blade 1 gains as a function of rotor azimuth

The mechanism can be explained by looking at the periodic gain matrix (Figure 3.2). The gain for blade 1 is negative for azimuth angles approximately between 90° and 270°; these angles correspond to the blade lying in the lower half section of the rotor. Therefore, given a negative platform pitch velocity, shown in Figure 3.1b, blades at the top with a positive controller gain are commanded to reduce blade pitch thus increasing thrust. Blades at the bottom with a negative controller gain are commanded to increase blade pitch and hence reducing thrust. This asymmetric aerodynamic loading generates a positive restoring pitching moment in addition to the restoring moment generated by the mean thrust load (as with collective pitch) as illustrated in Figure 3.1b.

Looking further at the periodic gain shown in Figure 3.2, it can be seen that the maximum positive peak is when the blade is at the top (12 o'clock) position. A more positive gain value means increased blade pitching, which indicates that the controller is making use of the combined effect of increased moment arm of the blades and wind shear.

Wind turbines are under-actuated systems where the number of controller degrees of freedom is more than the number of actuators available. Furthermore, having the wind turbine mounted on a floating platform makes it even more difficult to regulate the control objectives than turbines with fixed foundations by introducing six additional DOFs (surge, sway, heave, roll, pitch, and yaw). The use of IBP increases the number of available actuators from 2 to 4 (for a three bladed wind turbine and including the generator torque) which gives the controller more authority to better regulate multiple objectives. However, there are some issues that arise when implementing IBP that one must be aware of:

- Increased blade pitch actuation which may result in blade pitch saturation and/or increased blade loads (depending on the control objectives).
- Increased computational requirements by the control system.
- The possibility of exciting or destabilising other turbine modes due to coupling with unmodelled and/or unregulated DOFs.

In this work, state feedback controllers utilising individual blade pitching are implemented using MBC transformation as it utilises well established LTI control design methods without the computational complexity of direct periodic control.

3.3 Multi-Blade Coordinate Transformation

Wind turbine systems are usually modelled with degrees of freedom in the fixed and rotating frames of reference. Therefore, the effects of the DOFs in the rotating frame of reference (e.g. blades) on those in the fixed frame of reference (such as the tower) are periodic. MBC transformation is used to transform the DOFs that are in the rotating frame of reference to the fixed frame of reference [48]. For a three bladed wind turbine, transforming any three DOFs in the rotating frame of reference results in three DOFs in the fixed frame of reference that describe the effect of the whole rotor on the turbine system. These three transformed DOFs are often termed collective, cosine-cyclic, and sine-cyclic components. MBC transformation is also known as the Coleman transformation or Fourier coordinate transformation [48, 62, 63].

The state, input and output vectors of equations (3.5) and (3.6) contain entities that are defined in both frames of reference (fixed and rotating); this combination is referred to as the mixed frame of reference. MBC transformation of these equations yields a state-space model whose states are all in the non-rotating/fixed frame of reference given by equations (3.7) and (3.8) where the subscript NR indicates the transformed entity into the non-rotating frame of reference; the Δ symbol that indicates perturbation about an operating point is omitted for brevity and clarity. For more information on MBC transformation, please refer to Appendix A.

$$\dot{\underline{x}}_{\mathrm{NR}} = A_{\mathrm{NR}}\,\underline{x}_{\mathrm{NR}} + B_{\mathrm{NR}}\,\underline{u}_{\mathrm{NR}} + B_{d,\mathrm{NR}}\,\underline{u}_d \tag{3.7}$$

$$\underline{y}_{\mathrm{NR}} = C_{\mathrm{NR}}\,\underline{x}_{\mathrm{NR}} + D_{\mathrm{NR}}\,\underline{u}_{\mathrm{NR}} + D_{d,\mathrm{NR}}\,\underline{u}_d \tag{3.8}$$

This transformation is achieved by applying the transformation equations (3.9) to (3.11). Note that the disturbance vector $\underline{u}_d$ is assumed to have no inputs in the rotating frame of reference and hence the vector itself is not transformed. The transformation matrices are defined in Appendix A.

$$\underline{x} = T_s(\psi)\,\underline{x}_{\mathrm{NR}} \tag{3.9}$$

$$\underline{u} = T_c(\psi)\,\underline{u}_{\mathrm{NR}} \tag{3.10}$$

$$\underline{y} = T_o(\psi)\,\underline{y}_{\mathrm{NR}} \tag{3.11}$$

The transformed system in equations (3.7) and (3.8) is not time-invariant; it is still slightly periodic [48]. Strictly speaking, periodic analysis should follow the transformation but Stol *et al.* [50] found that by averaging the transformed matrices (A_{NR}, B_{NR}, $B_{d,\mathrm{NR}}$, C_{NR}, D_{NR}, and $D_{d,\mathrm{NR}}$), little or no information is lost and hence time-invariant control design can be used without affecting the controller performance. Therefore, with a controller designed by averaging the sys-

tem matrices *after* applying MBC transformation, the commanded actuator effort, $\underline{u}_{\mathrm{NR}}$, is time-invariant. However, individual blade pitching is achieved when this command is transformed back to the rotating frame of reference by expanding equation (3.10) into equation (3.12) where T_{Gen} is the applied generator torque, and θ_n is the commanded blade pitch angle for blade n. Equation (3.12) clearly shows that even if the controller commands are time-invariant in the non-rotating frame of reference, the actual blade commands are periodic resulting in individual blade pitching. Equation (3.12) is applicable for a three bladed wind turbine with $\underline{u}_{\mathrm{NR}}$ given by equation (3.13) where θ_o, θ_c, and θ_s are the collective, cosine-cyclic, and sine-cyclic terms of the blade pitch angles respectively.

$$\underline{u} = \begin{bmatrix} T_{Gen} \\ \theta_1 \\ \theta_2 \\ \theta_3 \end{bmatrix} = \begin{bmatrix} 1 & 0 & 0 & 0 \\ 0 & 1 & \cos(\psi) & \sin(\psi) \\ 0 & 1 & \cos\left(\psi + \frac{2\pi}{3}\right) & \sin\left(\psi + \frac{2\pi}{3}\right) \\ 0 & 1 & \cos\left(\psi + \frac{4\pi}{3}\right) & \sin\left(\psi + \frac{4\pi}{3}\right) \end{bmatrix} \underline{u}_{\mathrm{NR}} \tag{3.12}$$

where

$$\underline{u}_{\mathrm{NR}} = \begin{bmatrix} T_{Gen} & \theta_o & \theta_c & \theta_s \end{bmatrix}^{\mathrm{T}} \tag{3.13}$$

3.4 Implementation

MBC transformation allows the design of time-invariant controllers in the non-rotating frame of reference that are actually periodic in nature. Therefore, equation (3.3) still applies in the non-rotating frame (i.e. $\Delta\underline{u}_{\mathrm{NR}} = K_{\mathrm{NR}}\Delta\underline{x}_{\mathrm{NR}}$). The block diagram implementation of this equation is shown in Figure 3.3a [64]. This implementation, obviously has two transformations: to and from the non-rotating frame. From an implementation point of view, each transformation requires periodic matrix extraction and multiplication. Periodic matrices are 3D arrays/matrices where each layer in the "third dimension" contains the matrix data for a specified azimuth angle. Hence, at each simulation step, the 2D matrix data has to be extracted and interpolated according to the simulation azimuth angle before multiplication with $\Delta\underline{x}_{\mathrm{NR}}$.

A simpler implementation that does not require transformation to and from the non-rotating frame is possible by simple manipulation of the control law. By substituting $\Delta\underline{u}_{\mathrm{NR}} = -K_{\mathrm{NR}}\Delta\underline{x}_{\mathrm{NR}}$ and $\Delta\underline{x}_{\mathrm{NR}} = T_s^{-1}(\psi)\,\Delta\underline{x}$ into equation (3.10), we obtain equation (3.14) which only contains a single periodic controller gain matrix. This simpler approach (Figure 3.3b) is more computationally efficient and only requires the periodic controller gain matrix to be computed offline (equation (3.15)).

$$\begin{aligned} \Delta\underline{u} &= -T_c(\psi)\,K_{\mathrm{NR}}T_s^{-1}(\psi)\,\Delta\underline{x} \\ \therefore \Delta\underline{u} &= -K(\psi)\,\Delta\underline{x} \end{aligned} \tag{3.14}$$

where

$$K(\psi) = T_c(\psi) K_{\mathrm{NR}} T_s^{-1}(\psi) \tag{3.15}$$

Note that the control gain $K(\psi)$ depends on the azimuth angle. In this implementation, the actual azimuth angle is used instead of the desired angle ($\omega_{Rated} \times t$) for better accuracy. However, because azimuth angle is a system state, the controller becomes nonlinear. If speed regulation is maintained close to the rated rotor speed, then the effects of this nonlinearity are negligible. From this point forward, the controller is considered linear.

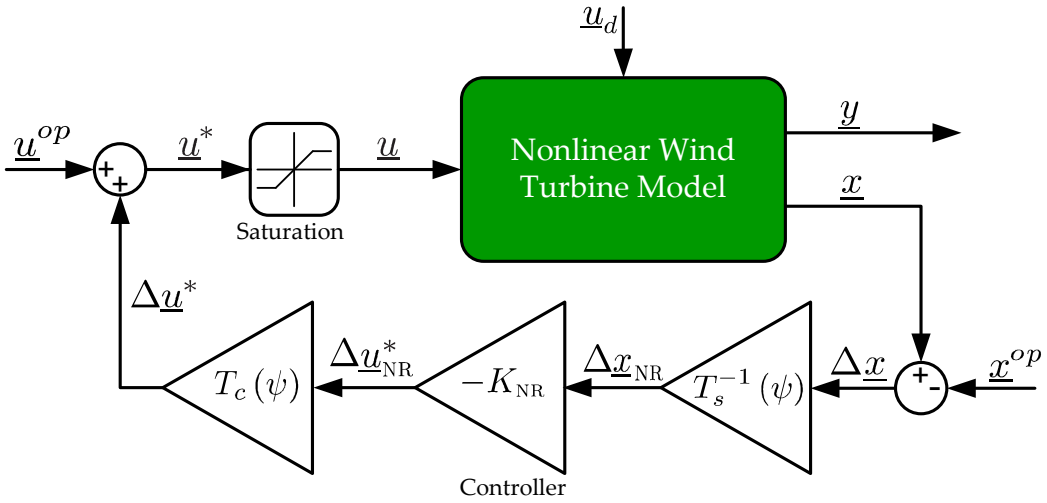

(a) Standard

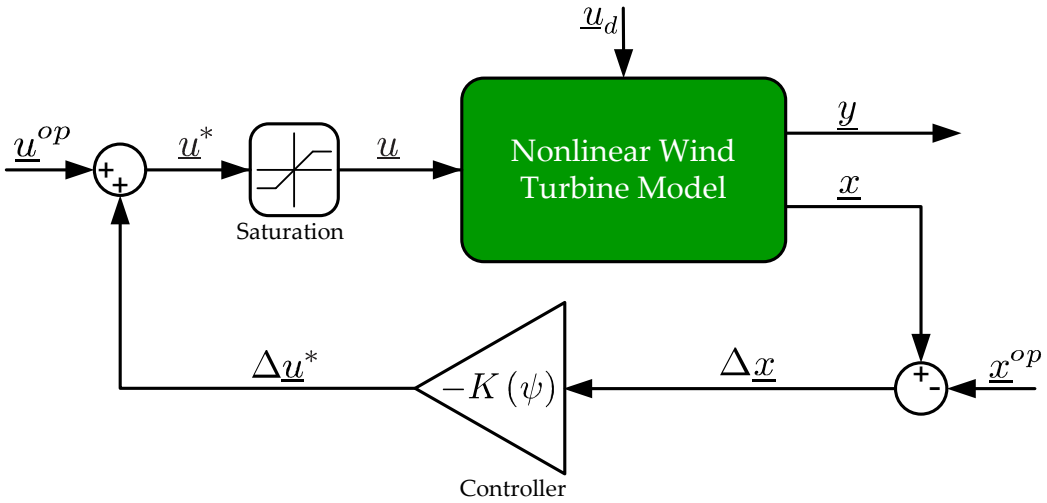

(b) Simplified

Figure 3.3: Standard and simplified block diagram implementations of an IBP state-space controller

3.4.1 Generator Torque

Wright [35] showed that generator torque can be used directly to influence some turbine states such as tower side-side motion and low speed shaft loads. Therefore, the generator torque is included in the design of the SFC as an additional actuator to help in regulating turbine states. When the generator torque is included in the model as an actuator, the controls input vector becomes $\Delta\underline{u} = \begin{bmatrix} \Delta T_{Gen} & \Delta\theta_1 & \Delta\theta_2 & \Delta\theta_3 \end{bmatrix}^{\mathrm{T}}$ where ΔT_{Gen} is the commanded torque perturbations and $\Delta\theta_n$ is blade n commanded perturbations about the linearisation point.

For the state feedback controller, direct power regulation via state regulation is not possible as generator power is not a state in the linearised models of the wind turbine obtained from FAST. One approach to regulate power is to vary the generator torque operating point according to equation (3.16) such that $T_{Gen} = \Delta T_{Gen} + T^{op}_{Gen}$ where $\omega_{Gen,f}$ is the filtered generator speed (as discussed in §2.1). This set-up, known as *constant power algorithm*, maintains the constant power objective by the Baseline torque control in addition to regulating turbine states through the commanded torque perturbations.

$$T^{op}_{Gen} = \frac{P_{Rated}}{\eta_{Gen}\omega_{Gen,f}} \tag{3.16}$$

Normally, the actuators' operating point vector is constant and based on the linearised state-space model. For the generator torque, the constant operating point is termed *constant torque algorithm*. Using the constant power algorithm improves power regulation but results in increased rotor speed fluctuations and slightly reduces the platform pitch damping when compared to the constant torque control algorithm [61]. Constant power algorithm is implemented on all the state feedback controllers used in this work.

3.4.2 Azimuth Angle Correction due to Platform Rolling

Due to the application of MBC transformation, any controller designed based on that transformation will require periodic matrix or matrices in its implementation which can be calculated offline for improved computational efficiency. These periodic matrices require the current rotor azimuth angle to be known at that time step. Since FSFB is used for the SFC, the current azimuth angle is available.

For floating wind turbines, the roll motion changes the effective azimuth angle ψ_a as the blades are rotated the additional roll angle ξ and therefore placing the blades in a different rotor orientation with respect to the incident wind field. The effect of the roll motion on the azimuth angle is illustrated in Figure 3.4 where the platform roll and rotor DOFs rotate about the positive x-axis [36]. If the effect of platform rolling is not taken into account, the data extracted from the periodic matrices become inaccurate and do not represent the system at that state.

The actual azimuth angle can be calculated using equation (3.17). This angle can then be used to extract data from the periodic matrices. However, equation (3.17) requires the roll angle to be measured. For the controllers implemented in Chapters 6, 7, and 8, the roll DOF is part of the controller design which allows the compensation of the azimuth angle due to roll motion.

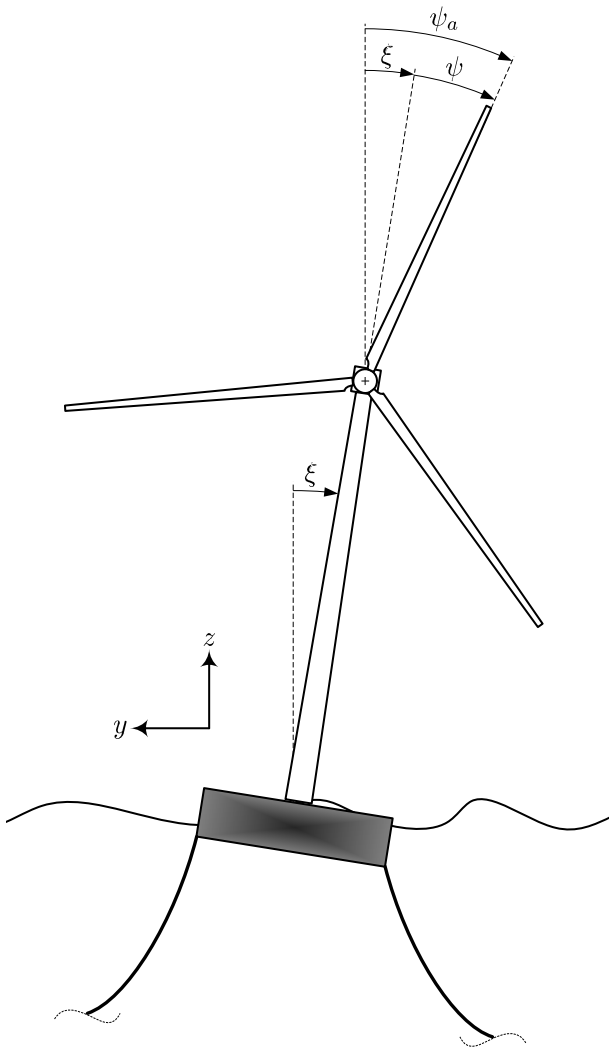

Figure 3.4: Azimuth angle correction due to platform roll motion

$$\psi_a = \psi + \xi \qquad 0 < \psi_a < 2\pi \tag{3.17}$$

The effect of rolling and pitching motion on changing the hub height is negligible. To cause a 5 m change in hub-height for a wind turbine with 90 m hub-height, it would require a roll/pitch angle of approximately 19°; this is an extreme angle which, with an on–board active controller, should never be reached. Furthermore, a 5m change in hub height would only cause the wind speed to change by 1% with a power law coefficient of 0.2 for the vertical wind shear.

3.4.3 Actuator Saturation

An important factor to consider when designing controllers is actuator limits. From a simulation point of view, these limits must be enforced to reflect the limits of the real actuator. For the the floating wind turbines considered, saturation and rate limits for the generator torque and blade pitch angles are enforced. The rate limits are used to limit how fast the control effort can

change in the absence of an actuator model (as defined in the scope of this work in §1.3). From a control design point of view, these limits must be avoided as reaching them may significantly affect the controller performance.

With individual blade pitching, the blade actions can be thought of as a collective blade pitch with periodic perturbations such that $\theta = \theta_o + \Delta\theta_i(\psi)$ where θ_o is the collective pitch angle that creates symmetric loads on the rotor and $\Delta\theta_i(\psi)$ is the individual periodic perturbation that is responsible for creating the asymmetric loads on the rotor. Therefore, during blade saturation, $\Delta\theta_i(\psi)$ is allowed to pass through and continue regulating certain objectives while limiting the collective term. MBC transformation facilitates this type of selective saturation because $\underline{u}_{\text{NR}}$ (equation (3.13)) has the three components already separated out. Therefore, by only saturating the collective term the selective saturation can be achieved.

3.4.4 Azimuth State Anti-windup

Integrator windup becomes a concern when actuator saturation is possible. With state feedback control, there are no explicit integrators present but windup is possible through certain states. Recall that the states vector of a first order state-space model contains the state and its derivative (i.e. $\underline{x} = \begin{bmatrix} \underline{q} & \underline{\dot{q}} \end{bmatrix}^{\text{T}}$). Therefore, $\underline{q}$ can be thought of as integrals of $\underline{\dot{q}}$.

For a floating wind turbine, the only state the can grow when the blades are saturated is the azimuth state. Therefore, an anti-windup scheme is used to stop that state from growing when the blades are saturated. Instead of directly feeding the change in azimuth state, $\Delta\psi$, to the linear state-space controller, the change in rotor speed, $\Delta\dot{\psi}$, is passed through a special integrator that stops integrating when the blades are saturated and holds its value. That way, $\Delta\psi$ will not grow to dominate the control effort when the blades are saturated.

3.5 Stability Assessment

LQR control design guarantees the closed-loop stability of the linear system it is designed to control. However, because wind turbines in general and especially floating wind turbines have many flexibilities and degrees of freedom, the linear model used for controller design is usually of a much lower order than the actual system. Therefore, the closed-loop stability of the controller with the full DOFs system must be assessed.

The stability of the closed-loop system can be assessed by finding the location of the closed-loop poles. For a system given in state-space form, the closed-loop poles can be found by evaluating the eigenvalues of the $(A_{\text{NR}} - B_{\text{NR}}K_{\text{NR}})$ matrix. Stol *et al.* [50] showed that there are no differences between the closed-loop poles calculated from using MBC transformed matrices compared to the poles found by doing a Floquet analysis on the full periodic system.

To assess the closed-loop stability of the controller with *all the model flexibilities* enabled, we need to introduce a boolean transition matrix T to account for the larger full degrees of freedom (DOFs) state-space matrices $A_{\text{NR},full}$ and $B_{\text{NR},full}$. The stability of the full DOFs system is given

by equation (3.18) where all the eigenvalues λ must lie in the left half of the complex plane (i.e. the real part must be negative).

$$Re\left(\lambda\left(A_{\mathrm{NR},full} - B_{\mathrm{NR},full}K_{\mathrm{NR}}T\right)\right) < 0 \tag{3.18}$$

The boolean transition matrix T, given by equation (3.19), has dimensions of $nd \times nf$ where nd is the number of design states (i.e. the number of states the controller was designed with) and nf is the number of the full system states. The elements of the matrix are either 1 or 0. The element $T_{i,j}$ is set to 1 to indicate that the i^{th} design state is thej^{th} state in the full DOFs system. A simple program is executed to automatically create the boolean matrix based on information contained within the FAST linearisation files of the controller and the full DOFs system.

$$T = \begin{bmatrix} T_{1,1} & \cdots & T_{1,nf} \\ \vdots & \ddots & \vdots \\ T_{nd,1} & \cdots & T_{nd,nf} \end{bmatrix} \tag{3.19}$$

When one or more poles are unstable it is possible to identify which bending mode or DOF the pole corresponds to. By looking at the associated eigenvector, one can identify which state has the most contribution in that eigenvector and therefore is most likely the state that is unstable. However, with complex flexible structures such as wind turbines, the unstable DOF may not be that easy to identify due to the number of DOFs and their associated coupling.

It is important to note that this approach can only assess the closed-loop stability of the *linearised* system which is a close approximation of the nonlinear system around the operating point. Therefore, away from the linearisation point, nothing can be inferred about the stability of the nonlinear system. This approach with its limitation is sufficient for the purposes of this work since it is only used to identify any instability caused by the controller that can arise from using individual blade pitching or using a low fidelity linear model.

3.6 Chapter Summary

State feedback control using individual blade pitching is one of the main controllers that are implemented on the three floating platforms. The state Feedback controller is designed using a linearised periodic state-space model of a floating wind turbine, can handle multiple objectives, and utilise all of the available actuators. The periodicity of the linear model is dealt with by using multi-blade coordinate system transformation to transform the model to a non-rotating frame of reference. By averaging the transformed system, a linear time-invariant model is created without loss of information which can then be used for controller design.

MBC transformation also facilitates the use of individual blade pitching. Individual blade pitching allows the controller to create asymmetric loads on the rotor in addition to symmetric ones created by collective blade pitching. These asymmetric loads help in better regulating certain objective/states than collective blade pitching.

4

Disturbance Accommodating Control

Contents

4.1 Introduction to DAC **43**
4.2 DAC Theory Overview **44**
4.3 DAC After MBC Transformation **47**
4.4 Implementation **48**
4.5 Wind Speed Disturbance Rejection **50**
4.6 Chapter Summary **53**

Disturbance Accommodating Control (DAC) is a type of feed-forward control used to minimise or cancel the effects of persistent disturbances [35, 47, 65]. In the case of floating wind turbines, the disturbances include the incident wind and waves. If the effects of wind and, more importantly, waves can be cancelled or reduced, then platform motions will be significantly reduced thus reducing the additionally induced loads on the wind turbine and improve power regulation.

In this chapter, the general approach of applying DAC to floating wind turbines is described where the effects of wind speed perturbations are considered. A disturbance estimator is derived to estimate the system disturbances, whose effects are to be minimised, since direct measurement of the disturbances is assumed to be unavailable. MBC transformation is used to deal with the periodicity of the wind turbine.

4.1 Introduction to DAC

Disturbance accommodating controllers have been designed and implemented, at least in simulations, on large scale wind turbines in the past; two examples are described next.

Wright [35] has designed and implemented a DAC on a 600 kW, two bladed, wind turbine. The wind disturbance was modelled as a superposition of a step change in horizontal hub-height wind speed and a periodically varying term to represent the changes in wind speed at the blade tip due to vertical wind shear as the blade completes a full revolution. The latter term facilitated IBP control without the need to resort to periodic control theory. Results were then compared to a standard PI controller under two distinct conditions: slow and fast actuator dynamics. With slow actuator dynamics, both controllers performed similarly but the PI controller behaved more robustly when the wind speed drifted away from the linearisation point. However, with fast actuator dynamics, DAC performance was significantly better than that of the PI controller. Under these conditions, the PI controller could not guarantee system stability (since it was a single-objective controller thus could not regulate/control other DOFs); in fact, certain DOFs were destabilised when the PI controller was used with an actuator with fast dynamics.

Stol and Balas [49] performed a study to evaluate the load mitigation capability (for blade flap) of three different control strategies: time-invariant PI, time-invariant DAC, and periodic DAC (utilising IBP control). The disturbance was modelled as a step change in hub-height wind speed. First, they tested these controllers under full state feedback conditions. Results showed that while all controllers gave similar speed regulation, loads were best mitigated by the periodic DAC, then the time-invariant DAC, while the PI controller had the highest loads. However, when state estimators were included in the design, the load mitigation capability of DACs were severely reduced. The time-invariant controllers had similar performance while the periodic DAC was able to reduce the loads further relative to the time-invariant controllers.

4.2 DAC Theory Overview

Disturbance accommodating controllers are implemented by modelling the disturbances using an assumed waveform model [35,65], similar to the use of an exo-system in reference tracking control theory. A generic linear system is given by equations (4.1) and (4.2). The objective is to modify the control law such that it cancels out the effects of the *persistent* disturbances $\underline{u}_d$ on system states.

$$\dot{\underline{x}} = A\underline{x} + B\underline{u} + B_d\underline{u}_d \tag{4.1}$$

$$\underline{y} = C\underline{x} + D\underline{u} + D_d\underline{u}_d \tag{4.2}$$

To cancel the effects of disturbances, we must first assume that the persistent disturbances can be represented by a waveform model. The disturbance waveform model is given by equations (4.3) and (4.4) where $\underline{z}$ is the disturbance states vector, Γ and Θ are assumed to be known but with unknown initial conditions $\underline{z}(0)$ [47,65]. The choice of matrices Γ, Θ, and initial conditions $\underline{z}(0)$ determines the nature of the assumed waveform (step, ramp, periodic, etc.).

$$\underline{u}_d = \Theta\underline{z} \tag{4.3}$$

$$\dot{\underline{z}} = \Gamma\underline{z} \tag{4.4}$$

The modified feedback control law that minimises or cancels the effects of disturbances is given by equation (4.5) where K is the state feedback controller gain matrix, and G_d is the disturbance minimisation gain matrix. The second term in equation (4.5) exhibits feed-forward action as it commands the blades based on an assumed disturbance model.

$$\underline{u} = -K\underline{x} + G_d\underline{z} \tag{4.5}$$

Substituting equations (4.3) and (4.5) into equation (4.1), we obtain equation (4.6) which clearly shows that in order to *cancel* the effects of persistent disturbances, equation (4.7) must hold true.

$$\begin{aligned} \underline{\dot{x}} &= A\underline{x} - BK\underline{x} + BG_d\underline{z} + B_d\Theta\underline{z} \\ &= (A - BK)\,\underline{x} + (BG_d + B_d\Theta)\,\underline{z} \end{aligned} \tag{4.6}$$

$$BG_d + B_d\Theta = 0 \tag{4.7}$$

Note that the disturbance accommodating controller is simply a state feedback controller with an additional feed-forward term that minimises the effects of persistent disturbances on the modelled system states. This additional feed-forward term has no impact on the closed-loop stability of the system. This is evident by examining equation (4.6) where the disturbance minimisation gain, G_d, does not affect state regulation.

Applying the Disturbance Accommodating Control law and equations in practice gives rise to two issues:

1. With a relatively complicated model, it is almost always impossible to completely cancel out the disturbances (unless these disturbances enter the system through the same channels such that $B = B_d$) [47, 65]. Therefore, to minimise the effect of disturbances on the system, G_d must be chosen to minimise $\|BG_d + B_d\Theta\|$. This can be achieved by applying the Moore-Penrose pseudoinverse (indicated by $^+$) such that G_d is calculated using equation (4.8).

$$G_d = -B^+B_d\Theta \tag{4.8}$$

2. Equation (4.5) assumes FSFB - meaning the controller has access to all states including the disturbance states. Practically, this is very hard to implement especially with the modelled disturbance states where they do not necessarily represent real physical entities. Therefore, a disturbance estimator has to be designed to reconstruct the system and disturbance states based on sensor measurements, $\underline{y}$.

4.2.1 Disturbance Estimator

In this work, it is assumed that the disturbance inputs cannot be measured, therefore, a disturbance state estimator is required. It is possible to use turbine measurements to estimate the

disturbance states thereby utilising the turbine as an instrument that measures the effects of the disturbances.

A disturbance state estimator can be designed by augmenting the turbine states with the disturbance states forming $\underline{w}$ in equation (4.9). By differentiating the new state vector with respect to time and utilising equations (4.1) to (4.4) a new and augmented state-space model is created and given by equations (4.10) and (4.11).

$$\underline{w} = \begin{bmatrix} \underline{x} & \underline{z} \end{bmatrix}^{\mathrm{T}} \tag{4.9}$$

$$\dot{\underline{w}} = \overline{A}\underline{w} + \overline{B}\underline{u} \tag{4.10}$$

$$\underline{y} = \overline{C}\underline{w} + D\underline{u} \tag{4.11}$$

where

$$\overline{A} = \begin{bmatrix} A & B_d\Theta \\ 0 & \Gamma \end{bmatrix} \tag{4.12}$$

$$\overline{B} = \begin{bmatrix} B \\ 0 \end{bmatrix}$$

$$\overline{C} = \begin{bmatrix} C & D_d\Theta \end{bmatrix}$$

The state estimator dynamics for the augmented state-space model are given by equations (4.13) and (4.14) [66] where K_e is the state estimator gain matrix; the $\hat{}$ symbol indicates an estimate.

$$\dot{\underline{\hat{w}}} = \overline{A}\underline{\hat{w}} + \overline{B}\underline{u} + K_e\left(\underline{y} - \underline{\hat{y}}\right) \tag{4.13}$$

$$\underline{\hat{y}} = \overline{C}\underline{\hat{w}} + D\underline{u} \tag{4.14}$$

Forming the error vector $\underline{e}$ such that $\underline{e} = \underline{w} - \underline{\hat{w}}$ and differentiating with respect to time results in equation (4.15). Therefore, if the pair $\left(\overline{A}, \overline{C}\right)$ is observable, then the augmented vector $\underline{w}$ can be fully estimated [66].

$$\begin{aligned} \dot{\underline{e}} &= \dot{\underline{w}} - \dot{\underline{\hat{w}}} \\ &= \overline{A}\left(\underline{w} - \underline{\hat{w}}\right) - K_e\overline{C}\left(\underline{w} - \underline{\hat{w}}\right) \\ \therefore \dot{\underline{e}} &= \left(\overline{A} - K_e\overline{C}\right)\underline{e} \end{aligned} \tag{4.15}$$

It is important to remember that although the above description involved simple linear state-space models for simplicity, the linear models used to describe the wind turbine are periodic

and are only perturbations about the linearisation point. Similar to state feedback control described in Chapter 3, MBC transformation is used to deal with turbine periodicity.

4.3 DAC After MBC Transformation

In this work, the disturbance states, $\underline{z}$, are modelled in the non–rotating frame of reference and therefore do not require a transformation matrix from the rotating frame of reference. After applying MBC transformation on a periodic system, DAC design becomes time-invariant. The DAC law in the non-rotating frame is given by equation (4.16) and the time-invariant DAC gain matrix is found by solving equation (4.17).

$$\begin{aligned} \underline{u}_{\mathrm{NR}} &= -K_{\mathrm{NR}}\underline{\hat{x}}_{\mathrm{NR}} + G_{d,\mathrm{NR}}\underline{\hat{z}} && (4.16)\\ G_{d,\mathrm{NR}} &= -B^{+}_{\mathrm{NR}}B_{d,\mathrm{NR}}\Theta && (4.17) \end{aligned}$$

The DAC law is now in the non-rotating frame and therefore blade pitch commands have to be transformed back to the mixed frame using equation (3.10). Equation (4.18) shows the DAC law transformed into the mixed frame of reference. The result is periodic gain matrices where $K_{\mathrm{MBC}}(\psi)$ and $G_{d,\mathrm{MBC}}(\psi)$ are the periodic state regulation and periodic disturbance minimisation gain matrices respectively.

$$\begin{aligned} \underline{u} &= -T_c(\psi)\,K_{\mathrm{NR}}T_s^{-1}(\psi)\,\underline{\hat{x}} + T_c(\psi)\,G_{d,\mathrm{NR}}\,\underline{\hat{z}} \\ &= -K_{\mathrm{MBC}}(\psi)\;\underline{\hat{x}} + G_{d,\mathrm{MBC}}(\psi)\;\underline{\hat{z}} && (4.18) \end{aligned}$$

Similar to the time-invariant DAC design, we form a *new* augmented states vector $\underline{w}_{\mathrm{NR}}$ given by equation (4.19). Equation (4.20) can then be used to transform between $\underline{w}_{\mathrm{NR}}$ and $\underline{w}$ where I is an identity matrix and nd is the number of disturbance states.

$$\begin{aligned} \underline{w}_{\mathrm{NR}} &= \begin{bmatrix} \underline{x}_{\mathrm{NR}} \\ \underline{z} \end{bmatrix} && (4.19)\\ \underline{w} &= \begin{bmatrix} T_s(\psi) & 0 \\ 0 & I_{nd\times nd} \end{bmatrix} \underline{w}_{\mathrm{NR}} = T_d(\psi)\;\underline{w}_{\mathrm{NR}} && (4.20) \end{aligned}$$

Given the definition of $\underline{w}_{\mathrm{NR}}$ above, we form a *new* disturbance estimator for the MBC transformed system (equations (3.7) and (3.8)). The disturbance estimator in the non-rotating frame is given by equation (4.21). This equation does *not* represent the MBC transformation of equation (4.13).

$$\underline{\hat{\dot{w}}}_{\mathrm{NR}} = \left(\overline{A}_{\mathrm{NR}} - K_{e,\mathrm{NR}}\overline{C}_{\mathrm{NR}}\right)\underline{\hat{w}}_{\mathrm{NR}} + \overline{B}_{\mathrm{NR}}\,\underline{u}_{\mathrm{NR}} + K_{e,\mathrm{NR}}\,\underline{y}_{\mathrm{NR}} \tag{4.21}$$

where

$$\overline{A}_{\mathrm{NR}} = \begin{bmatrix} A_{\mathrm{NR}} & B_{d,\mathrm{NR}}\Theta \\ 0 & F \end{bmatrix}$$
$$\overline{B}_{\mathrm{NR}} = \begin{bmatrix} B_{\mathrm{NR}} \\ 0 \end{bmatrix}$$
$$\overline{C}_{\mathrm{NR}} = \begin{bmatrix} C_{\mathrm{NR}} & D_{d,\mathrm{NR}}\Theta \end{bmatrix}$$

Since the actuator commands and the measurements are in the mixed frame of reference, we transform the input and measurement vectors into the non-rotating frame and combine the two vectors into one for easier implementation. The result is given by equation (4.22) where $\underline{v}$ is the augmented estimator inputs in the mixed frame of reference.

$$\begin{aligned} \underline{\hat{\dot{w}}}_{\mathrm{NR}} &= \left(\overline{A}_{\mathrm{NR}} - K_{e,\mathrm{NR}}\overline{C}_{\mathrm{NR}}\right)\underline{\hat{w}}_{\mathrm{NR}} + \underbrace{\overline{B}_{\mathrm{NR}}T_c^{-1}(\psi)\,\underline{u} + K_{e,\mathrm{NR}}T_o^{-1}(\psi)\,\underline{y}}_{\text{Inputs}} \\ &= \left(\overline{A}_{\mathrm{NR}} - K_{e,\mathrm{NR}}\overline{C}_{\mathrm{NR}}\right)\underline{\hat{w}}_{\mathrm{NR}} + \begin{bmatrix} \overline{B}_{\mathrm{NR}}T_c^{-1}(\psi) & K_{e,\mathrm{NR}}T_o^{-1}(\psi) \end{bmatrix}\begin{bmatrix} \underline{u} \\ \underline{y} \end{bmatrix} \\ &= \left(\overline{A}_{\mathrm{NR}} - K_{e,\mathrm{NR}}\overline{C}_{\mathrm{NR}}\right)\underline{\hat{w}}_{\mathrm{NR}} + E(\psi)\,\underline{v} \end{aligned} \tag{4.22}$$

4.4 Implementation

In the case of floating wind turbines, FSFB is used for the SFC part of the DAC which means the state estimates $\underline{\hat{x}}_{\mathrm{NR}}$ are not used. Therefore, the implemented control law is given by equation (4.23) where $\underline{x}_{\mathrm{NR}}$ is obtained by equation (4.24).

$$\underline{u}_{\mathrm{NR}} = -K_{\mathrm{NR}}\underline{x}_{\mathrm{NR}} + G_{d,\mathrm{NR}}\underline{\hat{z}} \tag{4.23}$$
$$\underline{x}_{\mathrm{NR}} = T_s^{-1}(\psi)\,\underline{x} \tag{4.24}$$

For the disturbance estimator, FSFB implementation and the availability of $\underline{x}_{\mathrm{NR}}$ requires rearranging equation (4.21) into equation (4.25). Equation (4.25) differs from equation (4.22) by having the disturbance estimator inputs in the nonrotating frame of reference.

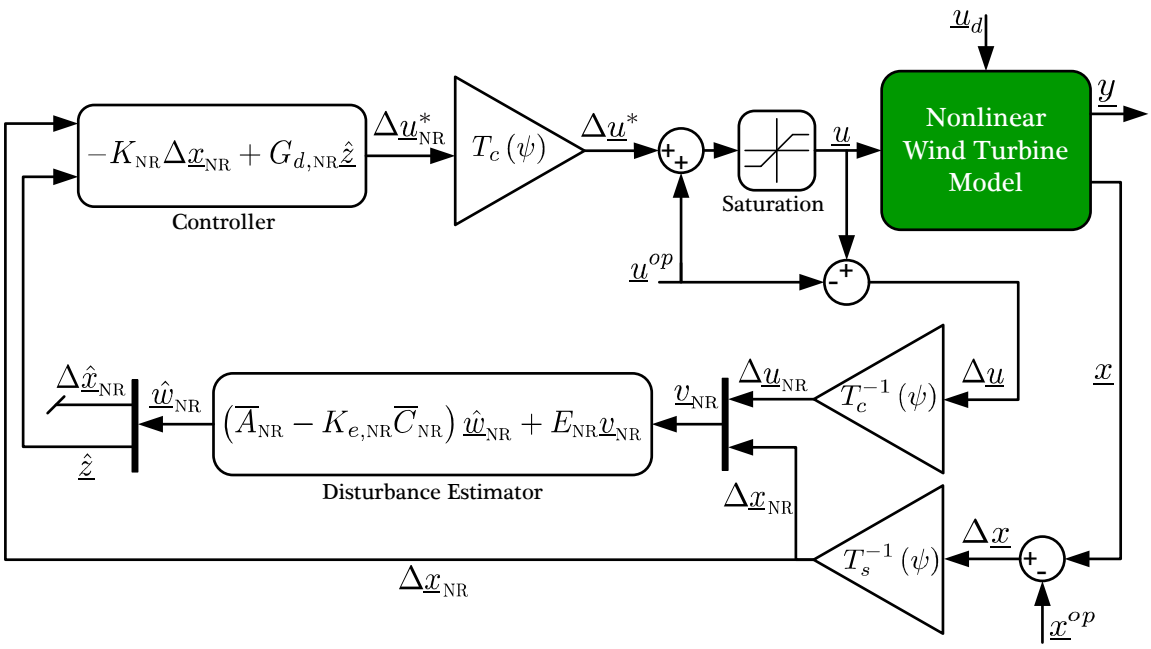

Figure 4.1: DAC with FSFB implementation for floating wind turbines

$$\begin{aligned}\dot{\hat{\underline{w}}}_{\mathrm{NR}} &= \left(\overline{A}_{\mathrm{NR}} - K_{e,\mathrm{NR}}\overline{C}_{\mathrm{NR}}\right)\hat{\underline{w}}_{\mathrm{NR}} + \begin{bmatrix} \overline{B}_{\mathrm{NR}} & K_{e,\mathrm{NR}} \end{bmatrix}\begin{bmatrix} \underline{u}_{\mathrm{NR}} \\ \underline{x}_{\mathrm{NR}} \end{bmatrix} \\ &= \left(\overline{A}_{\mathrm{NR}} - K_{e,\mathrm{NR}}\overline{C}_{\mathrm{NR}}\right)\hat{\underline{w}}_{\mathrm{NR}} + E_{\mathrm{NR}}\underline{v}_{\mathrm{NR}} \end{aligned} \tag{4.25}$$

Block diagram implementation of DAC after MBC transformation for floating wind turbines is shown in Figure 4.1. The implementation accounts for the controller being designed based on a linearised state-space model and actuator saturation.

Other implementation configurations, discussed in Appendix B, were considered. However, these implementation options cannot be applied for systems with slow actuator dynamics or when actuator saturation is possible.

4.4.1 DAC Limitations and Challenges

Since the DAC gain matrix is the result of a minimisation process (equation (4.8)) with no parameters to tune, the resultant gain matrix may cause severe actuator saturation if the actuators do not have enough control authority to reduce the effects of modelled disturbances on all or some of the system states. Therefore, one must be careful when applying DAC to a system with relatively low saturation limits.

One way to limit the effects of the minimisation process is to exclude certain states from the DAC design where the actuators have little control authority. That way, the DAC will not assign large gains in an attempt to limit the effect of disturbances on those states. To exclude

certain states from DAC design, the elements in the $B_{d,\mathrm{NR}}$ matrix that correspond to the selected states must be set to zero (example given in §4.5.1).

Another challenge when implementing a DAC is the choice of disturbance waveform model. Choosing a simple model may not accurately represent the actual disturbance but is computationally simple and only adds a few disturbance states $\underline{z}$. Conversely, using a complex waveform model will increase the number of disturbance states which may render the disturbance estimator unobservable. In such cases, increasing the turbine model fidelity or directly measuring some of the input disturbances (if possible) may resolve this issue.

4.5 Wind Speed Disturbance Rejection

For floating wind turbines, two types of disturbances are considered: change in horizontal hub-height wind speed and change in resultant pitching moment due to incident waves. Minimising the effects of wind speed fluctuations is discussed in this section. Wave disturbance rejection is discussed in Chapter 10.

Recall that the DAC design is based on a linearised state-space model about a chosen operating point. Linearisation also means that the disturbance input is wind speed perturbation about that operating point. Therefore, in an ideal case, the DAC cancels the effects of any wind speed fluctuations about the designed wind speed (operating point). For simplicity, a step change waveform model ($\dot{u}_d = 0$) is used for wind speed perturbations whose parameters are given by equation (4.26).

$$\text{step input} \begin{cases} \Gamma = 0 \\ \Theta = 1 \end{cases} \tag{4.26}$$

Because the disturbance estimator in this case uses state measurements to estimate the wind disturbances, the overall effect of a step waveform model with the disturbance estimator is essentially similar to an additional integral term to the SFC. However, the DAC formulation used in this chapter allows for more complicated waveform models to be used for disturbance rejection; e.g. Wright [35] used a periodic waveform model to reject the effects of wind shear.

To demonstrate that the DAC is able to reject wind speed perturbations, the DAC is compared to the SFC in a simple test case similar to what Wright [35] uses to prove that his DAC implementation cancels the effects of wind speed perturbations. The simulation set up and parameters are as follows:

- Single DOF nonlinear simulation. Only the generator/rotor DOF is enabled thereby removing all bias that can come from coupling between turbine modes.
- Step incident wind with no wind shear or turbulence. The wind speed is varied between 15 m/s to 22 m/s (well into the above rated wind speed region) in a step-like manner every 40 seconds.

- The DAC and SFC are designed based on a state-space model linearised at 18 m/s wind speed. The SFC and state feedback part of the DAC are identical.
- The system is simulated with FSFB for system and disturbance states – without a disturbance estimator (i.e. with measured hub-height wind speed).
- The SFC part is designed without the integrator effect. A state-space controller has no explicit integrator term. However, integral action can be achieved by including the integral of the state to be regulated as an additional system state. For example, to have an integral action to regulate the rotor speed, the rotor azimuth is included in the controller design since the azimuth angle is the integral of the rotor speed. Therefore, driving that state (change in azimuth angle $\Delta\psi$) to zero is similar to driving the integral error to zero. Integral action forces the system states to be driven to zero, even in the presence of disturbances, which is desirable. However, the purpose is to show that the disturbance accommodating part is rejecting the disturbances and not the integral action. The disturbance accommodating action is similar to the integral action to disturbances only but without the delay.

Figure 4.2 shows the rotor speed regulation (the only objective) for the two simulated controllers (SFC and DAC) under changing external disturbances – wind speed perturbations. Results clearly show that the DAC successfully rejected the effects of external disturbances by maintaining a relatively constant rotor speed. The SFC is unable to regulate the rotor speed to the rated without the integral action as the wind speed deviates away from the linearisation point. This clearly shows that the DAC implementation is correct and successful at minimising the effects of wind speed disturbances.

4.5.1 Collective Blade Pitch Drift

One issue exists when implementing a DAC to reject wind speed perturbation on wind turbines; collective blade pitch drifting [67]. Assuming a linear wind turbine system, the collective blade pitch commanded by the feed-forward action of the DAC to reject wind disturbances and maintain steady state is a linear function of the wind speed described by equation (4.27) where $\underline{u}^{op}$ is the actuators' collective pitch operating point. However, the collective blade pitch angle required to keep the floating wind turbine in steady state as the wind speed varies is a nonlinear function of wind speed as shown in Figure 4.3. With steady state conditions, the DAC forces the collective blade pitch away from the optimum angle as the turbine operates away from the linearisation point. The blade pitch is eventually driven back to the optimum angle by the state feedback part of the controller but after some delay due to the integral action.

$$\underline{u} = G\Delta\underline{x} + G_d\Delta\underline{z} + \underline{u}^{op} \tag{4.27}$$

A solution is to split the DAC into two components: a scheduled collective blade pitching component that follows the nonlinear optimum trajectory for rotor speed regulation and a state-

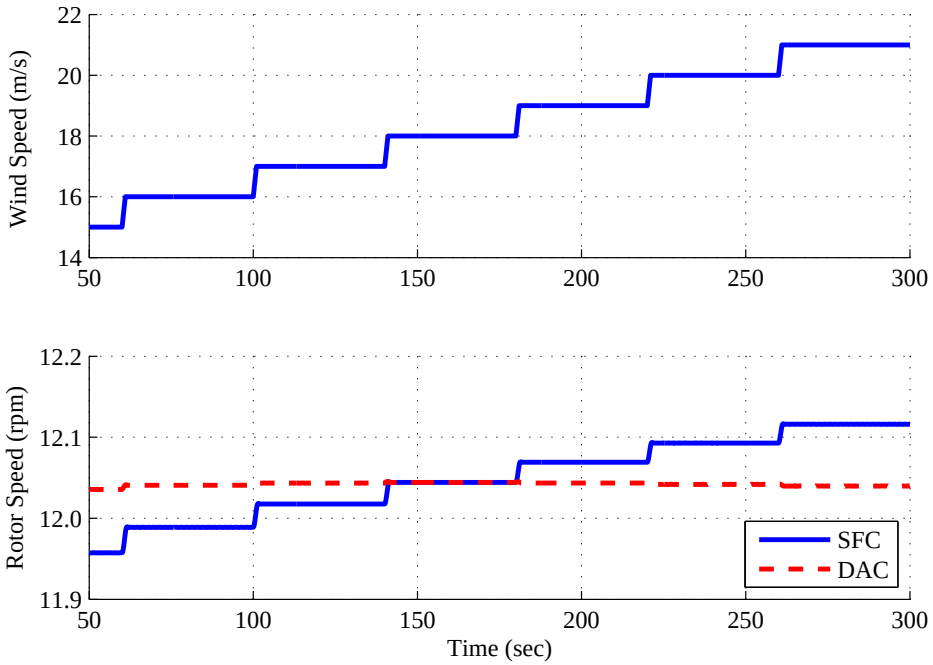

Figure 4.2: Single DOF nonlinear simulation results showing disturbance rejection by the DAC

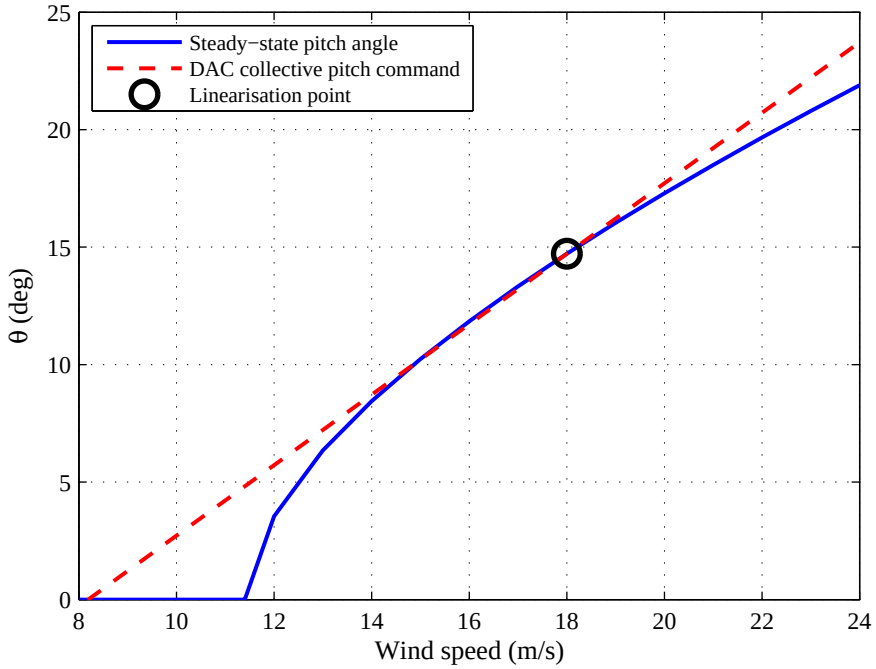

Figure 4.3: Collective blade pitch drift

space component that is designed to minimise the residual periodic effects on the remaining turbine states by only using cyclic blade pitch commands.

For MBC transformed systems, the solution can be easily implemented by just zeroing the elements in the B_{NR} matrix that corresponds to collective blade pitch θ_o since $\underline{u}_{\mathrm{NR}}$ is given by equation (4.28). This results in zero gains in elements of the disturbance minimisation gain $G_{d,\mathrm{NR}}$ that correspond to collective blade pitching. However, removing collective blade pitching results in the state-space component of the disturbance accommodating controller trying to compensate for that by increasing the gains on the remaining actuators (cosine- and sine-cyclic pitch) in an attempt to regulate all states including the rotor speed. To force the state-space part of the DAC to only remove residual periodic effects, the elements in the $B_{d,\mathrm{NR}}$ matrix that correspond to the drivetrain states must be set to zero *in addition* to any other state that periodic blade pitching has limited control authority over. This method is used in this work for disturbance accommodating controllers that reject wind speed perturbations.

$$\underline{u}_{\mathrm{NR}} = \begin{bmatrix} T_{Gen} & \theta_o & \theta_c & \theta_s \end{bmatrix}^{\mathrm{T}} \tag{4.28}$$

An alternative approach was implemented successfully in [68] where the elements in the disturbance minimisation gain, $G_{d,\mathrm{NR}}$, that correspond to collective pitch were set to zero after the controller was designed. This method produced a sub-optimal set of disturbance minimisation gain matrix as it will no longer minimised $\|BG_d + B_d\Theta\|$.

4.6 Chapter Summary

Disturbance accommodating control is a linear feed-forward add-on to the state feedback controller (described in Chapter 3) that minimises the effects of persistent disturbances. DAC requires knowledge of the disturbance inputs through direct measurements and how the disturbance inputs affect system states through the disturbance gain matrix. Where direct measurement of the disturbances is not possible, a disturbance estimator can be used to generate an estimate based measured system states and on an assumed disturbance waveform model. For wind turbines whose response is periodic, MBC transformation is utilised for time-invariant controller design in the non-rotating frame of reference.

Persistent disturbances that act on floating wind turbines include wind speed perturbations and waves. For wind speed disturbances, a step waveform model is used and is shown to be able to mitigate the effects of changes in the wind speed away from the linearisation point. However, due to the nonlinear nature of the wind turbine, DAC for wind tends to cause the collective blade pitch angle to drift away from the optimum pitch angle when the turbine is operating away from the linearisation point. This limitation is resolved by splitting the DAC into two components: a scheduled collective blade pitch angle for rotor speed regulation and cyclic actuation to remove residual effects of the wind speed on other turbine states via state-space implementation.

5

Modelling, Simulation, and Analysis Tools

Contents

5.1 Wind Turbine Modelling and Simulation Tools **55**
5.2 5MW Wind Turbine Model **60**
5.3 The IEC 61400-3 Standard **61**
5.4 Performance Metrics **62**
5.5 Simulation and Comparison Set Up **64**
5.6 Weibull Scaling **65**
5.7 Chapter Summary **68**

With floating wind turbines the simulation tool and its model must take into account the additional 6 DOFs (platform surge, way, heave, roll, pitch, and yaw) brought by the lack of rigid foundations. These 6 DOFs cannot be approximated by existing flexibilities in the modelled onshore wind turbines as they exhibit larger motion envelope, last for longer periods, and are independent of each other. Therefore, special offshore models and simulators are required. Many new simulation tools and modified existing ones are beginning to accommodate these additional 6 DOFs. This chapter mainly deals with the simulation tools, simulation conditions, and performance metrics used to obtain the results described in subsequent chapters.

5.1 Wind Turbine Modelling and Simulation Tools

As mentioned in Chapter 1, results presented in this work depend on computer simulations. Therefore, suitable simulation tools must be chosen to allow for reasonable high-fidelity simulations on floating offshore wind turbines.

Modelling the flexibilities of the wind turbine components becomes more critical as the size of the wind turbine increases. Furthermore, the interactions between the aerodynamics, hydrodynamics and structural dynamics for such large machines need to be modelled and taken into account. Several wind turbine simulation tools exist and they vary in their modelling approach, model fidelity, user customisation, interfacing capability with other software, etc.; Table 5.1 summarises the simulation tools that can accommodate additional DOFs of floating wind turbines.

The Offshore Code Comparison Collaboration (OC3) project [75] compared the simulation results of several simulation codes across four different phases. Phase IV of the OC3 project dealt with comparing simulation codes for floating wind turbines (Table 5.1) [69]. To summarise, the design codes compared quite well with minor differences attributed to modelling approach and fidelity.

FAST (Fatigue, Aerodynamics, Structures and Turbulence) was chosen as the simulation tool for this study for two simple reasons. First, at the start of this work, it was readily available and the first floating model of the barge in FAST format was kindly provided by Dr. Jason Jonkman at the National Renewable Energy Laboratory (NREL). Second, it was the only readily available simulation code out of those listed in Table 5.1 that allowed for interfacing with MATLAB® Simulink® (referred to hereafter as Simulink) for controller implementation.

5.1.1 FAST Simulation Code

FAST is a freely available design code developed by NREL [36]. It is of moderate complexity developed to analyse the structural dynamics of horizontal axis wind turbines. FAST models the tower, blades and the drivetrain as flexible elements and uses bending modeshapes for the analysis [13,36]. Each blade has two flapwise and one edgewise bending modes. The tower has two fore-aft and two side-side bending modes. The drivetrain flexibility is modelled through a linear spring and a damper for the low speed shaft. The remaining elements of the wind turbine (nacelle and hub) are modelled as rigid bodies. The fidelity of the model can be set by selecting which degrees of freedom are to be enabled in the nonlinear model.

FAST can also provide a linearised representation of the turbine's nonlinear model at specified trim conditions. The linearised *periodic* (i.e. time-varying) state space model is given by equations (5.1) and (5.2). Dealing with periodic models is discussed in § 3.1 on page 30.

$$\Delta\dot{\underline{x}} = A(\psi)\,\Delta\underline{x} + B(\psi)\,\Delta\underline{u} + B_d(\psi)\,\Delta\underline{u}_d \tag{5.1}$$

$$\Delta\underline{y} = C(\psi)\,\Delta\underline{x} + D(\psi)\,\Delta\underline{u} + D_d(\psi)\,\Delta\underline{u}_d \tag{5.2}$$

In addition to simulating a wind turbine, FAST allows for a control system to be integrated with the simulation environment. The wind turbine actuators (blade pitch, generator torque, and yaw drive) can be controlled either via a user specified control algorithm through a dynamic link library (DLL) file or through interfacing with Simulnik. The Simulink/FAST interface option is selected to allow for custom and complex controllers to be developed quickly and

Table 5.1: Floating wind turbine simulation codes (adapted from [69])

Code Name	Code Developer	OC3 Participant	Aerodynamics	Hydrodynamics	Control System (Servo)	Structural Dynamics (Elastic)
FAST [36]	NREL	NREL + POSTECH	(BEM or GDW) + DS	Airy^{+} + ME, Airy + PF + ME	DLL, UD, SM	Turbine: FEM^{P} + (Modal / MBS), Moorings: QSCE
Bladed [70]	GH	GH	(BEM or GDW) + DS	(Airy^{+} or Stream) + ME	DLL	Turbine: FEM^{P} + (Modal / MBS), Moorings: UDFD
ADAMS [71]	MSC + NREL + LUH	NREL + LUH	(BEM or GDW) + DS	Airy^{+} + ME, Airy + PF + ME	DLL, UD	Turbine: MBS Moorings: QSCE, UDFD
HAWC2 [72]	Risø - DTU	Risø - DTU	(BEM or GDW) + DS	Airy + ME	DLL, UD, SM	Turbine: MBS / FEM, Moorings: UDFD
3Dfloat	IFE - UMB	IFE - UMB	(BEM or GDW)	Airy + ME	UD	Turbine: FEM, Moorings: FEM, UDFD
SIMO [73]	MARINTEK	MARINTEK	BEM	Airy + PF + ME	DLL	Turbine: MBS, Moorings: QSCE, MSB
SESAM / DeepC [74]	DNV	Acciona Energia + NTNU	None	Airy^{+} + ME, Airy + PF + ME	None	Turbine: MBS, Moorings: QSCE, FEM

Legend:

Airy^{+}	Airy wave theory, $^{+}$with free surface corrections	MBS	multibody-dynamics formulation
		ME	Morison's equation
BEM	blade-element / momentum	MSC	MSC Software Corporation
DLL	external dynamic link library	NREL	National Renewable Energy Laboratory
DNV	Det Norsk Veritas	NTNU	the Norwegian University of Science and Technology
DS	dynamic stall	PF	linear potential flow with radiation and diffraction
DTU	Technical University of Denmark	POSTECH	Pohang University of Science and Technology
FEM^{P}	finite-element method ^{P}for mode processing only	QSCE	quasi-static catenary equations
		SM	interface to Simulink® with MATLAB®
GDW	generalised dynamic wake	UD	user-defined subroutines available
GH	Garrad Hassan & Partners Ltd.	UDFD	implementation through user-defined force-displacement relationships
IFE	Institute for Energy Technology		
LUH	Leibniz University of Hannover	UMB	the Norwegian University of Life Sciences

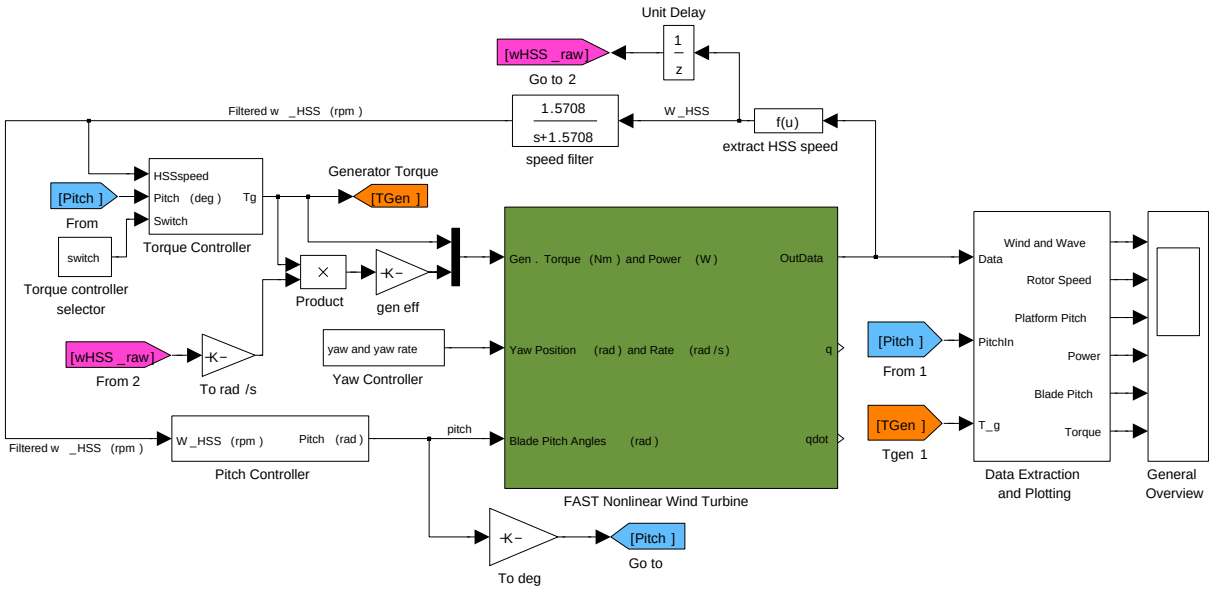

Figure 5.1: Baseline controller model showing Simulink/FAST interface

utilise MATLAB tools for control design. Figure 5.1 shows an example Simulink model where a Gain Scheduled Proportional-Integral (GSPI) controller (described in § 2.1 on page 19) is implemented using the Simulink/ FAST interface.

FAST and Floating Wind Turbines

Since 2006, Jonkman *et al.* [13, 76] have modified the standard version of FAST to include a hydrodynamics module to account for floating platform dynamics. The modified FAST now includes a hydrodynamics and a quasi-static mooring modules; the structure is shown in Figure 5.2. The hydrodynamics module, `HydroDyn`, uses linear/Airy wave theory to simplify the hydrodynamics problem into three separate components: hydrostatics, radiation, and diffraction. The quasi-static mooring module treats the system in equilibrium at every computation time to calculate the forces in the mooring lines. The mooring line module accounts for "the apparent weight in fluid, elastic stretching, and seabed friction of each line" [76]. It also accounts for the nonlinear geometric restoring force of the complete mooring system on the floating platform.

Hydrodynamics Module Assumptions

The onshore version of FAST coupled with AeroDyn have been certified by Germanischer Lloyd WindEnergie GmbH for use by the industry for wind turbine certification [78]. Since testing of full scale prototypes of floating wind turbines have just started, certification of FAST with HydroDyn and other similar codes is not yet possible. However, the OC3 project gives an indication that the models developed are acceptable. Therefore, it is important to know the limitations and assumptions of the simulation tool and keep it in mind when interpreting the simulation results. The newly developed offshore module has the following assumptions [13]:

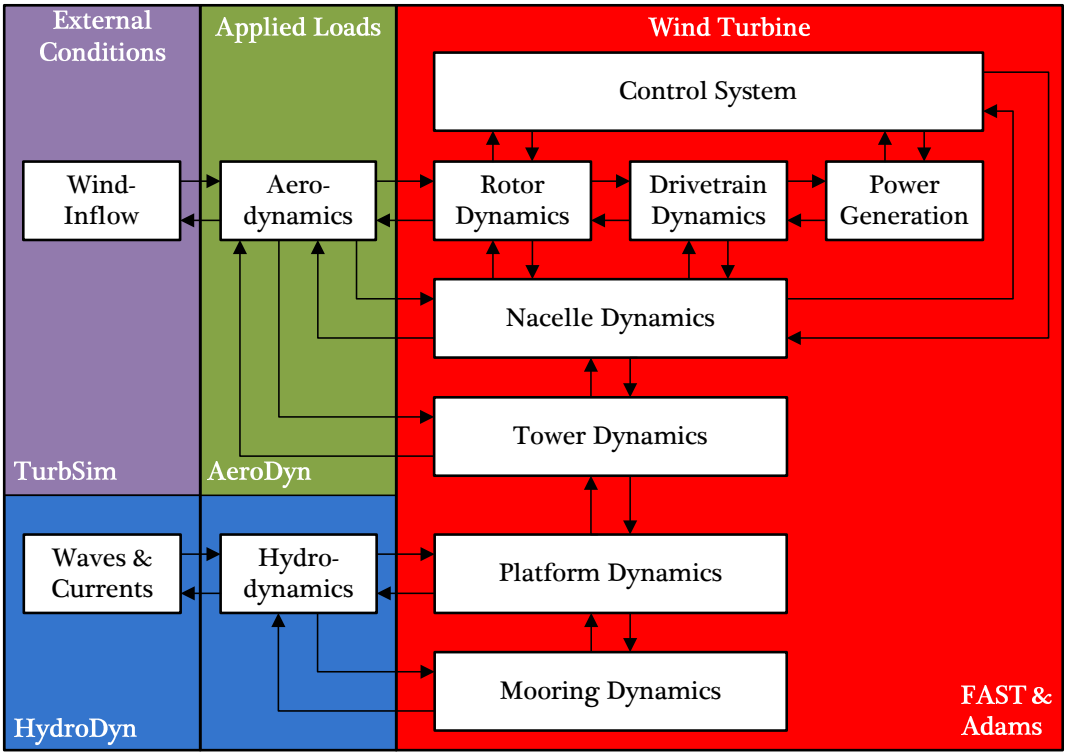

Figure 5.2: Offshore FAST structure (adapted from [77])

- The platform has 6 DOFs (surge, sway, heave, roll, pitch, and yaw) but the three rotational DOFs (roll, pitch, and yaw) have small angles. The effects of this assumption are not considered critical for angles smaller than 20°.
- The floating platform is modelled as a rigid body.
- The tower is perpendicular to the platform and is cantilevered.
- The inertia (excluding the wind turbine) and the centre of buoyancy lie on the centreline of the undeflected tower.
- Mooring lines do not have bending stiffness.
- The hydrodynamic forces are calculated based on linearisation of the hydrodynamic problem. Linearisation has the following consequences:
  - Wave heights are much smaller than wave lengths; a reasonable assumption in deep water. This allows the use of very simple wave kinematics equations and does not require the modelling of breaking or steep waves.
  - Translational displacements of the platform are small compared to the platform size (characteristic body length); however, this does not mean that the characteristic length of the body has to be small when compared to the wavelength. This allows the hydrodynamic problem to be split into 3 separate problems: radiation, scattering, and hydrostatics.

  - The linearisation of the hydrodynamics ignores:
    * the nonlinear and high order effects that are used to calculate the loads on the instantaneous wetted area; this is important for bodies with large displacements relative to their characteristic length.
    * second order mean- and slow-drift forces caused by multiple incident waves of varying frequencies. In some situations, these second order effects are important for platforms with small draft, large waterplane area, and a mooring system that does not resist motions in the surge and sway directions. This is relevant to a barge platform concept.
    * second order frequency effects on the platform caused by multiple incident waves of varying frequencies. In some situations, this second order effect can cause ringing in platforms with mooring lines that have high resistance to heave motion. This is relevant to a TLP concept.

- Loading from sea ice or floating debris is ignored.

5.2 5MW Wind Turbine Model

For this work, a single 5 MW wind turbine will be used for simulation on each of the three floating platforms. This wind turbine, commonly known as the "NREL 5 MW wind turbine", is a fictitious turbine whose properties are derived from a collection of publicly available information of similar sized wind turbines [37]. It is a three bladed upwind wind turbine with 126 m diameter rotor and 90 m hub height. Table 5.2 list all the main details about the wind turbine.

Since FAST models the system flexibilities through assumed modeshapes, the tower's modeshapes change when mounted on different platforms. This is the only change that occurs in the wind turbine properties when changing to another platform.

Table 5.2: NREL 5MW wind turbine properties

Power Rating	5 MW
Rotor orientation	Upwind
Control	Variable speed, variable pitch, active yaw
Rotor, hub diameter	126 m, 3 m
Hub height	90 m
Rated rotor, generator speed	12.1 rpm, 1173.7 rpm
Blade operation	Pitch to feather
Maximum blade pitch rate	8 deg/s
Rated generator torque	43,093 Nm
Maximum generator torque	47,402 Nm

5.3 The IEC 61400-3 Standard

The simulations are carried out in accordance with IEC 61400-3 standard [39] for DLC 1.2 – fatigue loads under normal operating conditions; these conditions are summarised in Table 5.3. The IEC 61400-3 standard is for offshore wind turbines with fixed foundations. Since no standards for floating turbines exist to date, the simulations will be carried out according to DLC 1.2 of this standard.

DLC 1.2 requires the wind and waves to be co-directional and multi-directional. However, because the platforms are axisymmetric, only one wind and wave direction is considered. Misaligned situations are covered by DLC 1.4, however, DLC 1.4 is used for ultimate load analysis and is outside the scope of this work. The IEC standard specifies for DLC 1.2 that a joint probability distribution for the wind speed, significant wave height, and wave period must be used. However, due to the unavailability of full site specific data, DLC 1.1 condition of using the expected significant wave height at given wind speed range is implemented.

Because the above rated wind speed region is the main focus of this study, the range of wind speed bins for DLC analysis is limited between 15 m/s and 24 m/s in 1 m/s speed increments. The IEC standard requires six 600-second turbulent wind and irregular waves with different random seeds to be used for each wind speed bin [79].

The wave conditions are selected based on the same reference site used by Jonkman [32] located north-east of Scotland. In the data for that site, there exists a single significant wave height and a range of wave periods for a corresponding average wind speed. In this work, the wave periods in each wind speed bin linearly range from the minimum to the maximum range of periods for that site that do not violate the assumptions of linear wave theory used by FAST; the use of linear wave theory is a reasonable assumption in deep water [39]. According to the IEC 61400-3 standard, for the linear wave theory to be applied in deep water, equation (5.3) must be satisfied where H is the wave height, T_w is the wave period, and g is the acceleration due to gravity.

$$\frac{H}{gT_w^2} \leq 0.002 \tag{5.3}$$

Full field stochastic wind conditions are generated using TurbSim [80] while the irregular stochastic waves are generated using HydroDyn. Appendix C lists the parameters used to generate these stochastic conditions for each DLC.

Table 5.3: DLC 1.2 conditions summary

DLC	Wind Condition	Waves	Wind and Wave Directionality	Sea Currents
1.2	Normal turbulence model $V_{in} < V_{hub} < V_{out}$	Normal sea state	Co-directional and multi-directional	No currents

V_{in} =cut-in wind speed; V_{hub} = hub-height wind speed; V_{out} = cut-out wind speed

5.4 Performance Metrics

To perform a DLC analysis, each controller is simulated in 60 different ten-minute simulations that span the above rated wind speed region. To quantify the performance of the controllers, 14 performance metrics are used to monitor key wind turbine components. Some of these metrics involve the calculation of a root mean square (RMS) or a fatigue damage equivalent load (DEL). Fatigue DELs are used as a metric to replace the stochastic loads on a component by a periodic load with a calculated magnitude at a given frequency (1 Hz in this work).

The performance metrics/indices are then averaged across their corresponding wind speed bin as well as averaged across all the simulations. However, a real wind turbine does not spend an equal amount of time in each wind speed bin. Hence, weighted averaging using a Weibull distribution (discussed in §5.6) for the weighting/scaling factors is used for the overall averaged performance metrics.

The performance metrics can broadly be grouped into three categories. The categories and a brief description of each performance index are given below:

Power and speed regulation, and actuator usage

1. RMS of the generator power error (from rated power) in kW. The smaller the error the better the power regulation and hence increased power quality.
2. RMS of the rotor speed error (from rated rotor speed) in rpm. The lower the value the better the rotor speed regulation.
3. Maximum RMS of the blade pitch rates in degrees per second (deg/s). This is used to indicate the level of actuator usage. A high value means high blade pitch actuator usage.

Fatigue damage equivalent loads of key components

4. Blade root flapwise bending fatigue DEL in kNm.
5. Blade root edgewise bending fatigue DEL in kNm.
6. Tower base Fore-Aft (FA) bending fatigue DEL in kNm.
7. Tower base Side-Side (SS) bending fatigue DEL in kNm.
8. Low Speed Shaft (LSS) torsion fatigue DEL in kNm.

Platform motions

9. Floating platform RMS roll in degrees. This is used as a measure for the platform rotation about its roll axis; this should be kept as low as possible to reduce tower side-to-side bending loads.

10. Floating platform RMS pitch in degrees. This is used as a measure for the platform rotation about its pitch axis; this should be kept as low as possible to reduce tower fore-aft bending loads.

11. Floating platform RMS yaw in degrees. This is used as a measure for the platform rotation about its yaw axis; this should be kept as low as possible to reduce rotor yaw error that will result in reducing the amount of captured power and increase asymmetric aerodynamic loading.

12. Floating platform RMS roll rate in deg/s. Reducing platform rolling, pitching, and yawing velocities will reduce their respective motion envelope thus reducing the loads associated with each motion direction.

13. Floating platform RMS pitch rate in deg/s.

14. Floating platform RMS yaw rate in deg/s.

With the fatigue load metrics (items 4 – 8), it is assumed that the turbine is designed such that all the main components fail roughly at the same time placing equal importance on each fatigue load metric. However, from the control objective point of view, the 14 metrics listed above are not considered equal when assessing the overall performance of each controller. Table 5.4 lists the metrics according to their relative importance.

Table 5.4: Relative importance of metrics in determining the overall performance of a controller

Level of Importance	Metrics
Primary	1, 2, 6, and 7
Secondary	3, 8, 10, and 13
Tertiary	4, 5, 9, 11, 12, 14

The results presented in subsequent chapters are normalised relative to a baseline controller. One might argue that this is an unfair comparison between the multi-objective and the Baseline controllers. However, in a noise-free environment, the baseline controller is essentially a single state feedback controller since the output/measurement of the baseline controller is a system state. Furthermore, the purpose of this comparison is not to compare these controllers against the Baseline controller. Instead, the comparison is used as a yardstick for measuring the level of improvement SFC and DAC bring to each of the floating platforms.

With all the performance metrics except for RMS blade pitch rate, the objective is to have a value of 1 or smaller indicating better or improved performance relative to the baseline controller. At this stage, dealing with the absolute values of these performance metrics in terms of detailed design or to assess whether the blades or tower are strong enough is outside the scope of this work.

Due to the range of simulated wind speeds, a single weighted average for each metric is not adequate to represent the full behaviour of the floating wind turbine. Therefore, trends of the

Table 5.5: Types of observed performance trends

Short Name	Description
Constant	A relatively constant level of performance across all wind speed bins indicating the robustness of the controller to maintain the same relative performance to the Gain Scheduled Baseline controller as the turbine operates away from the linearisation point.
Increasing	An upward or positive sloping trend with increasing wind speed. Taking the performance at 18 m/s as the starting point, a metric is better regulated at lower wind speeds and worse otherwise.
Decreasing	A downward or negative sloping trend with increasing wind speed. Taking the performance at 18 m/s as the starting point, a metric is better regulated at higher wind speeds and worse otherwise.
Parabolic	A parabolic-type function with the minimum located around the linearisation point. The parabolic-type trend indicates a metrics is best regulated around the linearisation point but is worse off away in either direction.

averaged and normalised performance metrics across wind speed bins are also discussed in subsequent chapters. Table 5.5 lists the types of trends observed; these are referred to using their short name.

In addition to the performance metrics, other metrics (such as maximum blade pitch rate) and the time series response of each simulation are inspected for unusual or undesirable behaviour such as prolonged or frequent actuator saturation.

5.5 Simulation and Comparison Set Up

Design load case simulations are carried out on 10 different controllers on four different platforms; a total of 600 DLC simulations. The simulations are carried out using FAST with HydroDyn with all 22 DOFs enabled using turbulent full field wind and irregular waves. The turbine yaw DOF is locked since no active yaw control is needed as the mean wind direction remains unchanged. Yaw error correction is not part of DLC 1.2 and is outside the scope of this work.

The performance metrics described above are used to evaluate the performance of the SFC and DAC relative to the Baseline controller. Two types of comparisons (summarised in Table 5.6) are made:

1. Comparing the performance of the SFC and DAC relative to the Baseline controller *on the same floating platform*; this type of comparison is made on the three platforms and discussed in chapters 6 – 8. The purpose of this comparison is to evaluate whether adding the disturbance minimisation component to the SFC has a measurable impact. This type of comparison also allows for identifying the benefits of individual over collective blade pitching and multi-objective over single-objective control on floating wind turbines.

2. Comparing the performance of the Baseline controller and the best performing multi-objective controller (SFC or DAC) on each platform relative to a Baseline controller *on an*

onshore wind turbine (5MW NREL onshore wind turbine). The purpose of this comparison is to allow for comparing the dynamic performance between the floating platforms in terms of power regulation and fatigue damage equivalent loads. These comparisons are made in Chapter 9.

Table 5.6: Simulated controllers' comparison summary

Chapter	Baseline		Controllers to be compared	Platform(s)
	Platform	Controller		
6	Barge	GSPI	SFC, DAC	Barge
7	TLP	GSPI	SFC, DAC	TLP
8	Spar–buoy	GSPI	SFC, DAC	Spar–buoy
9	Onshore	GSPI	GSPI, SFC, DAC	Barge, TLP, Spar–buoy

5.6 Weibull Scaling

As discussed in the previous section, a weighted average is used to obtain the overall averaged performance metrics such that it accounts for the wind speed probability distribution at a specific site. The overall average for performance metric $\overline{p}$ is given by equation (5.4) where s_i and p_i are the scaling factor and averaged performance metric for the ith wind speed bin respectively and n_{bins} is the number of wind speed bins.

$$\overline{p} = \frac{\sum_{i=1}^{n_{bins}} s_i p_i}{\sum_{i=1}^{n_{bins}} s_i} \tag{5.4}$$

The Weibull distribution is considered a good fit for annual mean wind speed distribution [29]. However, using data collected from 178 ocean buoys distributed around North America over several years, Morgan et. al. [81] show that the widely accepted 2-parameter Weibull distribution provides a poor fit for these offshore sites when compared to other, higher order distributions. However, for the purposes of providing weighted averages for the performance metrics, the 2-parameter Weibull distribution is considered adequate. What follows is a description of the approach used to obtain the scaling factors for each wind speed bin.

Using the same notation in [29], the Weibull distribution takes the form given by equation (5.5) where $F(U)$ is the fraction of time for which the hourly mean wind speed exceeds U , c is the scaling parameter, and k is the shape factor. The Weibull distribution's shape resembles the shape shown in Figure 5.3 for certain values of c, and k typical for annual wind speed distribution.

$$F(U) = \exp\left(-(U/c)^k\right) \tag{5.5}$$

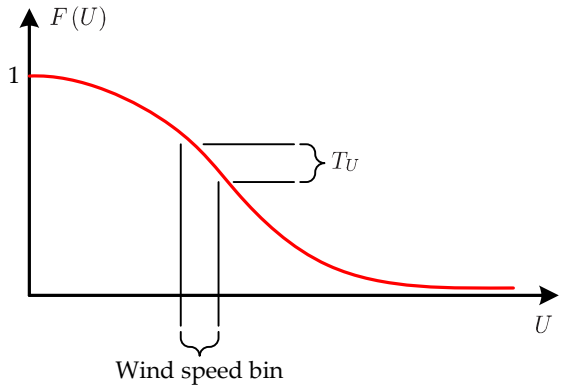

Figure 5.3: The Weibull distribution

Given a wind speed bin U whose wind speeds range from $U - 0.5\,\mathrm{m/s}$ to $U + 0.5\,\mathrm{m/s}$, the percentage time of the year the wind turbine spends in that wind speed bin T_U is given by equation (5.6).

$$T_U = (F(U - 0.5) - F(U + 0.5)) \times 100 \tag{5.6}$$

The Weibull scaling factors s_i from equation (5.4) are obtained by normalising T_U values by its maximum value giving the most weight (of 1) to the dominant wind speed bin. Figure 5.4 shows how values of T_U and the scaling factors change for each wind speed bin for selected Weibull distribution parameters.

The above approach requires knowledge of the site specific Weibull parameters c, and k at the turbine's hub height. However, site measurements are often given at the measurement mast height and not the wind turbine's hub height. Therefore, given c, and k at a reference height h_{ref}, the mean annual wind speed $\overline{U}$ is given by equation (5.7) [29].

$$\overline{U} = \int_0^\infty U f(U)\, dU \tag{5.7}$$

where

$$f(U) = k\frac{U^{k-1}}{c^k} \exp\left(-(U/c)^k\right)$$

Equation (5.7) can be used to calculate the annual mean wind speed at the reference height $\overline{U}_{ref}$ if the measured mean wind speed is not given. That reference wind speed can then be scaled to any height h according to the vertical shear law given by equation (5.8) where α is the vertical shear exponent; for offshore sites α is 0.14 [39].

$$\overline{U}(h) = \overline{U}_{ref}\left(\frac{h}{h_{ref}}\right)^{\alpha} \tag{5.8}$$

Assuming the Weibull shape factor k remains roughly the same between the measurement

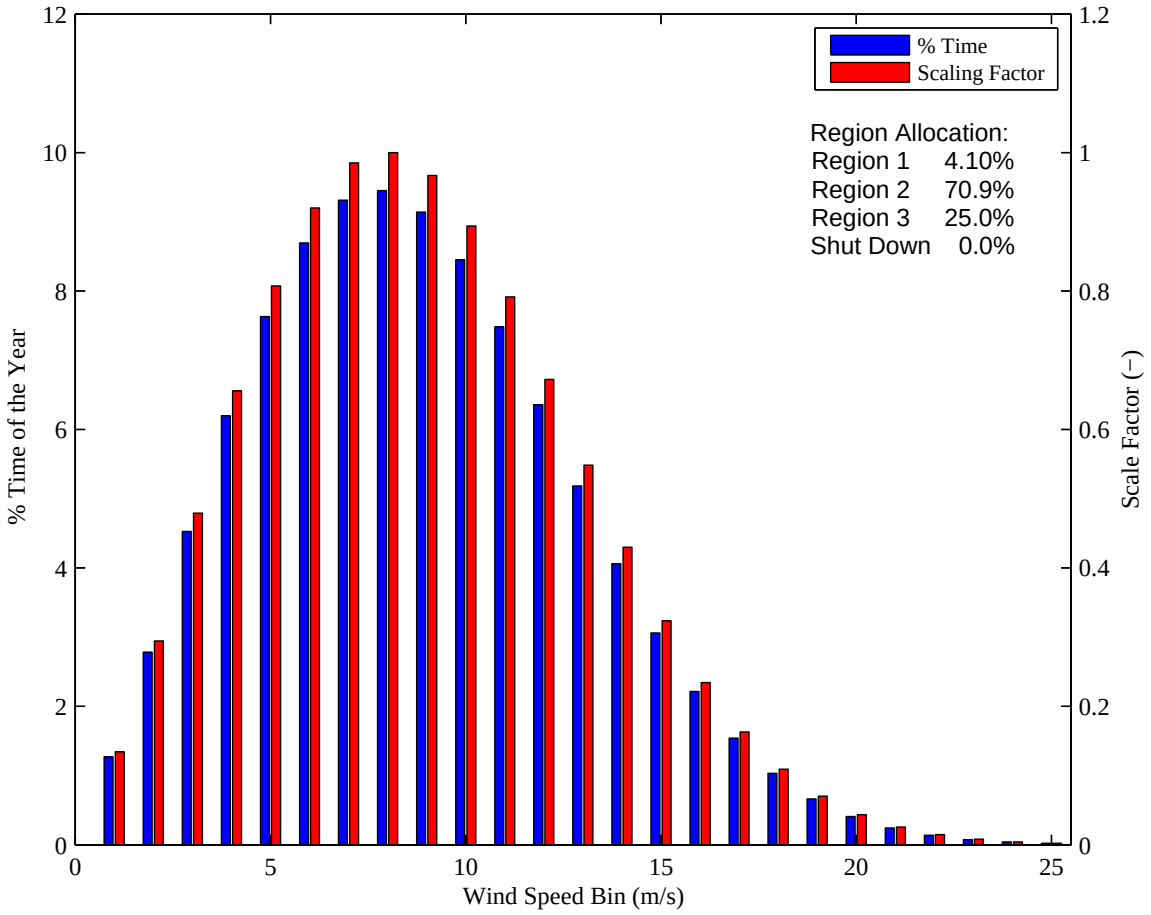

Figure 5.4: Weibull scaling factors

height and the hub height, the Weibull shape factor c can be calculated using the newly calculated mean hub height wind speed and equation (5.9) [29] where $\Gamma()$ is the gamma function and not to be confused with Γ which is the disturbance states matrix (equation (4.4)). The gamma function can be calculated using equation (5.10) [82].

$$\overline{U} = c\Gamma\left(1+\frac{1}{k}\right) \tag{5.9}$$

$$\Gamma(a) = \int_0^\infty t^{a-1}\exp(-t)\,dt \tag{5.10}$$

The Weibull parameters in this work are selected based on real data from Vindeby offshore wind farm in Denmark from 1993 to 1997 [83] because Weibull parameters for the chosen site in Scotland are not available. the selected Weibull parameters are $k = 2.3$, $c = 9.1$, and $\overline{U} = 8.1\,\mathrm{m/s}$ at a reference height of 48 m. These are then scaled to a hub height of 90 m where the resultant Weibull distribution is shown in Figure 5.4. The wind speed region calculations in Figure 5.4 are based on the wind speed ranges defined by Jonkman [32] and given by Table 5.7; these wind speed ranges are only used to calculate the time a wind turbine spends in each region.

Table 5.7: Wind speed region limits

Region	Wind Speed Range (m/s)
1	$0 \leqslant U < 3$
2	$3 \leqslant U < 11.4$
3	$11.4 \leqslant U < 25$
Shutdown	$U \geqslant 25$

5.7 Chapter Summary

For floating wind turbine simulation and design codes, they must take into account the additional 6 DOFs brought by the lack of rigid foundations as well as the nonlinear interaction with the waves. Several simulation tools have been developed and compared to each other in the Offshore Code Collaboration (OC3) project. However, none have been verified against real field data as the first full scale prototypes are still being tested. FAST with HydroDyn is selected to be the simulation tool in conjunction with MATLAB and Simulink.

The controllers described in previous chapters are simulated according to DLC 1.2 of the IEC–61400–3 standard for fixed offshore wind turbines since no standards for floating wind turbines are available to date. DLC 1.2 is designed to test for fatigue loads under normal operating conditions. To perform DLC analysis, each controller must be simulated in 60 different simulations across 10 different wind speed bins chosen to span the operational range of the above rated wind speed region.

To analyse the large volume of simulation results, 14 performance metrics are used to quantify the performance of the floating wind turbines in terms power and rotor speed regulation, fatigue damage equivalent loads of key turbine components, and platform motions. These metrics are averaged over each wind speed bin as well as over the entire range selected of wind speeds. The overall average is calculated using a weighted average whose weights are calculated based on a Weibull distribution of a selected offshore site. The Weibull scaling factors are used to weigh each wind speed bin according to the time the turbine is expected to operate in that wind speed in a year.

DLC simulations are carried out for 10 different controllers on four different platforms. The simulations are carried out using FAST with HydroDyn with all 22 DOFs enabled using turbulent full field wind and irregular waves. The turbine yaw DOF is locked since no active yaw control is needed because the mean wind direction remains unchanged.

Simulation results comparing the developed controllers on each floating platforms are presented in chapters 6 – 8. The platforms are compared to each other using results relative to an onshore wind turbine in Chapter 9.

6

The Barge Platform

Contents

6.1 The Barge Platform **70**
6.2 Controller Design **71**
6.3 Offshore DLC Results **75**
6.4 Chapter Summary **78**

Results from quantitative analyses using the state feedback and disturbance accommodating controllers described in chapters 3 and 4 on the barge platform are described in this chapter. The results obtained from running an extensive set of simulations described in Chapter 5 are normalised relative to a gain scheduled collective pitch PI controller. The normalised results are used to compare the impact of controller features such as multiple objectives, individual blade pitching, and disturbance accommodation on the barge platform. In addition to the simulation results, the order of the state-space model required for control design on floating platforms is specified based on physical insight into the floating system.

Although detailed and high-fidelity simulation results for the floating platforms have been published [32,38], the controllers used were single objective and utilised collective blade pitching. Therefore, the results presented in this chapter and chapters 7 and 8 are rather unique in terms of assessing how multi-objective controllers utilising individual blade pitching will behave on these floating platforms.

6.1 The Barge Platform

The barge platform (Figure 6.1) is originally designed by Willem Vijfhuizen at the universities of Glasgow and Strathclyde [24] and later modified by Jason Jonkman at the National Renewable Energy Laboratory (NREL) [32]. It is a simple rectangular platform that utilises buoyancy due to its large water-plane area to maintain stability. Its shallow draft design makes it independent of the minimum water depth required for installation. It is designed to be cost effective and easy to install on site. However, the barge is very sensitive to incident waves since most of the structure is above the water; that is, it rides the waves rather than pass through them. The main properties of the barge platform studied in this work are listed in Table 6.1.

The original design of the barge platform had an oscillating water column incorporated into the platform design to capture energy from the waves and perhaps add more damping to the system [24]. However, this feature was not modelled in FAST and therefore excluded from the barge model. For more details on the development of the barge model, please refer to [24, 25, 32, 84].

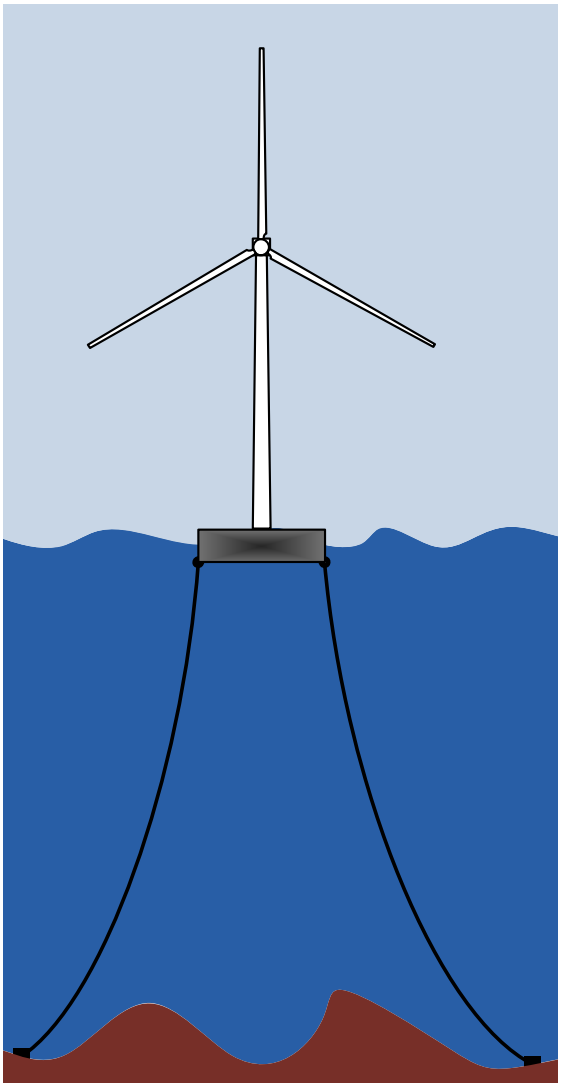

Figure 6.1: The barge platform

Table 6.1: Barge platform properties

Width	40 m
Length	40 m
Height	10 m
Draft	4 m
Water depth	150 m
Platform mass	5,452,330 kg

6.2 Controller Design

In this section, two issues are discussed that lead to the final controller designs on the barge platform but more importantly they define the approach used to design controllers on the other two platforms. First, the effectiveness of collective blade pitching on a multi-objective controller is evaluated. Second, coupling between platform rolling and pitching is identified that could destabilise the system.

6.2.1 Collective Blade Pitch State Feedback Control

A simple case study is used to demonstrate the effectiveness of a multi-objective controller using collective blade pitching [61]. The SFC is designed based on a 2 DOFs azimuth averaged linearised state-space model; DOFs include rotor and platform pitch. This form of the SFC is similar to the tower-top feedback loop implemented by Jonkman [32] (see § 2.1.1 on page 21 for a brief description). However, unlike the tower-top feedback controller, the SFC is able to reduce platform pitching without severely affecting rotor speed regulation (see Figure 6.2). Recall that a value of less than 1 indicates improvement relative to the Baseline controller. The results presented in Figure 6.2 are based on a single nonlinear full DOFs simulation case used to test the implementation of the CBP SFC.

Since both controllers use collective blade pitching, the physical principles used to achieve their control objectives remain the same. The difference in performance is attributed to better controller tuning and the use of constant torque control algorithm by the SFC to increase rotor speed damping in the above rated wind speed region. The SFC combines the two control objectives into a single optimal controller implementation.

A major drawback of using collective blade pitching with SFC is the issue of conflicting blade pitch commands. Adding more objectives to the control design only exacerbates the problem. Therefore, individual blade pitching is used in the final implementations of the SFC and DAC.

6.2.2 Platform Roll-Pitch Coupling

For the previous case study, Figure 6.2 shows that tower base side-side bending fatigue DEL is increased by 19%. Also, upgrading the SFC to use individual blade pitching further increases

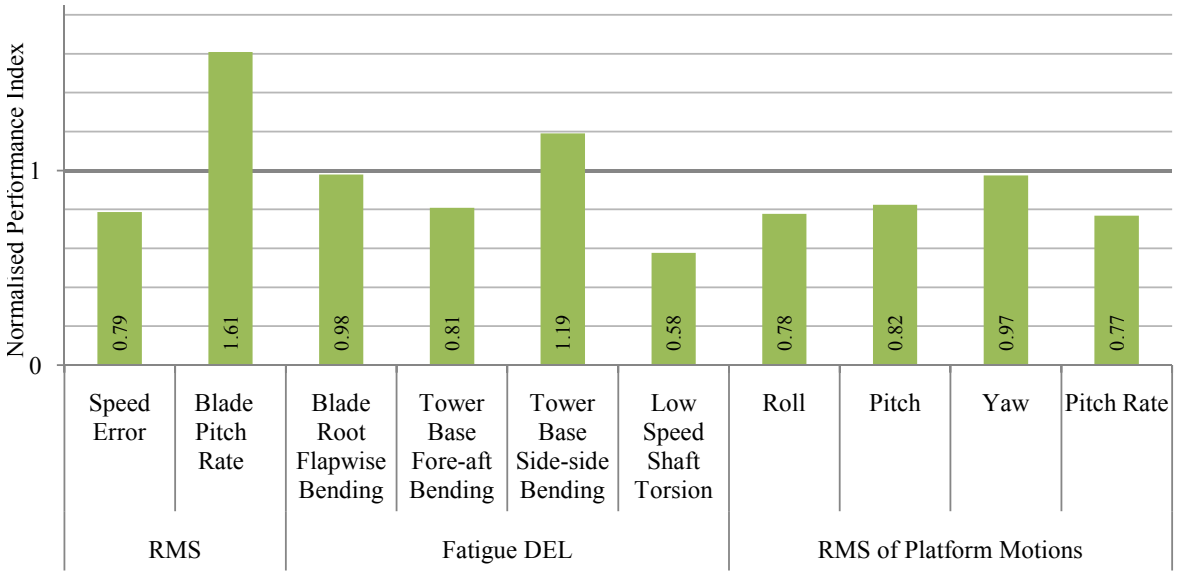

Figure 6.2: Normalised results for 2 DOFs CBP SFC relative to the Baseline controller

the tower side-side loads and platform rolling on a 2 DOFs nonlinear simulation model [61]. A similar behaviour is observed by Lackner [41] when he implemented IBP control to reduce blade loads on a floating platform (see § 2.2 on page 23).

The increase in tower base side-side bending loads is caused by a net sideways load due to an increase rotor torque load induced by the increased thrust of the rotor when regulating platform pitch motion. For a three bladed wind turbine, the aerodynamic torque generated by each blade is balanced given a uniform wind due to the blades' spatial symmetry. However, due to wind shear, rotor pre-cone, and shaft up-tilt this symmetry is broken and a net sideways load is generated.

In addition to affecting tower base side-side loading, this induced sideways load interacts with platform rolling motion which may lead to roll instability. This interaction is illustrated by examining some of the linearised turbine properties. In particular, the coupling relationship between platform roll and pitch is determined by looking at the periodic $B(\psi)$ matrix of equation (3.5); the relevant elements of that matrix are shown in Figure 6.3.

Figure 6.3 shows the effects of blade 1 pitch perturbations on the roll and pitch accelerations of the platform[7]; the zero azimuth position is when blade 1 is at the 12 o'clock position. Several interesting features can be inferred from the figure:

- The blades are most effective (most negative) at the top due to the effects of wind shear and the increased moment arm about the platform. An IBP controller utilises this effect to generate the maximum pitch restoring moment as described in §3.2.2.
- The mean effect of the blades on the rolling motion is not zero (small negative number) indicating that the collective effect of all three blades creates a rolling moment. Normally

[7]Blades 2 and 3 are 120° and 240° out of phase respectively.

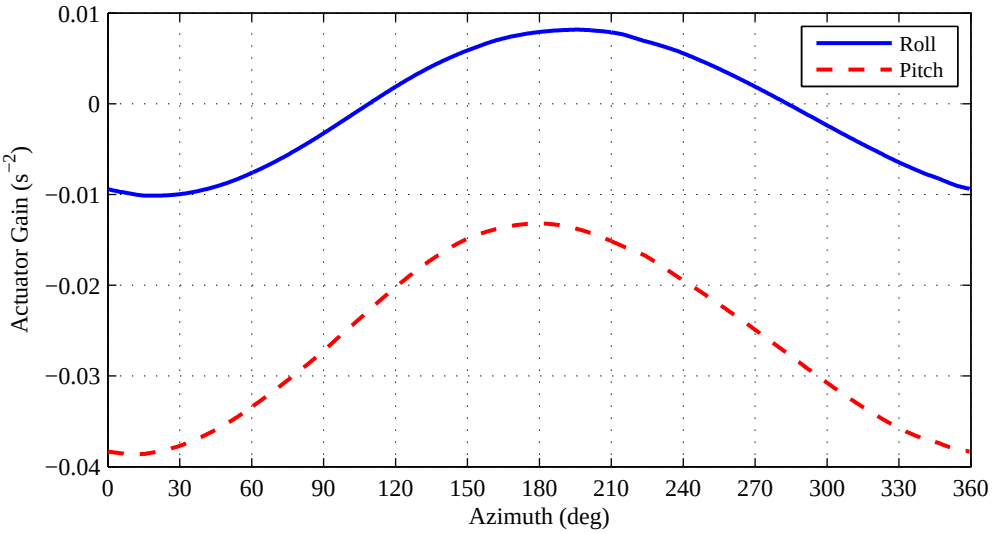

Figure 6.3: Blade 1 B matrix elements that correspond to platform roll and pitch acceleration for a 3 DOFs linearised state–space model

for a 3 bladed wind turbine the lateral loads on the rotor are balanced due to the 120° blade separation. However, wind shear, rotor pre-cone and shaft tilt angle create an imbalance and hence the net sideways force.

- The blades affect the platform roll the same way they affect platform pitch (with much less control authority) and the effect is almost in phase. Therefore, when the controller generates the restoring pitch moment it also induces a rolling moment.

All of the above observations coupled with the fact that there is little aerodynamic damping in the roll direction (compared to the pitch direction) explains the increase in rolling motion and tower side-side fatigue load. The second and third observations indicate that even a CBP controller designed to reduce platform pitch motion will generate a rolling moment (as shown in Figure 6.2); the IBP controller only amplifies the effect.

Roll Instability

Closed-loop stability analysis of the IBP SFC (designed based on a 2 DOFs linear model) on the floating platform with all the DOFs enabled results in two unstable poles. The unstable poles are determined to be those of the platform roll states using a three-step approach. First, the eigenvectors associated with the unstable poles give an indication of which states are most likely to contribute to that bending mode. With all 22 DOFs enabled and due to coupling, it is unclear if a single state is actually unstable or a coupled bending mode. For example, coupling between blade edgewise, tower side-side, and platform rolling motions allows for 10 possible states to have contributions to the eigenvector of the unstable vibrating mode. Second, the most likely unstable DOF is then included in a 3 DOFs model[8] including the rotor and platform

[8]The order of this model in subsequent stability analyses is equal to the order of the model used for controller design plus the additional unstable DOF.

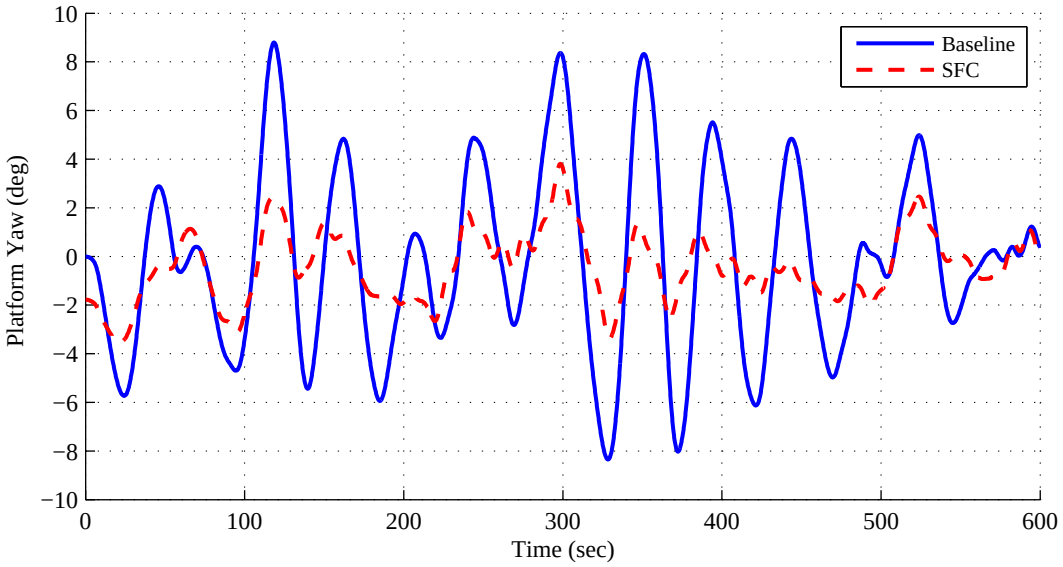

Figure 6.4: Typical platform yaw motion envelope for the barge platform

pitch DOFs where stability is assessed. The final step involves linearising the system with all the DOFs enabled *except* the unstable DOF from the second step and analysing the closed loop stability to make sure that no other coupled mode is being destabilised by the controller.

Of course, one could argue that by lowering the controller gains the system can be stabilised. However, lowering the gains to a stabilisable level makes the actual controller ineffective in terms of performance. Therefore, the roll DOF is added to the control design[9] to ensure closed loop stability for that model order around the linearisation point; full system stability is not guaranteed, however, and it has to be checked. Similarly, adding the roll DOF destabilises the first tower side-side bending mode and hence it is added to the control design. Adding a DOF that is strongly coupled to other existing DOFs in the linearised model for control design ensures that the correct coupling and natural frequencies are accounted for by the controller.

6.2.3 Final Controller Design

The final SFC is designed based on a 6 DOFs linearised model. The model includes the platform roll, pitch and yaw, first tower side-side bending mode, rotor and drivetrain twist DOFs. The drivetrain twist DOF is added to maintain or reduce the fatigue loads of the drivetrain. Due to large yaw motion experienced by the barge platform, the platform yaw DOF is added to improve overall performance [85]. Figure 6.4 shows a typical yaw motion envelope for the Baseline and State Feedback Controllers.

Controller tuning is carried out via careful selection of weighting matrices that emphasise the regulation of certain states more than others. Platform motions and velocities have the highest weighting to reduce motion and have a positive secondary effect on tower loads and power

[9]The roll DOF is added to the linearised state-space model used for control design.

regulation. The generator torque is part of the actuators used by the SFC and has a variable operating point for power regulation (§3.4.1). Of course, the tuned controller is by no means the optimum controller but its performance is deemed satisfactory during the tuning phase. Tuning is carried out using two design load cases in the 18 m/s wind speed bin (at the linearisation point).

Recall that the DAC consists of a SFC with an additional disturbance minimisation term (§4.2). Therefore, the DAC uses the same model order and weighting matrices as the SFC. To resolve the collective blade pitch drift issue discussed in §4.5.1, the column in the B_{NR} matrix that corresponds to the collective blade pitch is set to zeros and elements in the $B_{d,\mathrm{NR}}$ matrix that correspond to the drivetrain states are also set to zero.

6.3 Offshore DLC Results

In this section, simulation results from performing DLC analysis on the State Feedback and Disturbance Accommodating Controllers are compared and normalised to the Baseline controller (GSPI controller described in §2.1) on the barge platform.

6.3.1 Averaged Normalised Results

The overall averaged and normalised simulation results for both controllers relative to the Baseline controller on the barge platform are shown in Figure 6.5.

Looking at the performance of the State Feedback Controller relative to the Baseline, it can be seen that power and rotor speed regulation, and blade flapwise and edgewise bending, and low speed shaft torsion fatigue DELs are similar to that of the Baseline controller. However, tower fore-aft and side-side fatigue DELs are reduced by 33% and 51% respectively. Furthermore, platform roll, pitch, and yaw motions are reduced by 41%, 31% and 51% respectively. Platform roll, pitch, and yaw rates are reduced by 48%, 37%, and 60% respectively. These large and impressive reductions can be attributed to the multi-objective nature of the controller and most importantly to the use of individual blade pitching. Even though the tower fore-aft load is not an explicit control objective, it is noticeably reduced; this reduction is believed to be the result of the large reduction in platform pitching motion. The cost of this load reduction is the increased use of the blade pitch actuators. Blade pitching rate is increased by 103%; however, this increase does not result in blade saturation longer than 1 second at a time and, more importantly, does not increase the blade flapwise and edgewise fatigue DELs.

The Disturbance Accommodating Controller performance is almost identical to that of SFC despite an increase in blade pitch actuation. The reason for such a result is because the barge platform loads are dominated by incident waves rather than wind speed fluctuations which the DAC was designed to mitigate. Therefore, reducing the effects of wind speed perturbations has a minimal effect on overall platform behaviour.

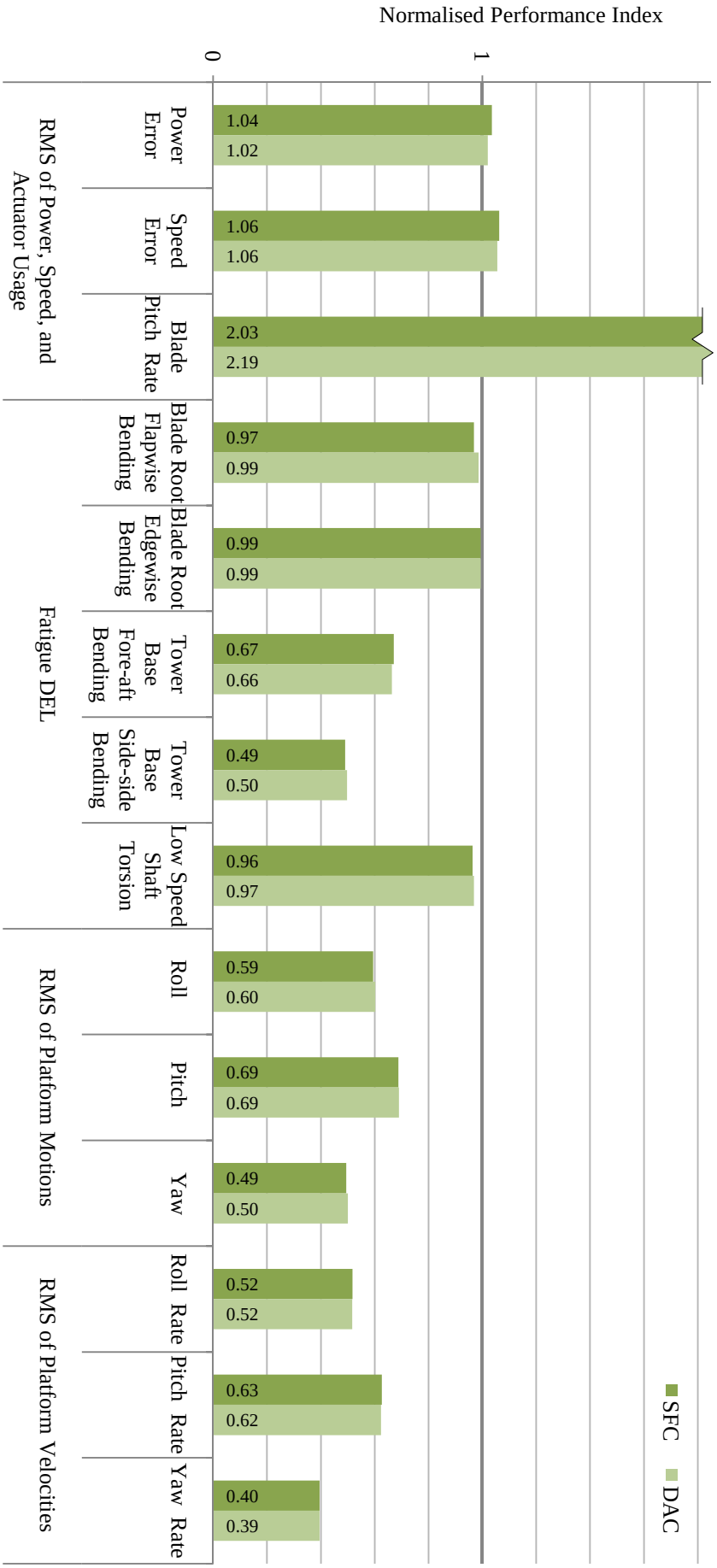

Figure 6.5: Averaged DLC results for the barge platform relative to the Baseline controller on the barge platform

Table 6.2: Performance trends of the barge platform controllers relative to Baseline controller

Trend	SFC	DAC
Constant	- Power and rotor speed errors - LSS fatigue DEL - Blade root flapwise fatigue DEL - Platform yaw and yaw rate	- Power and rotor speed errors - LSS fatigue DEL - Platform yaw and yaw rate
Increasing	- None	- None
Decreasing	- Blade root edgewise fatigue DEL - Tower FA and SS fatigue DELs - Platform roll and pitch motions	- Blade root flapwise and edgewise fatigue DELs - Tower FA and SS fatigue DELs - Platform roll and pitch motions
Parabolic	- None	- None

Table 6.2 summarises the average performance trends across wind speed bins for the SFC and DAC. These trends are categorised according to the 4 types of trends defined in Table 5.5. Plots of the trends are shown in figures D.1 and D.2 in Appendix D for the SFC and DAC respectively.

Both controllers have roughly the same trends with one noticeable difference. The DAC has lower blade flapwise bending DEL at high wind speeds but slightly worse at low wind speeds than the SFC. Despite having a lower blade flapwise DEL at high wind speeds, the overall average flapwise DEL for the SFC is lower than the DAC's due to the Weibull scaling putting more emphasis on lower, more dominant wind speeds.

The performance metrics that fall into the constant trend category demonstrate some degree of robustness of these controllers as they operate away from their linearisation point of 18 m/s. This relative robustness for these metrics does not mean that gain scheduling of state-space controllers is not needed, it only shows that these controllers are robust enough to maintain consistent performance improvement relative to the gain scheduled Baseline controller across a wide range of wind speeds. Gain scheduling may be beneficial in improving the performance in an *absolute* sense rather than in a relative sense.

Performance metrics with a decreasing trend, where they are better regulated at higher wind speed, are under-represented in the weighted average due to Weibull scaling. This variation in performance is due to to the nonlinearity of the system sensitivities with changing wind speeds.

Since the performance of the Disturbance Accommodating Controller is almost identical to that of the State Feedback Controller, the State Feedback Controller is deemed better suited on the barge platform as it is simpler and easier to implement than the DAC.

6.3.2 Time Series Results

A sample time series plot of a representative case is shown in Figure 6.6[10] where the SFC is compared to the Baseline controller on the barge platform. The figure shows the incident wind

[10]The figure starts at 100 s as this is the time period where differences in performance can be clearly identified.

and wave conditions, rotor speed, commanded blade 1 pitch angle, platform pitch angle, tower fore-aft and side-side base moments for the Baseline and State Feedback Controllers.

The improvement brought by individual blade pitching can be seen by the large reductions in platform pitching especially during the time between 140 and 180 seconds. During this period, the influence of platform pitch on tower fore-aft moment loads can also be seen coinciding with increased wave activity. In terms of rotor speed regulation, the SFC and Baseline have roughly the same performance; recall that the rated rotor speed is 12.1 rpm.

The "high frequency" content of the tower FA and SS moments shown in Figure 6.6 are those of the tower's FA and SS first bending mode natural frequencies. The "low frequency" variation of the tower moments is caused by the platform pitch and roll motions affecting the tower FA and SS loads respectively; platform roll motion is not shown in Figure 6.6. Since the tower side-side bending mode is part of the SFC, the controller is able to significantly reduce the amplitudes of the main frequency components of the tower side-side bending moment as shown in Figure 6.7. Adding the tower fore-aft DOFs to the SFC is expected to further reduce the tower loads; however, the tower loads relative to an onshore wind turbine (discussed in Chapter 9) remain, despite the massive reductions by the SFC, infeasibly high for practical deployment of the barge platform. Hence, the tower fore-aft DOFs are not added to the SFC design.

Interestingly, the platform pitch response for both controllers seems to be in phase. Such behaviour is caused by the dominance of the waves driving the platform pitch rather than observing the free decay of the platform pitch according to the open- and closed-loop damping ratios for the Baseline and State Feedback Controllers respectively.

The increase in blade pitching by the SFC is noticeable. This increased actuation has a higher frequency content than that of the Baseline controller mainly due to two reasons: First, using individual blade pitching adds a once-per-revolution (1p) frequency content that depends on the rotor speed. Second, blade pitching by the SFC contains the structural natural frequencies that the controller is designed to regulate and act upon.

It is important to note that for some of the DLC simulations, the platform pitch angle exceeds 10°; in some extreme cases such as DLC 55 (see Table C.1 for DLC parameters) the platform pitch angle is as high as 18° for the baseline controller. In such cases, the assumptions of the hydrodynamics module used by FAST (§5.1.1) no longer apply and the simulation results may no longer be an accurate representation of the true floating system.

6.4 Chapter Summary

The barge platform offers a simple and cost effective solution for a floating system that is easy to manufacture, transport and assemble. However, it suffers from being sensitive to the incident waves and thus experiences large platform motions that increase loading on the turbine.

When implementing multi-objective controllers on the barge platform, platform pitch to roll coupling due to blade pitch actuation is found to be present and applies for all floating platforms as it is a property of the wind turbine rather than the platform's. Due to this coupling,

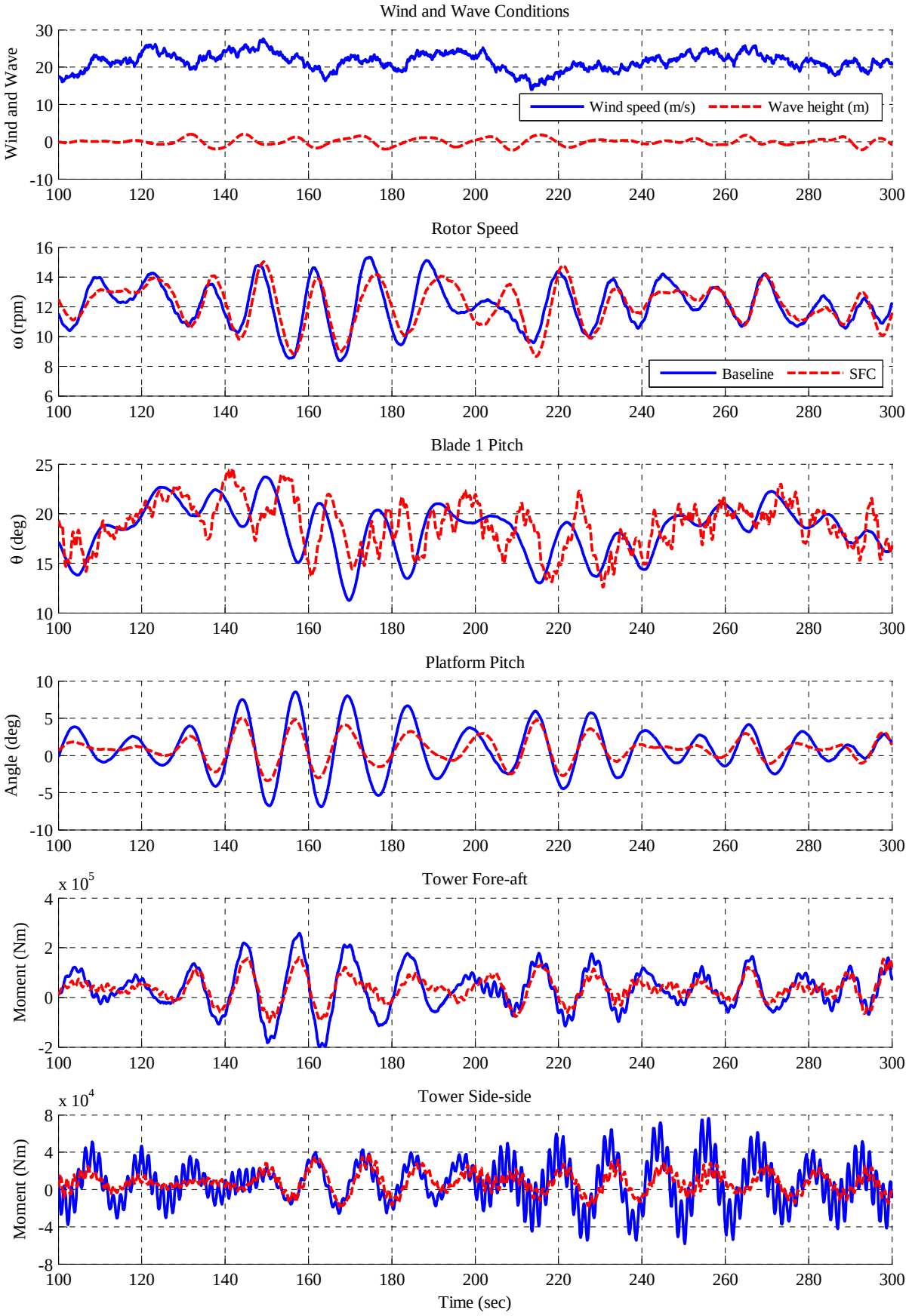

Figure 6.6: Sample time series response of Baseline and State Feedback Controllers on the barge platform

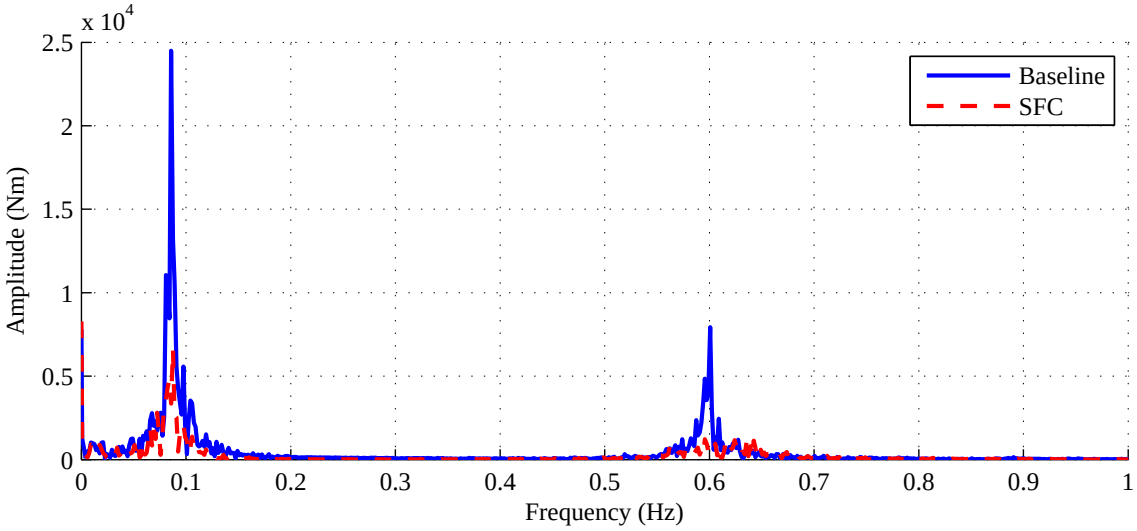

Figure 6.7: Frequency content of the tower side-side base moment

when a controller commands the blades to create a platform pitch restoring moment, it also induces a rolling moment. This coupling causes the SFC to destabilise the roll DOF and subsequently the first tower side-side bending mode. These DOFs are included in the state-space model used for control design to ensure the stability in a linear sense around the linearisation point.

For floating wind turbines, the recommended state-space model order for control design on floating platforms should include the following 6 DOFs: platform roll, pitch and yaw; first tower side-side bending mode; rotor and drivetrain twist DOFs. These DOFs are included to improve performance and maintain closed loop stability of the floating system.

Simulation results show that when compared to the Baseline controller, there is no difference in performance between the Disturbance Accommodating and State Feedback Controllers. The reason the DAC for wind speed perturbations is not able to improve the performance further than the SFC is because the barge platform is dominated by the waves rather than wind speed perturbations. However, both controllers manage to significantly reduce platform motions and tower fatigue damage equivalent loads without negatively affecting any monitored aspect of the wind turbine apart from an increase in blade pitch actuator usage. Since the DAC does not offer a noticeable improvement despite an increase in blade pitch usage, the SFC is deemed more suitable for the barge platform.

7

The Tension Leg Platform

Contents

7.1 The Tension Leg Platform **81**
7.2 Controller Design **83**
7.3 Offshore DLC Results **83**
7.4 Chapter Summary **86**

The tension leg platform uses taught mooring lines to maintain hydrostatic stability. This chapter gives a brief description of the tension leg platform and presents the analysed simulation results of the implemented State Feedback and Disturbance Accommodating Controllers when compared to the Baseline controller on the tension leg platform.

7.1 The Tension Leg Platform

The tension leg platform has a cylindrical hull with four spokes where the tensioned mooring lines are attached as shown in Figure 7.1. The TLP used in this work was originally designed at the Massachusetts Institute of Technology (MIT) [25] and was later modified by NREL to correct the platform roll and pitch inertias [38]; this TLP is also known as the MIT/NREL TLP. The main properties of the TLP are listed in Table 7.1.

The TLP concept has most of its hull underwater thus minimising the interaction with incident waves and therefore is not as sensitive to the waves as the barge platform. Furthermore, having taught mooring lines increases the stiffness of the platform in the roll, pitch, and heave motions. The major drawbacks of this design include the cost of anchors and dependency on seabed soil conditions to support large tensile forces.

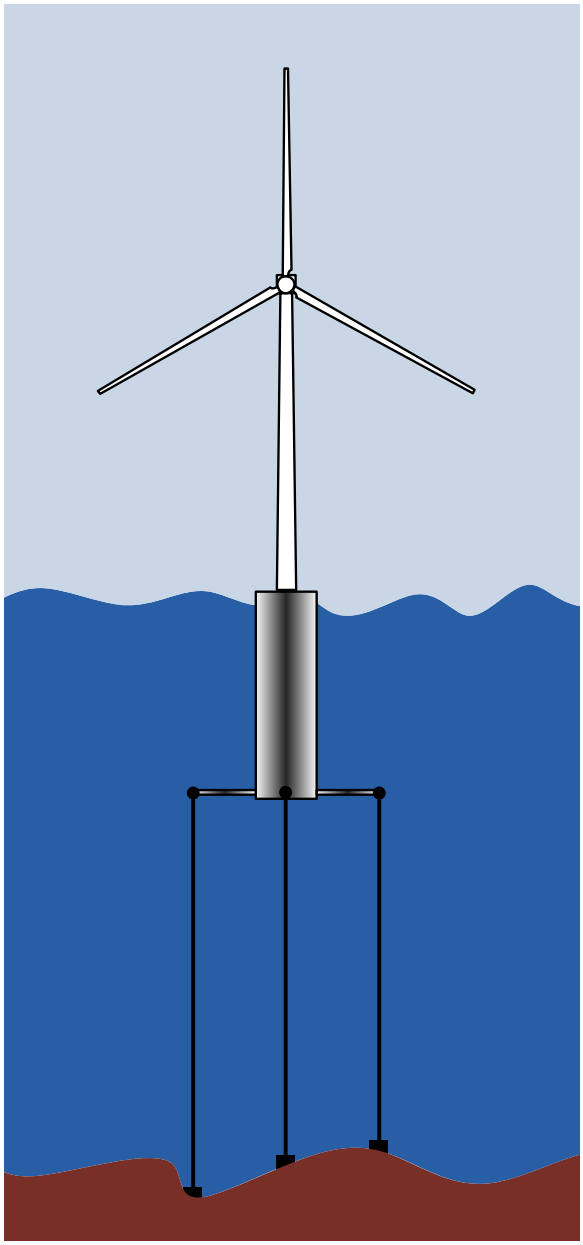

Figure 7.1: The tension leg platform

Table 7.1: Tension leg platform properties

Diameter	18 m
Number of spokes	4
Spoke length	18 m
Draft	47.89 m
Water depth	200 m
Platform mass	8,600,410 kg

7.2 Controller Design

The individual blade pitch State Feedback and Disturbance Accommodating Controllers on the TLP are designed based on a seven DOFs state-space model. The first six DOFs are the same used in designing the barge controllers (see §6.2.3), the seventh DOF is the tower fore-aft first bending mode. Although the TLP does not experience similar resonance issues as the barge platform, the physical mechanism behind these excitations still exists due to the individual blade pitch controller.

The addition of the tower fore-aft DOF is aimed at reducing the associated fatigue DEL. Design Load Case simulation results not shown here indicate that adding the tower fore-aft DOF does indeed reduce tower fore-aft fatigue DEL when compared to a State Feedback Controller designed without that additional DOF on the TLP. This DOF is not added to the barge controllers simply because the tower loads remain very high (when compared to an onshore wind turbine in Chapter 9) even after the large reductions from the State Feedback and Disturbance Accommodating Controllers. It is also believed that the reductions from adding this DOF to the barge controllers will not be significant due to the dominance of the waves. The 7 DOFs SFC for the TLP is by no means the optimum controller for the TLP but its performance is deemed satisfactory during the tuning phase.

For the Disturbance Accommodating Controller, the disturbance minimisation gain $G_{d,\mathrm{NR}}$ is obtained after modifying the B_{NR} and $B_{d,\mathrm{NR}}$ matrices to avoid the collective blade pitch drift discussed in §4.5.1. The column in the B_{NR} matrix that corresponds to the collective blade pitch is set to zeros and elements in the $B_{d,\mathrm{NR}}$ matrix that correspond to the drivetrain and first tower fore-aft bending states are also set to zero. The first tower FA states are removed from the $B_{d,\mathrm{NR}}$ matrix because the cosine- and sine-cyclic effects of the rotor have limited control authority over the tower FA states.

7.3 Offshore DLC Results

In this section, simulation results from performing a DLC analysis on the State Feedback and Disturbance Accommodating Controllers are compared and normalised to the Baseline controller on the TLP.

7.3.1 Averaged Normalised Results

The overall averaged and normalised results are shown in Figure 7.2. Both controllers improve power and rotor speed regulation considerably. The effect of adding wind speed disturbance rejection to the State Feedback Controller is more prominent than on the barge platform because the TLP is less influenced by the incident waves. The result is a noticeable improvement in rotor speed and hence power regulation by the DAC. The DAC is also able to further reduce tower base FA fatigue DEL.

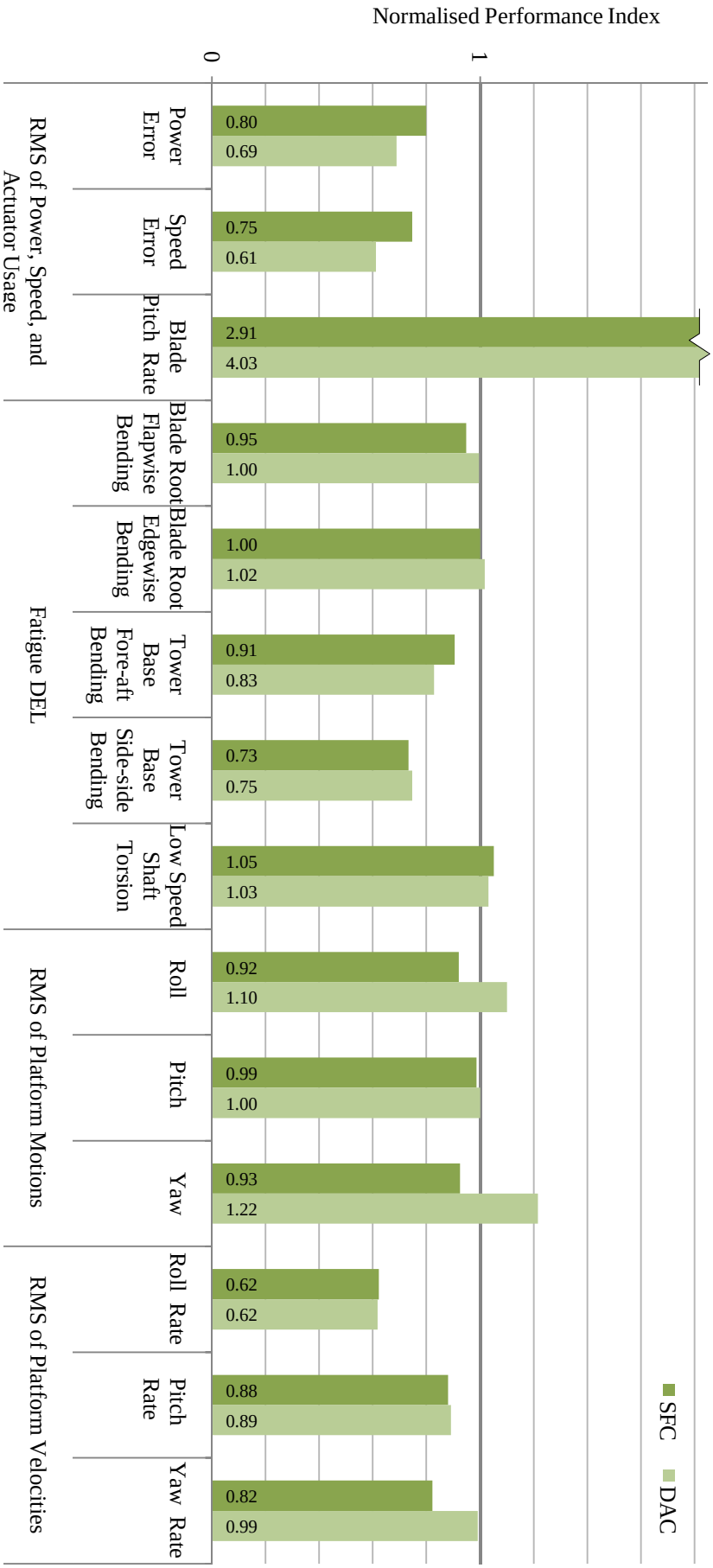

Figure 7.2: Averaged DLC results for the TLP relative to the Baseline controller on the TLP

The SFC is able to reduce platform roll, pitch, and yaw rates by an average of 38%, 12%, and 18% respectively while only managing to reduce the roll, pitch, and yaw angles by an average of 8%, 1%, and 7% respectively. The reason for such performance is due to two factors: first is the emphasis by the controller, through tuning, to primarily focus at regulating the platform velocities. The second is the TLP's stiffness in the roll and pitch directions where the angles remain very small (roll and pitch angles do not exceed 1 degree). Therefore, very little improvement can be achieved in these motions. The large increase in blade pitch actuation by the DAC is responsible for the increase in rolling and yawing motions. However, these angles remain small (less than 5 degrees) and do not result in a significant increase in fatigue DEL on any of the major turbine components.

Blade flapwise and edgewise bending and low speed shaft torsion fatigue DELs remain close to parity for both SFC and DAC indicating a similar performance to the Baseline controller. Whether the Baseline performance is adequate will be discussed in Chapter 9. Tower fore-aft DEL can be reduced by a maximum of 17% due to the addition of hub-height wind speed disturbance rejection. Tower side-side fatigue load is better reduced than fore-aft load due to better roll rate regulation and the availability of the generator torque to influence side-side loading. Tower side-side fatigue DEL can be reduced by up to 27% by the SFC relative to the Baseline controller.

Blade pitch actuation is increased, as expected, by at least 291%. However, like the barge controllers, this increase in actuation has no extensive saturation periods and does not result in an increase in blade fatigue damage equivalent loads.

In terms of performance trends across the simulation wind speed bins, Table 7.2 summarises the trends for the SFC and DAC according to the 4 types of trends defined in Table 5.5. For a plot of the trends, please refer to figures D.3 and D.4 in Appendix D.

For the metrics that fall into the decreasing trend category, the improvement in performance as wind speed increases is due to the nonlinearity of the system sensitivities with changing wind speed. Such a performance trend is under-represented in the weighted average results shown in Figure 7.2 due to the Weibull scaling factors placing more emphasis on performance

Table 7.2: Performance trends of the TLP controllers with increasing mean wind speed

Trend	SFC	DAC
Constant	- All except power and rotor speed errors	- Tower FA and SS fatigue DELs - LSS fatigue DEL - Platform pitch - Platform rotational velocities
Increasing	- None	- None
Decreasing	- Power and speed errors	- Power and rotor speed errors - Platform roll - Blade root edgewise fatigue DEL
Parabolic	- None	- Blade root flapwise fatigue DEL - Platform yaw

in lower wind speeds. The performance metrics that exhibit a parabolic trend are affected by the linearity of the DAC law; these metrics would benefit from gain scheduling. Gains scheduling of SFCs or DACs is outside the scope of this work.

Since the performance of the Disturbance Accommodating Controller is generally better than that of the State Feedback Controller, the Disturbance Accommodating Controller is deemed better suited for the TLP.

7.3.2 Time Series Results

A sample time series plot of the TLP using the same representative case for the barge platform is shown in Figure 7.3 for the Baseline and Disturbance Accommodating Controllers. The improvement in rotor speed regulation is reflected in the 200 second window where the DAC regulates the rotor speed closer to the rated speed of 12.1 rpm.

Noticeable reductions in tower side-side moment loads can be observed especially during the first 20 seconds shown in Figure 7.3. Figure 7.4 shows the reduction in the amplitudes of certain frequencies by the DAC for the tower fore-aft and side-side base moments. The difference in magnitude of the moments for the tower fore-aft and side-side moments (also in Figure 7.3) is mainly because the main rotor thrust and wave loads act in the fore-aft direction when no yaw errors are present.

It is important to note that platform pitch angle during the 200 second window shown does not exceed 0.3 degrees in magnitude. Consequently, further reducing platform pitching motion becomes difficult. This limited improvement is reflected by the almost identical pitching motion for both controllers on the TLP and, as shown by Figure 7.2, only moderate reductions in platform pitching velocity and tower fore-aft fatigue DEL are achieved when compared to the large reductions achieved by the SFC controller on the barge platform.

Finally, note that the mean blade pitch of the DAC closely follows the collective blade pitch of the Baseline controller. This suggests that most of the performance improvements brought by the DAC on the TLP are due to individual blade pitching.

7.4 Chapter Summary

The tension leg platform uses taught mooring lines to achieve hydrostatic stability in the water. The tensioned mooring lines increase the stiffness of the platform's roll, pitch, and heave motions. Furthermore, the design of the hull to have minimal water-plane area reduces the interaction with incident waves thus reducing the magnitude of induced motions. This design produces the smallest motion envelope out of the three platforms considered in this work.

The State Feedback Controller is designed based on a 7 DOFs linearised state-space model; the first six are the same DOFs used for control design on the barge platform in addition to the first bending mode of the tower fore-aft DOF. This DOF is added to further reduce the tower base fore-aft fatigue DEL.

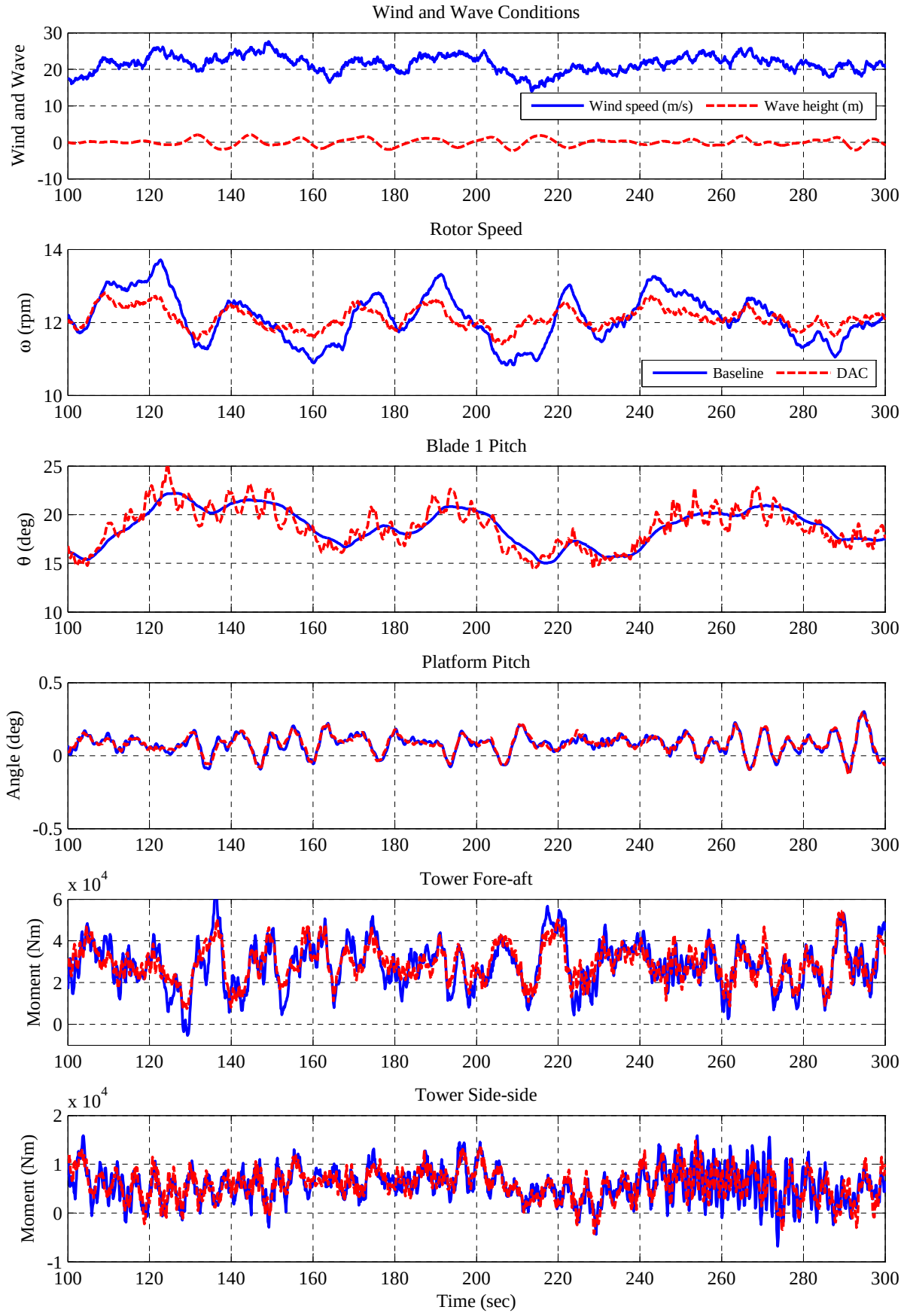

Figure 7.3: Sample time series response of Baseline and Disturbance Accommodating Controllers on the TLP

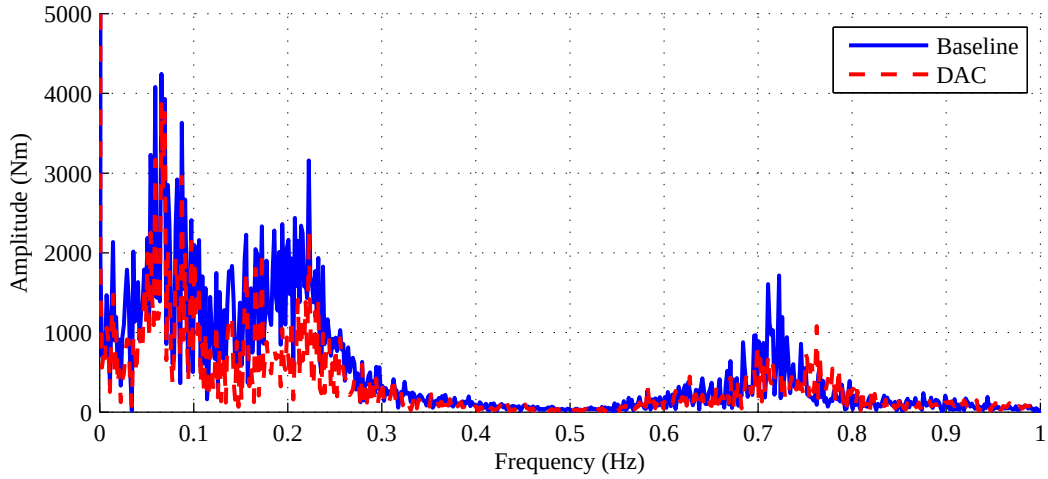

(a) Tower fore-aft

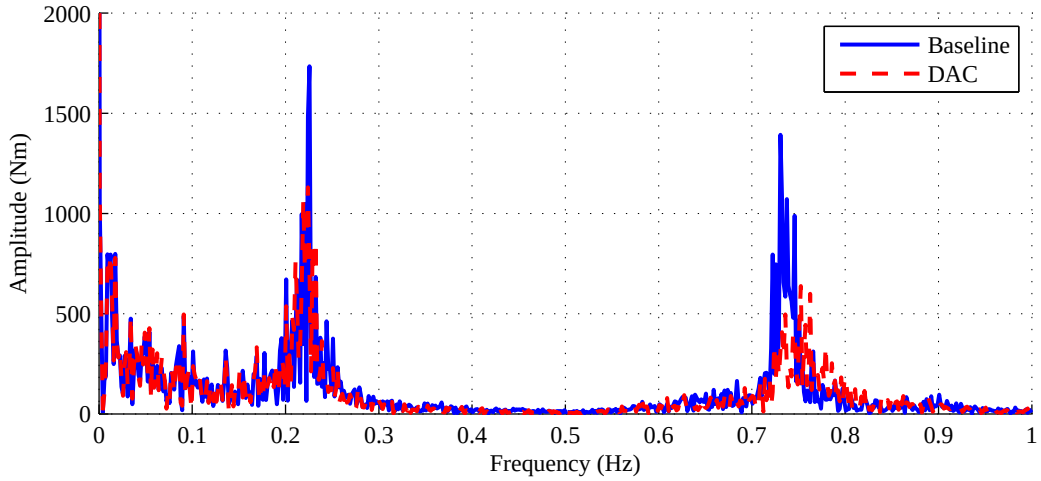

(b) Tower side-side

Figure 7.4: Frequency content of tower base moments

Simulation results show that the SFC manages to improve most of the performance metric, although, the magnitude of the reductions in platform motions is not as significant as the reductions achieved by the SFC on the barge platform. The reason for such limited improvement is because the platform roll and pitch motions are very small (typically less than 1 degree) leaving little room for improvement.

The DAC further improves power and rotor speed regulation and further reduces tower fore-aft fatigue DEL by rejecting wind speed fluctuations. However, the DAC increases the use of the blade pitch actuators which in turn increases the platform's rolling and yawing motions via coupling. The DAC is able to reject the effects of the wind speed perturbations with noticeable results due to the fact that the TLP motions are not very sensitive to incident waves compared to the barge platform. Since the performance of the Disturbance Accommodating Controller is generally better than that of the State Feedback Controller, the Disturbance Accommodating Controller is deemed better suited for the tension leg platform.

8

The Spar-Buoy Platform

Contents

8.1 The Spar-Buoy Platform **89**
8.2 Effects of Lowering the Platform's Pitch Natural Frequency in Control Design **91**
8.3 Offshore DLC Results **95**
8.4 Chapter Summary **99**

Spar-buoy platform concepts use ballast tanks to achieve hydrostatic stability and usually have deep drafts. This chapter presents the averaged DLC results for the State Feedback and Disturbance Accommodating Controllers relative to the Baseline controller on the OC3-Hywind Spar-buoy platform. The effects of the spar-buoy's low natural frequency and its implications on control design and individual blade pitching are also discussed.

8.1 The Spar-Buoy Platform

The spar-buoy platform utilises a deep-draft ballast to maintain hydrostatic stability and catenary mooring lines for station-keeping (Figure 8.1). The spar-buoy platform model used in this work is known as the "OC3-Hywind Spar-buoy". It is developed for Phase IV of the OC3 project and based on the Hywind Spar-buoy model [69, 86]. The main difference between the two models is that the Hywind Spar-buoy has a 2.3 MW wind turbine whereas the OC3-Hywind has a 5 MW wind turbine mounted on the platform. Recall that a full-scale prototype of the Hywind spar-buoy is currently being tested in Norway, therefore, assessing the potential and limitations of State Feedback and Disturbance Accommodating Control on a spar-buoy-type platform is important. Table 8.1 lists the main properties of the OC3-Hywind spar-buoy. More details on the OC3-Hywind spar-buoy can be found in [86].

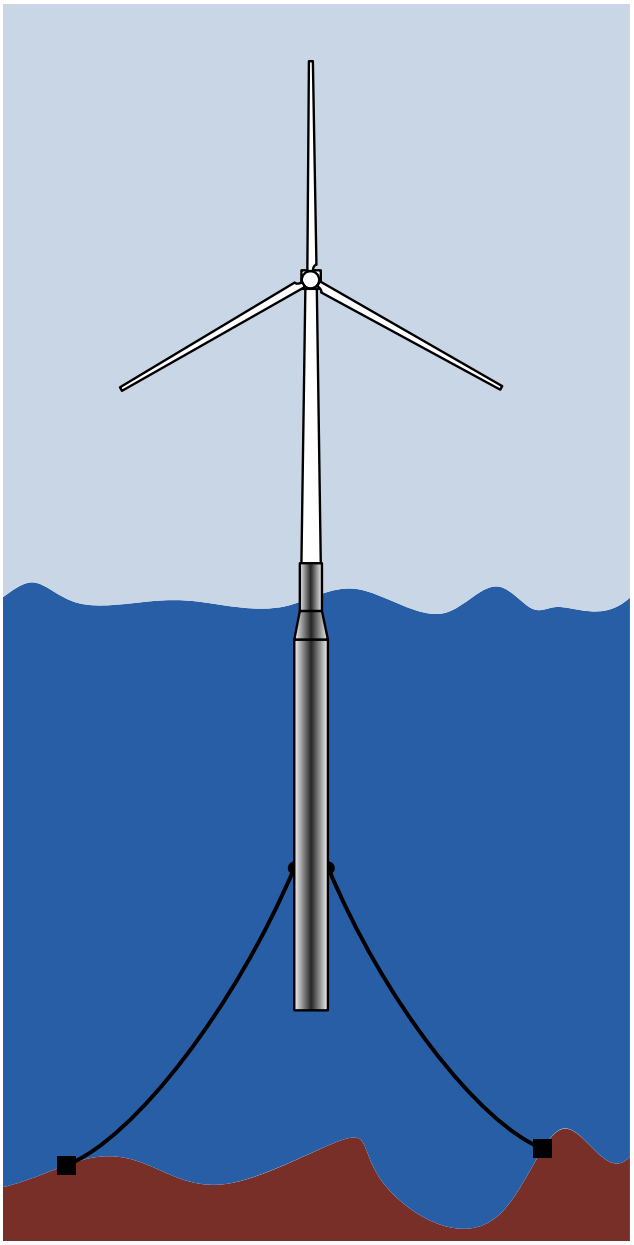

Figure 8.1: The spar-buoy platform

Table 8.1: Spar-buoy platform properties

Diameter above taper	6.5 m
Diameter below taper	9.4 m
Freeboard	10 m
Draft	120 m
Water depth	320 m
Platform mass	7,466,330 kg

Like the TLP, the spar-buoy has most of its hull underwater thus minimising the interaction with surface waves. However, for cost effectiveness, the spar-buoy uses catenary mooring lines which results in a larger motion envelope than the TLP. Due to the large ballast, the Spar-buoy is designed such that the platform's roll and pitch natural frequencies are below the wave excitation frequency of most sea states [86]. The spar-buoy's deep draft limits the locations where it can be deployed whereas the barge and tension leg platforms can be deployed in shallower sites.

8.2 Effects of Lowering the Platform's Pitch Natural Frequency in Control Design

A low platform pitch natural frequency (of about 0.21 rad/s or 0.03 Hz [86]) has a direct impact on control design and performance. Starting with the Baseline controller, the controller's design natural frequency is reduced from 0.6 rad/s to 0.2 rad/s to avoid the reduced or negative damping in the pitch direction and wave excitation frequency of most sea states [40, 86]. Furthermore, the torque control strategy in the above rated wind speed region is changed from constant power to constant torque to prevent a reduction in platform pitch damping; this has a direct impact on power regulation quality.

For the State Feedback Controller, recall that it is designed based on a linearised state-space model of the nonlinear system with only certain DOFs enabled. Having a low platform pitch natural frequency means that other low frequency DOFs, such as the platform surge, can interact with the platform pitch therefore altering its peak resonant frequency. Furthermore, the low platform pitch natural frequency reduces the effectiveness of important high-frequency individual blade pitch commands at regulating platform pitch. These two effects are discussed next.

8.2.1 Platform Surge DOF

For State Feedback Controllers designed for the barge and tension leg platforms, the surge DOF is not included in the controller design as it has little or no effect on the controller performance. However, because the spar-buoy's pitch frequency is now reduced, the surge DOF does have an impact on the model, changing the first pitch peak resonant frequency[11] by 68%. Figure 8.2a shows the change in the peak resonant frequency of the platform pitch when the platform surge is added to the linearised model. Compare that with the barge platform (Figure 8.2b) where adding the surge DOF does not change the main peak resonant frequency. The frequency responses shown in Figure 8.2 are based on 2 and 3 DOFs linearised (at 18 m/s) models transformed into the nonrotating frame of reference; note the actuator inputs are now collective, cosine- and sine-cyclic pitch. The DOFs include the rotor and platform pitch DOFs with the addition of the platform surge DOF. Therefore, if the SFC is designed based on a linear

[11] The peak resonant frequency is a function of the natural frequency ω_n and damping ratio ζ. It should not be confused with the damped natural frequency.

Table 8.2: DOFs list for Figure 8.3

# of DOFs	Description
6	Platform roll, pitch, and yaw, 1st tower SS bending mode, rotor and drivetrain
7	6 DOFs + platform surge
8	7 DOFs + 1st tower FA bending mode
21	All DOFs except nacelle yaw

model that does not include the surge DOF, then the controller will be trying to actuate the blades at the wrong frequency to have maximum impact on the platform pitch.

The frequency responses in Figure 8.2 use simple models to demonstrate the effect of including the surge DOF on the linearised model and compare with the barge platform. The effects of adding certain DOFs to the linearised state-space model (for control design) on the platform pitch frequency response are shown in Figure 8.3; the list of DOFs is given in Table 8.2. In the figure, only the collective blade pitch input is shown as the other two (cosine- and sine-cyclic pitch) display the same trends.

Figure 8.3 shows that by including the platform surge DOF, the correct peak frequency is attained and the low frequency gain is closer to the actual system (21 DOFs). Adding the first tower fore-aft bending mode to the linearised model (8 DOFs model) accounts for the second resonant peak which is in close proximity to the first resonant frequency. Adding more DOFs such as the second tower FA bending mode or the blade flap bending modes makes the frequency response of the model used for control design approach the real system. However, it is deemed that an 8 DOFs linear state-space model is adequate to account for the platform pitch dynamics.

8.2.2 Effectiveness of Individual Blade Pitching

The spar-buoy's platform pitch frequency is lower than the other two platforms mainly due to the significantly larger pitch inertia. Having a lower platform pitch natural frequency than the other two platforms means that high frequency blade pitch inputs are more attenuated thus reducing their effectiveness (Figure 8.4). For now, assume that the main frequency components of individual blade pitching occur at frequencies higher than 0.2 Hz (this is demonstrated in Chapter 9). Therefore, individual blade pitching on the spar-buoy platform is not as effective at regulating the platform pitch as on the other floating platforms when actuator saturation is taken into account. Explaining the differences in the frequency response of the three platforms (Figure 8.4) is discussed further in Chapter 9.

8.2.3 Final Controller Design

The final form of the State Feedback Controller used for DLC analysis is based on an 8 DOFs linearised state-space model that includes the DOFs listed in Table 8.2. However, the plat-

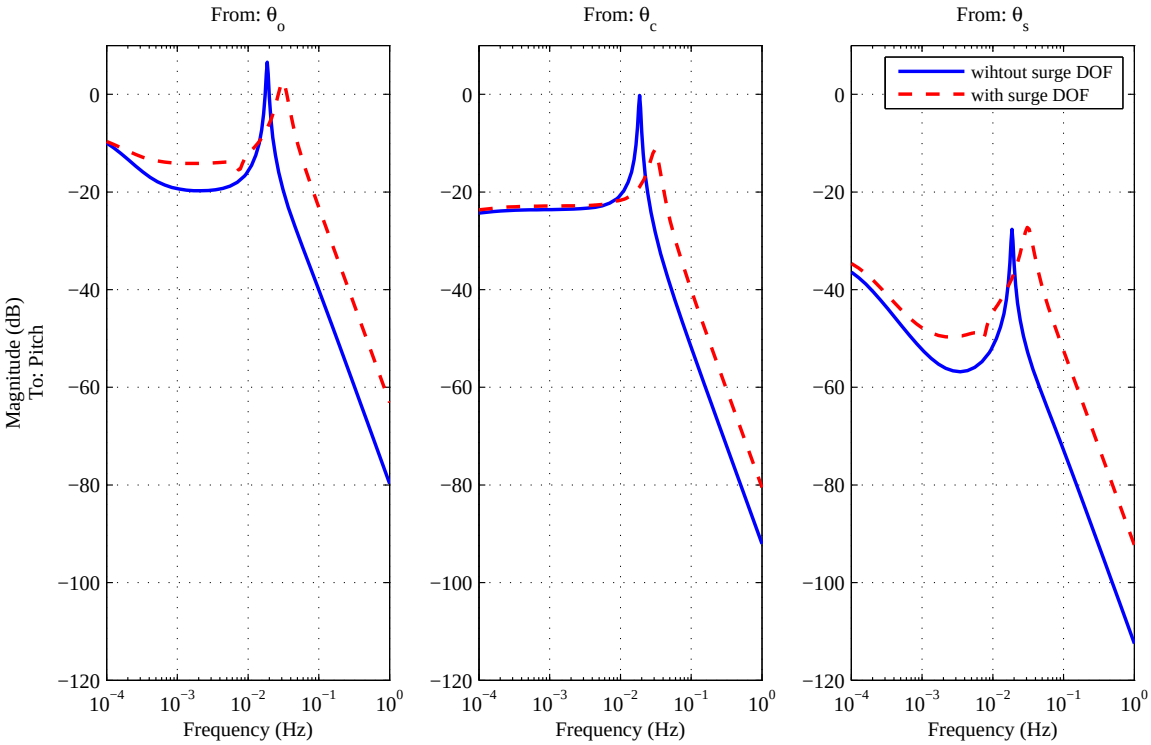

(a) Spar-buoy platform

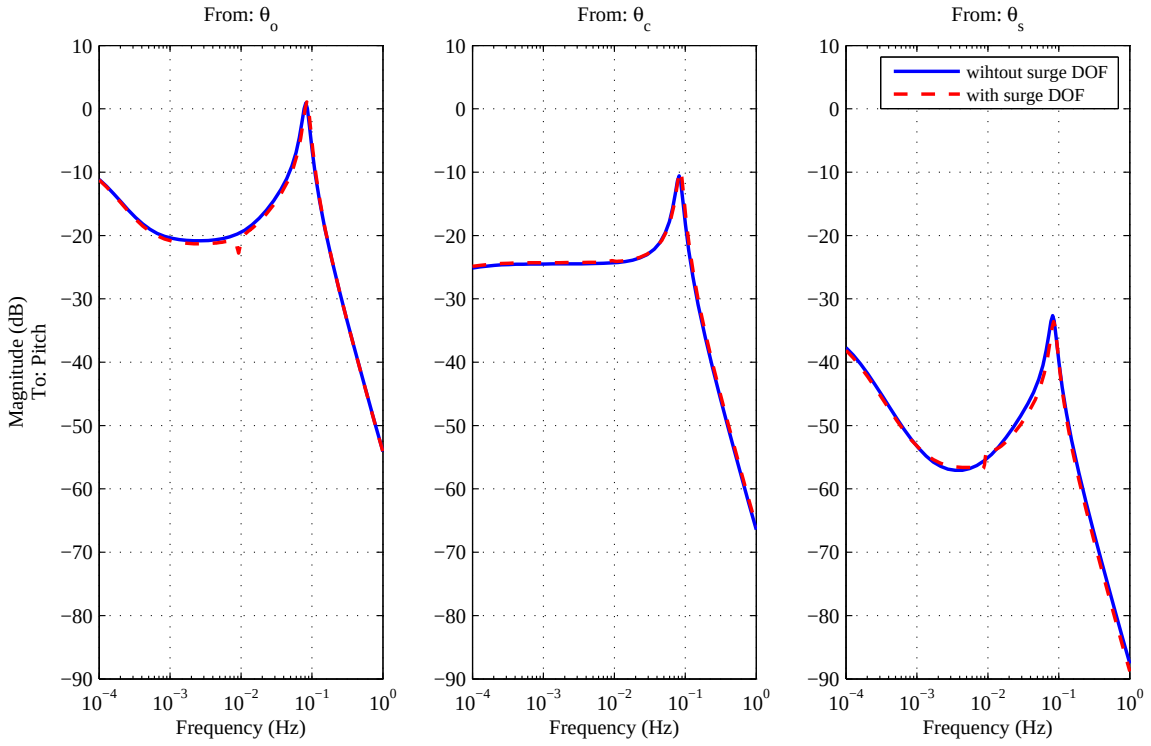

(b) Barge platform

Figure 8.2: Effects of adding the surge DOFs on frequency response

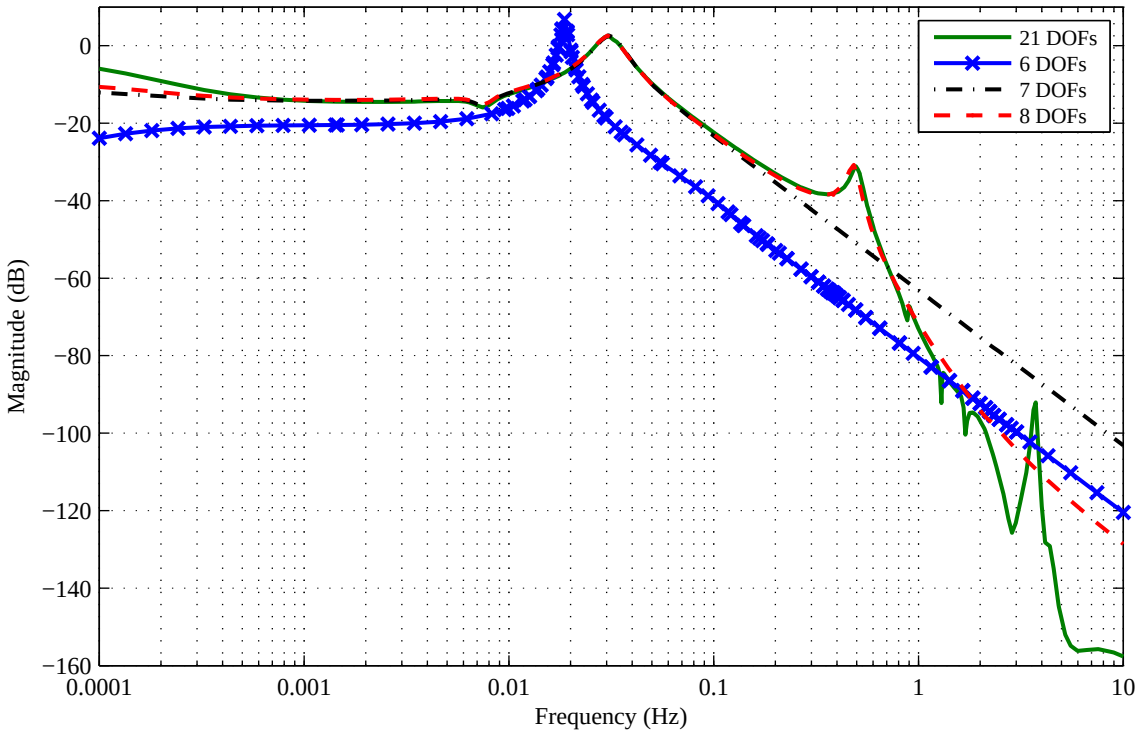

Figure 8.3: Spar-buoy platform pitch frequency response to collective blade pitch with different sets of DOFs

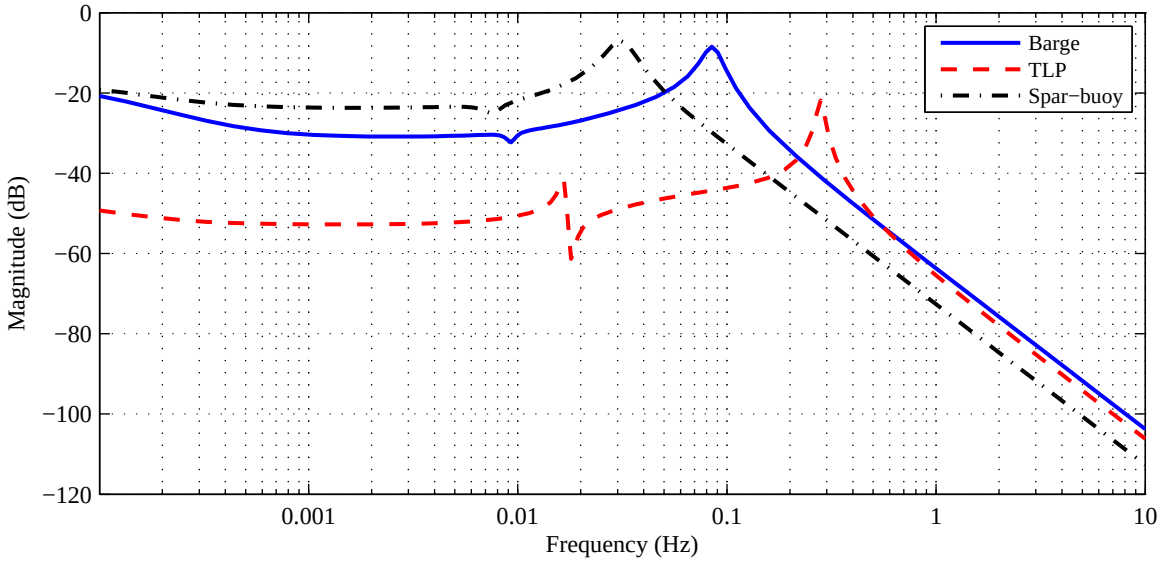

Figure 8.4: The three platforms' pitch frequency response to blade 1 pitch on a 3 DOFs model that includes the platform surge, platform pitch, and rotor DOFs

form surge state (position) is removed from the linear state-space model before the controller is designed; platform surge velocity is still part of the model. Regulating the platform surge position is not considered critical to normal operation, and by removing it as a control objective, an unnecessary increase in blade pitch actuation is avoided.

Recall that the Baseline controller's torque algorithm is changed from constant power to constant torque to improve the platform's pitch damping [38, 86]; using the constant torque algorithm and reducing the desired closed-loop natural frequency produces the best results for the Baseline controller. When tuning the 8 DOFs SFC, little or no difference is observed between the two torque algorithms in terms of platform pitch response. However, with the constant power algorithm, power regulation is significantly improved. Therefore, the constant power algorithm is used as the generator torque operating point for the SFC. Being a multi-objective controller gives the SFC an obvious advantage allowing it to use the constant power algorithm without suffering the negative or reduced platform pitch damping whereas the single-objective Baseline controller has to compensate by using the constant torque algorithm.

Tuning the SFC to achieve somewhat satisfactory performance involves sacrificing rotor speed regulation in favour of improved platform pitch regulation. Relaxing rotor speed control allows the controller to use the blade pitch to regulate the platform pitch but increases rotor speed fluctuations. However, since the constant power torque algorithm is used, power regulation is not significantly affected.

The wind speed perturbation Disturbance Accommodating Controller on the spar-buoy is configured using the same set-up used for the DAC on the TLP – discussed in §7.2.

8.3 Offshore DLC Results

In this section, simulation results from performing DLC analysis on the State Feedback and Disturbance Accommodating Controllers are compared and normalised to the Baseline controller on the spar-buoy platform.

8.3.1 Averaged Normalised Results

The overall averaged and normalised results are shown in Figure 8.5. The SFC manages to reduce the tower fatigue DELs by 9%. All other metrics remain close to parity except for RMS power error, blade pitch rate and low speed shaft torsion fatigue DEL. Since rotor speed regulation performance is essentially similar to the Baseline controller, the massive 64% reduction in power error is simply due to the use of the constant power algorithm for the torque operating point. The massive *relative* increase in blade pitch usage is thought to be having a negative impact on low speed shaft fatigue load.

There are two main reasons as to why most of the SFC's relative performance metrics are close to parity. First, unlike the barge platform, the Baseline controller's performance is good in the sense that rotor speed is closely regulated and platform motions remain below 5°. Second and

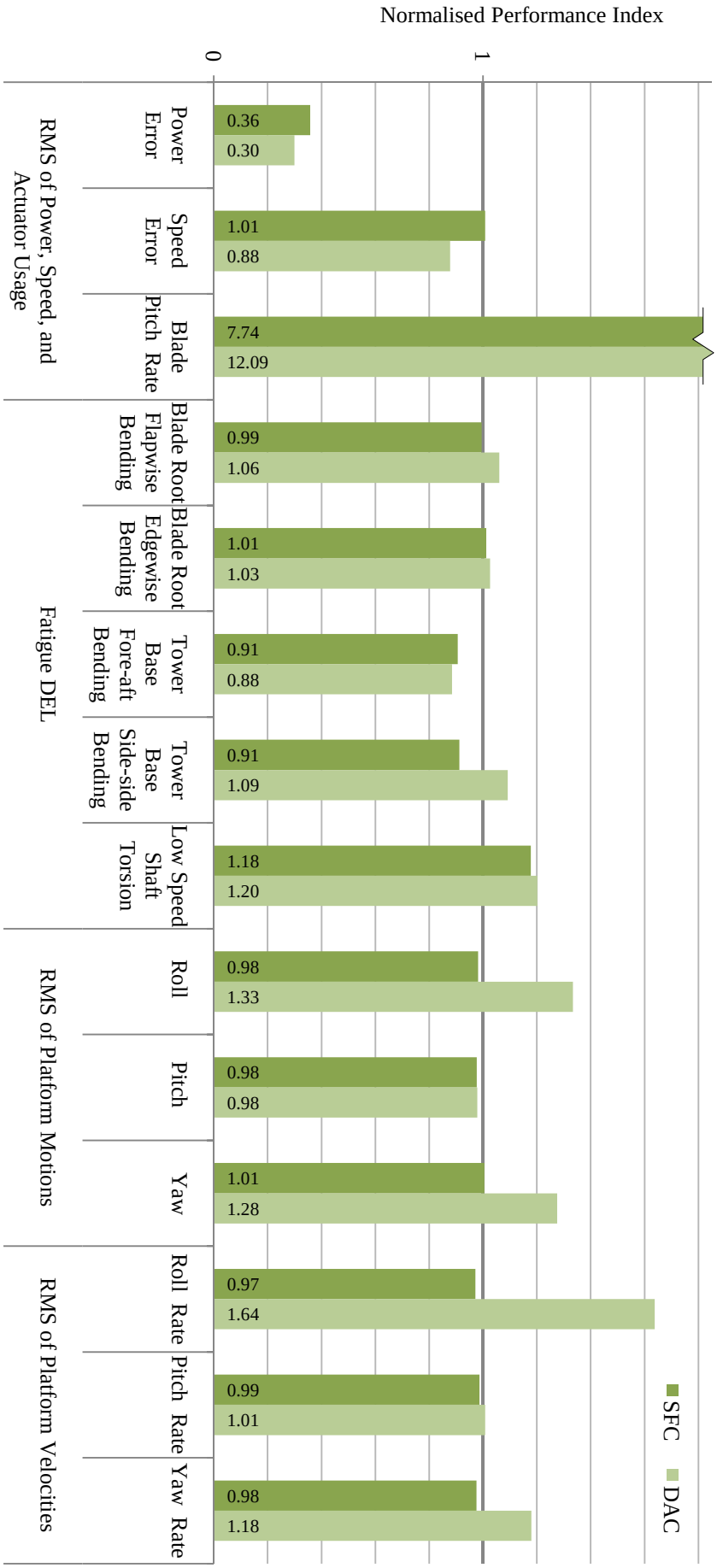

Figure 8.5: Averaged DLC results for the spar-buoy platform relative to the Baseline controller on the spar-buoy platform

as discussed earlier, the effectiveness of individual blade pitching is limited and therefore the controller requires to actuate the blades further to achieve the required actuation force. However, due to the presence of actuator saturation, individual blade pitching becomes of limited effect on the floating wind turbine. Therefore, the SFC can only have limited improvement on the spar-buoy relative to the Baseline controller.

The DAC manages to improve rotor speed regulation by reducing the effects of wind speed perturbations through increased blade pitch usage; power regulation is improved as a consequence. However, the increased blade pitch actuation does have a negative impact on platform roll and yaw motions, and as a result, tower side-side loads are increased by an average of 9%. The DAC's feed-forward term operates linearly away from the linearisation point; the further away from the linearisation point the turbine is operating, the more and further the blades are actuated. System nonlinearities mean that the DAC is either under- or over-actuating the blades to minimise the effects of wind speed perturbations away from the linearisation point. To be able to utilise the DAC's rejection of wind speed perturbations, tuning of the SFC can allow for the expected impact of the DAC by further relaxing rotor speed regulation. Further tuning is not considered here as the objective is to assess the performance of just adding the feed-forward term to the SFC.

In terms of performance trends across the simulation wind speed bins, Table 8.3 summarises the trends for the SFC and DAC according the 4 types of trends defined in Table 5.5. For a plot of the trends, please refer to figures D.5 and D.6 in Appendix D.

Interestingly, certain performance metrics for both controllers on the spar-buoy platform exhibit an increasing trend with increasing wind speed. Since both controllers have these specific metrics fall into this category, this indicates the actuators' limited influence on these metrics/control objectives. Such limitation is possibly due to the limited effectiveness of IBP and the presence of actuator saturation limiting the controller design from increasing the gain. The increasing trend over-represents the improvement of metric due to the Weibull scaling placing more emphasis on the lower wind speed range where it is better regulated.

Table 8.3: Performance trends of the spar-buoy platform controllers relative to the Baseline controller with increasing mean wind speed

Trend	SFC	DAC
Constant	- Blade root edgewise fatigue DEL - Tower FA and SS fatigue DELs - Platform velocities	- Tower FA fatigue DEL - LSS fatigue DEL - Platform pitch and yaw velocities
Increasing	- Blade root flapwise fatigue DEL - Platform motions	- Platform roll and pitch motions - Platform roll velocity
Decreasing	- Rotor speed error - LSS fatigue DEL	- Rotor speed error - LSS fatigue DEL - Blade root edgewise fatigue DEL
Parabolic	- Power error	- Power error - Platform yaw - Blade root flapwise fatigue DEL

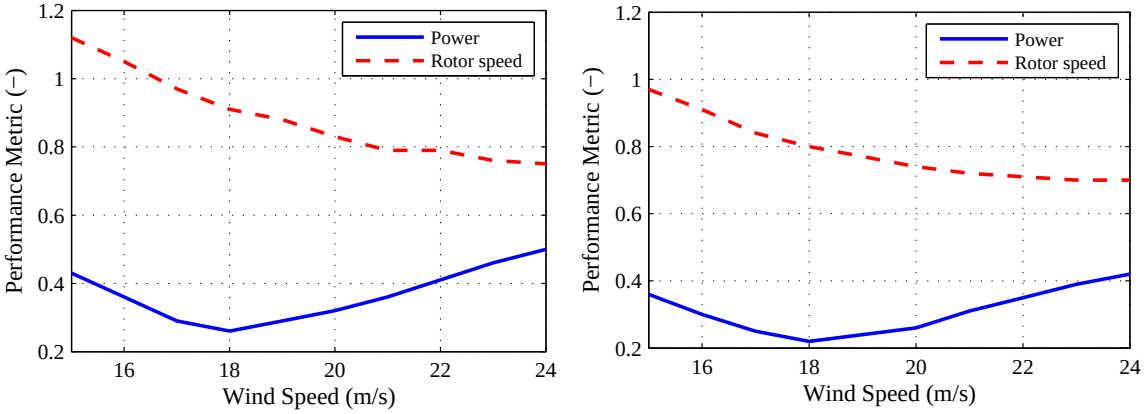

(a) SFC (b) DAC

Figure 8.6: Rotor speed and power regulation errors trends with increasing wind mean speed relative to the Baseline controller

The parabolic power error trend for the SFC (Figure 8.6a) and DAC (Figure 8.6b) may seem counter-intuitive as the rotor speed error improves with increasing wind speed suggesting that power error should follow suit. However, because both controllers have relaxed rotor speed control, the generator torque usage is increased to compensate, thus reaching its maximum saturation limit. As the wind speed increases, rotor speed fluctuations increase as well (recall that the trends are relative to the Baseline controller). This in turn increases the periods where generator torque is saturated resulting in worse power regulation than at lower wind speeds.

The tower side-side bending fatigue DEL for the DAC trend is not included in Table 8.3 as it does not belong to any of the four trend types convincingly. The metric fluctuates wildly following the effects of the platform rolling motion as shown in Figure 8.7.

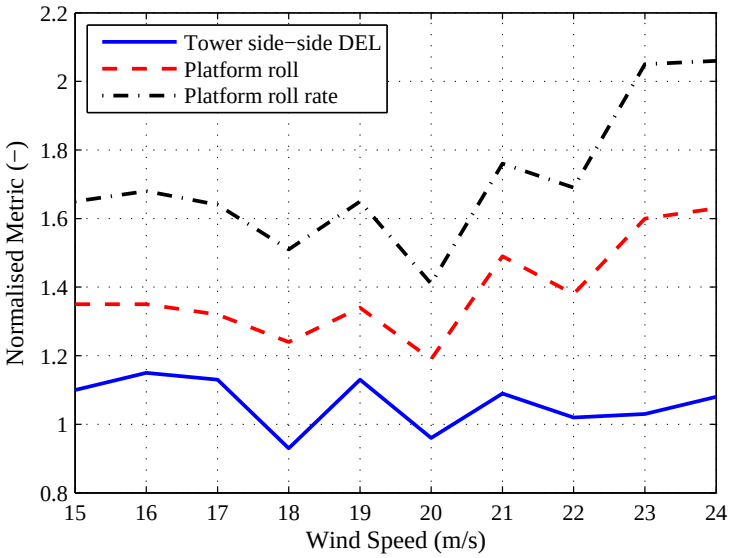

Figure 8.7: Effect of platform roll on tower SS bending trend

Since the performance of the State Feedback Controller is generally better than that of the Disturbance Accommodating Controller, the State Feedback Controller is deemed better suited for the spar-buoy platform given the current actuators' limitations.

8.3.2 Times Series Results

Figure 8.8 shows the time series response of the Baseline and State Feedback Controllers for the same representative case used for the barge and tension leg platforms. Since rotor speed regulation performance of the two controllers is almost identical, the generator power is shown instead. The SFC's power regulation is significantly better than the Baseline's due to the use of the constant power algorithm for the torque operating point as discussed earlier.

The reductions in tower fore-aft and side-side base bending loads are clearly noticeable in Figure 8.8. For the tower fore-aft base bending load, Figure 8.9a shows the reduction in the amplitudes of certain frequencies and especially at the platform pitch resonant frequency of 0.03 Hz. However, for the tower side-side base moment, there is an increase in the amplitude at the platform roll natural frequency of 0.03 Hz (Figure 8.9b). This increase is caused by the change in the platform roll resonant frequency due to excluding the platform sway from the linearised model based on the same principles discussed in §8.2.1. The platform sway DOF is not added to the control design as the blade pitch actuators are already reaching the limits of their effectiveness. Furthermore, the reduction in tower side-side loads due to the inclusion of the platform sway DOF is not expected to change the overall feasibility of the spar-buoy platform as tower side-side is not a main design driver; tower fore-aft is (see Chapter 9).

Note how the SFC's blade 1 pitch angle closely follows the Baseline's collective blade pitch trajectory. Since both controllers have similar rotor speed regulation performance, this suggests that most of the improvements brought by the SFC are achieved via individual blade pitching despite its limited effectiveness at high frequencies.

8.4 Chapter Summary

The spar-buoy platform achieves hydrostatic stability using a deep drafted ballast with catenary mooring lines for station-keeping. The deep draft of the spar-buoy increases the platform's rolling and pitching inertias significantly thus reducing their respective natural frequencies. This design feature puts the platform's roll and pitch frequencies below the wave excitation frequency of most sea states.

The platform's lower pitch frequency affects the choice of which DOFs to include in the control design of the State Feedback Controller. Adding the platform surge DOF and the first tower fore-aft bending mode to the linearised model captures all the essential features of the platform pitch dynamics. Not including these two DOFs (especially the platform surge) causes the model used for control design to incorrectly represent the nonlinear system.

Another effect caused by the platform's lower pitch frequency is the limited effectiveness of individual blade pitching to regulate the platform pitch. A lower natural frequency than the other platforms means that high frequency blade pitch inputs are further attenuated. Therefore, individual blade pitching on the spar-buoy is not as effective as on other platforms at high frequencies requiring the controller to increase actuation to get the same desired impact. How-

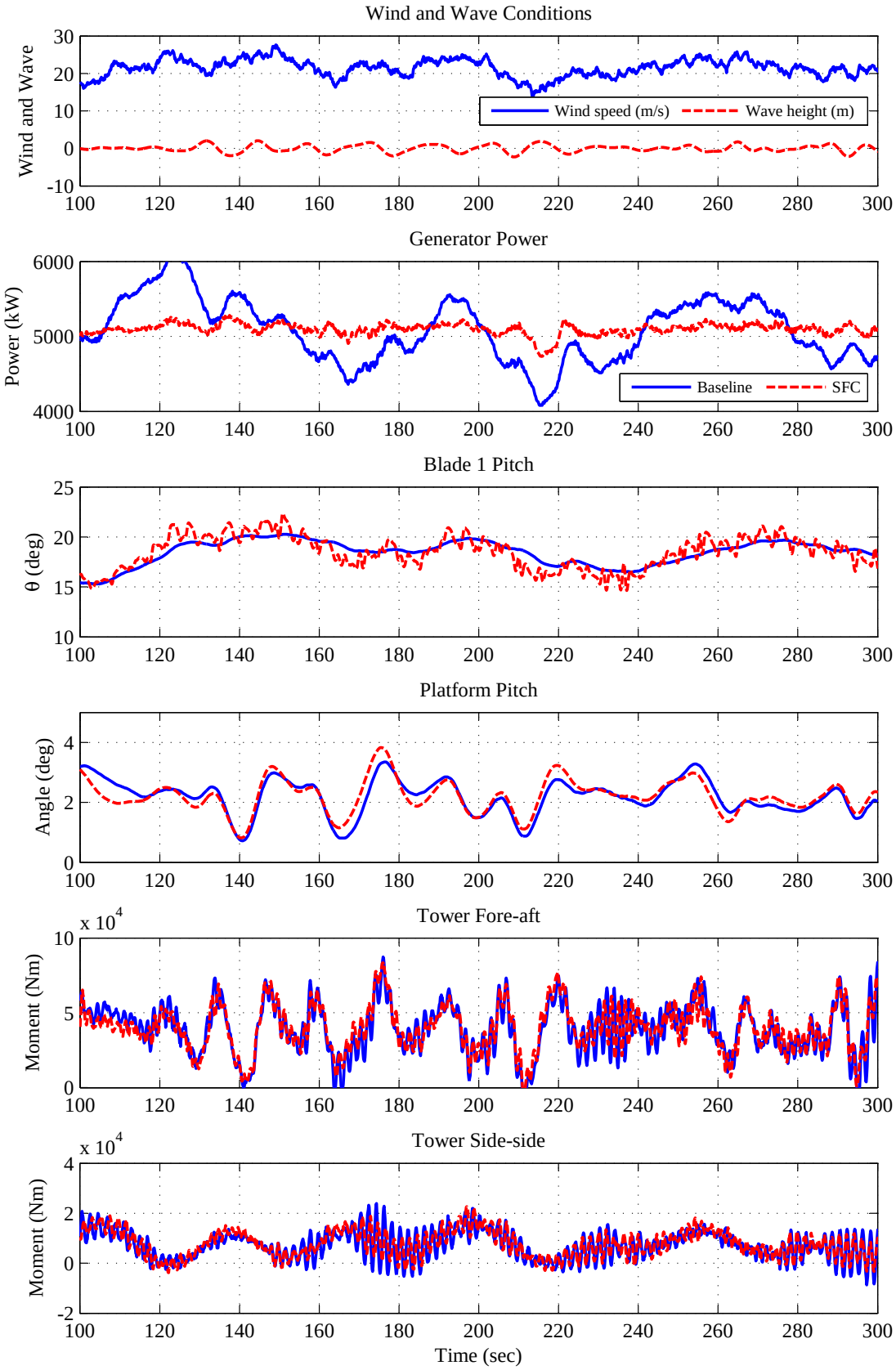

Figure 8.8: Sample time series response of Baseline and State Feedback Controllers on the spar-buoy platform

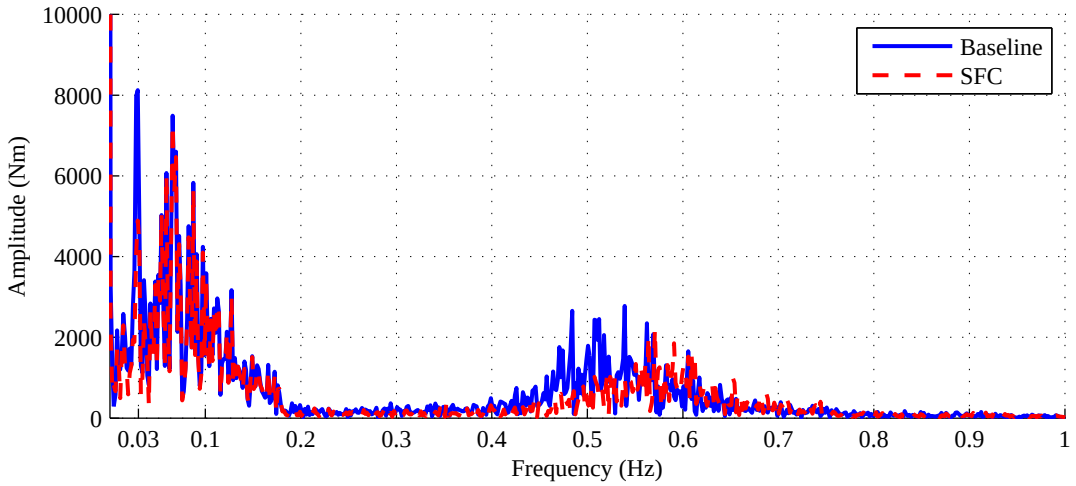

(a) Tower fore-aft

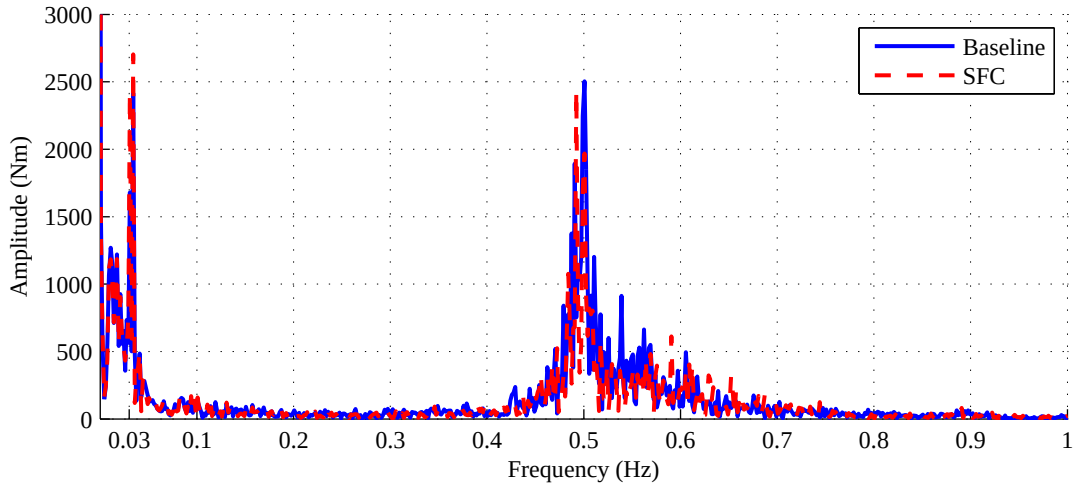

(b) Tower side-side

Figure 8.9: Frequency content of tower base moments

ever, blade pitch saturation limits impose an upper limit to the controller gains thus reducing the effectiveness of IBP on the spar-buoy platform.

Both controllers (SFC and DAC) use constant power for the torque control algorithm thus significantly improving power regulation over the Baseline controller which uses constant torque to improve platform pitch damping. The SFC is able to reduce tower fatigue damage equivalent loads by an average of 9% relative to the Baseline controller. All other metrics remain close to unity except for low speed shaft torsion DEL where it is increased by an average of 18%. This increase is thought to be due to the significant relative increase in blade pitch actuation.

The DAC is able to improve rotor speed regulation by rejecting wind speed perturbations through increased blade pitch actuation. This significant increase in blade pitch actuation has a negative impact on platform rolling and yawing motions. Therefore, the State Feedback Controller is deemed better suited for the spar-buoy platform given the current actuators' limitations.

9

Platform Comparisons

Contents

9.1 Comparison Approach **103**
9.2 Platform Pitch Input and Disturbance Sensitivities **104**
9.3 DLC Results Relative to an Onshore Wind Turbine **108**
9.4 Chapter Summary **111**

Early comparisons between the three floating platforms involved qualitative analysis; see Table 1.5 for an example. Then, numerical comparisons using hi-fidelity simulation models used results relative to an onshore wind turbine for comparing turbine loads when simulated with a Gain Scheduled PI controller.

In this chapter, the platforms' simulation results for the Baseline and multi-objective controllers from previous chapters are compared to each other using an onshore wind turbine as a reference to establish whether fatigue loads can be reduced to a level comparable to an onshore wind turbine. The differences in performance based on numerical results are then explained using physical insight into their properties through the frequency response of the platform pitch motion.

9.1 Comparison Approach

The platforms are compared in two different ways: The first is by examining certain properties of the frequency response of the platform pitch motion to establish certain differences that affect their dynamic behaviour. The second is by comparing their simulation results from previous chapters.

Table 9.1: Platform controllers to be compared to the onshore wind turbine

Platform	Controller	Blade Pitching	Torque Control	Other
Barge	Baseline	Collective	Const. Power	$\omega_n = 0.6\,\text{rad/s}$ and $\zeta = 0.7$
	SFC	Individual	Const. Power	6 DOFs linear state-space model
TLP	Baseline	Collective	Const. Power	$\omega_n = 0.6\,\text{rad/s}$ and $\zeta = 0.7$
	DAC	Individual	Const. Power	7 DOFs linear state-space model
Spar-buoy	Baseline	Collective	Const. Torque	$\omega_n = 0.2\,\text{rad/s}$ and $\zeta = 0.7$
	SFC	Individual	Const. Power	8 DOFs linear state-space model

Since all the floating platforms use the same 5 MW wind turbine, the main differences arise in the behaviour of their floating platform. Of most interest is the dynamics of the platform's pitch motion since both wind and wave conditions directly affect it. Furthermore, the platform pitch motion can have direct impact on power output and tower fore-aft and blade loads. Therefore, the frequency responses of the platform pitch motion to blade pitch, wind and wave inputs are analysed for each platform.

In previous chapters, the performance of the controllers are compared to the Baseline controller on their respective platform. To allow for a fair comparison between the platforms, the simulation results are normalised relative to the Baseline controller on a 5 MW onshore wind turbine. Comparing to an equivalent onshore system allows for:

- comparison between different floating platforms in terms of power and speed regulation as well as fatigue loads on the main wind turbine components (tower, blades, and drivetrain), and
- evaluation of the required turbine strength in relative terms to well established onshore wind turbine designs.

The comparisons are carried out between the baseline controllers on each platform as well as the best controller on each platform; these are summarised in Table 9.1. For more details on each controller, please refer to the corresponding platform chapter; the Baseline controller is described in Chapter 2.

9.2 Platform Pitch Input and Disturbance Sensitivities

Each of the three floating platforms uses a different principle to achieve hydrostatic stability and as a consequence have different dynamic properties. Compared to the barge platform, the TLP has higher stiffness while the spar-buoy has larger pitch inertia. These differences determine how the blades are able to influence the platform pitch for regulation as well as how the disturbances affect the platform pitch.

The platform pitch frequency responses to blade 1 pitch perturbations for each platform are shown in Figure 9.1. Each frequency response is based on a 21 DOFs state-space model linear-

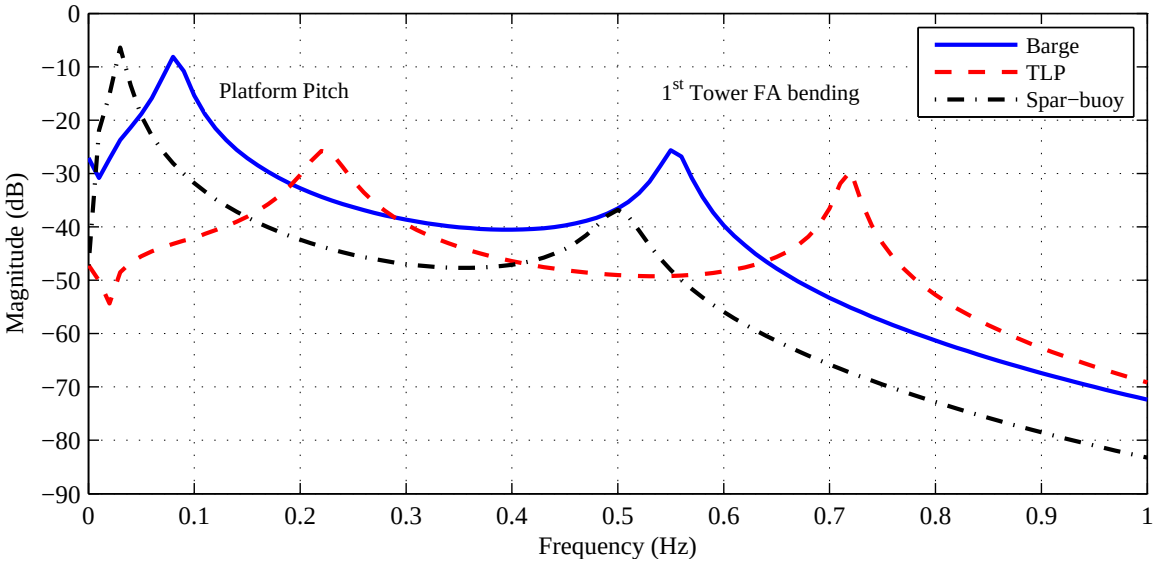

Figure 9.1: Platform pitch frequency response to blade 1 pitch input

ised at 18 m/s wind speed. The two major resonant frequencies are those of the platform pitch and first tower fore-aft bending mode respectively according to frequency.

To simplify the comparison, consider the frequency response of the barge platform as the median response. The TLP's low frequency gain is noticeably lower than the other two platforms. This difference is due to the high platform pitch stiffness brought by having taught mooring lines. Although the TLP is not as responsive to blade pitch commands as the other two platforms at low frequencies, it is as responsive as the barge platform at higher frequencies. Furthermore, since the TLP experiences little pitch motion, blade pitch demand is not as big as on the other platforms, therefore, the effect of TLP's stiffness on blade pitch sensitivity at low frequencies is not considered critical. The TLP's high stiffness also increases the peak frequency of the platform pitch.

As discussed in Chapter 8, the spar-buoy platform's lower pitch natural frequency is due to the large platform pitch inertia. The lower natural frequency attenuates high frequency blade pitch commands more than the other two platforms. This effect, coupled with blade pitch saturation, limits the effectiveness of individual blade pitching on the spar-buoy. Figure 9.2 shows the frequency content of blade 1 pitch commands for the representative case used for the time series response of the floating platforms (Figures 6.6, 7.3 and 8.8); note the logarithmic scale of the amplitudes in Figure 9.2 and the linear frequency range matches that of Figure 9.1. For the spar-buoy platform (Figure 9.2c), the SFC and DAC have noticeably more high frequency blade pitch actuation (higher than 0.2 Hz) than the Baseline controller. At frequencies higher than 0.2 Hz, the effectiveness of the blade pitch is almost consistently lower than the other two platforms (Figure 9.1) thus limiting the effectiveness of individual blade pitching because increasing the controller gain would results in actuator saturation.

The frequency content of the Disturbance Accommodating Controllers on the tension leg (Figure 9.2b) and spar-buoy (Figure 9.2c) platforms shows an increase in actuation over the other controllers around the rotor frequency of 0.2 Hz. This increase in once-per-revolution (1p) ac-

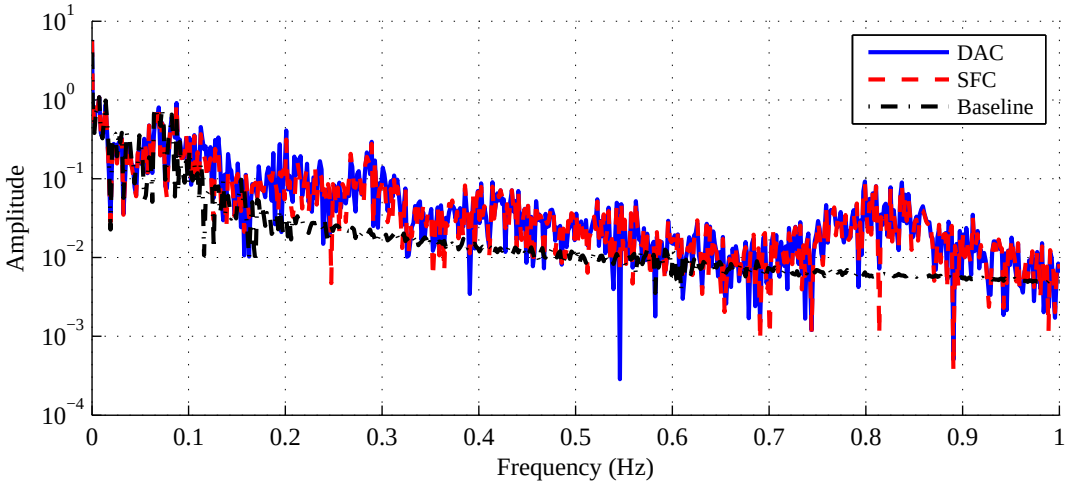

(a) Barge platform

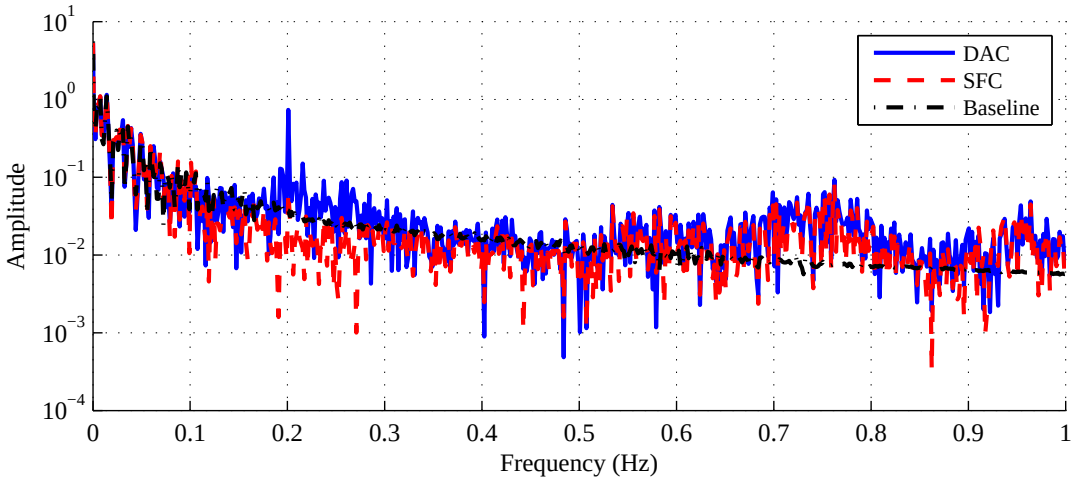

(b) TLP platform

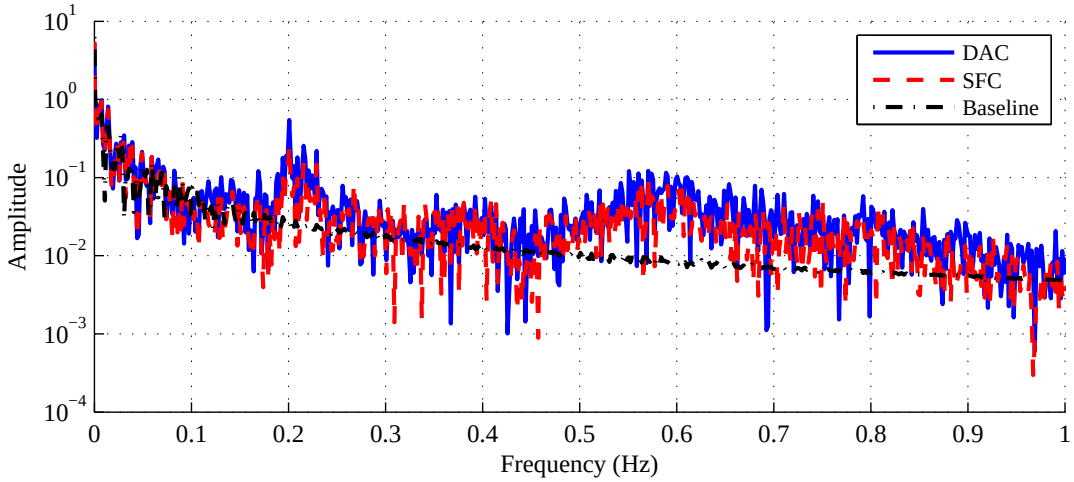

(c) Spar-buoy platform

Figure 9.2: Blade pitch frequency content

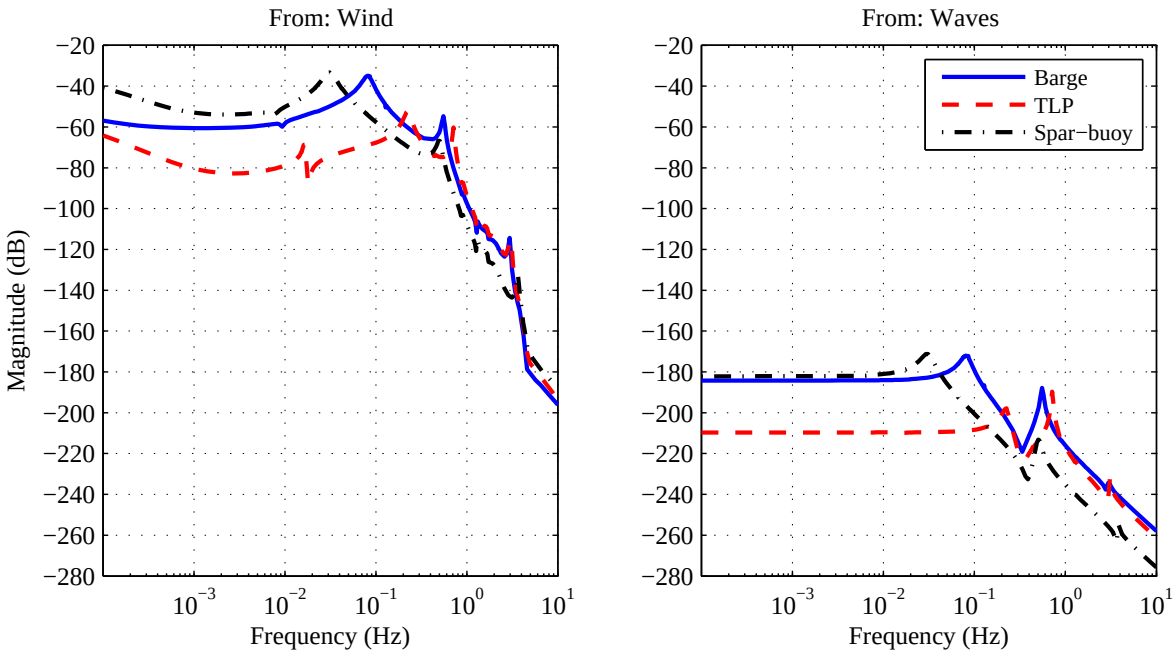

Figure 9.3: Platform pitch frequency response to disturbance inputs

tuation frequency is due to the DACs actively reducing asymmetric loads on the rotor caused by wind shear. The DACs reduce the fluctuations in rotor torque and thrust loads thus improving rotor speed regulation and tower fore-aft bending loads; this is reflected in the averaged DLC results from previous chapters. For the barge platform (Figure 9.2a), there is a moderate increase in actuation around the rotor frequency and thus limited impact on rotor speed regulation; recall that the barge platform is dominated by incident wave disturbances.

The platforms' pitch frequency responses to wind speed perturbation and wave moment disturbance inputs are shown in Figure 9.3. The frequency responses are based on the same linearised models used in Figure 9.1.

For wind speed perturbations, the spar-buoy platform's pitch is most sensitive at low frequencies while TLP is the least sensitive due to its high stiffness. At high frequencies, all the platforms have similar sensitivities to wind speed perturbations. Since wind speed perturbations affect the platform pitch through the blades, the low frequency magnitude of the pitch response to wind speed perturbations is similar to that of blade pitch perturbation (Figure 9.1). However, the magnitude itself is small (around -40 dB for the spar-buoy platform) thus requiring a large blade pitch or wind speed perturbations to noticeably affect the platform pitch.

The frequency response of a wave disturbance input represents a perturbation in the resultant wave moment on the platform pitch; it does not include the hydrodynamic interaction between the incident waves and the platform or the mooring lines. Due to the platform properties, the behaviour is similar to wind speed perturbations with one exception. Since the wave disturbance enters the system through the platform pitch dynamics, the low frequency response is constant and does not depend on the dynamics of the load path (blades and drivetrain flexibilities). The frequency response shown is for 1 Nm perturbation of the resultant wave moment, hence the considerably lower gain. However, the wave moment perturbations are in the or-

der of 10^8 Nm (+160 dB) or higher, depending on sea conditions and platform hydrodynamics, thus having a noticeable impact on platform pitch response. Note that the frequency response to wave moment disturbances shown in Figure 9.3 does not represent the sensitivity of the platform to incident wave conditions as the latter depends on the platform's hydrodynamic properties. That is, a 1 m incident wave, for example, creates a larger resultant wave moment on the barge platform than on the TLP and spar-buoy platform.

9.3 DLC Results Relative to an Onshore Wind Turbine

In this section the DLC simulation results of the three platforms are compared relative to the Baseline controller on an equivalent 5 MW onshore wind turbine. The results are normalised across each individual wind speed bin and then averaged according to the Weibull distribution to obtain the overall averaged results shown in Figure 9.4. Here, a value of less than 1 indicates better performance than the onshore system. The direct averaged simulation results of the Baseline controller (not shown here) agree with DLC 1.2 results presented by Matha [38] for the three floating platforms.

Recall that these results are based on simulations only and therefore are bound by the limitation of the simulation tools used and their associated assumptions. Furthermore, these results are for the above rated wind speed region only. Below rated wind speed region operation and region transition on floating wind turbines are outside the scope of this work.

An interesting result shown in Figure 9.4 is the independence of blade root edgewise bending fatigue DEL from the floating platform type, controller, or whether the turbine is mounted onshore or offshore. The same trend applies for the blade root flapwise bending fatigue DEL except on the barge platform where excessive platform pitching increases the fatigue DEL.

9.3.1 The Barge Platform

The barge platform experiences large motions due to its sensitivity to incident waves. These large motions directly affect power and rotor speed regulation and tower loads. For the Baseline controller on the barge platform, tower FA and SS fatigue loads are 6.9 and 4.48 times that of an onshore wind turbine respectively. Despite the impressive reductions by the SFC reported in Chapter 6, tower FA and SS fatigue DELs remain 4.6 and 2.18 times larger than the onshore wind turbine. Low speed shaft fatigue DEL is also increased by at least 56%. Power fluctuations are almost 4 times larger than the onshore wind turbine, however, the power regulation of the onshore wind turbine is excellent. In terms of percentage of rated power, the barge platform's average power fluctuation is around 5.8% of the rated power of 5 MW; slightly higher than the acceptable 5% error.

The large increase in the fatigue DEL on the main turbine components suggest that, unless the effects of incident waves on the barge are reduced, the barge platform is not suitable for deployment in such harsh sea conditions. Perhaps, as Matha suggested [38], the barge platform can offer a cost-effective solution to sheltered sites such as the Great Lakes in the USA.

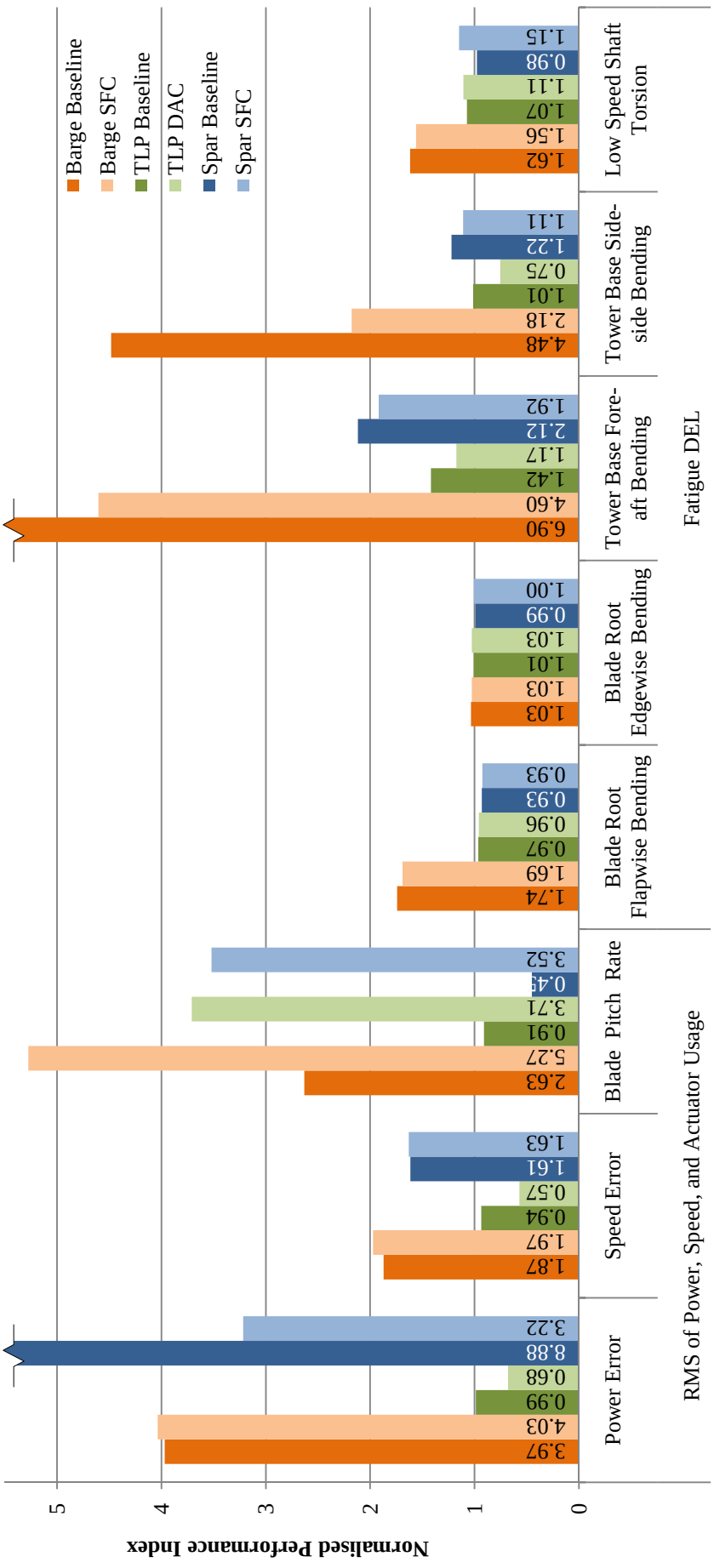

Figure 9.4: Averaged DLC results for all floating platforms relative to the Baseline controller on an onshore wind turbine

9.3.2 The Tension Leg Platform

For the tension leg platform, it is worthy to note that the performance of the Baseline controller relative to the onshore system is almost at parity across most metrics with the exception of RMS power and speed errors, RMS blade pitch rate, and tower fore-aft fatigue DEL. As a result of this parity, the performance of the Disturbance Accommodating Controller relative to the onshore system almost mirrors that of the offshore case in Chapter 7 with the exception of the tower fore-aft fatigue DEL. The Disturbance Accommodating Controller manages to have better power and speed regulation and reduce tower side-side fatigue DEL relative to the onshore system. It may be argued that this is an unfair comparison but recall that the Baseline controller is gain scheduled to account for the nonlinearities present in the system that affect rotor speed regulation. However, tower fore-aft fatigue DEL remains 17% more than that of an onshore wind turbine. The almost parity performance of the TLP controllers relative to the onshore turbine demonstrates the effectiveness of the TLP concept. That is, because platform motions and rotations are kept small, turbine fatigue loads were of a comparable level to an onshore wind turbine with the same controller.

From these results, the TLP demonstrates that with slight strengthening of the turbine tower and when coupled with the improvement in performance brought by using the DAC, it is possible to deploy wind turbines on a floating platform without having to redesign the well established onshore wind turbines.

9.3.3 The Spar-buoy Platform

The dynamic performance of the spar-buoy platform is somewhere between that of the barge platform and the TLP; platforms motions are not as small as the TLP but not as large as the barge platform. As a result, its performance in terms of the tower and low speed shaft fatigue DELs lies between the two platforms. Tower FA and SS fatigue DELs are 2.12 and 1.22 times the onshore loads respectively with the Baseline controller on the spar-buoy platform; the SFC reduces these loads to 1.92 and 1.11 times the onshore wind turbine respectively. Power fluctuations for the Baseline controller, that uses constant torque control algorithm, is 8.88 times that of the onshore wind turbine power variations. These fluctuations are noticeably reduced by the SFC to a factor of 3.22 through the use of constant power control algorithm. In terms of percentage of the turbine's rated power, the Baseline and State Feedback Controllers have average power fluctuations of 11.52% and 4.6% of rated power respectively.

The increase in loading on the tower would require some degree of strengthening of the turbine tower to withstand these loads. Although no information/properties of the deployed 2.3 MW Hywind prototype are publicly available, it is likely that the turbine tower has been strengthened and/or the offshore site where the prototype is deployed is relatively "calmer" than the site used for simulations in this work.

9.4 Chapter Summary

Comparing the simulation results obtained in previous chapters and comparing them relative to an onshore wind turbine allows for direct comparison between the platforms as well as evaluation of the required turbine strength in relative terms to well established onshore wind turbine designs.

Simulation results for the Baseline controller on each floating platform relative to the onshore wind turbine agree with previously published results. The main benefit of using individual blade pitching with the State Feedback and Disturbance Accommodating Controllers is the large reduction in tower fatigue bending loads.

The barge platform experiences large motions due to its sensitivity to incident waves. These motions induce tower loads that are at least 2.18 times that of the onshore wind turbine. Therefore, the current design of the barge platform is not suitable for open sea deployment, however, it may offer a cost effective solution for sheltered sites.

Due to the TLP's extra stiffness from the taught mooring lines, platform motions are kept to a minimum resulting in loads that are comparable to the onshore wind turbine. The additional stiffness reduces the platform's sensitivity to incident wind and wave disturbances. The DAC on the TLP is able to improve power and rotor speed errors and tower base side-side DEL over the onshore wind turbine. Only the tower base fore-aft DEL remains 17% more than the onshore wind turbine. Therefore, with minor strengthening of the tower and using the DAC, the TLP makes an excellent candidate for open sea deployment. However, the economic feasibility of the TLP concept could be a limiting factor.

The spar-buoy platform's large inertia limits the effectiveness of individual blade pitching with the current actuator's saturation limits; this limits the potential of the SFC to improve the platform pitch performance. The spar-buoy platform experiences large enough motions to more than double the tower fore-aft fatigue loads of an onshore wind turbine. Therefore, strengthening or redesign of the tower is required for open sea deployment.

10

Wave Disturbance Rejection: A Case Study

Contents

10.1 Wave Disturbance Rejection **113**
10.2 Case Study: Wave Disturbance Rejection on Floating Wind Turbines **116**
10.3 Chapter Summary **123**

Floating wind turbines are subject to an additional disturbance input over onshore wind turbines: waves. These waves can have a large impact on the dynamic performance of the floating wind turbines and can induce large loads. Therefore, if a Disturbance Accommodating Controller can minimise the effects of incident waves on turbine motion (especially roll and pitch motions), then further load reductions are possible to those achieved by the State Feedback and Disturbance Accommodating Controllers described in previous chapters.

This chapter describes the formulation and implementation of a disturbance accommodating controller designed to minimise the effects of the resultant wave moment on the platform. Wave disturbance rejection is unique to this work where a simplified approach is used to include the effects of waves on system dynamics for disturbance rejection.

10.1 Wave Disturbance Rejection

Implementing wave disturbance rejection on a floating wind turbine requires a slightly different approach to the general DAC formulation described in Chapter 4. To be able to design a DAC for wave disturbance rejection (referred to hereafter as *DAC for waves*), the effects of the input disturbances on system states must be known in the form of the B_d matrix; recall that DAC formulation requires the linearised system to be in the form given by equation (10.1). For

wind disturbances, the effect is readily available from FAST linearisation. However, FAST linearisation does not include waves as a disturbance input. Therefore, to be able to implement wave disturbance rejection, a new B_d matrix must be evaluated.

$$\Delta\dot{\underline{x}}_{\mathrm{NR}} = A_{\mathrm{NR}}\Delta\underline{x}_{\mathrm{NR}} + B_{\mathrm{NR}}\Delta\underline{u}_{\mathrm{NR}} + B_{d,\mathrm{NR}}\Delta\underline{u}_d \tag{10.1}$$

There are many factors that add complexity to this issue. Incident waves are periodic with a spectrum of frequencies whereas FAST linearises the wind turbine based on a fundamental frequency that is a multiple of rotor period. Therefore, it will be extremely difficult to correctly linearise the interaction of incident waves with the periodic wind turbine states. Furthermore, what parameters can be used to describe the incident waves that can be perturbed during linearisation? Irregular waves are described by a wave spectrum, significant wave height, peak spectral period, and random seed numbers, none of which are suitable for linearisation. A simplified approach is used in this work to allow for wave disturbance rejection.

10.1.1 Simplified Modelling Approach

Instead of considering some wave parameters as disturbance inputs, their resultant effect on the platform in terms of moments is considered as the disturbance input. This approach bypasses all the complexity of the nonlinearity and randomness of the waves and their nonlinear interaction with the platform.

The set of nonlinear equations of motion for the floating system, equation (10.2), is in the same format used by FAST [32] where $\underline{q}$ is a vector of the DOFs modelled, and M is the mass matrix.

$$M\left(\underline{q},\underline{u},t\right)\dot{\underline{q}} = \underline{f}\left(\dot{\underline{q}},\underline{q},\underline{u},\underline{u}_{d,wind},t\right) \tag{10.2}$$

Given an incident wave with an arbitrary direction, the resultant moment vector is expressed along the global inertial axes (roll, pitch, and yaw). This additional moment vector results in a term appended to equation (10.2) giving equation (10.3), where $\underline{u}_{d,wave}$ is a 3×1 moment vector (moments long the inertial axes) and $F_{d,wave}$ is a $n_{dof} \times 3$ matrix that applies the resultant moments to the correct differential equations. The term $F_{d,wave}\underline{u}_{d,wave}$ is a nonlinear function of wave height, wave period, current, platform yaw angle, and wave direction.

$$M\left(\underline{q},\underline{u},t\right)\dot{\underline{q}} = \underline{f}\left(\dot{\underline{q}},\underline{q},\underline{u},\underline{u}_{d,wind},t\right) + F_{d,wave}\underline{u}_{d,wave} \tag{10.3}$$

Equation (10.3) is in a generic form that can accommodate incident waves with changing direction. For simplicity, it is assumed that platform yaw angles remain small such that the wave moment components only act on their respective axis. For example, if waves are modelled to act only in the pitch direction for DAC implementation, then the resultant pitch moment only acts on the pitch DOF and has no components in the roll or yaw directions. This assumption reduces $F_{d,waves}$ to a known time-invariant boolean matrix.

Linearisation of equation (10.3) assuming still water (no waves) and without underwater currents results in equation (10.4) where C_d is the damping matrix, K_s is the stiffness matrix, and F

is the actuators gain matrix for a 2nd order system. All the terms in equation (10.4) except for the last term on the right side of the equation can be obtained numerically from FAST linearisation.

$$M(\psi)\,\Delta\underline{\ddot{q}} + C_d(\psi)\,\Delta\underline{\dot{q}} + K_s(\psi)\,\Delta\underline{q} = F(\psi)\,\Delta\underline{u} + F_{d,wind}(\psi)\,\Delta\underline{u}_{d,wind} + F_{d,wave}\Delta\underline{u}_{d,wave} \tag{10.4}$$

where

$$\underline{u}_{d,wave} = \Delta\underline{u}_{d,wave} + \underline{u}^{op}_{d,wave}$$

The moment vector operating point $\underline{u}^{op}_{d,wave}$ contains the hydrostatic and mooring line moments that keep the system in equilibrium at the operating point. Now, let

$$\begin{aligned} \Delta\underline{u}_d &= \begin{bmatrix} \Delta\underline{u}_{d,wind} & \Delta\underline{u}_{d,wave} \end{bmatrix}^{\mathrm{T}} \text{ and} \\ F_d(\psi) &= \begin{bmatrix} F_{d,wind}(\psi) & F_{d,wave} \end{bmatrix} \end{aligned} \tag{10.5}$$

such that

$$M(\psi)\,\Delta\underline{\ddot{q}} + C_d(\psi)\,\Delta\underline{\dot{q}} + K_s(\psi)\,\Delta\underline{q} = F(\psi)\,\Delta\underline{u} + F_d(\psi)\,\Delta\underline{u}_d \tag{10.6}$$

Equation (10.6) is a standard linearised second order state-space equation. All FAST linearisations used in this work are in the second order form (to give access to the mass, damping, and stiffness matrices) which are then converted to first order state-space models for control design.

The first order representation of equation (10.6) is given by equation (10.7) where the $A(\psi)$, $B(\psi)$, and $B_d(\psi)$ matrices can be calculated using equations (10.8) to (10.10) respectively where n, m, and nd are the number of states, control inputs, and disturbance inputs respectively.

$$\Delta\underline{\dot{x}} = A(\psi)\,\Delta\underline{x} + B(\psi)\,\Delta\underline{u} + B_d(\psi)\,\Delta\underline{u}_d \tag{10.7}$$

where

$$A(\psi) = \begin{bmatrix} 0 & I_{ndof\times ndof} \\ -M(\psi)^{-1}K_s(\psi) & -M(\psi)^{-1}C_d(\psi) \end{bmatrix}_{n\times n} \tag{10.8}$$

$$B(\psi) = \begin{bmatrix} 0 \\ M(\psi)^{-1}F(\psi) \end{bmatrix}_{n\times m} \tag{10.9}$$

$$B_d(\psi) = \begin{bmatrix} 0 \\ M(\psi)^{-1}F_d(\psi) \end{bmatrix}_{n\times(nd,wind+nd,wave)} \tag{10.10}$$

Since the new disturbance inputs vector contains wind and wave disturbance inputs, the B_d matrix is partitioned accordingly in equation (10.11). The first element $B_{d,wind}$ is readily available from FAST linearisation. By substituting equation (10.5) into equation (10.10), the second

element $B_{d,wave}$ can be calculated using equation (10.12).

$$B_d(\psi) = \begin{bmatrix} B_{d,wind}(\psi) & B_{d,wave}(\psi) \end{bmatrix} \tag{10.11}$$

$$= \begin{bmatrix} 0 & 0 \\ M(\psi)^{-1} F_{d,wind}(\psi) & M(\psi)^{-1} F_{d,wave}(\psi) \end{bmatrix}$$

$$\therefore B_{d,wave}(\psi) = \begin{bmatrix} 0 \\ M(\psi)^{-1} F_{d,wave}(\psi) \end{bmatrix}_{n \times nd,wave} \tag{10.12}$$

The above derivation allows for a DAC design that rejects wind speed perturbations only, resultant wave moment perturbations only, or both depending on which B_d matrix is used. Once the final form of the B_d matrix is obtained, MBC transformation is used to facilitate the time-invariant DAC design discussed in Chapter 4.

10.2 Case Study: Wave Disturbance Rejection on Floating Wind Turbines

To verify that the aforementioned approach minimises the effects of the wave moment on a floating wind turbine, it is implemented on a low-order linearised model of the spar-buoy platform. The spar-buoy platform is chosen as a test case because it is less sensitive to incident waves than the barge at high frequencies (see Figure 9.3) and not as stiff as the TLP. Nonlinear simulations are then used to evaluate the performance of DAC for waves where actuator saturation and system nonlinearities have an impact on performance. Similar to wind speed disturbance rejection, it is assumed that the wave moment cannot be measured and therefore a disturbance estimator is used.

10.2.1 Linear Time-varying Model

The linear model is based on a 2 DOFs model (rotor and platform pitch DOFs) transformed in the non-rotating frame of reference; MBC transformation is used to account for the periodicity of the wind turbine. The linear model is implemented without actuator saturation to test the full potential of the Disturbance Accommodating Controller.

The floating wind turbine is subjected to constant periodic wave moments of a similar magnitude observed in nonlinear simulations of the spar-buoy platform. Wind speed is held constant at 18 m/s – the linearisation point – thereby having no impact on the turbine dynamics. The DAC is implemented with a gain scaling factor α to "tune" the controller such that $\underline{u}_{\mathrm{NR}} = -K_{\mathrm{NR}}\underline{x}_{\mathrm{NR}} + \alpha G_{d,\mathrm{NR}}\hat{\underline{z}}$; α ranges from 0 to 1.

The disturbance estimator is designed with an assumed waveform of a periodic input with an offset such that $\hat{\underline{u}}_d = a\sin(\omega t) + b\cos(\omega t) + c$. The waveform model is given by equations (10.13) – (10.15). For simplicity, the assumed waveform frequency ω used to design the

disturbance estimator matches the incident wave moment period in the linear simulation.

$$\Gamma = \begin{bmatrix} 0 & 0 & 0 \\ 0 & 0 & 1 \\ 0 & -\omega^2 & 0 \end{bmatrix} \tag{10.13}$$

$$\Theta = \begin{bmatrix} 1 & 1 & 0 \end{bmatrix} \tag{10.14}$$

$$\underline{z}(0) = \begin{bmatrix} c & b & a\omega \end{bmatrix}^{\mathrm{T}} \tag{10.15}$$

The simulation starts with $\alpha = 0$ (i.e. the DAC becomes a State Feedback Controller) and the DAC is fully activated ($\alpha = 1$) at $t = 50$ seconds. Figure 10.1 shows the output of the linear simulation. When the DAC is activated, there is a large increase in blade pitch actuation. This increased actuation is generating the required moment to resist the incident wave moment; of course, such actuation magnitude and rate are not realistic for a floating wind turbine such as the spar-buoy.

The estimate of the incident wave moment closely follows the actual moment (Figure 10.1). Consequently, the restoring moment generated by the blades is in phase with the incident wave moment and, therefore, the DAC is able to reject almost all of the wave effects on system states. Note that complete cancellation can only occur if the disturbances enter the system through the same channel as the actuators [47]; for floating wind turbines, the wave moment affects the system through the floating platform while the restoring moments are generated via the blades, hence, wave disturbance cancellation is not possible.

Table 10.1 summarises the effectiveness of the DAC for waves on a linear system with different values of the gain scaling factor α. Recall that to minimise or cancel the effect of input disturbances, the norm $\|B\alpha G_d + B_d\Theta\|$ must be minimised (equation (4.6)). When the DAC is fully activated, the norm is essentially zero when compared to the full effect of disturbance states ($\alpha = 0$). Therefore, for wave disturbance rejection on a linear system, the DAC can be considered to be cancelling the effects of incident wave moments. When the DAC is operating at 10%, the norm is reduced by 10%; the reduction in the norm is linear with different values of α.

Figure 10.1 shows that after the DAC is activated and the effect of incident wave moment is cancelled, the platform pitch angle enters a damped oscillatory response in which the performance is determined by the design of the SFC-part of the DAC. In fact, the damping ratio of this motion is calculated, using the logarithmic decrement approach described in [87, p. 598], to be that of the closed loop damping ratio of the system which verifies the analysis. Since wind

Table 10.1: Effect of DAC gain scaling factor α on $\|B\alpha G_d + B_d\Theta\|$ for a 2 DOFs linear wind turbine model

α	$\|B\alpha G_d + B_d\Theta\|$	Comment
0.0	1.41	Full effect of disturbance states on system states
0.1	1.27	DAC operating at 10% capacity
1.0	4.1×10^{-10}	DAC operating at 100% capacity

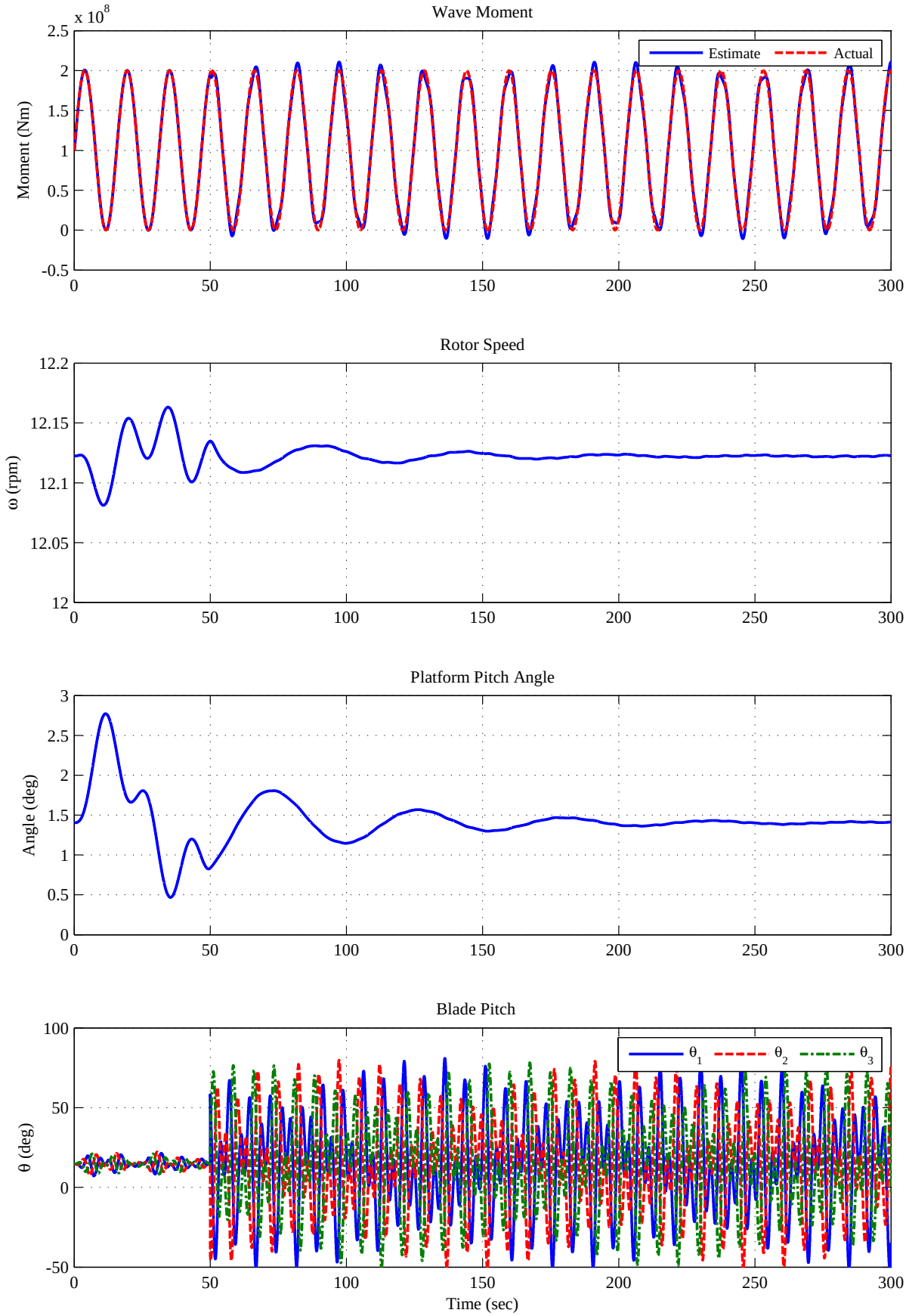

Figure 10.1: Wave disturbance rejection on a linear 2 DOFs model (DAC activated at $t = 50$ seconds)

speed is kept constant, the fluctuations in rotor speed are primarily due to platform pitching velocity affecting the wind speed relative to the rotor.

When the disturbance waveform model only accounts for the wave moment disturbance, a wind speed perturbation is incorrectly interpreted as an incident wave thus leading to a wrong moment estimate. Because the rotor is generating the large wave minimising moment, an error in the estimate causes this large moment to be applied out of phase thus exacerbating the platform pitch moment rather than minimising it. To overcome this limitation, a model of the wind speed perturbation is included in the disturbance waveform model.

This case study demonstrates that wave disturbance rejection based on the approach described in §10.1 is valid for linear systems.

10.2.2 Nonlinear Periodic Model

This case study is used to test the robustness of the DAC for waves when simulated using a nonlinear 2 DOFs model of the spar-buoy with constant wind, regular waves, and actuator saturation. To establish the limit for continuous blade saturation, five simulations are carried out using a different value of the DAC gain scaling factor α.

Figure 10.2 shows the trends of selected performance metrics (relative to the Baseline controller) with α. Note that $\alpha = 0$ represents a SFC without any feed-forward disturbance rejection component. Platform pitch and pitch rate regulation are noticeably improved for $\alpha \leqslant 0.1$ where platform pitch error and pitch rate are reduced by 35% and 20% relative to the baseline controller respectively. For simulations with $\alpha \geqslant 0.15$, the blade pitch rate is periodically saturated to $\pm 8\,\mathrm{deg/s}$ for longer periods as shown in Figure 10.3 and performance degradation is reflected in figures 10.2 and 10.4. When the blades are frequently saturated for $\alpha \geqslant 0.15$, the improvement trend in platform pitch regulation is reversed and rotor speed error is drastically increased.

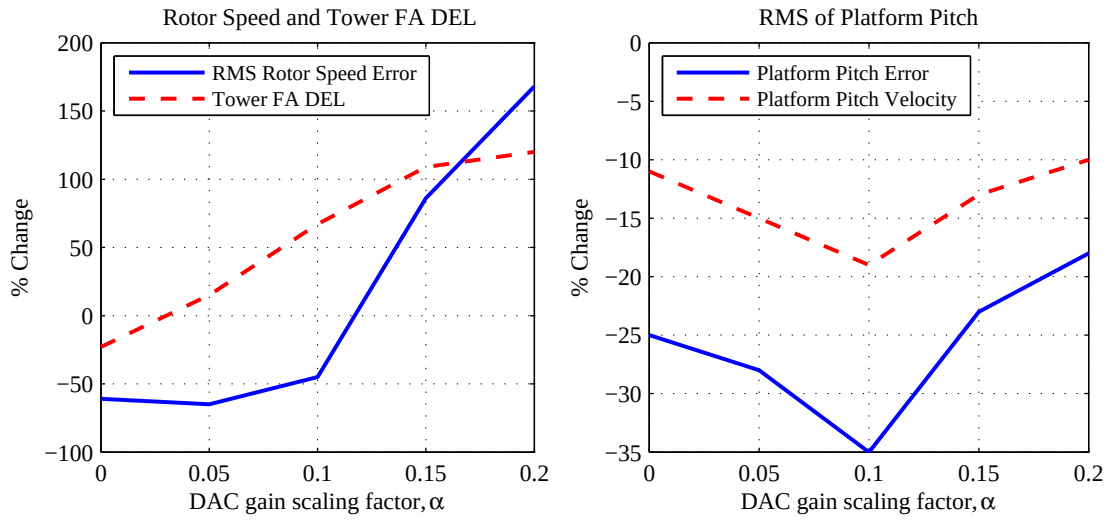

Figure 10.2: Wave disturbance rejection performance relative to the Baseline controller on a nonlinear 2 DOFs model

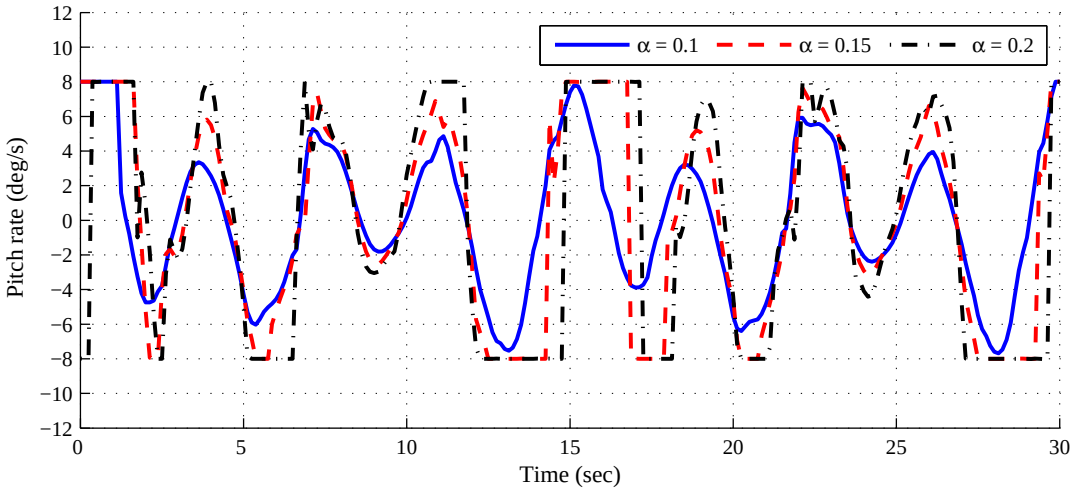

Figure 10.3: Blade 1 pitch rates with different α

The main purpose for implementing wave disturbance rejection is to reduce platform motion such that tower loads caused by the offset gravity load of the Rotor-Nacelle Assembly (RNA) is reduced. However, despite the DAC for waves reducing platform pitch motion and pitching velocity, tower loads suffer a significant increase (up to 67% increase for a non-saturated actuator). This increase in tower fore-aft load can be explained by studying the load path on the tower when a wave moment hits the tower (Figure 10.5). When the floating wind turbine is subjected to an incident wave moment (M_{WAVE} in Figure 10.5), the DAC would, ideally, generate an equal and opposite moment (M_{DAC}) instantly. These two moments bend the tower in the same direction thus increasing the bending loads in the fore-aft direction. This increased bending load is larger than the load reduction brought by reducing the moment created by the offset gravity load of the Rotor-Nacelle Assembly (F_{RNA}).

Figure 10.5 illustrates a fundamental limitation to minimising the effects of wave moments on platform motion by using the blades to generate the restoring moment. Therefore, to reject wave disturbances and reduce tower loads, additional actuators are needed to generate the wave minimisation moment at the platform or mooring line level such that the load is not transferred through the tower. Adding and analysing the effectiveness of additional actuators on floating wind turbines is beyond the scope of this work.

10.2.3 Case Study Summary

Despite the effectiveness of wave disturbance rejection on a linear wind turbine model, there are several factors that limit the performance of DAC for waves on a nonlinear (or more realistic) wind turbine model.

- The incident wave moments are large in magnitude requiring large actuation forces to minimise their effect. Therefore,

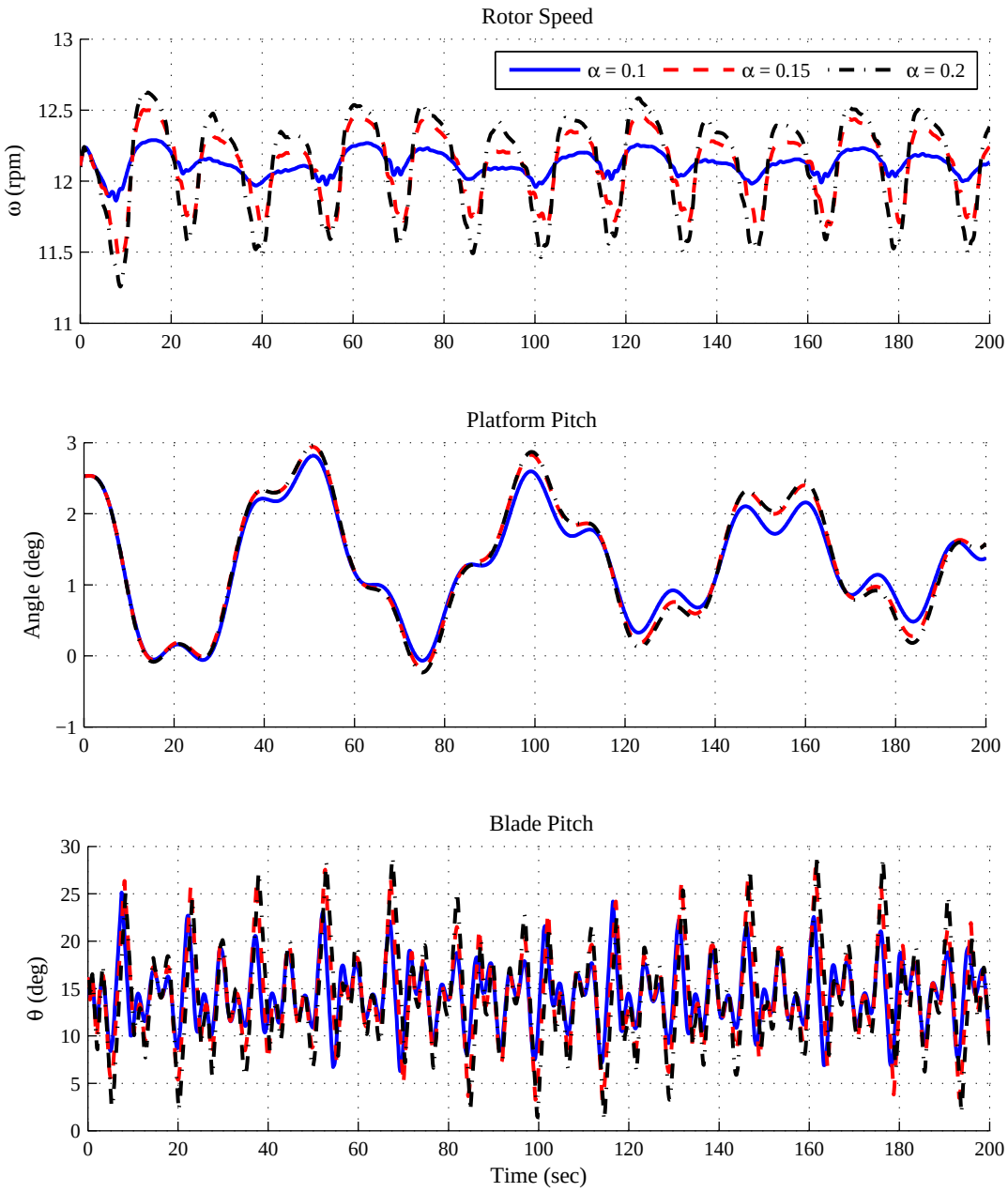

Figure 10.4: Wave DACs with different α simulated with a nonlinear 2 DOFs model

- actuator saturation becomes an important limiting factor in the successful implementation of wave disturbance rejection; and
- accuracy of the disturbance estimates becomes important as a relatively small estimation error causes the large actuation force(s) to be applied out of phase which may excite the platform motions rather than reducing them.

- The approach described in §10.1 and the underlying DAC theory are based on linear systems. Therefore, system nonlinearities can have an impact on performance especially if the DAC is forcing the system or the actuator far away from the linearisation point. For example, Figure 10.1 shows the blade pitch angles range from -50° to 80°. Saturation issues aside, the effectiveness of the blade pitch at these angles varies greatly from the

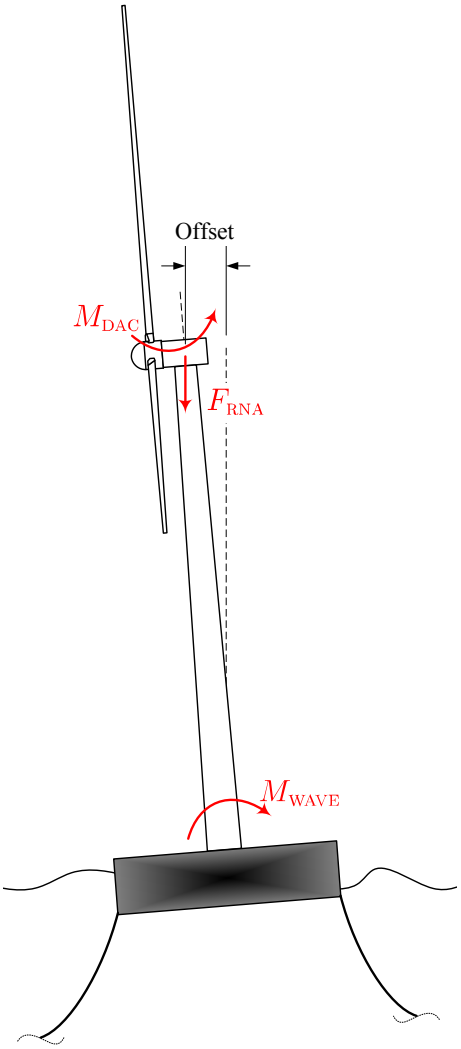

Figure 10.5: Wave minimisation moment load path

linearisation point[12] due to the nonlinearities associated with the blade aerodynamics and blade pitch angle.

- Using the blades to generate the wave minimising moment increases the bending moment on the tower despite the reduction in platform motions. For reducing tower loads, the wave minimising moment must not be transferred through the tower.

Due to the above limitations, further analysis of wave disturbance rejection using full DOFs nonlinear simulation with stochastic wind and irregular waves is not warranted for this work.

The simplified waveform model used in the above approach assumes a constant wave frequency. Irregular waves are usually modelled using a spectrum of frequencies. However, they can also be modelled as having a dominant frequency that slowly changes with time and a randomly varying amplitude depending on sea conditions. Appendix (E) describes the limitations of this approach and introduces an empirical approach to deal with periodic disturbances with a slowly changing frequency.

[12]The DAC, based on the linear model, assumes the blade pitch effectiveness is constant for all operating blade pitch angles.

10.3 Chapter Summary

Implementation of wave disturbance rejection requires manipulation of the linearised state-space model produced by FAST because FAST linearisation currently does not include waves as disturbance inputs. By only considering the resultant moments due to incident waves as disturbance inputs, the effects of these moments on system states can be calculated and thereby facilitating DAC design. This simplified approach bypasses all the nonlinear interaction between the waves and the platform structure but it requires a disturbance estimator because direct measurement of the resultant moments is not possible.

Implementing wave disturbance rejection on a linear model of a floating wind turbine shows that the Disturbance Accommodating Controller can cancel the effects of input periodic wave moments. However, due to actuator saturation and system nonlinearities most of the benefits of wave disturbance rejection are lost when applied on a nonlinear wind turbine model using FAST. Furthermore, using the turbine blades to generate the wave minimisation moment results in increasing the tower bending loads despite reductions in platform motion.

11

Conclusions and Recommendations

Having no rigid foundations, floating offshore wind turbines experience additional motions in 6 directions: platform surge, sway, heave, roll, pitch, and yaw. These additional motions, especially the platform pitch motion, can significantly affect power regulation and turbine loads. Interaction with the waves adds another source of loading on the wind turbine as well as inducing platform motions; incident waves are considered as a disturbance input from a control system point of view.

There are several floating wind turbine designs currently being investigated with some of them reaching a full scale prototype stage. In this work, only the three main floating wind turbine concepts are considered. Each platform uses a different principle to achieve hydrostatic stability. The three floating concepts are: a buoyancy stabilised barge platform, a mooring line stabilised tension leg platform (TLP), and a ballast stabilised spar-buoy platform.

The main objective of this research is to quantify the performance of multi-objective state feedback and disturbance accommodating controllers applied to the three main floating platform concepts. The results presented in this thesis are based entirely on hi-fidelity simulations and, therefore, the results are bound by the limitations of the simulation tools used and their associated assumptions. However, the results are presented in a relative sense with the main conclusions drawn based on physical insight of the floating systems.

The controllers implemented to date on floating wind turbines range from a Gain Scheduled Proportional-Integral (GSPI) controller to account for system nonlinearities over a wide range of wind speeds, a variable power pitch controller that changes the captured power to improve platform pitching, to passive and active tuned mass dampers to add damping to platform pitch. All of these controllers have mainly used collective blade pitching for their actuation. None of the implemented controllers use multi-objective state feedback or disturbance accommodating

controllers to improve platform pitch response *and* regulate rotor speed in a single controller implementation.

Table 11.1 summarises the state of the art in floating wind turbine control. The main contributions of this thesis are included in the last three rows of the table. These controllers use individual blade pitching in a multi-objective controller implementation for state feedback regulation and disturbance rejection of wind speed and wave moment perturbations.

To help categorise the main conclusions of this thesis, this chapter answers the 6 research questions introduced in Chapter 1:

1. ***Does using individual blade pitching help improve the performance over collective blade pitching on a floating wind turbine?***

   Individual blade pitching (IBP) allows the controller to create asymmetric loads on the rotor in addition to the symmetric loads that can be created using collective blade pitching. These asymmetric loads help in better regulating some objective/states, such as the platform pitch DOF, over collective blade pitching alone. Individual blade pitching also prevents the controller from issuing blade pitch commands that conflict when simultaneously regulating rotor speed and platform pitch motion (or tower fore-aft motion, to a lesser extent, on onshore wind turbines). IBP effectively increases the number of available actuators from 2 (generator torque and collective blade pitch angle) to 4 (generator torque and each blade's pitch angle). Therefore, individual blade pitching does help improve the performance on floating wind turbines. For example, IBP with a state feedback controller is able to reduce platform roll, pitch, and yaw rates on the barge platform by 48%, 37%, and 60% respectively relative to the Baseline controller while maintaining rotor speed regulation to a similar level.

2. ***Similarly, does using a multi-objective controller help improve the performance relative to a single-objective Gain Scheduled Proportional-Integral controller on floating wind turbines, consistent with findings for onshore wind turbines?***

   Two types of multi-objective controllers are implemented on the three floating platforms: State Feedback Controller (SFC) and Disturbance Accommodating Controller (DAC) for rejecting wind speed perturbations. Simply put, the DAC consists of the SFC with a feed-forward term for rejecting modelled persistent disturbances. The SFC is implemented with full state feedback as adding a state estimator only degrades the performance. Therefore, the state estimator is excluded from the system design because the objective is to assess the effectiveness/potential of advanced control strategies on floating platforms under ideal estimation conditions.

   Overall, both the SFC and DAC result in better performance in terms of better tower load reductions and reduced platform motions relative to the Baseline controller – collective blade pitch GSPI. The magnitude of relative improvement depends on the performance of the Baseline controller, the dynamics of each platform, its responsiveness to individual blade pitching and sensitivities to external wind and wave disturbances. For example, the SFC on the barge platform reduces the platform roll angle by 41% relative to the

Table 11.1: Summary of most important controllers applied on floating wind turbines to date

Controller Name	Blade Pitch Control	Torque Control	Additional Control Features	Simulation Code	Number of Simulations	Model Fidelity	Simulation Regions	Platform
GSPI	CBP GSPI	Constant power	TTF loop, pitch to stall, or detuned gains	FAST	Extensive	High	2, 3	Barge, TLP, Spar-buoy
GSPI Hywind	CBP GSPI	Constant torque	Constant speed region just below rated with PI torque control loop	HAWC2 / SIMO-RIFLEX	Limited	High	2, 3	Hywind spar-buoy
VPPC	CBP GSPI	Constant torque	Variable rotor speed set-point. IBP for blade load reduction	FAST	Limited	High	3	Barge
EBC	Unknown	Unknown	Wind turbine estimator to hide tower dynamics	HywindSim / SIMO-RIFLEX	Limited	Low	3	Hywind spar-buoy
ASC	Unknown	Unknown	Tuned mass damper with active control	FAST-SC	Moderate	High	3	Barge
IBP SFC	IBP SFC	Constant Power + SFC	Full State Feedback (no state estimator)	FAST	Extensive	High	3	Barge, TLP, Spar-buoy
DAC Wind	IBP SFC	Constant Power + SFC	Wind speed disturbance rejection only	FAST	Extensive	High	3	Barge, TLP, Spar-buoy
DAC Waves	IBP SFC	Constant Power + SFC	Wave moment disturbance rejection only	FAST	Limited	Low	3	Spar-buoy

Legend:

ASC	Active Structural Control	TTF	tower-top feedback
CBP	Collective Blade Pitch	VPPC	variable power pitch control
DAC	Disturbance Accommodating Control		
EBC	Estimator Based Control	Number of Simulations Guide:	
GSPI	Gain Scheduled Proportional-Integral control	Limited	<10
IBP	Individual Blade Pitch	Moderate	<100
SFC	State Feedback Control	Extensive	>100

platform's Baseline controller. The SFC on the TLP only manages an 8% reduction due to the TLP's high stiffness in the roll direction resulting in very small rolling motion for the Baseline and SFC.

3. ***Can a Disturbance Accommodating Controller designed to reject wind and wave disturbances help improve the performance?***

   On the barge platform, there are no differences in performance between the SFC and DAC for wind speed disturbance rejection because of the platform's sensitivity to incident waves thereby dominating the platform motions. However, on the tension leg and spar-buoy platforms, the DAC better regulates rotor speed thus improving power quality and further reduces tower fore-aft bending loads. These improvements are obtained through significant increase in blade pitch actuation without reaching saturation. The increase in blade pitch actuation negatively affects platform roll and yaw motions on the spar-buoy platform.

   Rejecting the effects of incident wave moments on the floating platform using the rotor increases the bending on the tower thus defeating one of the main reasons for implementing the DAC. The increase in tower bending is caused by the load path of the restoring moment generated at the rotor going through the tower; ideally, this restoring moment should be generated at the platform level or lower. Furthermore, to cancel the effects of incident wave moments, the restoring moment requires a large actuation force that, realistically, cannot be generated using the blades.

4. ***How will the three floating platforms perform when compared to each other under normal operating conditions especially when controlled by multi-objective controllers?***

   Comparing between platforms is carried out by normalising the simulation results relative to an equivalent onshore wind turbine. With a single-objective GSPI controller, the TLP has the best overall performance, followed by the spar-buoy and then the barge platform. Despite having a different magnitude in relative improvement in performance brought by implementing the multi-objective controllers on each platform, the ranking of the platforms' performance remains unchanged. However, the resultant loads are closer to that of the onshore wind turbine with the multi-objective controllers.

   The barge platforms is the most sensitive to incident waves due to its large water-plane area forcing it to ride the waves. As a results, it experiences the largest motions and thus the largest tower and blade loads. Multi-objective controllers help reduce these motions and loads, but even the massively reduced loads remain too high for practical deployment in open seas. For example, with the Baseline controller, tower fore-aft (FA) and side-side (SS) fatigue loads are 6.9 and 4.48 times higher than the onshore wind turbine tower loads respectively. The SFC manages to reduce these load factors to 4.6 and 2.18 for tower FA and SS loads respectively.

   Due to the TLP's extra stiffness in the roll, pitch, and heave motions brought by having taught mooring lines, it experiences significantly less rolling and pitching motion than the barge platform. Furthermore, since most of the TLP's hull is underwater, its sensitivity to incident waves is also minimised. As a result of these features and when coupled

with the improvement in performance brought by using the Disturbance Accommodating Controller, the TLP's performance closely resembles that of an onshore wind turbine with slightly higher tower fore-aft bending (17%) and low speed shaft torsion (11%) fatigue loads. Compare these results to the loads of the Baseline controller on the TLP with 42% increase in tower FA load and 7% increase in low speed shaft load relative to the onshore wind turbine; the increase in low speed shaft load for the DAC is due to increased blade pitch actuation.

The spar-buoy platform's motion envelope is not as large as the barge platform but not as good as the TLP's. Therefore, in terms of loads, it falls between the other two platforms. The effectiveness of individual blade pitching and hence the multi-objective controllers is limited on the spar-buoy platform due to its large pitch inertia; performance is marginally better than the GSPI. For example, tower FA fatigue loads ratios to the onshore wind turbine are 2.12 and 1.92 for the Baseline and state feedback controllers respectively. The large pitch inertia results in a low natural frequency that attenuates important high frequency individual blade pitching commands.

5. ***Is it possible to maintain fatigue loads to a level comparable to an onshore wind turbine of similar size?***

   The TLP has the best performance in terms of fatigue loads relative to an onshore wind turbine. Tower base fore-aft bending and low speed shaft torsion fatigue damage equivalent loads (DELs) are only on average 17% and 11% higher than an onshore wind turbine respectively with a Disturbance Accommodating Controller. The DAC manages to reduce tower base side-side bending fatigue DEL by 25% relative to the onshore wind turbine with a GSPI controller.

   The other two platforms experience loads that are much higher than the onshore wind turbine loads especially for the tower base fore-aft bending loads; for example, tower fore-aft bending loads on the barge and spar-buoy platforms are, on average, at least 4.6 and 1.92 times those of an onshore wind turbine respectively. These large loads make the barge and spar-buoy platforms impractical in their current form for open sea deployment.

   Fatigue DELs for the blade root edgewise bending on all three platforms and blade root flapwise bending on the tension leg and spar-buoy platforms are indifferent to the platform and controller used; these loads remain similar to the loads on an onshore wind turbine.

6. ***With the addition of the platform's 6 degrees of freedom, are the current actuators capable of addressing the control needs of the system?***

   The answer to this question depends on the control objectives; for example, wave disturbance rejection with the current actuators is not possible. Actuator saturation especially for the blade pitch actuator does limit the potential of the implemented multi-objective controllers; however, the performance improvements obtained with the current saturation limits are more than satisfactory. Of course, additional actuators that directly affect platform motions are expected to improve the performance noticeably.

In addition to answering the above questions, an interesting behaviour is observed for floating wind turbines. There is coupling between platform pitch and roll in the presence of a controller that only regulates the platform pitch motion and not both. This coupling is caused by the way the blades affect the platform roll and pitch motions and asymmetry in the rotor due to rotor pre-cone, shaft tilt, and wind shear. The result is that the controller induces a rolling moment as it regulates platform pitch. This coupling applies to any controller but is exacerbated by individual blade pitching. This coupling is resolved by including the roll degree of freedom (DOF) in the linear state-space model used for controller design.

Finally, for floating wind turbines, the recommended state-space model order for control design should include the following 6 DOFs: platform roll, pitch and yaw; first tower side-side bending mode; rotor and drivetrain twist. These DOFs are included to improve performance, resolve coupling, and maintain closed loop stability of the floating system.

Below is a list of topics that are yet to be explored yet have the potential to improve the response of floating systems when coupled with advancements in other wind turbine fields (such as blade design and materials). These topics are listed below in no particular order of importance.

- Verification of simulation and controller responses against full scale prototypes. This is a critical issue. The verification process may take some time, but when successful verification of simulation tools is achieved, it will increase the confidence in the predicted controllers' performance.
- A detailed look at region transition to and from above and below rated for floating wind turbines is yet to be investigated. There is a potential for limit cycle oscillations (continuously switching between regions regardless of wind conditions) due to the lack of rigid foundations.
- The effectiveness of passive (or active) structural dampers in extreme conditions. A reduction in platform motions in extreme conditions where the blades are feathered is expected. However, the extent of this reduction needs to be established.

This work showed that the implemented controllers' performance is limited mainly due to actuator saturation, under-actuation, and system nonlinearities. Therefore, the following is suggested:

- Including additional active or passive actuators on the platform to help regulate the platform motions and reduce the usage of the blade pitch actuators. Additional actuators may help improve the motion response of the floating platform. An example would be to use structural control techniques with individual blade pitching in a single controller implementation to regulate rotor speed and reduce platform pitching.
- Applying more advanced controllers such as model predictive and nonlinear control on such systems that take actuator and state saturation and other system nonlinearities into account. The benefits of implementing such complex controllers are yet to be evaluated on floating wind turbines.

Appendices

A

MBC Transformation of Linear State-Space Models

Multiblade coordinate system transformation of linear state-space systems is derived here. The derivation of MBC transformation for second order equations of motion is described in detail by Bir [48]. MBC transformation of state-space systems is only briefly described by Bir giving the final transformation results, however.

A.1 Overview of Approach and Notation

In this derivation we will use the same notation used by Bir [48] where possible; some variable names are changed as they conflict or don't match with previously defined variables.

The equations of motion of a 2nd order dynamic system is given by equation (A.1). The elements in the DOFs vector $\underline{q}$ are sorted such that the fixed DOFs come first followed by those in the rotating frame of reference.

$$M\underline{\ddot{q}} + C_d\underline{\dot{q}} + K_s\underline{q} \quad = \quad F\underline{u} + F_d\underline{u}_d \tag{A.1}$$

MBC transformation is a linear transformation between the non-rotating (NR) and the mixed frames of reference. Equation (A.2) defines this transformation for the DOFs vector $\underline{q}$.

$$\underline{q} = T_1\underline{q}_{\text{NR}} \tag{A.2}$$

The transformation matrix T_1, given by equation (A.3), consists of block diagonal sub-matrices where F_n is the number of states defined using fixed coordinates. Note that T_1 is a periodic matrix since the transformation sub-matrix $\tilde{t}$ is a function of rotor azimuth. For brevity of derivation the periodicity is implied and the notation is omitted. The transformation sub-matrix $\tilde{t}$, given by equation (A.4), is the fundamental transformation matrix used to transform a set of three rotating states between the rotating and non-rotating coordinate systems where ψ_b, given by equation (A.5), is the azimuth angle of blade b.

$$T_1 = \begin{bmatrix} I_{F_n \times F_n} & & \\ & \tilde{t} & \\ & & \ddots \\ & & & \tilde{t} \end{bmatrix} \tag{A.3}$$

$$\tilde{t} = \begin{bmatrix} 1 & \cos\psi_1 & \sin\psi_1 \\ 1 & \cos\psi_2 & \sin\psi_2 \\ 1 & \cos\psi_3 & \sin\psi_3 \end{bmatrix} \tag{A.4}$$

$$\psi_b = \Omega t + \frac{(b-1)\,2\pi}{N_{blades}} \tag{A.5}$$

Similarly, equations (A.6) and (A.7) define the transformations for the control inputs and output measurements respectively where the transformation matrices T_c and T_o are defined by equations (A.8) and (A.9) respectively. F_c and F_o are the number of control inputs and outputs defined using fixed coordinates respectively.

$$\underline{u} = T_c\, \underline{u}_{\mathrm{NR}} \tag{A.6}$$

$$\underline{y} = T_o\, \underline{y}_{\mathrm{NR}} \tag{A.7}$$

$$T_c = \begin{bmatrix} I_{Fc \times Fc} & & \\ & \tilde{t} & \\ & & \ddots \\ & & & \tilde{t} \end{bmatrix} \tag{A.8}$$

$$T_o = \begin{bmatrix} I_{Fo \times Fo} & & \\ & \tilde{t} & \\ & & \ddots \\ & & & \tilde{t} \end{bmatrix} \tag{A.9}$$

Similar to the derivation of MBC transformation equations for 2$^{\mathrm{nd}}$ order equations of motion, we need to differentiate vectors and matrices with respect to time. Below, we define some relationships that will be useful for the derivation. Let

$$\tilde{t}_2 = \begin{bmatrix} 0 & -\sin\psi_1 & \cos\psi_1 \\ 0 & -\sin\psi_2 & \cos\psi_2 \\ 0 & -\sin\psi_3 & \cos\psi_3 \end{bmatrix}$$
$$\tilde{t}_3 = \begin{bmatrix} 0 & -\cos\psi_1 & -\sin\psi_1 \\ 0 & -\cos\psi_2 & -\sin\psi_2 \\ 0 & -\cos\psi_3 & -\sin\psi_3 \end{bmatrix}$$

such that

$$\dot{\tilde{t}} = \Omega\tilde{t}_2 \tag{A.10}$$
$$\dot{\tilde{t}}_2 = \Omega\tilde{t}_3 \tag{A.11}$$

Similarly, let

$$T_2 = \begin{bmatrix} 0_{F_n \times F_n} & & & \\ & \tilde{t}_2 & & \\ & & \ddots & \\ & & & \tilde{t}_2 \end{bmatrix}$$
$$T_3 = \begin{bmatrix} 0_{F_n \times F_n} & & & \\ & \tilde{t}_3 & & \\ & & \ddots & \\ & & & \tilde{t}_3 \end{bmatrix}$$

such that

$$\dot{T}_1 = \Omega T_2 \tag{A.12}$$
$$\dot{T}_2 = \Omega T_3 \tag{A.13}$$

Note that equations (A.12) and (A.13) utilise the relationships defined by equations (A.10) and (A.11).

A.2 The State Equation

In order to make use of the already defined transformation equation (equation (A.2)) for a second order state-space model given by equation (A.1), we must define the system in state-space notation given by equation (A.14) by defining a state vector. The state vector is defined by equation (A.15) while its non-rotating equivalent is given by equation (A.16).

$$\dot{\underline{x}} = A\underline{x} + B\underline{u} + B_d\underline{u}_d \tag{A.14}$$

$$\underline{x} = \begin{bmatrix} \underline{q} & \dot{\underline{q}} \end{bmatrix}^{\mathrm{T}} \tag{A.15}$$

$$\underline{x}_{\mathrm{NR}} = \begin{bmatrix} \underline{q}_{\mathrm{NR}} & \dot{\underline{q}}_{\mathrm{NR}} \end{bmatrix}^{\mathrm{T}} \tag{A.16}$$

To transform equation (A.14) to the non-rotating frame, we must first derive the transformation equations of the variables $\dot{\underline{x}}$, $\underline{x}$, and $\underline{u}$; recall that we assumed the disturbance inputs $\underline{u}_d$ is always in the fixed frame. For the actuators vector $\underline{u}$, the transformation equation is defined by equation (A.6).

For the states vector, we start by differentiating the equation (A.2) with respect to time and substituting in equation (A.12). The result is given by equation (A.17).

$$\begin{aligned} \dot{\underline{q}} &= \dot{T}_1\underline{q}_{\mathrm{NR}} + T_1\dot{\underline{q}}_{\mathrm{NR}} \\ &= \Omega T_2\underline{q}_{\mathrm{NR}} + T_1\dot{\underline{q}}_{\mathrm{NR}} \end{aligned} \tag{A.17}$$

Substituting equations (A.2) and (A.17) into equation (A.15) and in conjunction with equation (A.16) we arrive at equation (A.18). Note that equation (A.18) is actually equation (3.9) that was used to define the state transformation in Chapter 3.

$$\begin{aligned} \underline{x} &= \begin{bmatrix} T_1\underline{q}_{\mathrm{NR}} \\ \Omega T_2\underline{q}_{\mathrm{NR}} + T_1\dot{\underline{q}}_{\mathrm{NR}} \end{bmatrix} = \begin{bmatrix} T_1 & 0 \\ \Omega T_2 & T_1 \end{bmatrix} \underline{x}_{\mathrm{NR}} \\ \therefore \underline{x} &= T_s\underline{x}_{\mathrm{NR}} \end{aligned} \tag{A.18}$$

where

$$T_s = \begin{bmatrix} T_1 & 0 \\ \Omega T_2 & T_1 \end{bmatrix}$$

The transformation equation for $\dot{\underline{x}}$ can be derived by differentiating equation (A.18) with respect to time as shown by equation (A.19). The time differential of the state transformation matrix T_s is given by equation (A.20).

$$\dot{\underline{x}} = \dot{T}_s\underline{x}_{\mathrm{NR}} + T_s\dot{\underline{x}}_{\mathrm{NR}} \tag{A.19}$$

$$\begin{aligned} \dot{T}_s &= \begin{bmatrix} \dot{T}_1 & 0 \\ \dot{\Omega}T_2 + \Omega\dot{T}_2 & \dot{T}_1 \end{bmatrix} \\ &= \begin{bmatrix} \Omega T_2 & 0 \\ \dot{\Omega}T_2 + \Omega^2 T_3 & \Omega T_2 \end{bmatrix} \end{aligned} \tag{A.20}$$

Substituting equation (A.20) into equation (A.19) and collecting similar terms of $\underline{\dot{q}}_{\mathrm{NR}}$ in the second row of equations of $\underline{\dot{x}}$ results in the transformation equation for $\underline{\dot{x}}$ given by equation (A.21).

$$\begin{aligned}\underline{\dot{x}} &= \begin{bmatrix} T_1 & 0 \\ \Omega T_2 & T_1 \end{bmatrix} \begin{bmatrix} \underline{\dot{q}}_{\mathrm{NR}} \\ \underline{\ddot{q}}_{\mathrm{NR}} \end{bmatrix} + \begin{bmatrix} \Omega T_2 & 0 \\ \dot{\Omega} T_2 + \Omega^2 T_3 & \Omega T_2 \end{bmatrix} \begin{bmatrix} \underline{q}_{\mathrm{NR}} \\ \underline{\dot{q}}_{\mathrm{NR}} \end{bmatrix} \\ &= \begin{bmatrix} T_1 & 0 \\ 0 & T_1 \end{bmatrix} \underline{\dot{x}}_{\mathrm{NR}} + \begin{bmatrix} \Omega T_2 & 0 \\ \dot{\Omega} T_2 + \Omega^2 T_3 & 2\Omega T_2 \end{bmatrix} \underline{x}_{\mathrm{NR}} \end{aligned} \tag{A.21}$$

Finally, substituting equations (A.18), (A.21), and (3.10) into the state equation (equation (A.14)), we get

$$\begin{bmatrix} T_1 & 0 \\ 0 & T_1 \end{bmatrix} \underline{\dot{x}}_{\mathrm{NR}} + \begin{bmatrix} \Omega T_2 & 0 \\ \dot{\Omega} T_2 + \Omega^2 T_3 & 2\Omega T_2 \end{bmatrix} \underline{x}_{\mathrm{NR}} = AT_s \underline{x}_{\mathrm{NR}} + BT_c \underline{u}_{\mathrm{NR}} + B_d \underline{u}_d$$

Rearranging for $\underline{\dot{x}}_{\mathrm{NR}}$ we get equation (A.23) which is the same as equation (3.7) and matrices A_{NR}, B_{NR}, and $B_{d,\mathrm{NR}}$ can be inferred from equation (A.22).

$$\begin{aligned}\underline{\dot{x}}_{\mathrm{NR}} &= \begin{bmatrix} T_1^{-1} & 0 \\ 0 & T_1^{-1} \end{bmatrix} \left[AT_s - \begin{bmatrix} \Omega T_2 & 0 \\ \dot{\Omega} T_2 + \Omega^2 T_3 & 2\Omega T_2 \end{bmatrix} \right] \underline{x}_{\mathrm{NR}} + \\ &\quad \begin{bmatrix} T_1^{-1} & 0 \\ 0 & T_1^{-1} \end{bmatrix} BT_c \underline{u}_{\mathrm{NR}} + \\ &\quad \begin{bmatrix} T_1^{-1} & 0 \\ 0 & T_1^{-1} \end{bmatrix} B_d \underline{u}_d \end{aligned} \tag{A.22}$$

$$\underline{\dot{x}}_{\mathrm{NR}} = A_{\mathrm{NR}} \underline{x}_{\mathrm{NR}} + B_{\mathrm{NR}} \underline{u}_{\mathrm{NR}} + B_{d,\mathrm{NR}} \underline{u}_d \tag{A.23}$$

A.3 The Output Equation

The output equation for a state-space model is given by equation (A.24).

$$\underline{y} = C\underline{x} + D\underline{u} + D_d \underline{u}_d \tag{A.24}$$

To obtain the output equation transformed in the non-rotating frame, we substitute equations (A.6), (A.7), (A.18), and (A.21) into equation (A.24). The result is equation (A.7) which is the same as equation (3.8) and matrices C_{NR}, D_{NR}, and $D_{d,\mathrm{NR}}$ can be inferred from equation (A.25).

$$
\begin{aligned}
T_o \underline{y}_{\text{NR}} &= C T_s \underline{x}_{\text{NR}} + D T_c \underline{u}_{\text{NR}} + D_d \underline{u}_d \\
\underline{y}_{\text{NR}} &= T_o^{-1} C T_s \underline{x}_{\text{NR}} + T_o^{-1} D T_c \underline{u}_{\text{NR}} + T_o^{-1} D_d \underline{u}_d \qquad \text{(A.25)} \\
\therefore \underline{y}_{\text{NR}} &= C_{\text{NR}} \underline{x}_{\text{NR}} + D_{\text{NR}} \underline{u}_{\text{NR}} + D_{d,\text{NR}} \underline{u}_d \qquad \text{(A.26)}
\end{aligned}
$$

Note that in Bir's derivation [48], the state transformation matrix T_s (equation (A.18)) is not defined. Hence, his definition of C_{NR}, given by equation (A.27), is different from that given by equation (A.36). Starting with equation (A.36), one can arrive at Bir's expression, given in equation (A.27), by expanding T_s and appropriately partitioning the C matrix.

$$
C_{\text{NR}} = T_o^{-1} \begin{bmatrix} C_1 T_1 + \Omega C_2 T_2 & C_2 T_1 \end{bmatrix} \text{ where } C = \begin{bmatrix} C_1 & C_2 \end{bmatrix} \qquad \text{(A.27)}
$$

A.4 Summary

Given a linear periodic state-space model in the mixed frame of reference (given by equations (3.5) and (3.6)) is transformed into a time-invariant model given by equations (A.28) and (A.29) using equations (A.30) to (A.32).

$$
\begin{aligned}
\dot{\underline{x}}_{\text{NR}} &= A_{\text{NR}}\, \underline{x}_{\text{NR}} + B_{\text{NR}}\, \underline{u}_{\text{NR}} + B_{d,\text{NR}}\, \underline{u}_d \qquad \text{(A.28)} \\
\underline{y}_{\text{NR}} &= C_{\text{NR}}\, \underline{x}_{\text{NR}} + D_{\text{NR}}\, \underline{u}_{\text{NR}} + D_{d,\text{NR}}\, \underline{u}_d \qquad \text{(A.29)} \\
\underline{x} &= T_s(\psi)\, \underline{x}_{\text{NR}} \qquad \text{(A.30)} \\
\underline{u} &= T_c(\psi)\, \underline{u}_{\text{NR}} \qquad \text{(A.31)} \\
\underline{y} &= T_o(\psi)\, \underline{y}_{\text{NR}} \qquad \text{(A.32)}
\end{aligned}
$$

The definitions of the newly transformed matrices A_{NR}, B_{NR}, $B_{d,\text{NR}}$, C_{NR}, D_{NR}, and $D_{d,\text{NR}}$ are given by equations (A.33) to (A.38) respectively.

$$
\begin{aligned}
A_{\text{NR}} &= \begin{bmatrix} T_1^{-1} & 0 \\ 0 & T_1^{-1} \end{bmatrix} \left[A T_s - \begin{bmatrix} \Omega T_2 & 0 \\ \Omega^2 T_3 + \dot{\Omega} T_2 & 2\Omega T_2 \end{bmatrix} \right] \qquad \text{(A.33)} \\
B_{\text{NR}} &= \begin{bmatrix} T_1^{-1} & 0 \\ 0 & T_1^{-1} \end{bmatrix} B T_c \qquad \text{(A.34)} \\
B_{d,\text{NR}} &= \begin{bmatrix} T_1^{-1} & 0 \\ 0 & T_1^{-1} \end{bmatrix} B_d \qquad \text{(A.35)} \\
C_{\text{NR}} &= T_o^{-1} C T_s \qquad \text{(A.36)} \\
D_{\text{NR}} &= T_o^{-1} D T_c \qquad \text{(A.37)} \\
D_{d,\text{NR}} &= T_o^{-1} D_d \qquad \text{(A.38)}
\end{aligned}
$$

B

Other Implementation Options for DAC After MBC Transformation

Various implementation options are developed and considered for implementing disturbance accommodating controllers for periodic systems after applying multi-blade coordinate transformation. These options are described in this appendix. However, these options are not suitable for systems with slow actuator dynamics or actuator saturation. This appendix follows the discussion in § 4.4 on page 48.

There are two implementation options for DAC after MBC transformation. The first option, illustrated in Figure B.1a, uses equation (B.1) instead of equation (B.2) since the output of the disturbance estimator is already in the nonrotating frame. The controller commands are then transformed into the mixed frame by applying equation (B.3).

$$\underline{u}_{\mathrm{NR}} = -K_{\mathrm{NR}}\underline{\hat{x}}_{\mathrm{NR}} + G_{d,\mathrm{NR}}\underline{\hat{z}} \tag{B.1}$$

$$\underline{u} = -K_{\mathrm{MBC}}(\psi)\,\underline{\hat{x}} + G_{d,\mathrm{MBC}}(\psi)\,\underline{\hat{z}} \tag{B.2}$$

$$\underline{u} = T_c(\psi)\,\underline{u}_{\mathrm{NR}} \tag{B.3}$$

In the second option, equation (B.2) is applied. For this implementation option, the disturbance estimator output $\underline{\hat{w}}_{\mathrm{NR}}$ must be transformed back into the mixed frame using equation (B.4) before the control law is applied. This implementation is shown in Figure B.1b. Implementation option 1 is preferred as it requires periodic gain calculations only for two matrices ($E(\psi)$ and $T_c(\psi)$) whereas option 2 requires periodic gain calculations for four matrices ($E(\psi)$, $K_{\mathrm{LQR}}(\psi)$, $G_{d,\mathrm{MBC}}(\psi)$ and $T_d(\psi)$).

$$\underline{w} = \begin{bmatrix} T_s(\psi) & 0 \\ 0 & I_{nd\times nd} \end{bmatrix} \underline{w}_{\mathrm{NR}} = T_d(\psi)\, \underline{w}_{\mathrm{NR}} \tag{B.4}$$

Another variant of implementation option 1 is used to avoid the redundant transformation of $\Delta\underline{u}_{\mathrm{NR}}$ to $\Delta\underline{u}$ and then back to $\Delta\underline{u}_{\mathrm{NR}}$. This is achieved by rewriting equation (B.5) into equation (B.6) where $\Delta\underline{u}_{\mathrm{NR}}$ is obtained directly from the controller output and $\Delta\underline{y}_{\mathrm{NR}}$ is the only input that is transformed to the non-rotating frame. In block diagram, this is shown in Figure B.1c. Note that the disturbance estimator now includes matrix E_{NR} instead of the identity matrix in the previous two implementation options. This option does not require the computation of the $T_c^{-1}(\psi)$ matrix which is part of the $E(\psi)$ matrix given by equation (4.22).

$$\dot{\underline{\hat{w}}}_{\mathrm{NR}} = \left(\overline{A}_{\mathrm{NR}} - K_{e,\mathrm{NR}}\overline{C}_{\mathrm{NR}}\right)\underline{\hat{w}}_{\mathrm{NR}} + \overline{B}_{\mathrm{NR}}\,\underline{u}_{\mathrm{NR}} + K_{e,\mathrm{NR}}\,\underline{y}_{\mathrm{NR}} \tag{B.5}$$

$$\begin{aligned} \dot{\underline{\hat{w}}}_{\mathrm{NR}} &= \left(\overline{A}_{\mathrm{NR}} - K_{e,\mathrm{NR}}\overline{C}_{\mathrm{NR}}\right)\underline{\hat{w}}_{\mathrm{NR}} + \begin{bmatrix} \overline{B}_{\mathrm{NR}} & K_{e,\mathrm{NR}} \end{bmatrix} \begin{bmatrix} \underline{u}_{\mathrm{NR}} \\ \underline{y}_{\mathrm{NR}} \end{bmatrix} \\ &= \left(\overline{A}_{\mathrm{NR}} - K_{e,\mathrm{NR}}\overline{C}_{\mathrm{NR}}\right)\underline{\hat{w}}_{\mathrm{NR}} + E_{\mathrm{NR}}\underline{v}_{\mathrm{NR}} \end{aligned} \tag{B.6}$$

Unfortunately, option 3 cannot be implemented if actuator saturation limits exist because the limits cannot be transformed to the non-rotating frame. Furthermore, this set up cannot be used if the actuator dynamics are sufficiently slow. Otherwise, if the controller output in the non-rotating frame is passed directly to the disturbance estimator, it could lead to wrong estimates as the passed control inputs do not match the actual inputs to the plant.

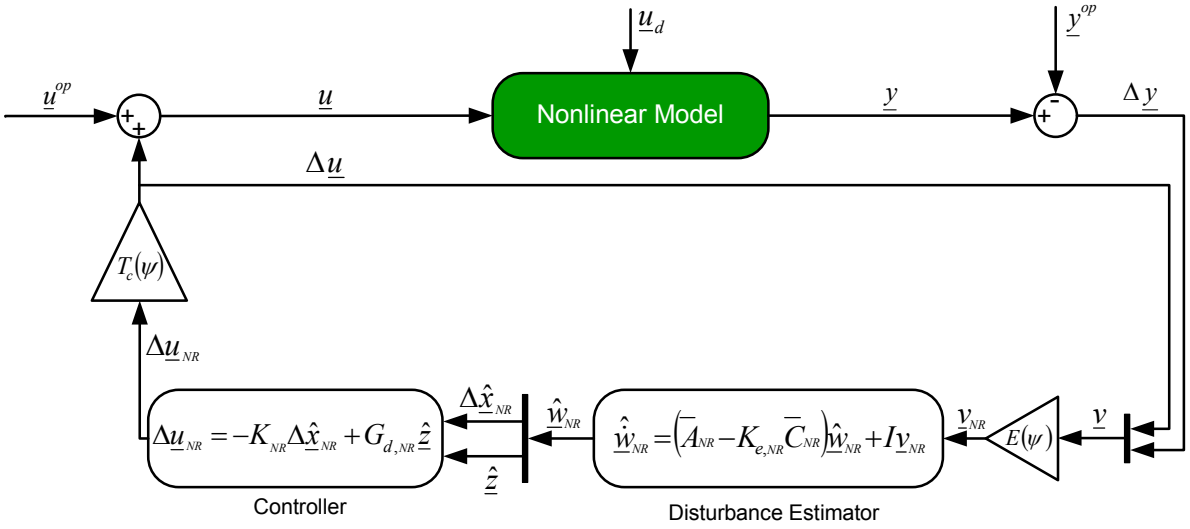

(a) Option 1

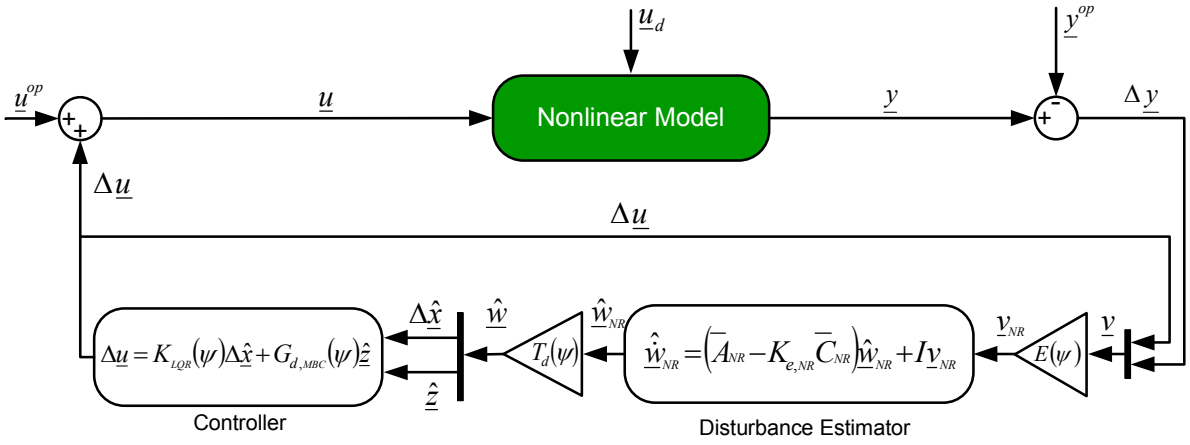

(b) Option 2

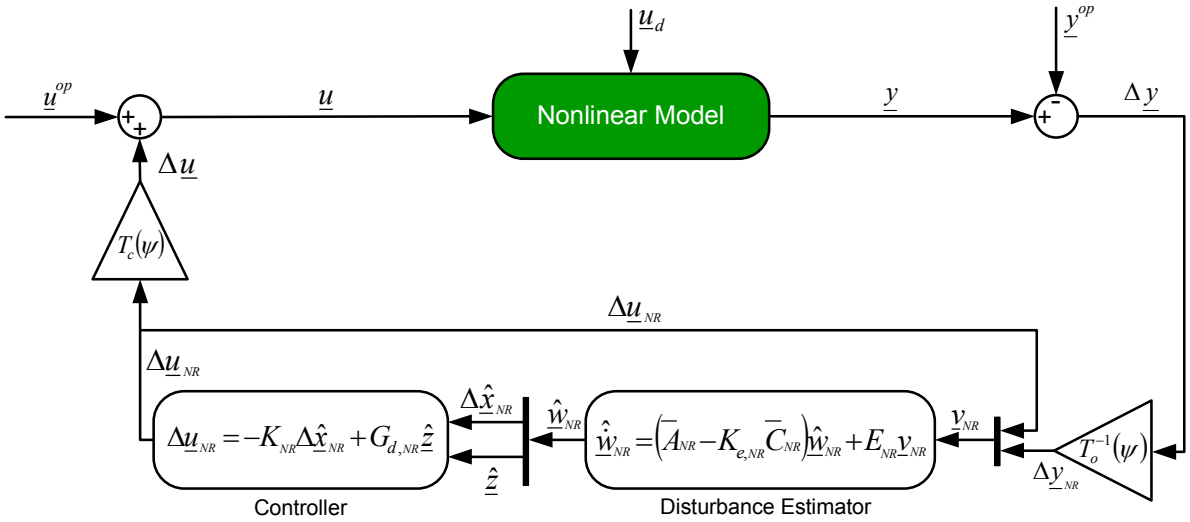

(c) Option 3

Figure B.1: General DAC implementation options

C

Design Load Cases

In this appendix, Table C.1 lists the parameters used to generate the stochastic wind and wave conditions used for DLC analysis specified by the IEC 61400-3 standard [39]. The full field stochastic wind speed profiles are generated using TurbSim [80] while the irregular waves are generated using the HydroDyn module of FAST.

Table C.1: Stochastic wind and wave parameters used for DLC analysis

Wind Speed Bin (m/s)	Wind Random Seed 1	Wind Random Seed 2	Wave Height (m)	Wave Period (s)	Wave Random Seed 1	Wave Random Seed 2	DLC #
15	905792	126987	3.4	13.164	957506835	157613082	1
	134974	988776		14.331	970592782	485375649	2
	357689	98366		15.498	800280469	141886339	3
	5687	12767		16.666	327229303	758402255	4
	229702	848597		17.833	1773428449	1763500767	5
	113949	50647		19.000	1156081573	33078631	6

Table continues on next page ...

... continued from previous page.

Wind Speed Bin (m/s)	Wind Random Seed 1	Wind Random Seed 2	Wave Height (m)	Wave Period (s)	Wave Random Seed 1	Wave Random Seed 2	DLC #
16	310923	466202	3.6	13.451	2139183008	92392911	7
	800281	141887		14.361	167880670	362903324	8
	651998	630206		15.271	950644343	1393964863	9
	66161	230300		16.181	229035080	1571361853	10
	275432	579885		17.090	2065660392	1391023859	11
	281821	603157		18.000	9951921	968351283	12
17	880067	599880	3.8	13.917	1664107546	1174692648	13
	444331	448428		14.734	1755145296	636344083	14
	755915	35424		15.550	1865507668	1599215621	15
	603297	513815		16.367	181324597	405777804	16
	783266	407731		17.183	858526699	1474839008	17
	113931	108047		18.000	558067439	394087205	18
18	814724	585268	4.0	14.278	1718133973	791314643	19
	157613	957167		15.583	926454137	1343505625	20
	485376	421761		16.887	1955600811	1675525653	21
	459876	506795		18.191	390513519	174216262	22
	450883	199926		19.496	566512448	1995841168	23
	551141	427194		20.800	312542580	1665830287	24
19	805405	168691	4.1	14.456	292205004	1045377067	25
	700851	751695		15.465	1866790795	935999189	26
	872236	368351		16.473	1244906118	959460793	27
	52193	941818		17.482	1180815788	657880480	28
	219682	17173		18.491	311288058	1092014019	29
	459643	829056		19.500	1831870370	1096873578	30

Table continues on next page ...

... continued from previous page.

Wind Speed Bin (m/s)	Wind Random Seed 1	Wind Random Seed 2	Wave Height (m)	Wave Period (s)	Wave Random Seed 1	Wave Random Seed 2	DLC #
20	958534	626591	4.6	15.312	1335853219	1755842128	31
	790046	538747		16.050	753664497	1706887465	32
	451875	650508		16.787	1102194991	1383662644	33
	333429	726630		17.525	862876179	813057456	34
	59096	94489		18.262	163137228	1742855757	35
	740906	877574		19.000	515216015	1144234235	36
21	678735	757740	4.9	15.803	264825396	753180718	37
	392227	655478		16.243	394938967	2016490493	38
	97541	278499		16.682	515294124	1881072858	39
	14363	796180		17.121	896074205	1181451746	40
	294303	691192		17.561	106632077	1336755064	41
	179915	345308		18.000	1938568078	1260668899	42
22	926295	946817	5.1	16.123	2028915034	446123175	43
	68181	520191		16.898	1054122609	646921566	44
	581094	953814		17.674	1050662037	1011300187	45
	637152	73596		18.449	725246908	494969554	46
	651270	207032		19.225	1932850911	1813139320	47
	864623	775028		20.000	792951422	418253126	48
23	55953	914188	5.2	16.280	238806098	485163329	49
	816856	782551		17.524	1675578552	366592739	50
	528923	295535		18.768	836957777	488905355	51
	694351	151846		20.012	519028083	935655797	52
	212405	847911		21.256	867394725	668087071	53
	543280	784855		22.500	207134515	1982942675	54

Table continues on next page ...

... continued from previous page.

Wind Speed Bin (m/s)	Wind Random Seed 1	Wind Random Seed 2	Wave Height (m)	Wave Period (s)	Wave Random Seed 1	Wave Random Seed 2	DLC #
24	702521	270832	5.8	17.194	283410487	923863335	55
	956435	227811		17.715	2023038232	396890024	56
	444543	321024		18.236	2053283283	1943217077	57
	85398	829562		18.757	1235251048	2103993614	58
	57341	822183		19.279	128375591	942466088	59
	629451	570683		19.800	504186023	238626715	60

D

Relative Performance Trends for Controllers on Floating Platforms

Performance trends of the State Feedback and Disturbance Accommodating Controllers on each floating platform across wind speed bins for the IEC 61400-3 standard are presented in this appendix. The performance metrics are relative to the respective platform's Baseline controller. A summary of the performance trends is presented in each of the platform's respective chapter.

Figures D.1 and D.2 show the performance trends of the SFC and DAC on the barge platform respectively. Both Controllers are designed based on a 6 DOFs linear state-space model. The barge platform's performance trends are discussed in § 6.3.1 on page 75.

For the tension leg platform, figures D.3 and D.4 show the performance trends of the SFC and DAC on the barge platform respectively. Both Controllers are designed based on a 7 DOFs linear state-space model. The tension leg platform's performance trends are discussed in § 7.3.1 on page 83.

Finally, the performance trends of the SFC and DAC on the spar-buoy platform are shown in figures D.5 and D.6 respectively. Both Controllers are designed based on a 8 DOFs linear state-space model. The spar-buoy platform's performance trends are discussed in § 8.3.1 on page 95.

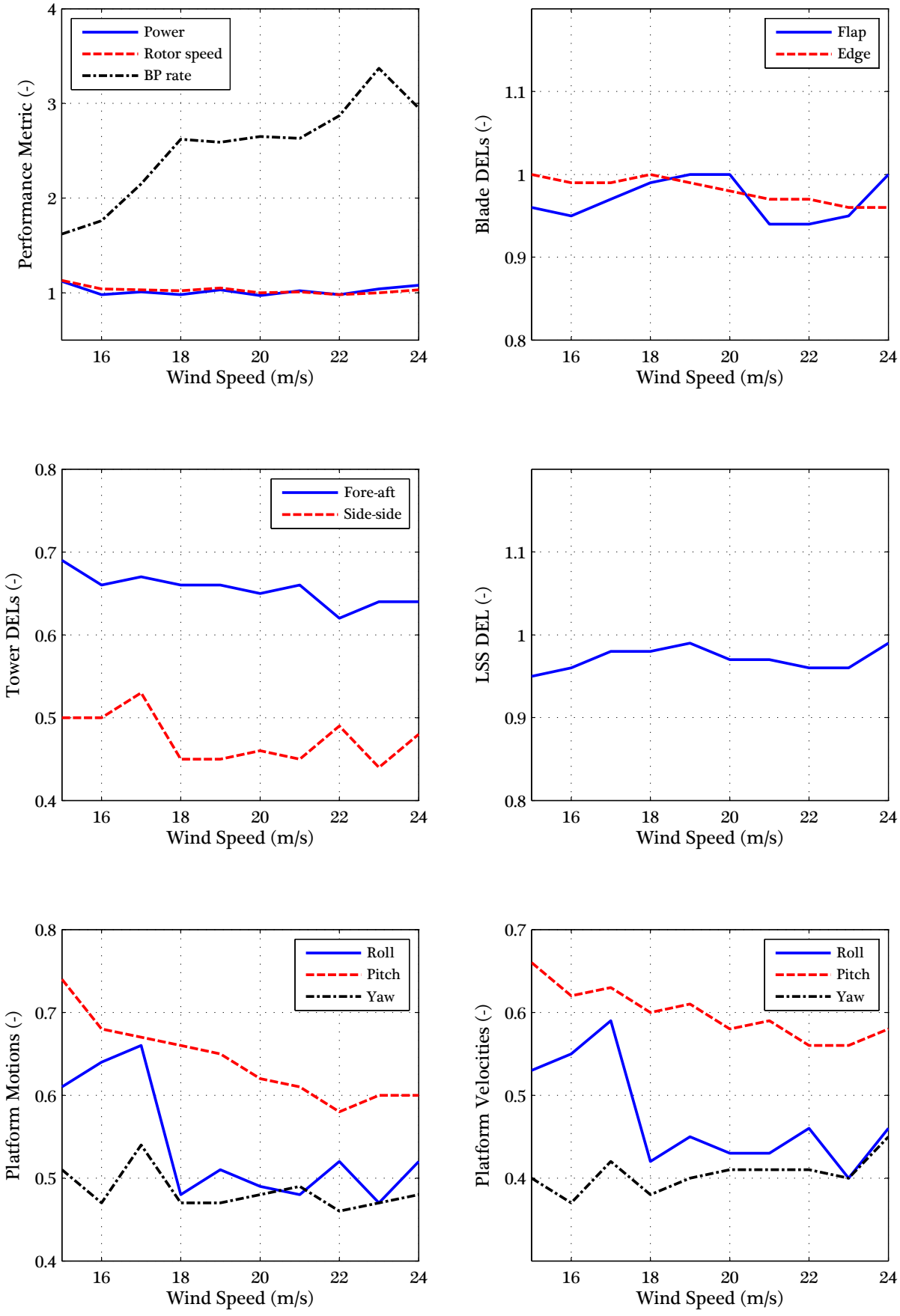

Figure D.1: Performance trends for the SFC on the barge platform

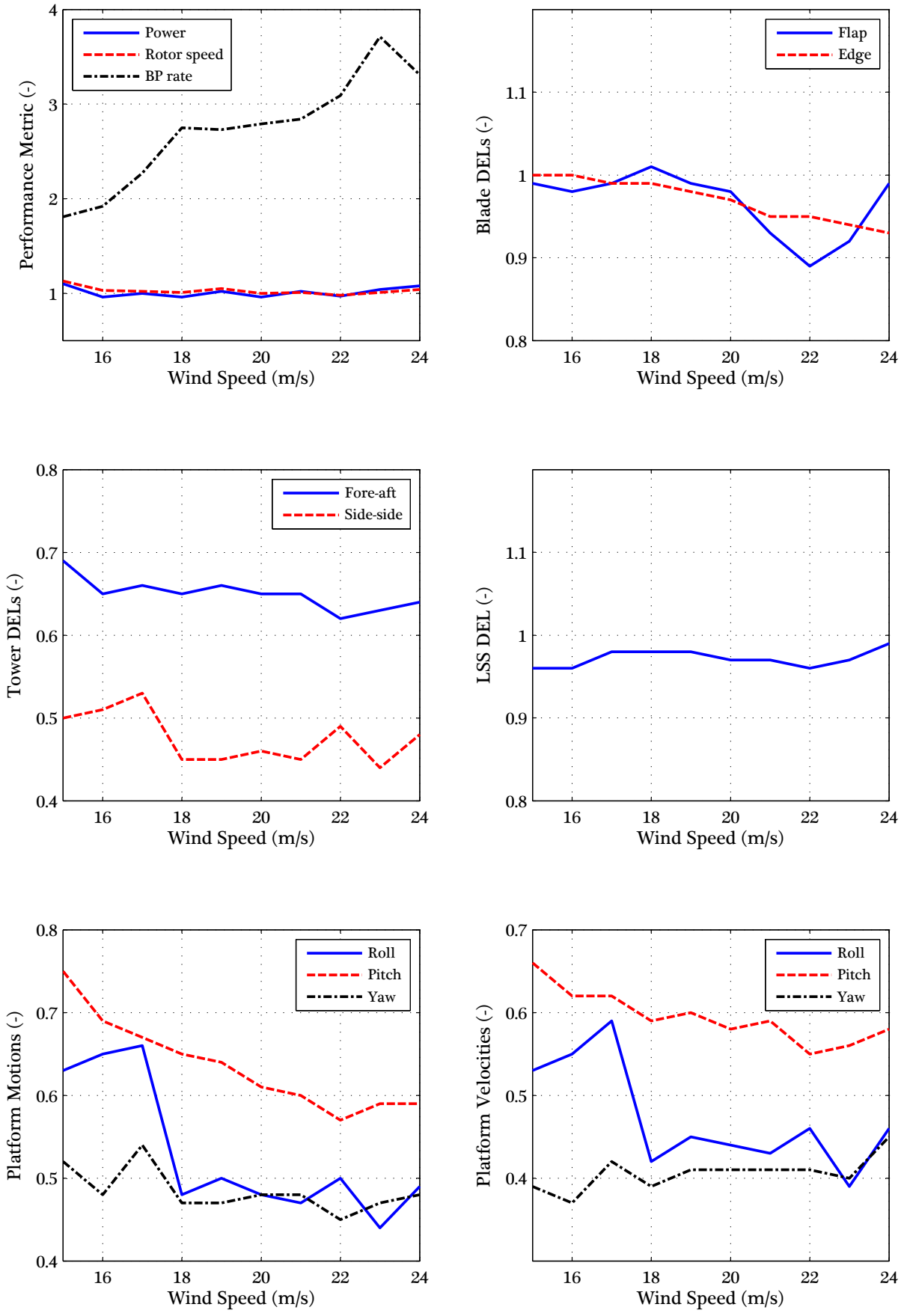

Figure D.2: Performance trends for the DAC on the barge platform

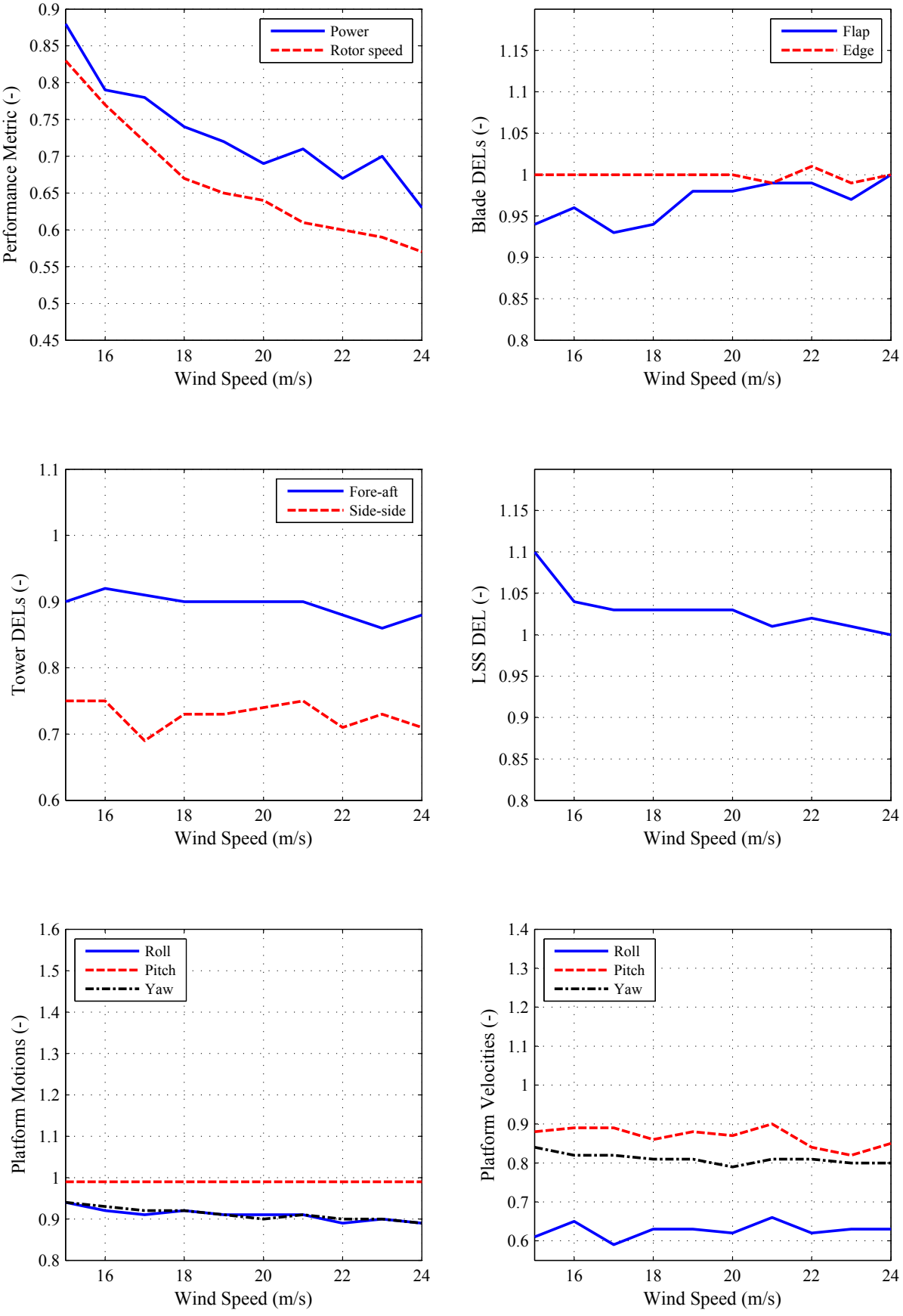

Figure D.3: Performance trends for the SFC on the TLP

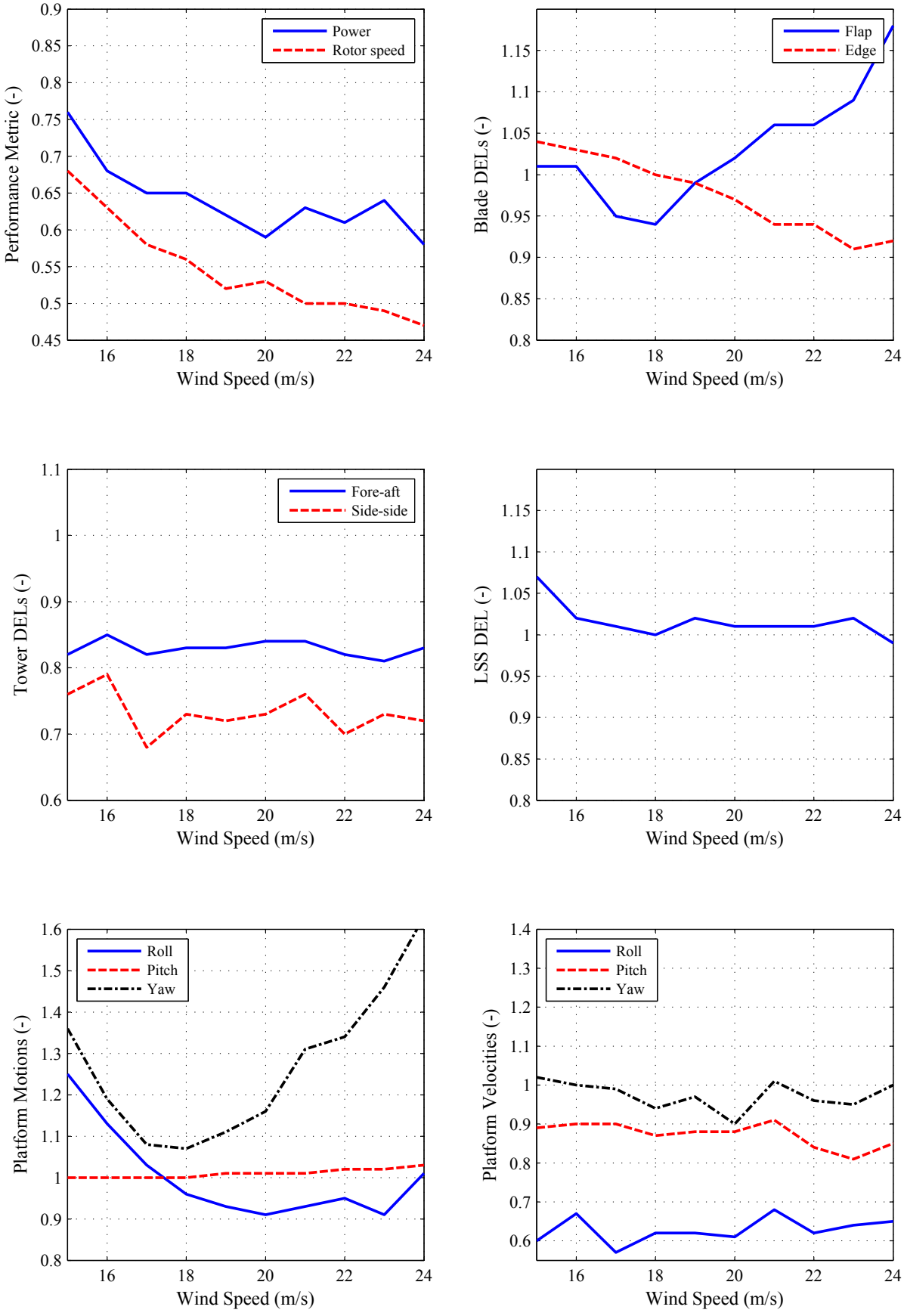

Figure D.4: Performance trends for the DAC on the TLP

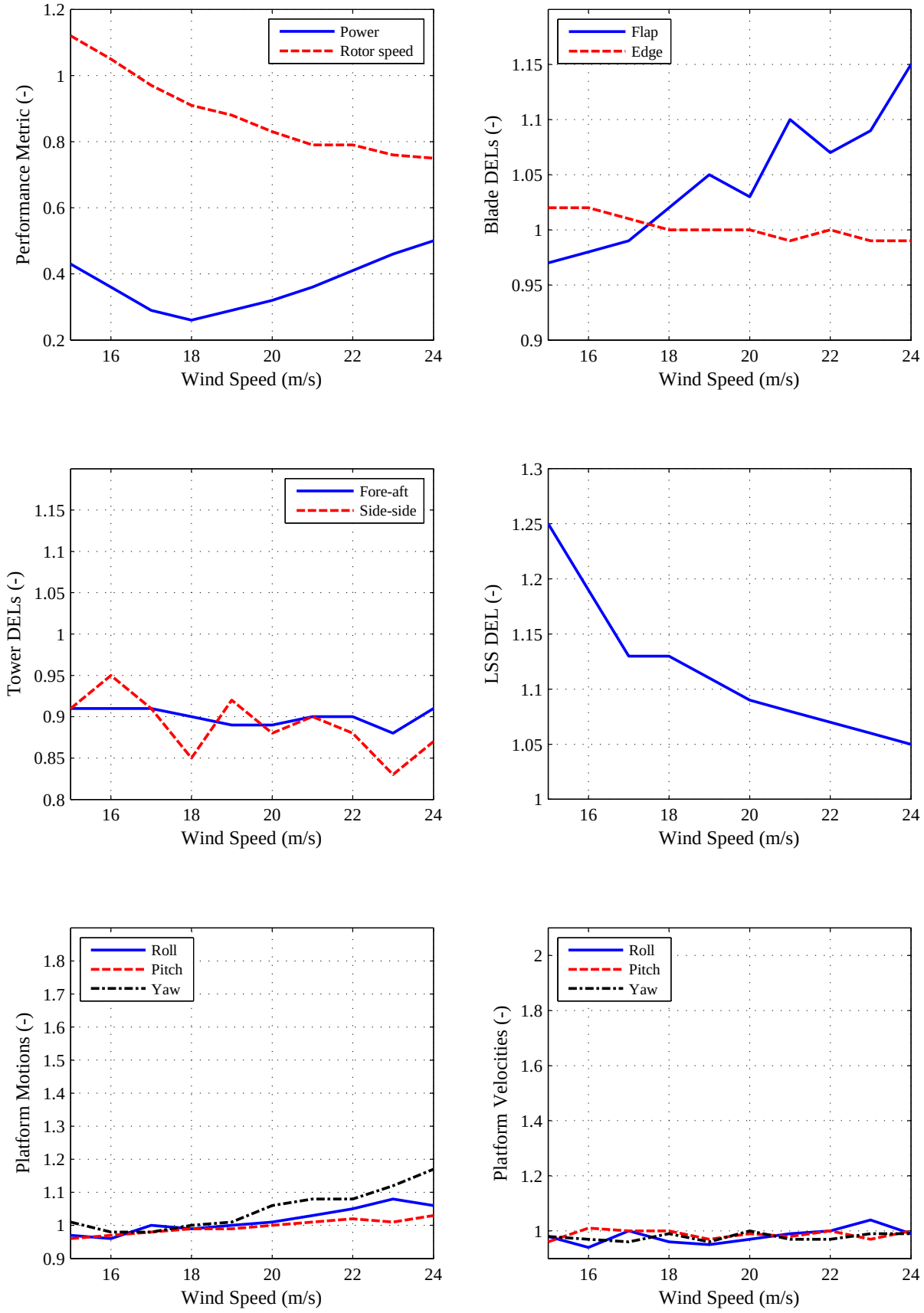

Figure D.5: Performance trends for the SFC on the spar-buoy platform

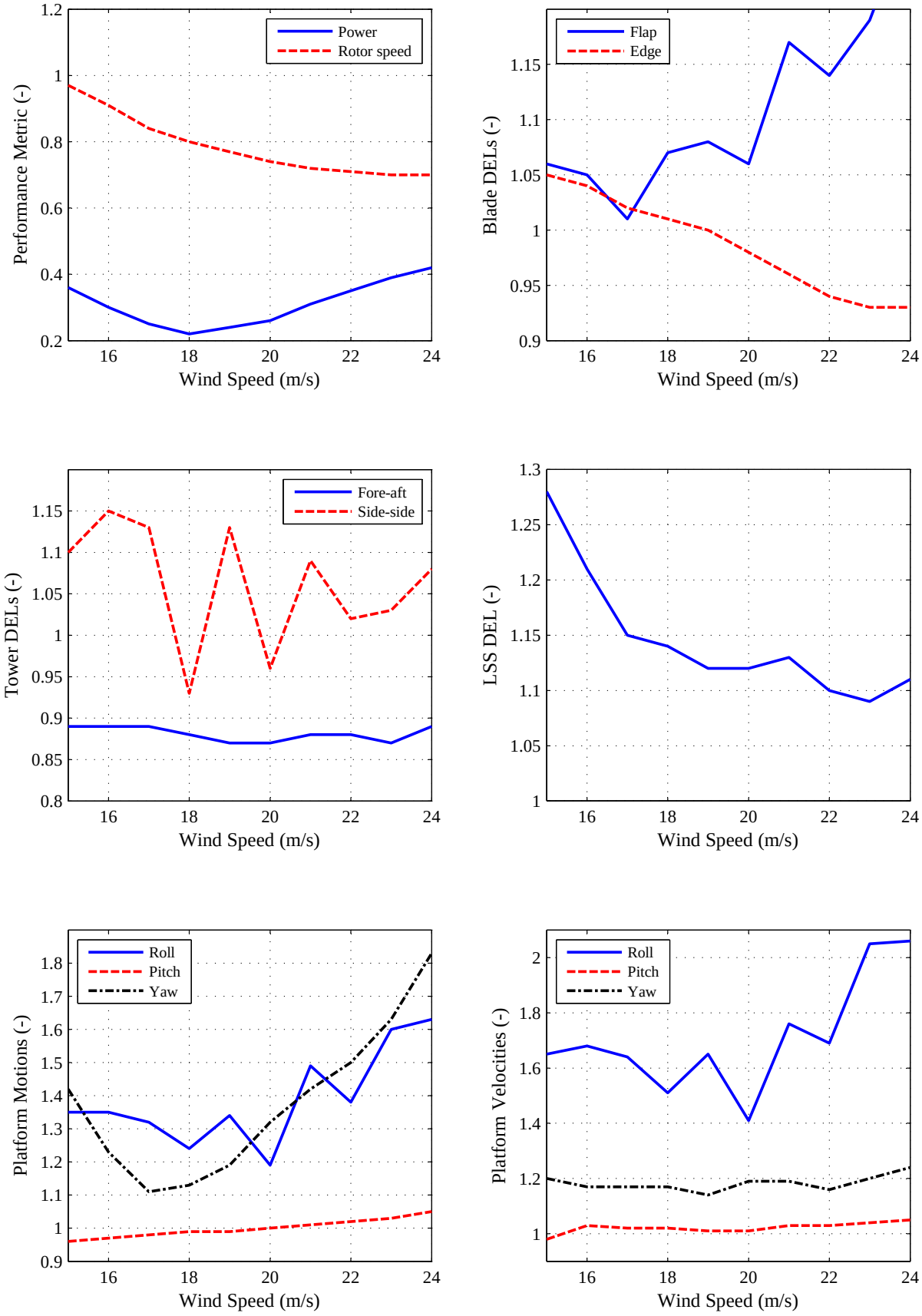

Figure D.6: Performance trends for the DAC on the spar-buoy platform

E

Adaptive Disturbance Estimator

Irregular waves are modelled using a spectrum of frequencies. They can also be modelled as having a dominant frequency that slowly changes with time and a randomly varying amplitude depending on sea conditions. In this appendix, the limitations of using a periodic waveform model for periodic disturbance estimation are highlighted when the assumed design frequency is mismatched from the input disturbance frequency. An empirical method to account for the change in period/frequency is introduced in §E.2.

E.1 Dealing with Periodic Waves

To reject periodic disturbances of the form $a\sin(\omega t) + b\cos(\omega t)$, the waveform model parameters are given by equations (E.1) - (E.3); the static offset of the waveform from the previous implementation is removed for simplicity.

$$\Gamma = \begin{bmatrix} 0 & 1 \\ -\omega^2 & 0 \end{bmatrix} \tag{E.1}$$

$$\Theta = \begin{bmatrix} 1 & 0 \end{bmatrix} \tag{E.2}$$

$$\underline{z}(0) = \begin{bmatrix} b & a\omega \end{bmatrix}^{\mathrm{T}} \tag{E.3}$$

This waveform model allows the DAC to minimise or cancel persistent disturbances only if the assumed frequency ω matches the actual frequency of the persistent disturbance. Also, a disturbance estimator based on this waveform matches the amplitude and phase of the input disturbance provided that the assumed frequency is matched.

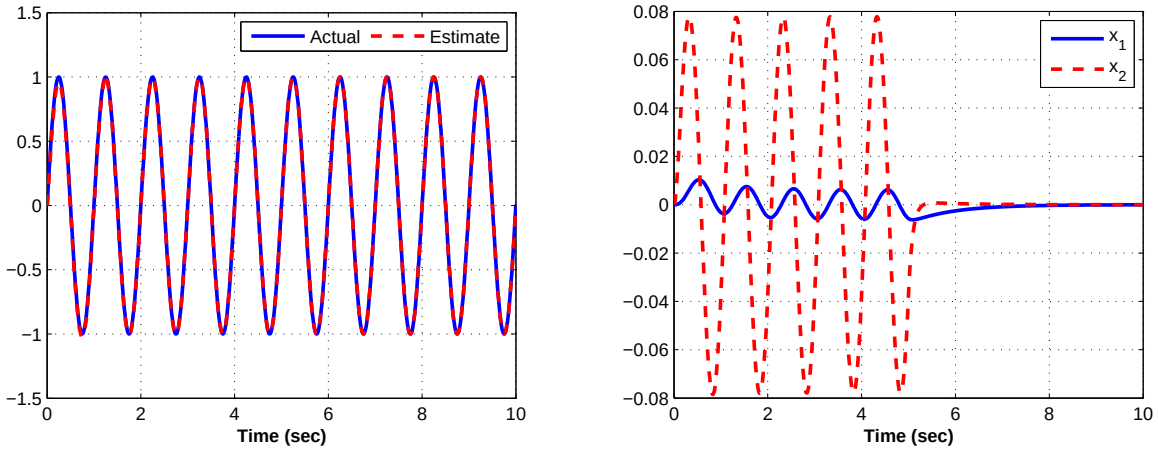

(a) Disturbance estimate

(b) States

Figure E.1: Periodic disturbance cancellation with matched estimator frequency

E.1.1 Case Study: Simple Linear System Subjected to Periodic Disturbances

In this section, the effectiveness of a DAC at cancelling periodic disturbances when the assumed frequency matches the actual disturbance frequency is demonstrated. The effects of frequency mismatch are also demonstrated.

The model considered here is a simple non-dimensional linear second order system with the following matrices:

$$A = \begin{bmatrix} -1 & 0.5 \\ 0 & -5 \end{bmatrix} \quad B = \begin{bmatrix} 0 \\ 10 \end{bmatrix} \quad B_d = \begin{bmatrix} 0 \\ 1 \end{bmatrix} \quad C = \begin{bmatrix} 1 & 0 \\ 0 & 1 \end{bmatrix} \quad D = \begin{bmatrix} 0 \\ 0 \end{bmatrix}$$

For simplicity, all the states are measured for state regulation. Furthermore, the disturbance is assumed to enter the system through the same channel as the actuator (B and B_d matrices are linearly dependent). This allows for disturbance cancellation rather than minimisation even though the B matrix is not a square matrix.

The controller is an optimal linear quadratic regulator that is designed to drive the states to zero. The DAC is set up to start 5 seconds after the simulation has started.

Matched Frequency

The system is subjected to periodic disturbances that match the assumed frequency of the disturbance estimator. Figure E.1a shows that the disturbance estimator correctly estimates the input disturbance. Therefore, when the DAC is activated 5 seconds after the start of the simulation, the system states are driven to zero as shown in Figure E.1b. The states' decay envelope for $t > 5$ seconds is governed by the SFC-part of the DAC.

Since the assumed estimator frequency matches the actual disturbance frequency, the estimates for the disturbance states eventually match the actual disturbance and hence the DAC is able to completely cancel the effects of the persistent periodic disturbance.

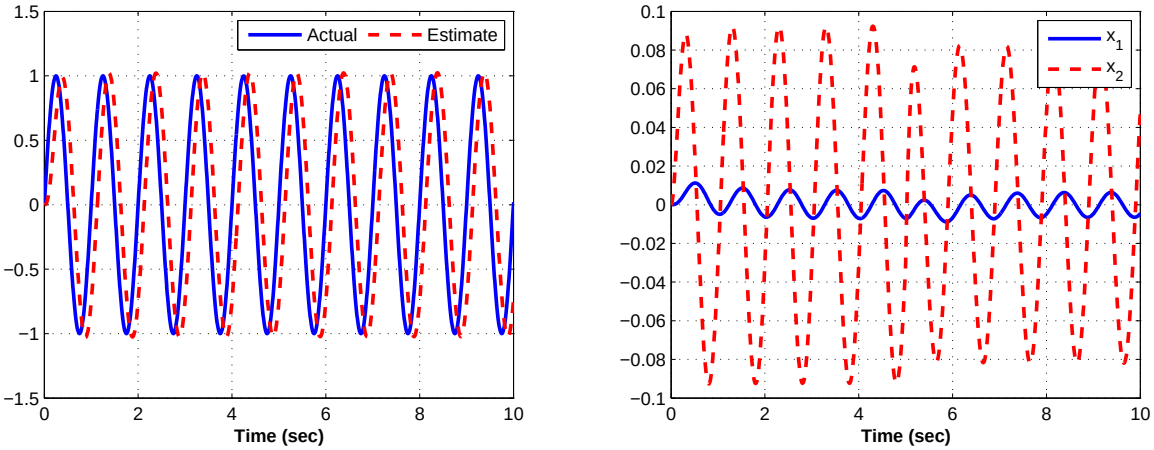

(a) Disturbance estimate

(b) States

Figure E.2: Mismatched frequency disturbance estimate and state regulation

Mismatched Frequency

When the assumed frequency does not match that of the actual disturbance, the disturbance estimates become out of phase and have a different amplitude as shown in Figure E.2a. The amount of phase lag and amplitude are determined by the dynamics of the state estimator. Slow dynamics increase the phase lag and reduce the amplitude (i.e. a low-pass filtered response).

This phase lag, regardless of how small, prevents the DAC from completely cancelling the effects of the periodic disturbance. Whether the DAC is able to minimise the effects of the disturbance or degrade the performance depends on the phase lag. Figure E.2b shows that little minimisation is being achieved by the DAC after 5 seconds.

E.2 Adaptive Disturbance Estimator for Disturbances with Variable Frequency

As demonstrated in §E.1.1, any mismatch in the assumed frequency degrades the DAC performance. Furthermore, for systems with periodic disturbances that change frequency with time, the problem is made more difficult as careful selection of a design frequency is no longer relevant as soon as the frequency changes.

One possible solution is to assume a disturbance waveform model with multiple periodic terms with different frequencies to form a Fourier series. However, one major limitation of this approach is to ensure that the system remains observable with all the additional disturbance states as discussed in §4.4.1.

The field of unknown input observers [88–92] deals with cases such as changing frequency of a periodic signal or having no knowledge of the estimated signal. However, these methods are

usually demonstrated on simple abstract models that do not necessarily represent a real physical system. Below is a new empirical method that is relatively quick and easy to implement but has not yet proven mathematically to guarantee stability.

The new approach, termed Adaptive Disturbance Estimator (ADE), consists of two modules: the first module dynamically estimates the frequency/period of the disturbance and the second module updates the disturbance estimator model, similar to direct model reference adaptive control. This involves on-line estimator design and update of variables.

E.2.1 Frequency Estimation

Starting with a hypothetical situation, assume that the input disturbance can be measured and is a perfect sinusoidal signal with zero offset. The frequency can be extracted by detecting when the signal crosses zero and measuring the time between the crossings (which corresponds to half the period). The frequency can then be calculated using equation (E.4). However, the input disturbance signal can have an offset and therefore may not cross at zero. Furthermore, as discussed earlier, the input disturbance cannot always be measured. Therefore, the actual disturbance signal cannot be used to detect the period.

$$\omega = \frac{\pi}{\Delta t} \tag{E.4}$$

The same approach can be used to detect the period of the disturbance estimator. Since the estimator is estimating the periodic disturbance input (as well as the system states), its outputs that correspond to the disturbance states $\underline{z}$ are sinusoidal with no offset. When subjected to periodic input, the steady-state output of the estimator matches the disturbance frequency but with a different amplitude and with a phase lag. Therefore, the output of the estimator can be used to detect the input frequency when the system reaches steady state.

The output of the disturbance states $\underline{z}$ are periodic *with zero offset* because when constructing the disturbance waveform model (equations (E.1) and (E.2)), the defined disturbance states (given by equation (E.5)) are periodic in order to create a waveform given by equation (E.6). Therefore, the outputs corresponding to these states can be used to measure the frequency of the input disturbance.

$$\underline{z} = \begin{bmatrix} \sqrt{a^2+b^2}\sin\left(\omega t + \tan^{-1}\left(a/b\right)\right) \\ \omega\sqrt{a^2+b^2}\cos\left(\omega t + \tan^{-1}\left(a/b\right)\right) \end{bmatrix} \tag{E.5}$$

$$u_d = a\sin\left(\omega t\right) + b\cos\left(\omega t\right) \tag{E.6}$$

One limitation of this approach is that it gives a discrete response. As a result, the lower the frequency the longer it takes to reach the correct input frequency because the estimate is updated every half a period of the disturbance state output. A sample response is shown in Figure E.3 where the input frequency is set to 1 Hz and the design frequency is assumed to be 0.5 Hz.

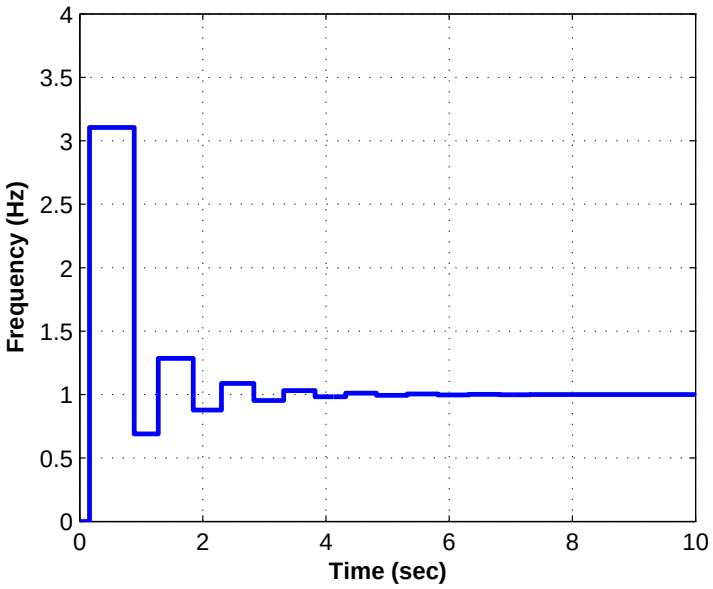

Figure E.3: Quantised response of the estimated frequency

E.2.2 On-line Estimator Design

Once an estimate of the frequency is obtained, the disturbance estimator must be updated. The change in frequency affects the Γ, $\overline{A}$, and K_e matrices as described by equations (E.1), (4.12), and (4.13) respectively. Therefore, these matrices are updated on-line which in turn update the dynamics of the disturbance estimator.

One important issue is how often the disturbance estimator variables are updated. The frequency estimate depends on the dynamics of the state estimator and the plant. Therefore, the update rate of the estimator variables should be longer than the time it takes for the transients of the estimator and the plant to decay. This is because when the state estimator is updated, it introduces new transients unless bump-less transfer [93, pp. 381–388] is implemented (not considered here). For the case study considered, the Adaptive Disturbance Estimator is updated every 10 seconds. The ADE implementation block diagram is shown in Figure E.4.

Stability and convergence assessment of the ADE is difficult as it contains continuous time, triggered, and time-sampled modules. Stability analysis of such systems is considered beyond the scope of this work.

E.2.3 Case Study: ADE Performance with Mismatched Frequency

In this case study the same fictitious plant and controllers in §E.1.1 are used with the ADE. The performance of the DAC with ADE are compared to the LQR controller and the DAC with a fixed frequency estimator.

The disturbance estimators start with an assumed frequency of 0.01 Hz and are subjected to a disturbance signal that has a sinusoidally varying frequency. The estimators are designed to have fast dynamics to accommodate a range of input frequencies. Of course, the higher the

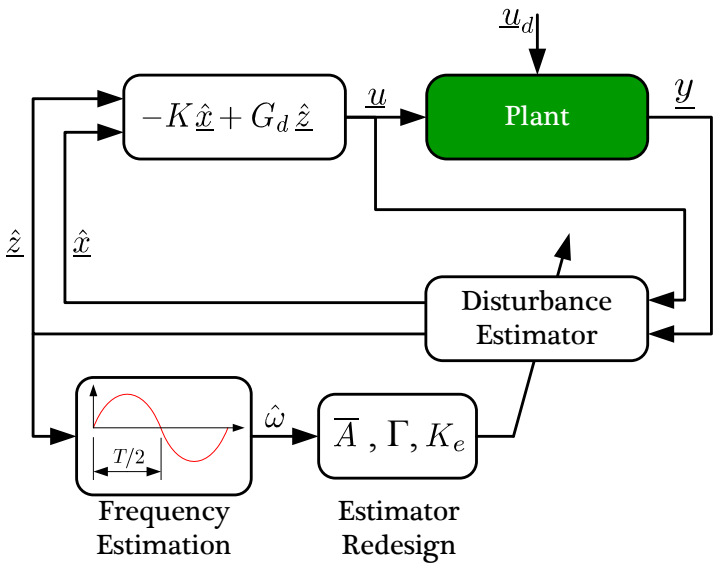

Figure E.4: Adaptive disturbance estimator implementation block diagram

disturbance frequency the faster the dynamics of the estimator need to be. The effect of noise on the quality of the estimates is not considered here. The disturbance frequency ranges from 0.05 Hz to 0.15 Hz with a frequency of 0.05 Hz (given by equation (E.7)) .

$$\omega\,(t) = (0.05 \times 2\pi)\sin\,(0.05 \times 2\pi t) + 0.1 \times 2\pi \tag{E.7}$$

Higher frequencies have been tested (with linearly varying frequency up to 4 Hz) but since the results are similar to those presented here, they are not included. The "low" range frequencies are chosen to be in the range of the irregular waves expected at sea.

The time series results of the disturbance estimates and state regulation are shown in Figure E.5. Due to fast estimator dynamics, the fixed frequency disturbance estimator has relatively good performance but the ADE has more accurate estimates especially at the low frequency range.

The effects of the accuracy of the estimates can be clearly seen in the regulation of the states. In general, the DAC with ADE has better disturbance rejection especially at the low frequency range as the estimate is more accurate. At higher frequencies, the DAC with ADE can still improve performance but the transients from updating the estimator become more significant.

E.2.4 Case Study: ADE Performance on a Linear Periodic Floating Wind Turbine Model

This case study is used to assess the performance of an Adaptive Disturbance Estimator with a wave Disturbance Accommodating Controller on the linear time-varying floating wind turbine model used in §10.2.1.

Two cases are tested: the first is with a constant frequency that does not match the assumed waveform frequency by the disturbance estimator. The second is where the wave moment frequency is continuously changing with time.

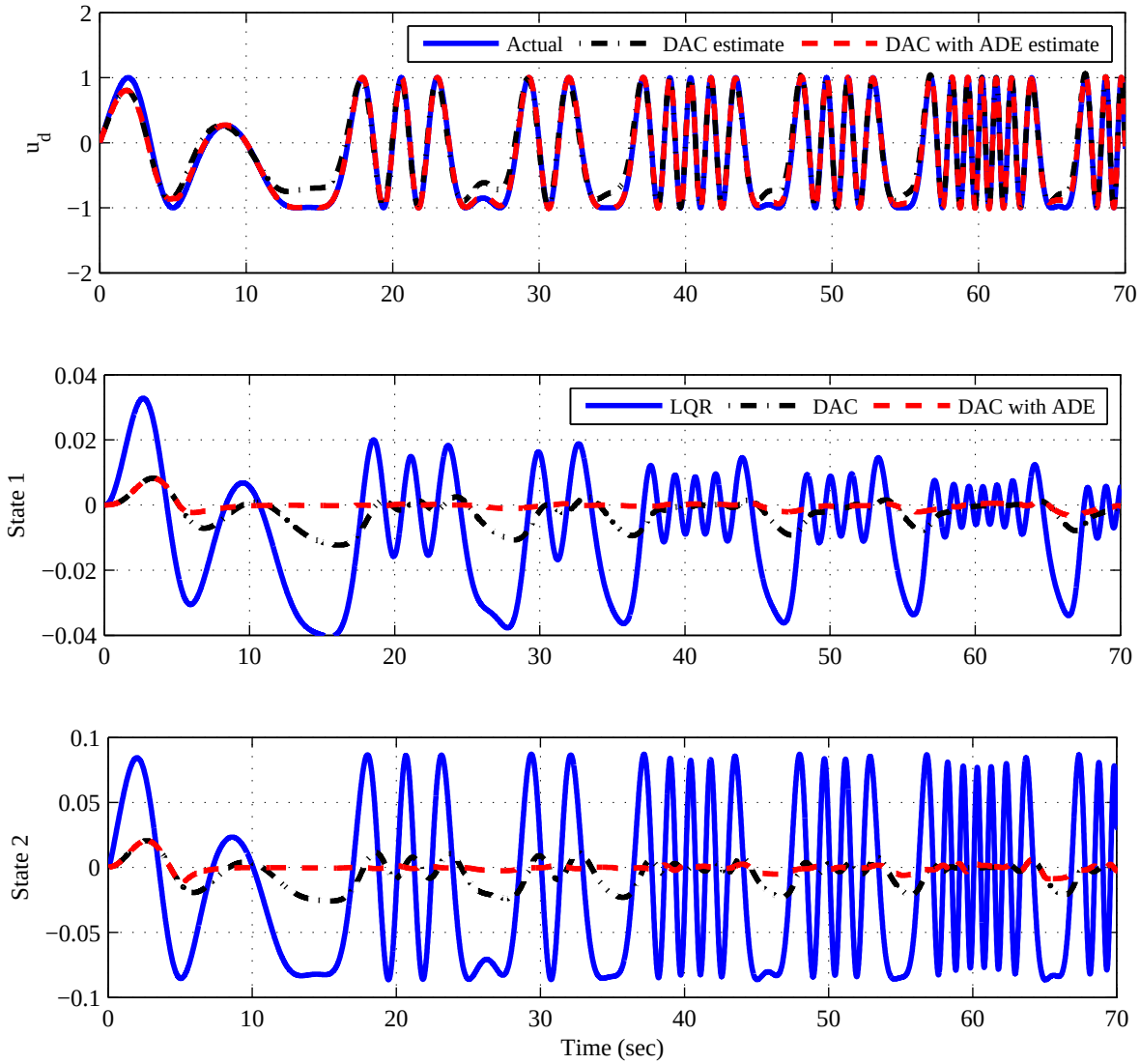

Figure E.5: Disturbance estimates and state regulation with a variable frequency disturbance input

Constant Mismatched Frequency Case

The 2 DOFs floating wind turbine model is subjected to wave moments with a constant period of 30 seconds (an extreme case for the site chosen for the floating wind turbines). The performance of the DAC with ADE at regulating the platform pitch is compared to a State Feedback Controller and a DAC with a fixed-frequency disturbance estimator that has an assumed wave period of 15 seconds. The state regulating part of the DACs has the same gains and weightings as the SFC.

Figure E.6 shows the platform pitch and disturbance moment estimates for the different controllers and estimators. Looking at the wave moment estimates, there are no significant differences between the actual wave moment and both estimates of the DAC and DAC with ADE. The phase lag for both estimators is not as prominent as the phase lag in the simple non-dimensional model shown in Figure E.2a because the state estimators are designed to have fast

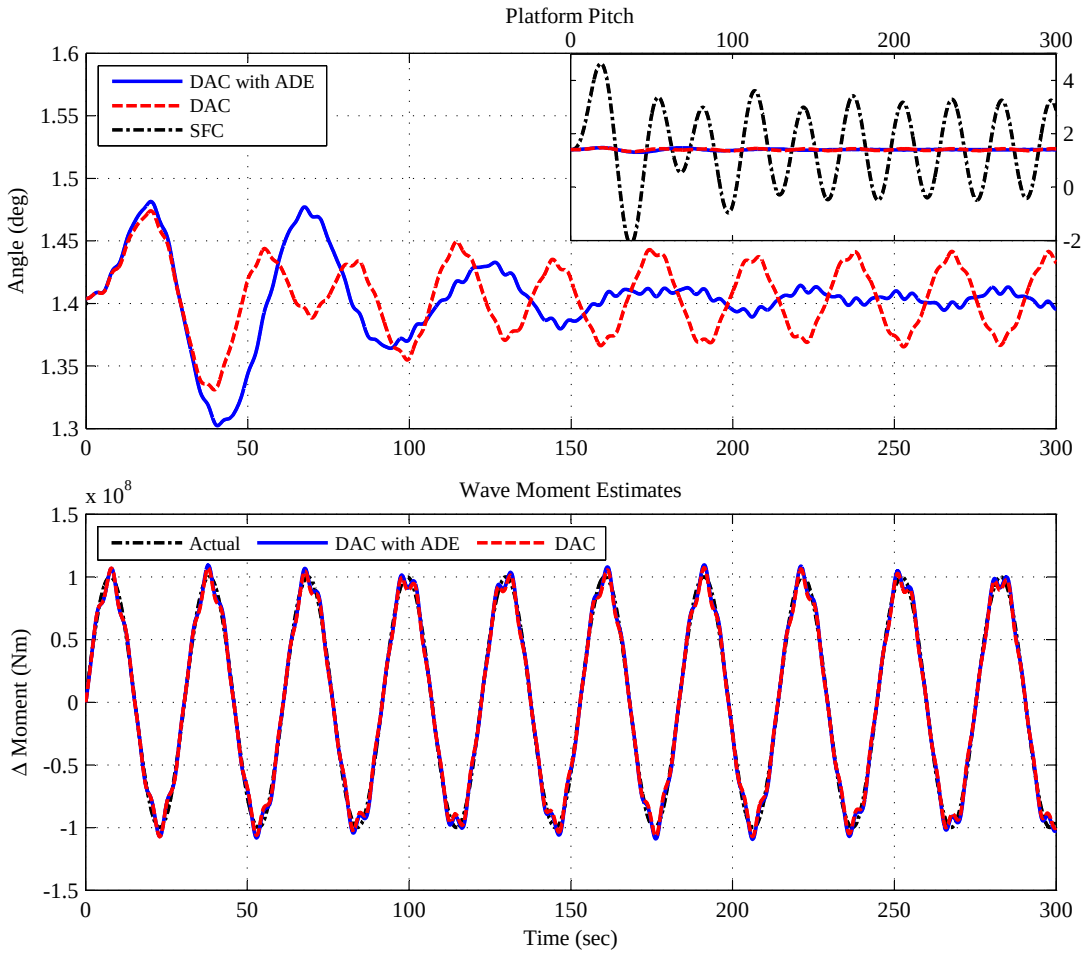

Figure E.6: Constant mismatched frequency case

dynamics. However, DAC with ADE does eventually (when the estimated frequency is close to the actual) regulate the platform pitch angle closer to the operating point of 1.4°, therefore, suggesting that there is a difference in wave estimate accuracy.

Putting the differences between the DAC and DAC with ADE in perspective, the difference between them in terms of platform pitch regulation is insignificant when compared to the performance of the SFC (see top right inset in Figure E.6). Both Disturbance Accommodating Controllers have excellent platform pitch regulation.

Continuously Varying Frequency Case

For wave disturbances with continuously changing frequency, the wave period T_w is made to vary from 5 seconds to 20 seconds (values typical for the chosen site [32]) tracking a periodic trajectory with a period of 600 seconds as defined by equation (E.8).

$$T_w = -7.5 \cos\left(\frac{2\pi}{600} t\right) + 12.5 \tag{E.8}$$

The simulation results are shown in Figure E.7; the disturbance estimates are not shown be-

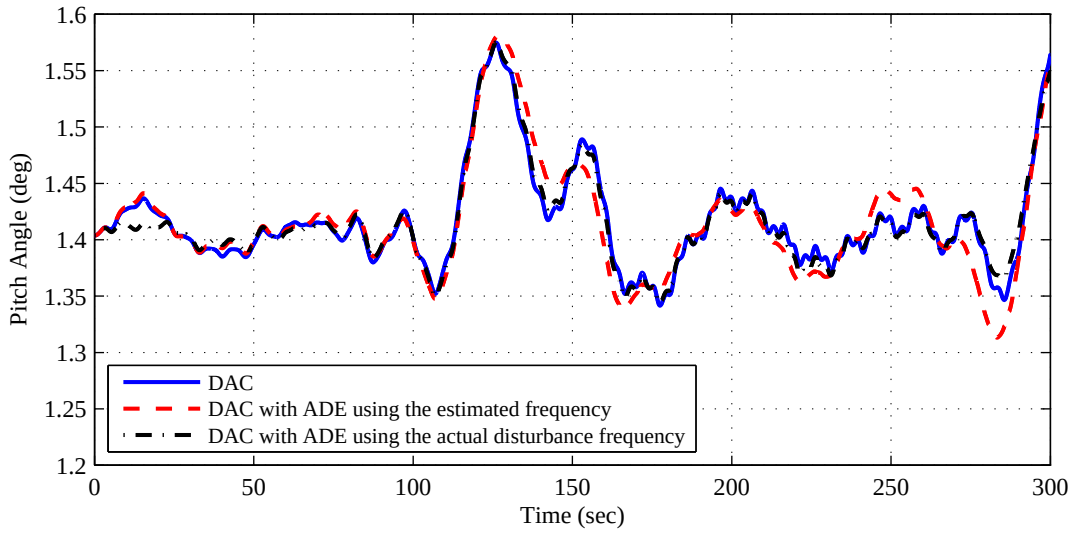

Figure E.7: Platform pitch angle regulation with continuously changing wave disturbance frequency

cause there are no significant differences that can be easily identified. In addition to comparing the performance between the DAC and DAC with ADE, another configuration is included where the ADE is designed based on the actual wave frequency rather than the estimated one to remove the quality of the frequency estimates from the DAC performance.

In this simulation case, the performance of the DAC with ADE that uses the estimated frequency has slightly larger fluctuations than the other two. This is mainly due to poor estimate of the wave frequency which is caused by slow dynamics of the floating wind turbine and the low frequency of the waves. By the time it takes for the disturbance states to complete half a period and trigger the system to get an estimate of the period, the actual wave frequency has changed. Furthermore, due to the slow dynamics of the wind turbine, it takes a long time for the system to reach steady state to match the period of the waves (recall that disturbance estimates are based on system states measurements). Although it may seem unlikely, however, in this case the frequency is changing too fast for the ADE to give accurate estimates of the frequency.

E.3 Summary

Irregular waves are modelled using a spectrum of frequencies. They can also be represented as having a variable amplitude and a dominant frequency that slowly change with time depending on sea conditions. Therefore, using a periodic disturbance waveform may actually make the performance worse caused by wrong estimates due to frequency mismatch. A new and empirical method (termed Adaptive Disturbance Estimator) is used to dynamically estimate the input disturbance frequency and redesign the disturbance estimator on-line. Test cases show that this approach can improve the accuracy of disturbance estimates and thereby improving the DAC performance. However, in cases where the frequency is changing rapidly

relative to the system dynamics and input disturbance frequencies, an accurate estimate of the disturbance frequency may not be achieved; the speed at which the wave frequency changes is not available for this work. Despite the limitations of the Adaptive Disturbance Estimator method, it can be applied on a variety of systems outside the realm of Disturbance Accommodating Control or floating wind turbines. An example application would be on a periodic system whose properties slowly change with time (such as a spring wearing out thus changing the natural frequency of the system).

References

[1] "Monthly electricity statistics: May 2011," Retrieved August 17, 2011 from: http://www.iea.org/stats/surveys/mes.pdf.

[2] H. Chandler, "Technolgy roadmap: Wind energy," International Energy Agency, Tech. Rep., 2009.

[3] S. Mathew, *Wind Energy : Fundamentals, Resource Analysis and Economics*. Berlin: Springer, 2006.

[4] A. Pullen and S. Sawyer, "Global wind report: Annual market update 2010," Global Wind Energy Council, Tech. Rep., 2010.

[5] J. Wilkes, C. Kjaer, and R. Gruet, "Pure power: Wind energy targets for 2020 and 2030," European Wind Energy Association, Tech. Rep., 2011.

[6] Parliamentary Commissioner for the Environment, "Wind power, people, and place," New Zealand Office of the Parliamentary Commissioner for the Environment, Wellington, Tech. Rep., 2006.

[7] "Operational offshore wind farms in europe, end 2010," Retrieved August 18, 2011 from http://www.ewea.org/fileadmin/ewea_documents/documents/statistics/110214__public_offshore_wind_farms_in_Europe_2010.pdf.

[8] Shikha, T. S. Bhatti, and D. P. Kothari, "Aspects of technological development of wind turbines," *Journal of Energy Engineering*, vol. 129, no. 3, pp. 81–95, 2003.

[9] S. Brennan, "Offshore wind energy resources," Workshop on Deep Water Offshore Wind Energy Systems, 15-16 October 2003.

[10] F. G. Nielsen, T. D. Hanson, and B. Skaare, "Integrated dynamic analysis of floating offshore wind turbines," in *Proceedings of the 25th International Conference on Offshore Mechanics and Arctic Engineering*, Hamburg, 4 - 9 June 2006, pp. 671–679.

[11] P. Goldman, "Offshore wind energy," Workshop on Deep Water Offshore Wind Energy Systems, 15-16 October 2003.

[12] A. R. Henderson, C. Morgan, B. Smith, H. C. Sørensen, R. J. Barthelmie, and B. Boesmans, "Offshore wind energy in europe - a review of the state-of-the-art," *Wind Energy*, vol. 6, no. 1, pp. 35–52, 2003.

[13] J. M. Jonkman and P. D. Sclavounos, "Development of fully coupled aeroelastic and hydrodynamic models for offshore wind turbines," in *Proceedings of the 44th AIAA Aerospace Sciences Meeting and Exhibit*, Reno, NV, 9-12 January 2006, pp. CD–ROM.

[14] A. R. Henderson, "Support structures for floating offshore windfarms," Workshop on Deep Water Offshore Wind Energy Systems, 15-16 October 2003.

[15] "Largest and deepest offshore wind turbine installed," *Refocus*, vol. 7, no. 5, p. 14, 2006.

[16] W. Musial, S. Butterfield, and B. Ram, "Energy from offshore wind," in *Offshore Technology Conference*, Houston, Texas, USA, 1-4 May 2006, pp. 1888–1898.

[17] B. Bulder, J. Peeringa, J. Pierik, A. R. Henderson, R. Huijsmans, E. Snijders, M. v. Hees, G. Wijnants, and M. Wolf, "Floating offshore wind turbines for shallow waters," in *European Wind Energy Conference*. Madrid, Spain: ECN Wind Energy, 16-19 June 2003.

[18] W. Musial, S. Butterfield, and A. Boone, "Feasibility of floating platform systems for wind turbines," in *23rd ASME Wind Energy Symposium*. Reno, NV: NREL, 5-8 January 2004.

[19] I. Ushiyama, K. Seki, and H. Miura, "A feasibility study for floating offshore windfarms in Japanese waters," *Wind Engineering*, vol. 28, no. 4, pp. 383–397, 2004.

[20] S. Butterfield, W. Musial, J. Jonkman, P. Sclavounos, and L. Wayman, "Engineering challenges for floating offshore wind turbines," in *Copenhagen Offshore Wind 2005 Conference and Expedition Proceedings*. Copenhagen, Denmark: Danish Wind Energy Association, 25-28 October 2005.

[21] K. C. Tong, "Technical and economic aspects of a floating offshore wind farm," *Journal of Wind Engineering and Industrial Aerodynamics*, vol. 74-76, pp. 399–410, 1998.

[22] "Hydro and Siemens cooperate on technology for full-scale demonstration of floating wind turbines," Retrieved December 12, 2007 from: http://www.powergeneration.siemens.com/press/press-releases/releases/2007/PG200706-051.htm.

[23] "Model testing of floating wind turbine facility," *Review*, vol. 1, no. 1, p. 6, April 2006.

[24] W. M. Vijfhuizen, "Design of wind and wave power barge," Master's thesis, Universities of Glasgow and Strathclyde, 2006.

[25] E. N. Wayman, "Coupled dynamics and economic analysis of floating wind turbine systems," Master's thesis, Massachusetts Institute of Technology, 2006.

[26] D. Biester, "Hywind: Siemens and StatoilHydro install first floating wind turbine," Retrieved July 3, 2009 from: http://www.siemens.com/press/pool/de/pressemitteilungen/2009/renewable_energy/ERE200906064e.pdf, Siemens AG.

[27] "SWAY successfully deployed prototype," Retrieved August 18, 2011 from: http://www.sway.no/.

[28] E. Hau, *Wind Turbines : Fundamentals, Technologies, Application, Economics*, 2nd ed. Berlin; New York: Springer, 2006.

[29] T. Burton, D. Sharpe, N. Jenkins, and E. A. Bossanyi, *Wind Energy Handbook*. Chichester ; New York: Wiley, 2001.

[30] L. Pao and K. Johnson, "A tutorial on the dynamics and control of wind turbines and wind farms," in *2009 American Control Conference*, 10–12 June 2009, pp. 2076–2089.

[31] US Department of Energy, "How wind turbines work," Retrieved December 17, 2007 from: http://www1.eere.energy.gov/windandhydro/wind_how.html.

[32] J. M. Jonkman, "Dynamics modeling and loads analysis of an offshore floating wind turbine," Ph.D. dissertation, University of Colorado, 2007.

[33] E. A. Bossanyi, "The design of closed loop controllers for wind turbines," *Wind Energy*, vol. 3, no. 3, pp. 149–163, 2000.

[34] J. Laks, L. Pao, and A. Wright, "Control of wind turbines: Past, present, and future," in *American Control Conference, 2009. ACC'09.* St. Louis, MO: IEEE, 10 - 12 June 2009, pp. 2096–2103.

[35] A. D. Wright, "Modern control design for flexible wind turbines," National Renewable Energy Lab, Tech. Rep. NREL/TP-500-35816, 2004.

[36] J. M. Jonkman and M. L. Buhl Jr., "FAST user's guide," National Renewable Energy Laboratory, Tech. Rep. NREL/EL-500-38230, August 2005.

[37] J. M. Jonkman, S. Butterfield, W. Musial, and G. Scott, "Definition of a 5-MW reference wind turbine for offshore system development," National Renewable Energy Laboratory, Tech. Rep. TP-500-38060, 2007.

[38] D. Matha, "Modelling and loads & stability analysis of a floating offshore tension leg platform wind turbine," Master's thesis, National Renewable Energy Lab's National Wind Turbine Center and University of Stuttgart, 2009.

[39] *Wind Turbines - Part 3: Design Requirements for Offshore Wind Turbines*, International Electrotechnical Commission (IEC) Std. 61 400-3 Ed. 1, 2009.

[40] T. J. Larsen and T. D. Hanson, "A method to avoid negative damped low frequency tower vibrations for a floating pitch controlled wind turbine," *Journal of Physics: Conference Series*, vol. 75, 2007.

[41] M. A. Lackner, "Controlling platform motions and reducing blade loads for floating wind turbines," *Wind Engineering*, vol. 33, no. 6, pp. 541 – 553, 2009.

[42] E. A. Bossanyi, "Wind turbine control for load reduction," *Wind Energy*, vol. 6, no. 3, pp. 229–244, 2003.

[43] B. Skaare, T. D. Hanson, and F. G. Nielsen, "Importance of control strategies on fatigue life of floating wind turbines," in *Proceedings of the 26th International Conference on Offshore Mechanics and Arctic Engineering*, San Diego, CA, 10 - 15 June 2007, pp. 493–500.

[44] M. Rotea, M. A. Lackner, and R. Saheba, "Active structural control of offshore wind turbines," in *48th AIAA Aerospace Sciences Meeting and Exhibit*, Orlando, FL, 4-7 January 2010, pp. CD–ROM.

[45] L. C. Henriksen, "Model predictive control of a wind turbine," Master's thesis, Technical University of Denmark, 2007.

[46] K. Stol, "Dynamics modeling and periodic control of horizontal-axis wind turbines," Ph.D. dissertation, University of Colorado, 2001.

[47] M. J. Balas, Y. J. Lee, and L. Kendall, "Disturbance tracking control theory with application to horizontal axis wind turbines," in *Proceedings of the 1998 ASME Wind Energy Symposium*, Reno, Nevada, 12-15 January 1998, pp. 95–99.

[48] G. Bir, "Multi-blade coordinate transformation and its application to wind turbine analysis," in *46th AIAA Aerospace Sciences Meeting and Exhibit*, Reno, NV, 7-10 January 2008, pp. CD–ROM.

[49] K. Stol and M. J. Balas, "Periodic disturbance accommodating control for blade load mitigation in wind turbines," *Journal of Solar Energy Engineering*, vol. 125, no. 4, pp. 379 – 385, 2003.

[50] K. Stol, H.-G. Moll, G. Bir, and H. Namik, "A comparison of multi-blade coordinate transformation and direct periodic techniques for wind turbine control design," in *47th AIAA Aerospace Sciences Meeting and Exhibit*, Orlando, FL, 5-8 January 2009, pp. CD–ROM.

[51] A. Kumar and K. Stol, "Scheduled model predictive control of a wind turbine," in *47th AIAA Aerospace Sciences Meeting and Exhibit*, Orlando, FL, 5-8 January 2009, pp. CD–ROM.

[52] J. Freeman and M. Balas, "An investigation of variable speed horizontal-axis wind turbines using direct model-reference adaptive control," in *18th ASME Wind Energy Symposium*, Reno, NV, Jan 1999, pp. 66–76.

[53] S. Frost, M. Balas, and A. Wright, "Direct adaptive control of a utility-scale wind turbine for speed regulation," *International Journal of Robust and Nonlinear Control*, vol. 19, no. 1, pp. 59–71, 2009.

[54] B. Boukhezzar and H. Siguerdidjane, "Nonlinear control of variable speed wind turbines without wind speed measurement," in *Decision and Control, 2005 and 2005 European Control Conference. CDC-ECC '05. 44th IEEE Conference on*, 2005, pp. 3456–3461.

[55] L. Zhao and Q. Guo, "Adjustable-pitch and variable-speed control of wind turbines using nonlinear algorithm," in *Electrical Machines and Systems, 2003. ICEMS 2003. Sixth International Conference on*, vol. 1, 2003, pp. 270–273 vol.1.

[56] T. v. Engelen, "Control design based on aero-hydro-servo-elastic linear models from TURBU (ECN)," in *Proceedings of the European Wind Energy Conference*, Milan, 7-10 May 2007, pp. 68–81.

[57] E. A. Bossanyi, "Individual blade pitch control for load reduction," *Wind Energy*, vol. 6, no. 2, pp. 119–128, 2003.

[58] K. Stol, W. Zhao, and A. D. Wright, "Individual blade pitch control for the controls advanced research turbine (CART)," *Journal of Solar Energy Engineering, Transactions of the ASME*, vol. 22, pp. 16 478–16 488, 2006.

[59] M. A. Lackner and G. v. Kuik, "A comparison of smart rotor control approaches using trailing edge flaps and individual pitch control," *Wind Energy*, vol. 13, no. 2-3, pp. 117–134, 2010. [Online]. Available: http://dx.doi.org/10.1002/we.353

[60] H. Namik and K. Stol, "Individual blade pitch control of floating offshore wind turbines," *Wind Energy*, vol. 13, no. 1, pp. 74–85, 2010.

[61] H. Namik, K. Stol, and J. Jonkman, "State-space control of tower motion for deepwater floating offshore wind turbines," in *46th AIAA Aerospace Sciences Meeting and Exhibit*, Reno, NV, 7-10 January 2008, pp. CD–ROM.

[62] W. Johnson, *Helicopter Theory*. Princeton, N.J.: Princeton University Press, 1980.

[63] P. Skjoldan and M. Hansen, "On the similarity of the Coleman and Lyapunov-Floquet transformations for modal analysis of bladed rotor structures," *Journal of Sound and Vibration*, vol. 327, no. 3-5, pp. 424–439, 2009.

[64] H. Namik and K. Stol, "Performance analysis of individual blade pitch control of offshore wind turbines on two floating platforms," *Mechatronics*, vol. 21, no. 4, pp. 691–703, 2011.

[65] C. D. Johnson, "Theory of disturbance-accommodating controllers," *Advances in Control and Dynamic Systems*, vol. 12, pp. 387–489, 1976.

[66] G. H. Hostetter, C. J. Savant, and R. T. Stefani, *Design of Feedback Control Systems*, 2nd ed. Saunders College Publishing, New York, 1989.

[67] H. Namik and K. Stol, "Control methods for reducing platform pitching motion of floating wind turbines," in *European Offshore Wind 2009*, Stockholm, 14-16 September 2009, pp. CD–ROM.

[68] ——, "Individual blade pitch control of a floating offshore wind turbine on a tension leg platform," in *48th AIAA Aerospace Sciences Meeting and Exhibit*, Orlando, FL, 4-7 January 2010, pp. CD–ROM.

[69] J. M. Jonkman, T. Lasren, A. Hansen, T. Nygaard, K. Maus, M. Karimirad, Z. Gao, T. Moan, I. Fylling, J. Nichols, M. Kohlmeier, J. Pascual Vergara, D. Merino, W. Shi, and H. Park, "Offshore code comparison collaboration within IEA wind task 23: Phase IV results regarding floating wind turbine modeling," in *European Wind Energy Conference 2010*, Warsaw, 20-23 April 2010.

[70] "Bladed: Wind turbine design software," Retrieved May 5, 2011 from: http://www.gl-garradhassan.com/en/GHBladed.php.

[71] "MD Adams: Multidiscipline multibody dynamics," Retrieved May 5, 2011 from: http://www.mscsoftware.com/Products/CAE-Tools/MD-Adams.aspx.

[72] "Aeroelastic wind turbine simulations and investigations," Retrieved May 5, 2011 from: http://www.risoe.dtu.dk/business_relations/Products_Services/consultancy_service/VEA_aeroelastic_simulation.aspx.

[73] "SIMO," Retrieved May 5, 2011 from: http://www.sintef.no/home/MARINTEK/Software-developed-at-MARINTEK/SIMO/.

[74] "DeepC," Retrieved May 5, 2011 from: http://www.dnv.in/services/software/products/sesam/SesamFloatingStructures/DeepC.asp.

[75] P. Passon, M. Kühn, S. Butterfield, J. M. Jonkman, T. Camp, and T. J. Larsen, "OC3 - benchmark exercise of aero-elastic offshore wind turbine codes," *Journal of Physics: Conference Series*, vol. 75, no. 1, p. 012071, 2007. [Online]. Available: http://stacks.iop.org/1742-6596/75/i=1/a=012071

[76] J. M. Jonkman and M. L. Buhl Jr., "Development and verification of a fully coupled simulator for offshore wind turbines," in *45th AIAA Aerospace Sciences Meeting and Exhibit*, Reno, Nevada, 8-11 January 2007, pp. 28–53.

[77] J. M. Jonkman and M. L. Buhl Jr, "Loads analysis of a floating offshore wind turbine using fully coupled simulation," in *WindPower 2007 Conference & Exhibition*, Los Angeles, CA, 3-6 June 2007.

[78] M. Buhl Jr and A. Manjock, "A comparison of wind turbine aeroelastic codes used for certification," in *44th AIAA Aerospace Sciences Meeting and Exhibit*, Reno, NV, 9-12 January 2006, pp. CD–ROM.

[79] *Wind Turbines - Part 1: Design Requirements*, International Electrotechnical Commission (IEC) Std. 61 400-1 Ed. 3, 2005.

[80] B. Jonkman and M. L. Buhl Jr., "Turbsim user's guide," National Renewable Energy Laboratory, Tech. Rep. NREL/TP-500-41136, April 2007.

[81] E. C. Morgan, M. Lackner, R. M. Vogel, and L. G. Baise, "Probability distributions for offshore wind speeds," *Energy Conversion and Management*, vol. 52, no. 1, pp. 15 – 26, 2011.

[82] M. Abramowitz and I. Stegun, *Handbook of Mathematical Functions with Formulas, Graphs, and Mathematical Tables.*, 10th ed., ser. Applied mathematics series. Washington, D.C.: National Bureau of Standards, 1972, no. 55.

[83] R. Barthelmie, O. Hansen, K. Enevoldsen, J. Højstrup, S. Frandsen, S. Pryor, S. Larsen, M. Motta, and P. Sanderhoff, "Ten years of meteorological measurements for offshore wind farms," *Journal of Solar Energy Engineering*, vol. 127, pp. 170–176, 2005.

[84] E. N. Wayman, P. D. Sclavounos, S. Butterfield, J. Jonkman, and W. Musial, "Coupled dynamic modeling of floating wind turbine systems," in *2006 Offshore Technology Conference*, Houston, Texas, USA, 1-4 May 2006.

[85] H. Namik and K. Stol, "Disturbance accommodating control of floating offshore wind turbines," in *47th AIAA Aerospace Sciences Meeting and Exhibit*, Orlando, FL, 5-8 January 2009, pp. CD–ROM.

[86] J. Jonkman, "Definition of the floating system for phase IV of OC3," National Renewable Energy Laboratory, Tech. Rep. NREL/TP-500-47535, May 2010.

[87] J. Meriam and L. Kraige, *Engineering mechanics. Vol. 2, Dynamics*, 5th ed. New York ; Chichester: Wiley, 2003.

[88] Y. Lee, M. Balas, and H. Waites, "Disturbance accommodating control for completely unknown persistent disturbances," in *American Control Conference, 1995. Proceedings of the*, vol. 2. IEEE, 1995, pp. 1463–1468.

[89] M. Bodson and S. Douglas, "Adaptive algorithms for the rejection of sinusoidal disturbances with unknown frequency," *Automatica*, vol. 33, no. 12, pp. 2213–2221, 1997.

[90] L. Brown and Q. Zhang, "Periodic disturbance cancellation with uncertain frequency," *Automatica*, vol. 40, no. 4, pp. 631–637, 2004.

[91] M. Bodson, "Rejection of periodic disturbances of unknown and time-varying frequency," *International Journal of Adaptive Control and Signal Processing*, vol. 19, no. 2-3, pp. 67–88, 2005.

[92] S. Hui and S. Zak, "Observer design for systems with unknown inputs," *International Journal of Applied Mathematics and Computer Science*, vol. 15, no. 4, pp. 431–446, 2005.

[93] W. S. Levine, *The Control Handbook*. IEEE Press, CRC Press, 1999, vol. 1.